UNIVERSITY OF SOUTHAMPTON

FACULTY OF ENGINEERING, SCIENCE AND MATHEMATICS

SCHOOL OF CHEMISTRY

March 2007

# LIQUID CRYSTALS: ORDER, SYMMETRY AND DYNAMICS

BY

AZIZAH MAINAL

A dissertation submitted for the
Degree of Doctor of Philosophy

UNIVERSITY OF SOUTHAMPTON

ABSTRACT

FACULTY OF ENGINEERING, SCIENCE, AND MATHEMATICS
SCHOOL OF CHEMISTRY

Doctor of Philosophy

**LIQUID CRYSTALS: ORDER, SYMMETRY AND DYNAMICS**

By
Azizah Mainal

This Thesis describes a range of liquid crystal research which concerns the microscopic properties of liquid crystals such as their orientational order, macroscopic properties such as the phase symmetry and the rate at which their field-induced alignment occurs. The main investigative tool employed is Nuclear Magnetic Resonance spectroscopy (NMR).

The first orientational order study involves a new class of solute known as *iptycenes*, and dramatically whose orientational behaviour in a nematic host is essentially solvent-dependent. While there is no appreciable pattern to link the values of the order parameter to the molecular structure of the liquid crystal host, the deuterium NMR results show very dramatic behaviour of the probe. One particularly significant phenomenon is the behaviour of two iptycenes, with $D_{3h}$ symmetry, which behave like biaxial molecules in their liquid crystal hosts.

The effect of a gelator on the macroscopic orientational ordering of a nematic liquid crystal has been studied. The NMR results suggest that the director order parameter increases with the concentration of the gelator, implying that the spacing between the fibres decreases. In addition, the deformation of the director in the gelled liquid crystal causes the nematic – isotropic transition temperature to decrease.

One of the latest debates in liquid crystal science concerns the existence of the thermotropic biaxial nematic phase. Our phase symmetry study is our contribution to this hot discussion to show how the phase symmetry can be unambiguously identified using NMR spectroscopy. For this, we have chosen the crystal E phase as our model because its biaxiality is not in doubt. Our results show that the phase symmetry is very sensitive to the probe molecule used but that the biaxiality is found to be high.

The director dynamics in the nematic phase is well-studied and understood, but not its smectic counterpart. An extensive study of the alignment process of the director in the smectic A phase of 8CB-$d_2$ by a magnetic field has been undertaken. The NMR spectral pattern and, hence, the alignment process, have been found to be dependent on the angle the director makes with the magnetic field in its initial state.

# CONTENTS

# LIST OF FIGURES

# LIST OF TABLES

**ACKNOWLEDGEMENT**

In the name of ALLAH, the Most Merciful, the Most Compassionate. May peace and blessings be upon Rasulullah SAW, his family and companions. Alhamdulillah, through ALLAH's blessings, I am given this opportunity, strength and will to go through this journey and complete my PhD. To embark on this journey is probably the best decision I have ever made in my life, and despite the roller coaster ride, the outcome has been both emotionally fantastic and intellectually gratifying.

I would like to thank especially Professor Geoffrey Luckhurst, my most esteemed, kind and *superwonderful*$^{\infty}$ supervisor in every way. He has been so inspirational throughout my years as his student, and I must be one of the most fortunate ones for having him as my guru (although...he does sometimes complain, "Oh, I'm not paid enough to do this job!") Indeed, I would not be where I am without his guidance, supervision and especially his belief in me. Most importantly, he was always the first one to make me smile when times were hard.

I would like to extend my gratitude to Professor George Attard for being my co-supervisor and for his kind help especially in the process of completing my studies. My deepest appreciation also goes to my mentor, Dr. Bakir Timimi (Tim), and his wife, Mary, for making me feel at home in Southampton. Tim was the first person to teach me how to use the NMR spectrometer. He has always been very supportive and kind, and I hope to keep learning from him so that I can be a great experimentalist like him. My special thanks also goes to Professor Jim Emsley for the fruitful discussions I had with him on the subject matter, and for lending me his textbooks for a few years, perhaps without him even realizing it! I would also like to express my gratitude to Professor Rauzah Hashim from Universiti Malaya for shaping me up before I came to Southampton. Since I first knew her, she would always take the role of being the tough person in making me strive. For that reason, I really adore her. I would also like to express my appreciation to the collaborators who have contributed to my research, namely, Professor Akihiko Sugimura, Professor Takashi Kato, Professor Roman Dabrowski, Professor Tim Swager, Professor Duncan Bruce, Dr. Susanne Klein, and Angela Downing.

Along this tremendous journey, I have made many friends and they are the reasons for my enjoyable and conducive working and living environment. I would like to thank the people from my group – Rozid, Daniel and the previous members, Sophie and Katsuhiko for their friendships throughout the years. I would also like to thank my colleagues from Professor Malcolm Levitt's group (past and present) whom I am so attached to. They are – Ole, Marina, Linda, Natala, Madhu, Xin, Ildefonso, Jacco, Giancarlo, Darren, Axel, Maria, Peppe and Salvatore. Many thanks to Ildefonso, Marina, Ole, Linda, Rozid, and my dearest friends from other research groups like Hartini, Cle'lia, Rosa, and Soad for always bringing sunshine to my days even when it is pouring

outside! My special thanks to my wonderful Ildefonso, for being such a great friend in need, and for his kind help in the printing of this Thesis. My special tribute also goes to Ole for all the good laughs, and especially for all the technical trouble-shootings, even though he keeps asking me to pay him for each help! But at one point we both agree that he should just request for Geoffrey's credit card! Thanks also to Mariana who has been a dear friend to me and to whom I promise, after my PhD, I will work on my guitar lesson. I would also like to thank the staffs in the School of Chemistry especially Karl, Bevy and Nikki for being so kind, cooperative and always helpful to me. And a great thank you to all other students and staffs in the School who have, in one way or another, touched my heart; you guys know who you are.

Next, I would like to thank the Malaysian community here especially those in the Muslimah Soton and Keluarga Soton group. Of particular, I would like to thank Rosmilah and Mohd. Taib, and Noor Shamsiah and Ustaz Fadhil, for their wonderful friendship and sheer kindness. They have such divine characters and I feel so blessed that they are my friends. I would also like to pay a special tribute to their lovely children, namely, Tasnim, Raihan, Kauthar, Jannah and Khadijah for making my stay here seem so worthwhile. A big thank you to Aniza, Hidayah, Shima, Shaza, Mazwana, Normah, Nani, Syakila and Syakila Sajad for being such gems. My sincere appreciation also goes to Norisah, and her hubby, Abdul Rahman, and family for their kind and moral support while I am here.

During my time here, I met the most wonderful people from Tanzania who has become like my own family. Abeid, Zainah, Jaminah, and their latest edition, Ibtisam, are four people I know who are so much larger than life. They make me so happy throughout my stay here and I can never ever repay the kindness they have given me. I love them so dearly and I look forward to visit them in Tanzania one day to enjoy my trip to Serengeti Safari and Zanzibar, as what we have planned! Through them too, I came to know the doting and wonderful Maryam who has been so kind and generous to me and always making my day throughout my stay in Southampton. My special thanks also goes to Ummu Ghid and Nagham for their moral support and love towards me. My deepest appreciation also goes to Dmitri who just gets to know me, but yet believes in me.

Across the Atlantic Ocean, I would like to thank my best friend, Amai and her hubby, Jeff, for their kindness, moral support and for being such good fun people! Across the Mediterranean Sea, I would like to thank my dearest friend and sister, Hind, for her kindness throughout our friendship. Having to meet Hind unexpectedly outside Raudhah in Masjid Nabawi in Madinah was truly miraculous.

Back home, I would like to thank my UMich girlfriends for being such wonderful, understanding and supportive friends. I would also like to thank Nor Aliah for her constant support and for being

caring. My deepest appreciation also goes to Mrs. Wan Nor Laili and Ms. Siti Balkis from Universiti Malaya for their kindness and help in making my stay here smooth.

My deepest gratitude also goes to Umi, for her love and support towards me throughout the years.

Most importantly, I would like to thank my beloved siblings – Abdul Karim, Seti Hamidah, Siti Aminah, and my in-laws - Zulkifli, Norliah and Faridah for their unconditional love and support. Through thick and thin, they are always and forever my strongest pillars. I would also like thank my wonderful and gifted nieces and nephews who are forever my best and favourite cheerleaders!

All the time, I wish that my beloved father and brother, Mohd. Ramzan, were here. Nonetheless, I know that they are always and forever present in my heart. But the one person I can never thank enough is my mother. She is my source of strength, love, wisdom and inspiration. Her words always soothe my heart and I love her ever so much. I truly hope that she will be pleased to see this Thesis.

Last but certainly not least, I would like to thank the Government of Malaysia and Universiti Malaya for the sponsorship of my PhD and for entrusting me with this fantastic opportunity.

Well... I did not say that this will be a short acknowledgement!

Finally, I truly hope that anyone who reads this Thesis will find it enjoyable, if not helpful!

*For what it's worth*
*It was worth all the while*
*It's something unpredictable*
*But in the end it's right*
*I hope you have the time of your life*

*by Green Day*

*To My Beloved*

*Mak and Abah*

# Chapter 1

# Liquid Crystals: The Phase with an Attitude

## 1.1 Introduction

The term *liquid crystal* is literally an oxymoron, contradictory, but nonetheless the designation is appropriate to depict this particular state of matter. Indeed, a liquid crystal is a unique state of matter which possesses both the anisotropic characteristic of a crystal and the flowing characteristic of a liquid. While we are very accustomed to the three states of matter – solid, liquid, and gas, the liquid crystalline state is still foreign to many. In fact, liquid crystals play an omnivital role in our life. Biologically, cell membranes are made up of liquid crystals to suit the functionality of intercellular transportation. Perhaps, a more apparent use of liquid crystals is in electro-optical visual displays where they have a wide and lucrative commercial application [1]. The complexity of having certain properties of a crystal and a liquid simultaneously is in fact a gift to the field of display technology and has resulted in liquid crystal displays found in numerous consumer everyday items such as watches, calculators, stereos, mobiles, personal organisers, and laptops. Further, liquid crystals have also found applications in detergency and cosmetics where soaps, cream and lotions are some of the products. Another useful and remarkable exploitation of liquid crystals is in the production of Kevlar® [2], a synthetic fibre which is five times stronger than steel per unit weight, and is very heat-resistant, decomposing above 400°C. Kevlar® is used in bullet-proof vests, fire suits, extreme sporting equipment (e.g. windsurfing sails), composites for aircraft construction, fibre optic and electromechanical cables. This almost schizophrenic characteristic of liquid crystals to complement the delicate functionality in the biological system [3] to the robust application in Kevlar® does somehow reflect the versatility of liquid crystals as the phase with an attitude [4].

Just like most great discoveries that of liquid crystals was also accidental. It was fortuitously discovered by an Austrian botanist, Friedrich Reinitzer (see Figure 1), in

1888, when he encountered a strange phenomenon in the material he was studying, namely cholesteryl benzoate. He discovered that cholesteryl benzoate had two melting points - at 145.5°C, the solid melts into a turbid liquid, and at 178.5°C, the turbid liquid becomes clear [5]. This phenomenon is also reversible. The turbid liquid between the solid and the liquid phases was, of course, the liquid crystal phase. Not understanding this strange behaviour of the material, Reinitzer sought help from Otto Lehmann, a German crystallographer who was actively studying the crystallisation properties of various materials using a polarising microscope equipped with a heating stage, which he had ingeniously constructed. When Lehmann observed Reinitzer's material under the microscope, he noted some similarity in behaviour to some of his own samples, namely organic crystals. He first referred to the phase as *Fliessende Kristalle* (flowing crystals) and later, still indecisive, he replaced the name with *Kristalline Flüssigkeit* (crystalline fluid). Gradually, he became convinced that a chemically uniform substance had been discovered. The turbid liquid was, in fact, a uniform fluid phase that also affected polarised light in a manner typical of crystals. Eventually, he coined the term *Flüssige Kristalle* (liquid crystals) which we use to the present day [6, 7, 8 and references therein]. However, occasionally, the term *mesophase*, meaning intermediate phase, is used interchangeably with *liquid crystals*. In addition, compounds which are capable of forming liquid crystal phases are called *mesogens* and molecules constituting such compounds are known as *mesogenic molecules*.

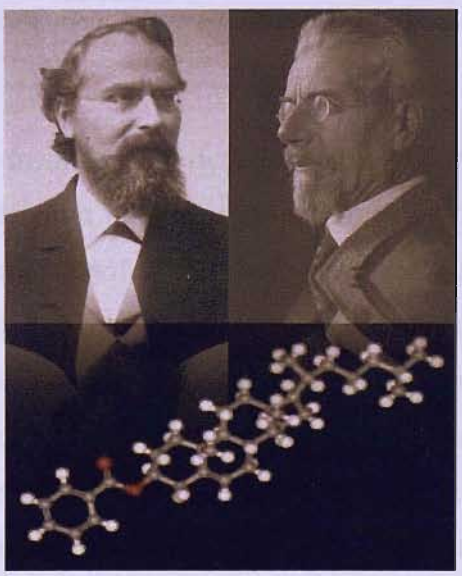

**Figure 1** History in the making - Friedrich Reinitzer (top right), Otto Lehmann (top left), and a molecular model of cholesteryl benzoate (bottom).

## 1.2 Molecular Prerequisites for Liquid Crystal Phases

The most fundamental characteristic of a liquid crystal lies in the existence of its long-range orientational order [9]. Another important and related feature of liquid crystals is that they are formed by molecules with high geometrical anisotropy in their shapes, such as rod- or disc-like objects. Figure 2 shows a schematic illustration of a liquid crystal phase, namely, the nematic phase, formed by rod- and disc-like molecules. A nematic phase is the simplest liquid crystal phase; further details of nematics will be addressed in Section 1.3. Although the rod- and disc-like structures are the established molecular shapes to form liquid crystal phases, other unconventional molecular shapes are also plausible like V-shaped molecules [10], as well as a combination of the rod- and disc-like molecules [11]. These unconventional molecular shapes are especially significant in searching for the elusive biaxial nematic phase, which will be described in detail in Chapter 7.

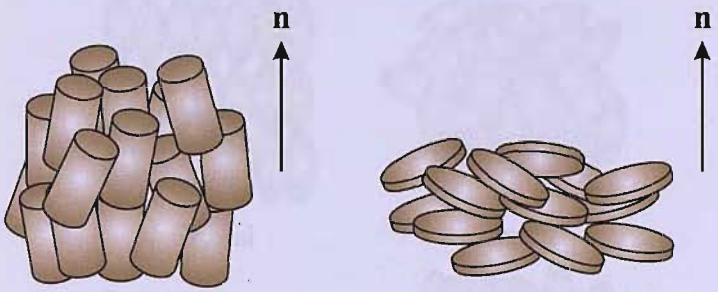


**Figure 2** Schematic illustration of the nematic phase formed from conventional rod- and disc-like molecules.

Molecules which deviate from the spherical shape may exhibit three types of order in the bulk, giving rise to different liquid crystalline phases [12]; they are *orientational order*, *positional* or *translational order*, and *bond orientational order*. Briefly, orientational order indicates that there are long-range orientational correlations between the molecules even when separated by large distances. The second type of order, positional order, refers to the extent to which molecular positions are correlated even though separated by large distances, often resulting in a layer structure [13]. The third is bond orientational order, where the "bonds" are the vectors that join the centres of mass of the nearest neighbouring molecules [14]. If the orientation of these bonds is preserved over a long range, then the system is said to possess bond

orientational order; this will certainly exist if there is long-range positional order but can also occur when the positional order is just short-range. This phenomenon is encountered in a category of smectic phases called the *hexatic smectics*. In these phases, the molecules within a smectic plane possess bond orientational order and since the molecules can best pack in a hexagonal fashion, locally the orientation of the bonds possess six-fold symmetry [12]. We shall discuss the smectic phases further in Section 1.3.

In a crystal, both positional and orientational order are present, such that the molecules are constrained both to occupy specific sites on a lattice and to align their molecular axes in specific directions. In marked contrast, the molecules in a liquid are distributed randomly throughout the sample container. When a crystal, which consists of anisotropic molecules is heated to the melting point, the following possibilities exist [15] (see Figure 3):

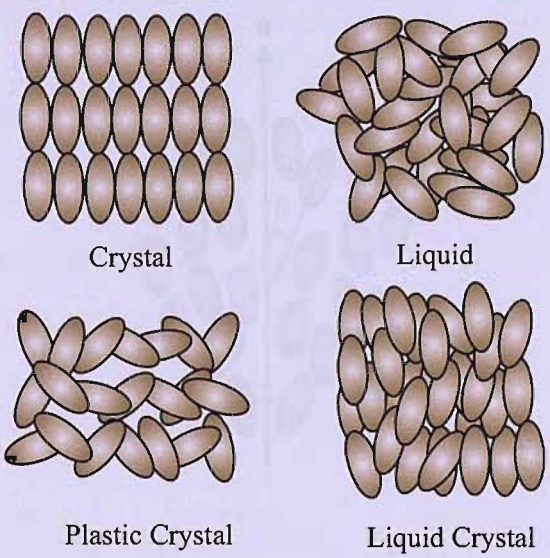


**Figure 3** Schematic illustration of the molecular organisation in crystal, liquid, plastic crystal and liquid crystal.

- § Both types of long-range order, positional and orientational, disappear altogether in the *isotropic liquid* but these correlations are present at short range;
- § Only the long-range orientational order disappears leaving the positional order intact, to give a *plastic crystal* phase;

§ The long-range positional order disappears, either fully or partially, while some long-range orientational order is maintained, the resulting phase is called a *liquid crystal* or *mesophase*. Some mesogenic compounds are *polymorphic*, *i.e.*, they exhibit more than one liquid crystal phase between the crystal and isotropic phases.

In the liquid crystal phase, the assumed molecular symmetry axes are on average parallel to a well-defined spatial direction, **n**, also known as the *director*, where **n** is identical to $-\mathbf{n}$ (see Figure 4). This definition is valid so long as the molecules approximate to cylindrical symmetry. However, for many mesogenic molecules this is not the case and for mesogens formed from such molecules a more appropriate definition is given by Frank [16] in terms of a macroscopic second-rank tensorial quantity such as the dielectric tensor, $\tilde{\varepsilon}$. For most liquid crystals the tensor is cylindrically symmetric and the symmetry axis is correctly identified as the director.

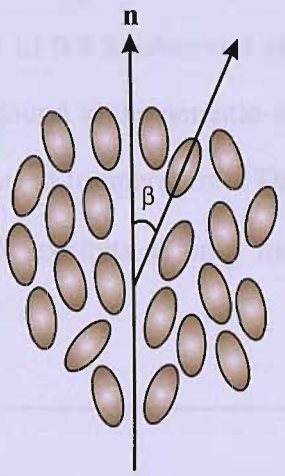


**Figure 4** Schematic molecular arrangement in a nematic phase showing the director.

A quantitative way to define the orientational order in the liquid crystal is *via* the second-rank *orientational order parameter*, $\overline{P}_2$, defined using the average of the second Legendre polynomial [17]. In some liquid crystal textbooks, this orientational order parameter is denoted by S, following the Russian scientist, Tsvetkov [18], who introduced this scalar order parameter for liquid crystals. In essence, $\overline{P}_2$ is defined for

apolar molecules with $D_{nh}$ symmetry (or $C_{nv}$ for polar molecules), with $n \geq 3$, and is expressed as

$$\bar{P}_2 = \left\langle \frac{3\cos^2\beta - 1}{2} \right\rangle, \qquad (1)$$

in which the brackets denote an average over many molecules at the same time, or the average over time for a single molecule; the equality of these assumes ergodic behaviour. The angle between the molecular symmetry axis of an individual molecule and **n** is $\beta$. This definition is convenient, since in a disordered liquid, $\bar{P}_2$ vanishes, whereas conversely, in an ordered crystalline state, $\bar{P}_2$ takes the limiting value of unity.

In addition, the orientational order parameter is typically a function of temperature such that it decreases with increasing temperature, and vanishes in the isotropic phase [19]. Figure 5 shows the typical temperature dependence of $\bar{P}_2$ for a nematic liquid crystal. Usually, an upper limit of 0.8 is observed at low temperature ($T/T_{NI} = 0.8$) and a lower limit of ~0.3-0.4 is found at the nematic-isotropic transition ($T/T_{NI} = 1.0$); here $T/T_{NI}$ is known as the reduced temperature. The nematic-isotropic transition is a first-order transition, hence, $\bar{P}_2$ exhibits a jump from the nematic to the isotropic phase, as shown in Figure 5.

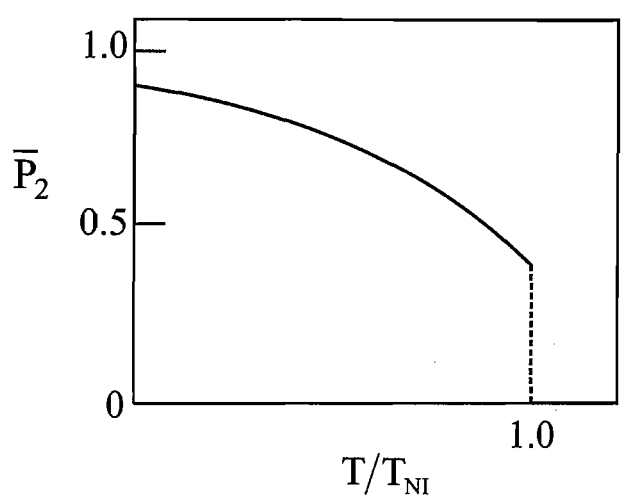


**Figure 5** The A typical temperature dependence of the order parameter, $\bar{P}_2$ for a nematic phase; here $T/T_{NI}$ is the reduced temperature and $T_{NI}$ is the nematic (N) - isotropic (I) transition temperature.

The orientational order parameter, $\overline{P}_2$, can be measured in various ways including diamagnetism, optical birefringence, and nuclear magnetic resonance (NMR). The basic principle of these methods is that they yield a value for some anisotropic property which, when scaled with the value for the crystal, *i.e.*, for perfect orientational order, gives a measure of the orientational order. In this Thesis, NMR spectroscopy has been employed to determine the order parameters, and so a more comprehensive discussion of the order parameters and the NMR technique will be given in the following two chapters. In addition, higher rank order parameters can also be defined, but are more difficult to measure. For example, the average of the fourth Legendre polynomial could be used, where

$$\overline{P}_4 = \left\langle \frac{35\cos^4\beta - 30\cos^2\beta + 3}{8} \right\rangle. \qquad (2)$$

As for $\overline{P}_2$, $\overline{P}_4$ takes the limiting value of zero in the isotropic phase and unity in a perfectly ordered crystalline phase. The measurement of $\overline{P}_4$ is not straightforward but it can be achieved using Raman scattering and with ESR spectroscopy; in addition these techniques also give the second rank order parameter. Values of $\overline{P}_4$ are important because they provide a more detailed characterisation of the phase structure and so give a more detailed test of theories and simulations.

In general, the odd Legendre polynomials can also be used to define orientational order parameters and these provide a measure of the polar order for the phase. For example, the first odd Legendre polynomial is

$$P_1(\cos\beta) = \cos\beta. \qquad (3)$$

However, the nematic phase is apolar, that is the directions $\mathbf{n}$ and $-\mathbf{n}$, are equivalent and so the averages of all of the odd Legendre polynomials vanish.

## 1.3 Thermotropic Liquid Crystals

Liquid crystalline materials are generally divided into two broad categories, the *thermotropic* mesophase and the *lyotropic* mesophase. In the case of the thermotropic, the prefix *therm-* originates from a Greek word *thérmē*, which means heat. As the name clearly suggests, the thermotropic mesophase refers to a liquid crystal where the transition into the mesophase is brought about by a thermal process *i.e.*, by heating. The other class, *lyotropic* liquid crystal, is such that the transition into the mesophase is solvent-driven. A lyotropic mesogenic molecule consists of a hydrophobic group and a hydrophilic group, which make it capable of forming ordered structures in both polar and non-polar solvents. These result because the amphiphile first forms micelles which may be anisotropic and it is the anisotropic interactions between these that lead to the formation of a liquid crystal phase. Thus, we see that the micelle for a lyotropic plays the same role as the molecule does for a thermotropic liquid crystal. However, this Thesis is focused only on thermotropic liquid crystals; for that reason, nothing else will be said about the lyotropics.

Thermotropic liquid crystals are generally further classified with respect to the molecular shape of the constituent molecules, being called *calamitic* for rod-like, and *discotic* for disc-like molecules as mentioned in Section 1.2. The following subsections will elaborate more on these two extremes although a wide range of other anisotropic molecular shapes are also capable of forming liquid crystal phases.

### *1.3.1 Calamitic Liquid Crystals*

*Calamitic* liquid crystals are liquid crystals consisting of elongated rod-like molecules, in which one molecular axis is much longer than the other two and such materials are the most numerous. The length-to-breadth ratio found to be necessary for the formation of a liquid crystal is ~ 3:1 or greater. The criterion of having an elongated, linear molecule to form liquid crystals is called Vorländer's Rule [20]. These rod-like molecules possess some rigidity at some portion of their length since it must maintain an elongated shape in order to produce anisotropic interactions that favour orientational order. Two common liquid crystal phases are the *nematic* and *smectic*

phases, in which the nomenclatures for the different phases of liquid crystals were proposed by the French chemist, Georges Friedel [21].

*Nematic Phases*

*Nematic* liquid crystals are named after the dark threads (from the Greek word, *νημα* (nēmat-) – "thread") visible in a typical nematic texture under a polarising microscope. These dark threads are a consequence of the differences in the director distribution caused by defects in the director field, known as *disclinations* [19]. These disclinations appear dark due to the optical extinction caused by the crossed polarisers. In order for this optical extinction to occur the director must be aligned in the direction of either of the two polarisers. These disclinations can meet at points, which give rise to defects known as *brush defects*, the most common of which is the *four-brush defect*. A nematic texture observed when the sample is in planar alignment is known as the *Schlieren texture* (see Figure 6), a colourful birefringent texture with dark threads.

**Figure 6** A Schlieren texture of a nematic film with four-brush defects [22].

As we have seen, the nematic phase is the simplest and most common type of liquid crystal, in which the molecules possess only long-range orientational order, and no positional order. Most nematics are uniaxial ($N_U$), which means that second-rank tensorial properties such as the dielectric anisotropy are cylindrically symmetric about the director. The existence of the biaxial nematic ($N_B$) phase has also been predicted [23], and in this phase, the three principal components of, for example, the dielectric

tensor will be different. In addition, the principal axes associated with the principal components define the three directors for this phase which are denoted by **l**, **m** and **n**.

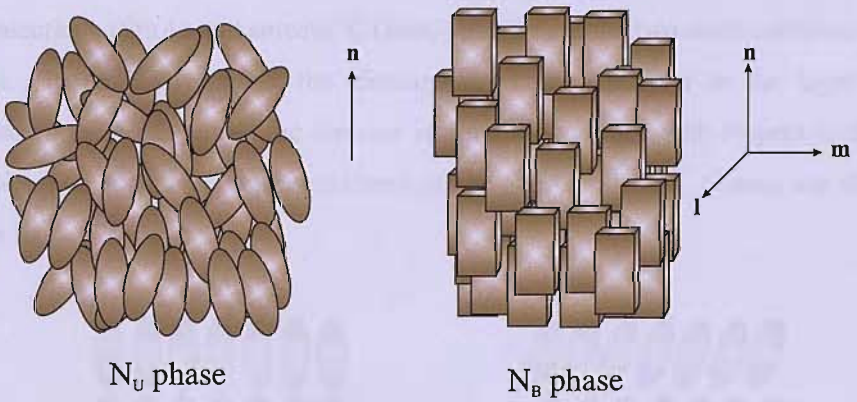


**Figure 7** Schematic illustration of the molecular organisation of a uniaxial nematic phase, $N_U$, and a biaxial nematic phase, $N_B$.

The biaxial nematic are made up of block-like molecules (see Figure 7), although other molecular shapes are also plausible, like the V-shaped molecule [10, 24, 25]. For the block-shaped molecules the preferred orientations of the molecular symmetry axes can be used to identify the directors but for many biaxial molecules there are no symmetry axes and for these the tensorial approach is clearly preferred. The pursuit of the biaxial nematic has proven to be challenging, especially in characterising the existence of the phase unambiguously [26]. While the existence of the biaxial nematic phase in the lyotropic system [27] is irrefutable and the biaxiality is large [28], the biaxiality for the thermotropic system is invariably a matter of debate [24]. The biaxial nematic is further discussed in Chapter 7.

*Smectic Phases*

The word *smectic* is derived from the Greek word, *σμηγμα* (smēktikós), which means "soap". Unlike the nematic phase, the smectic phase possesses both orientational and positional order. They have layered structures with a well-defined interlayer spacing which can be measured *via* X-ray diffraction. The interlayer attractions are usually weak compared to the lateral forces between the molecules, and so these layers are

able to slide over one another relatively easily, hence their name, giving the fluid property of the system [15].

The smectic A (SmA) and smectic C (SmC) phases are the two most common smectic phases. In the SmA phase, the director, **n**, is perpendicular to the layer planes, whereas in the SmC phase, the director is tilted by an angle with respect to the layer normal. The schematic representations of the SmA and SmC phases are shown in Figure 8.

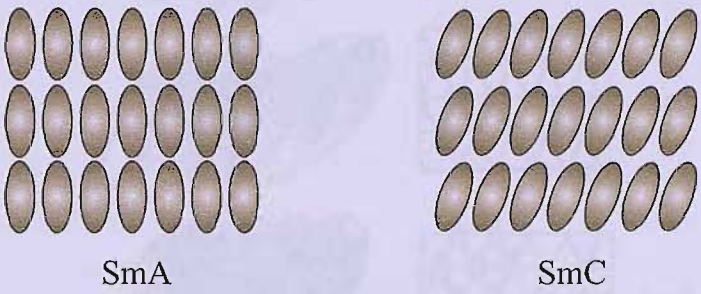


**Figure 8** Schematic illustration of the molecular organisation in the two common smectic phases, SmA and SmC.

*The Hexatic Smectic Phases (SmB, SmI, SmF)*

In this category of smectic phase, within a layer, the translational order is locally hexagonal but at long range, this positional order vanishes. However, the bonds, linking the molecules in the local hexagonal arrangement, are correlated at long range, so that there is long-range bond orientational order. Figure 9 shows the insertion of a defect in the hexagonal lattice that destroys the long-range positional order, while the bond orientational order is preserved across the defect [14].

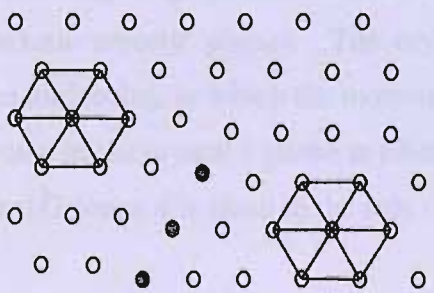

**Figure 9** The schematic illustration of bond-orientational order in hexatic smectic phases. The closed circles represent the defects in the hexagonal net.

The orthogonal hexatic smectic phase, comparable to SmA but now with bond-orientational order, is called the SmB, and has the director pointing along the smectic layer normal. The tilted versions of the hexatic smectic phases, SmI and SmF, only differ in their tilt direction. In the SmI phase the molecules are tilted towards the apex of the hexagon, while in the SmF phase the molecules are tilted towards its side, as shown in Figure 10.

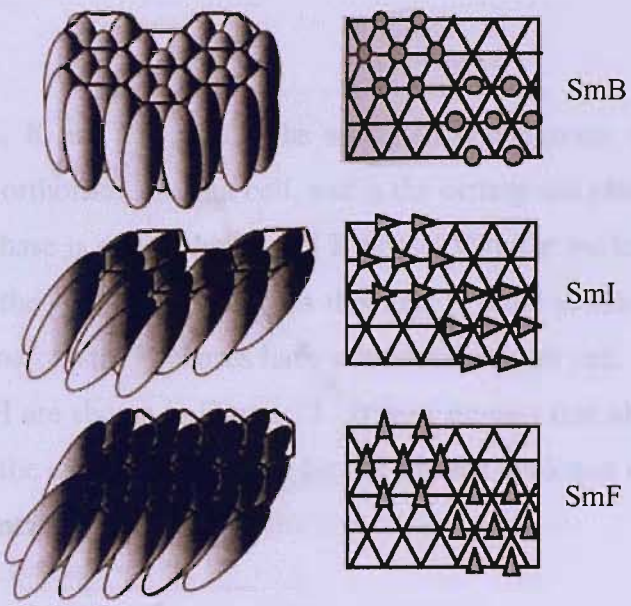


**Figure 10** The idealised structure of the molecular organisation in the SmB, SmI, and SmF phases [14, 19].

*The Soft Crystal Phases (B, J, G, E, K, H)*

The structures of the soft crystal phases, B, J and K, shown in Figure 11; they are very similar to those of the hexatic phases, SmB, SmI and SmF, respectively. However, they differ in that they exhibit long-range positional order within the layer, which is only short-range for the hexatic smectic phases. The crystal B phase exhibits an orthogonal orientation of the molecules, in which the molecular long axis is parallel to the layer normal. The director in the crystal J phase is tilted towards the apex of the hexagon, while for the crystal G phase it is tilted to the side of the hexagon.

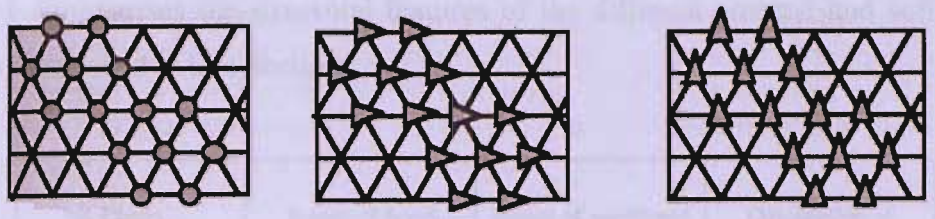


**Figure 11** A plan view of crystals B, J, and G [19].

The crystal phases, E, K and H, exhibit the so-called herringbone structure. The crystal E phase has an orthorhombic unit cell, and is the orthogonal phase of the three. The respective tilted phase is called the crystal K phase, with the molecular long axis tilted to side *a*, while the crystal H phase, has this axis is tilted to side *b* (see Figure 12). Both crystal K and crystal H phases have a monoclinic unit cell. Plan views of the crystals E, K and H are shown in Figure 13. It is of interest that although there is a smectic analogue of the crystal B phase, so far the smectic analogue of the crystal E phase has not been identified.

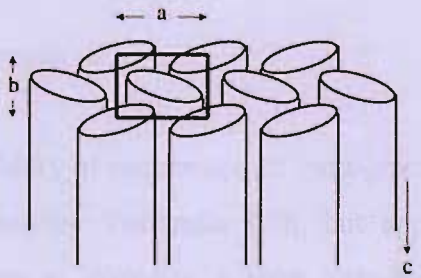


**Figure 12** The model structure of the crystal E phase with a herringbone molecular organisation. The crystal K phase has its molecular long axis tilted towards side *a*, while that of the crystal H phase is tilted towards side *b* [14].

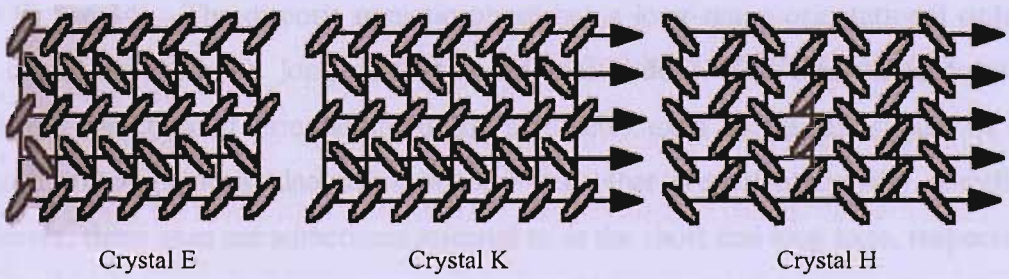


**Figure 13** A plan view of crystals E, K, and H [19].

Table 1 summarises the structural features of the different smectic and soft crystal phases mentioned in this Section.

| Phase | Range of bond orientational order | Range of positional order within a layer | Orientation of molecular long axis |
|---|---|---|---|
| SmA | short | short | orthogonal to layer |
| SmC | short | short | tilted to layer |
| SmB | long | short | orthogonal to layer |
| SmI | long | short | tilted (to apex) |
| SmF | long | short | tilted (to side) |
| B | long | long | orthogonal to layer |
| J | long | long | tilted (to apex) |
| G | long | long | tilted (to side) |
| E | long | long | orthogonal to layer |
| K | long | long | tilted (to side *a*) |
| H | long | long | tilted (to side *b*) |

**Table 1** A summary of the general characteristic of the structural features of smectic and soft crystal phases [14].

### *1.3.2 Discotic Liquid Crystals*

It was found that the feasibility of occurrence of mesogenicity is not restricted to rod-like molecules as suspected by Vorländer [20], but applies also to flat, disc-like organic compounds, known as *discotics*, a term introduced by Billard *et al.* [29]. Discotic liquid crystals were first discovered by Chandrasekhar *et al.* in 1977 for the hexa-alkanoyloxy benzenes [30, 31]. The two most common discotic mesophases are the *discotic nematic*, $N_D$ (see Figure 2), and the *ordered hexagonal columnar*, $Col_{ho}$ (see Figure 14). The discotic nematic phase has a long-range orientational order of the discs, but with no long-range translational order. The director denotes the preferred direction of orientation of the symmetry axes of the discs; just as in a calamitic nematic it is also the symmetry axes that are orientationally correlated. However, these axes are sometimes referred to as the short and long axes, respectively. Although this usage is quite common it should be avoided because it masks the similarity between the nematic phases formed from rod-like and from disc-like molecules. Just as rods can form liquid crystal phases with translational order, that is

the smectics, so too can discs. The translationally ordered phases formed by the disc-like molecules are the columnar phases so called to indicate that the discs are arranged in columns. The columns can then be organised within a plane perpendicular to the column axis to give a two-dimensional lattice. Several columnar structures have been identified with different arrangements of the columns, such as hexagonal, rectangular, and oblique. In some cases, the columns are liquid-like, *i.e.*, the centres of the molecules within the column are irregularly spaced, while in others they are arranged in a regular, ordered fashion [32]. In addition, there are other discotic mesophases including the tilted disordered columnar, and tilted ordered columnar phase as shown in Figure 14.

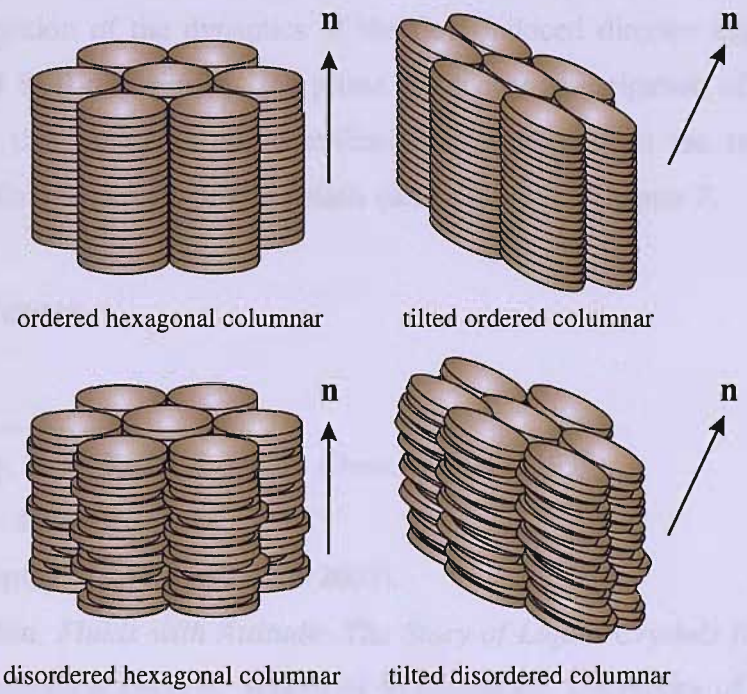


**Figure 14** Schematic representation of the molecular organisation in ordered hexagonal columnar phase ($Col_{ho}$), tilted ordered columnar phase ($Col_{to}$), disordered hexagonal columnar phase ($Col_{hd}$), and tilted disordered columnar phase ($Col_{td}$).

## 1.4 Synopsis of Thesis

This Thesis is entitled *Liquid Crystals: Order, Symmetry and Dynamics* for a very good reason. By the employment of Nuclear Magnetic Resonance Spectroscopy (NMR), which is a well-known and powerful tool, widely differing liquid crystal projects have been studied. The first three chapters in this Thesis serve to introduce

the liquid crystal systems under investigation, and the primary technique used to study these systems, which is NMR. In this Chapter, we have briefly discussed the historical background and the different classes of liquid crystal phases of particular relevance. A more quantitative approach can be found in Chapter 2, where the long-range orientational order, the essence of the liquid crystals, is described in detail. The discussion of the NMR technique employed in the studies will follow in Chapter 3. The last four chapters describe the results and their interpretation for the experiments we have conducted. Chapter 4 discusses the results obtained for the orientational order of the iptycenes, a new class of probe molecule for liquid crystal studies. The effect of gelators on the director distribution and the orientational order in the liquid crystal can be found in Chapter 5 on liquid crystal gels. This is followed in Chapter 6 by the investigation of the dynamics of the field-induced director alignment in the SmA phase of 8CB-$d_2$. Finally, the phase symmetry investigation of the crystal E phase can be thought of as our contribution to help unravel the mystery of the thermotropic biaxial nematic phase; details can be found in Chapter 7.

## 1.5 References


[1] G. W. Gray, S. M. Kelly, *J. Mater. Chem.*, **9**, 2037 (1999).

[2] http://www.dupont.com

[3] G. T. Stewart, *Liq. Cryst.*, **30**, 541 (2003).

[4 ] T. J. Sluckin, *Fluids with Attitude: The Story of Liquid Crystals from Oddity to Technology*, Inaugural Lecture, School of Mathematics, University of Southampton (2001).

[5] F. Reinitzer, *Monatsh. Chem.*, **9**, 421 (1888); *Liq. Cryst.*, **5**, 7 (1989).

[6] O. Lehmann, *Z. Phys. Chem.*, **5**, 427 (1890).

[7] H. Kelker, *Mol. Cryst. Liq. Cryst.*, **21**, 1 (1973).

[8] T. J. Sluckin, D. A. Dunmur, H. Stegemeyer (Eds.), *Crystals That Flow*, Taylor & Francis, London and New York (2004).

[9] A. J. Leadbetter, in *Critical Reports on Applied Chemistry, Vol. 22: Thermotropic Liquid Crystals*, (Ed. G. W. Gray), John Wiley & Sons, Great Britain, (1987), Chap. 1.

[10] G. R. Luckhurst, *Thin Solid Films*, **393**, 40 (2001).

[11] K. Praefcke, B. Kohne, B. Gundogan, D. Singer, D. Demus, S. Diele, G. Pelzl, U. Bakowsky, *Mol. Cryst. Liq. Cryst.*, **198**, 393 (1991).

[12] S. Kumar, *Liquid Crystals: Experimental Study of Physical Properties and Phase Transitions*, Cambridge University Press, Cambridge (2001).

[13] http://plc.cwru.edu/tutorial/

[14] I. Dierking, *Textures of Liquid Crystals*, Wiley-VCH, Weinheim (2003).

[15] S. Singh, *Phys. Rep.*, **324**, 107 (2000).

[16] F. C. Frank, *Proceedings of the International Conference on Liquid Crystals, Bangalore*, (Ed. S. Chandrasekhar), Hayden & Son, London, (1979), 1.

[17] P. H. Hermans, P. Platzek, Kolloid-Z, **88**, 68 (1939).

[18] V. Tsetkov, *Acta Physicochim. (USSR)*, **16**, 132 (1942).

[19] P. J. Collings, M. Hird, *Introduction to Liquid Crystals: Chemistry and Physics*, Taylor & Francis Ltd., London, (1997), Chap. 1.

[20] D. Vorländer, *Ber. Dtsch. Chem. Ges.*, **40**, 1970 (1907).

[21] G. Friedel, *Ann. Phys.*, **18**, 273 (1922).

[22] O. Lavrentovich, http://www.lci.kent.edu/polmicpic.html.

[23] M. J. Freiser, *Phys. Rev. Lett.*, **24**, 1041 (1970).

[24] L. A. Madsen, T. J. Dingemans, M. Nakata, E. T. Samulski, *Phys. Rev. Lett.*, **92**, 145505 (2004).

[25] B. R. Acharya, A. Primak, S. Kumar, *Phys. Rev. Lett.*, **92**, 145506 (2004).

[26] Y. Galerne, *Mol. Cryst. Liq. Cryst.*, **323**, 211 (1998).

[27] L. J. Yu, A. Saupe, *Phys. Rev. Lett.*, **45**, 1000 (1980).

[28] F. P. Nicoletta, G. Chidichimo, A. Golemme, N. Picci, *Liq. Cryst.*, **10**, 665 (1991).

[29] J. Billard, J. C. Dubois, N. H. Tinh, A. Zann, *Nouv. J. Chim.*, **2**, 535 (1978).

[30] S. Chandrasekhar, B. K. Sadashiva, K. A. Suresh, *Pramana*, **9**, 471 (1977).

[31] S. Chandrasekhar, in *Handbook of Liquid Crystals, Vol. 2B: Low Molecular Weight Liquid Crystals II*, (Eds. D. Demus, J. Goodby, G. W. Gray, H. W. Spiess, V. Vill), WILEY-VCH, Weinheim, (1998), Chap. VIII.

[32] S. Chandrasekhar, S. K. Prasad, *Contemp. Phys.*, **40**, 237 (1999).

# Chapter 2

# Long-range Orientational Order of Liquid Crystals

## 2.1 Introduction

The defining characteristic of a liquid crystal phase is its long-range orientational order. For rod-like mesogenic molecules, the molecular symmetry axes tend to be correlated over large distances and are, on average, parallel to the director [1]. In general, the extent of the molecular alignment with respect to the director can be described by an infinite set of orientational order parameters. However, in Chapter 1, only the second-rank order parameter, $\overline{P}_2$, was used to describe quantitatively the degree of such alignment in a uniaxial liquid crystal, like the nematic phase. On the other hand, when the mesogenic molecule deviates from cylindrically symmetry, as is true for all cases, the single order parameter, $\overline{P}_2$, must be replaced by an ordering matrix which we shall discuss in this Chapter. Similarly, the description of the ordering when both the molecule and the phase deviate from uniaxial symmetry also becomes both rich and complicated, as we shall see.

## 2.2 The Orientational Order Parameters

In dealing with a case where the flexibility of the molecule is ignored, the orientation of a rigid molecule with respect to an arbitrary laboratory frame can be specified by the three Euler angles, $\alpha$, $\beta$, and $\gamma$, collectively denoted as $\Omega$. These three angles are shown in Figure 1 where XYZ denotes the laboratory frame, and xyz is the molecular frame; the Euler angles, $\beta$ and $\alpha$, can best be visualised as the spherical polar angles made by the molecular z axis in the XYZ frame and $\beta$ and $\gamma$ as the spherical polar angles made by the laboratory Z axis in the xyz frame.

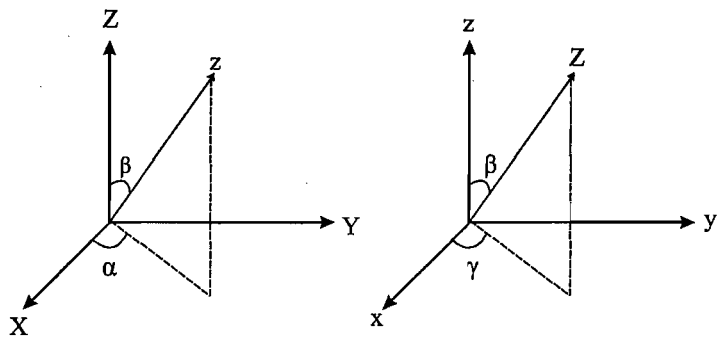


**Figure 1** The Euler angles, α, β and γ, relating a molecular frame (xyz) to a laboratory frame (XYZ).

The distribution of molecular orientations in the liquid crystal phase is described by the singlet orientational distribution function, $f(\Omega)$, which gives the probability density for the orientation of the molecule. In other words, $f(\Omega)d\Omega$ is defined as the probability of finding a molecule with an orientation between $\Omega$ and $\Omega + d\Omega$. By definition, the distribution function is normalised, *i.e.*,

$$\int_0^{\pi} f(\Omega) \sin\Omega \, d\Omega = 1. \tag{1}$$

It can be expanded in a basis of Wigner rotation matrices [2]:

$$f(\Omega) = \sum_{Lmn} f_{Lmn} D^{L}_{mn}(\Omega), \tag{2}$$

where $f_{Lmn}$ are, as yet, unknown expansion coefficients. However, as we shall see, these lead to the definition of a complete set of orientational order parameters related to the molecular symmetry and that of the phase. The expansion coefficients are obtained from the orthogonality of the Wigner rotation matrices,

$$\int D^{L*}_{mn}(\alpha\beta\gamma) D^{L'}_{m'n'}(\alpha\beta\gamma) d\alpha \sin\beta \, d\beta \, d\gamma = \frac{8\pi^2}{2L+1} \delta_{mm'} \delta_{nn'} \delta_{LL'}, \tag{3}$$

and so, the expansion coefficients are found to be

$$f_{Lmn} = \left(\frac{2L+1}{8\pi^2}\right)\overline{D}^{L*}_{mn}, \tag{4}$$

where the averages $\overline{D}^{L*}_{mn}$ represent a complete set of order parameters which define $f(\Omega)$ and the orientational order of the molecule in the phase. Rewriting Equation (2), we now have the general singlet orientational distribution function as

$$f(\Omega) = \sum_{Lmn}\left(\frac{2L+1}{8\pi^2}\right)\overline{D}^{L*}_{mn} D^{L}_{mn}(\Omega). \tag{5}$$

Equation (5) can be simplified by considering specific symmetries of the mesophase and its constituent molecules. In the following subsections, we shall look at different cases of molecular and mesophase symmetries in defining the singlet orientational distribution function, and more importantly, the orientational order parameters. Our discussion begins with the simplest case, *i.e.*, uniaxial molecules in a uniaxial phase such as the nematic or smectic A phases.

## 2.3 Uniaxial Molecules in a Uniaxial Phase

For an ordering tensor of a given rank L, $\overline{D}^{L}_{mn}$, there are a total of $(2L+1)^2$ components since n and m each take $2L+1$ values from $-L...L$. This number can be drastically reduced by exploiting the symmetry properties of the mesophase and of its constituent molecules [2]. We shall first treat the case of a uniaxial molecule in a uniaxial mesophase and define the symmetry axis of the phase, the director, to be along the Z laboratory axis. Thus, rotating the sample about the director does not change the singlet distribution function. This means that the probability for a molecule to have orientation $(\alpha\beta\gamma)$ should be the same whatever the angle, $\alpha$, is, since $\alpha$ describes a rotation around the laboratory Z axis (see Figure 1). In addition, because the molecule also possesses uniaxial symmetry, the distribution should be independent of the angle, $\gamma$, which is defined as a rotation around the molecular z axis [3] (see Figure 1) so that $f(\Omega)$ can now be simplified to $f(\beta)$, which gives the

probability of finding the molecule at an angle between $\cos\beta$ and $\cos\beta + d\cos\beta$ with respect to the director. The normalisation condition (see Equation (1)) for the distribution is

$$\int_0^{\pi} f(\beta)\sin\beta d\beta = 1. \tag{6}$$

$f(\beta)$ can be expanded in terms of a complete basis set of Legendre polynomials, $P_L(\cos\beta)$, which gives the singlet orientational distribution function as

$$f(\beta) = \sum_{L=0}^{\infty} f_L P_L(\cos\beta), \tag{7}$$

where $f_L$ are the expansion coefficients. The first few Legendre polynomials are

$$P_0(\cos\beta) = 1,$$

$$P_1(\cos\beta) = \cos(\beta),$$

$$P_2(\cos\beta) = \frac{(3\cos^2\beta - 1)}{2}, \tag{8}$$

$$P_3(\cos\beta) = \frac{(5\cos^3\beta - 3\cos\beta)}{2},$$

$$P_4(\cos\beta) = \frac{(35\cos^4\beta - 30\cos^2\beta + 3)}{8}.$$

However, the rank L is restricted to even values due to the mirror plane orthogonal to the director for apolar phases, which requires

$$f(\beta) = f(\pi - \beta), \tag{9}$$

so that the odd expansion coefficients must vanish. The even expansion coefficients are obtained from Equation (4) for the general case by setting m and n equal to zero, using the fact that $\overline{D}^{L}_{00} = \overline{P}_L$ and integrating out the dependence on $\alpha$ and $\gamma$; the result is

$$f_L = \frac{2L+1}{2}\overline{P}_L. \tag{10}$$

Here, the averages of the Legendre polynomials, $\overline{P}_L$ completely define the orientational distribution function and so constitute an infinite set of orientational order parameters when all ranks are considered. They are all zero in an isotropic liquid, while in a perfectly ordered system the order parameters take the limiting value of unity. There is also another limiting form of interest and that is when the molecules are orthogonal to the director but randomly distributed in this plane. Then $\overline{P}_2$ is $-1/2$, $\overline{P}_4$ is 3/8 and $\overline{P}_6$ is $-5/16$. Rewriting Equation (7), the distribution function for a uniaxial molecule in a uniaxial phase is given by

$$\begin{aligned} f(\beta) &= \sum_{0}^{L} \frac{2L+1}{2}\overline{P}_L P_L(\cos\beta), \\ &= \frac{1}{2} + \frac{5}{2}\overline{P}_2 P_2(\cos\beta) + \frac{9}{2}\overline{P}_4 P_4(\cos\beta) + \ldots \end{aligned} \tag{11}$$

The first non-trivial term contains the second-rank order parameter, $\overline{P}_2$. This order parameter, introduced by Tsvetkov [4], is easily measured and so is often used to quantify the orientational order in liquid crystals; sometimes $\overline{P}_2$ is denoted by the letter S. It is worth stressing that Equation (11) is only exact as an infinite expansion, but that, in practice, it does not give a very good approximation to the distribution when we truncate it after the first few terms, except in the limit of low order. For example, if we have $\overline{P}_2 = 0.5$, $f(\beta)$, as given by the expansion truncated at the second-rank level, is shown in Figure 2. We see that $f(\beta)$ constructed in this way can even become negative, which is certainly not physical since $f(\beta)$ is a probability density and so must be positive. $\overline{P}_2$ is calculated correctly using this form for $f(\beta)$,

however, for higher order parameters calculated with the second-rank approximation are zero because of the orthogonality of the Legendre polynomials. Thus, the approximation is exact for $\overline{P}_2$, but tells us nothing about the higher order parameters [3].

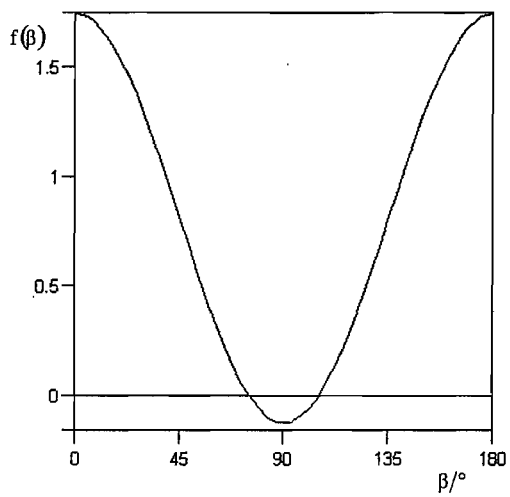


**Figure 2** The orientational distribution function corresponding to $\overline{P}_2 = 0.5$ obtained from the expansion in Equation (11) truncated to the second rank.

A different approach in finding an approximate form for the orientational distribution is provided by the maximum entropy (ME) principle [5, 6]. When a measurement of an arbitrary observable, A, is made in a uniaxial macroscopic system, it results in an ensemble average

$$\begin{aligned} \langle A(\beta)\rangle &= \int_0^{\pi} A(\beta) f(\beta) \sin\beta \, d\beta \\ &= \overline{A}, \end{aligned} \tag{12}$$

in which $f(\beta)$ is the orientational distribution function. According to the ME method, the best form for $f(\beta)$ is given by

$$f(\beta) = Z^{-1} \exp(-aA(\beta)), \tag{13}$$

where Z is the normalisation parameter

$$Z = \int_0^{\pi} \exp(-aA(\beta))\sin\beta d\beta . \tag{14}$$

The parameter a, is found by fitting the experimental value, $\overline{A}$, to the right-hand side of Equation (12). For example, we might take $\overline{A}$ to be $\overline{P}_2$ and assume $\overline{P}_2 = 0.5$, a typical value for a nematic phase close to the nematic-isotropic transition ($T/T_{NI} = 1.0$). Then by employing the principle of the ME method, it is found that the most probable distribution consistent with this, is

$$f(\beta) = Z^{-1} \exp\left(-a\left(\frac{3\cos^2\beta - 1}{2}\right)\right), \tag{15}$$

with Z = 3.62, and a = -2.32. This function is displayed in Figure 3.

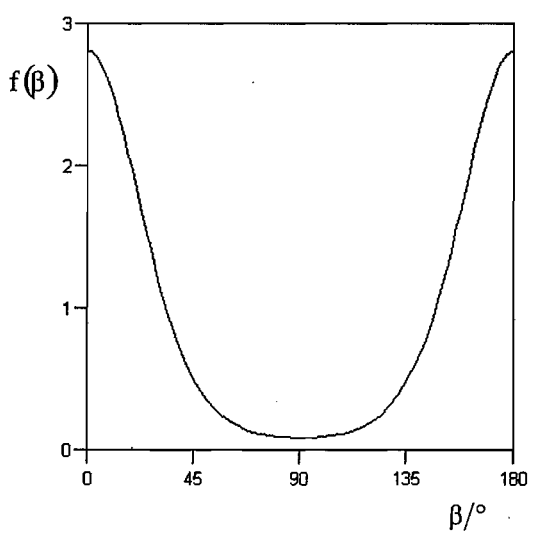


**Figure 3** The singlet orientation distribution function in Equation (15) obtained from the maximum entropy theory.

From the plot in Figure 3, it is apparent that the probability of finding a molecule at a certain angle between the director and the molecular symmetry axis is largest for $\beta$ = 0 and $\beta = \pi$, *i.e.*, when the molecule is oriented with its symmetry axis parallel or anti-parallel to the director as might have been expected. The comparison between the truncated orthogonal expansion and the maximum entropy theory for the singlet

orientation distribution function is shown in Figure 4. It is apparent that although both distributions give the same value of $\overline{P}_2 (= 0.5)$, the distribution from the truncated expansion is unrealistic and that from the maximum entropy principle is not.

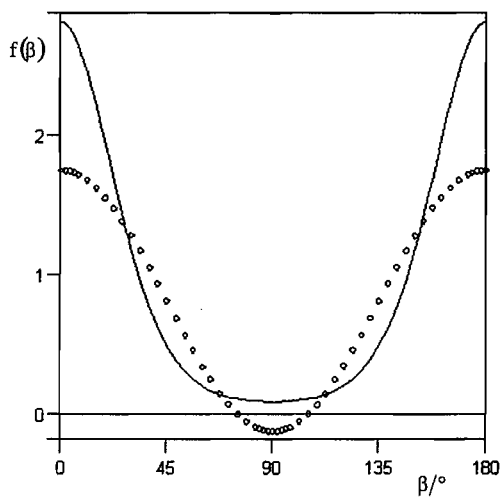


**Figure 4** Combining Figure 2 and Figure 3 to compare the orientational distribution obtained from the truncated orthogonal expansion (points) and from the maximum entropy principle (continuous line).

## 2.4 Biaxial Molecules in a Uniaxial Phase

When a mesogenic molecule or one dissolved in a uniaxial phase, deviates from cylindrical symmetry, we need two angles, $\beta$ and $\gamma$, collectively denoted by $\omega$, to define its orientation with respect to the director. $\beta$ is the angle between the molecular z axis and the director, and as stated earlier, $\gamma$ is the angle of rotation of the laboratory Z axis around the molecular z axis (*i.e.*, the azimuthal angle). The probability density, $f(\omega)$, of finding the molecule at a specific orientation between $\omega$ and $\omega + d\omega$, can be expanded in a complete set of modified spherical harmonics, $C_{Ln}(\omega)$. Thus, we find

$$f(\omega) = \sum_{Ln} f_{Ln} C_{Ln}(\omega), \tag{16}$$

where L is an integer denoting the rank of the spherical harmonic and $n \equiv -L...L$, giving a total of 2L + 1 components for the expansion coefficients, $f_{Ln}$. When n is

zero, the modified spherical harmonic is independent of the azimuthal angle $\gamma$, and hence, is equal to the Legendre polynomial of the same rank, *i.e.*,

$$P_L(\cos\beta) = C_{Ln}(\beta\gamma)\delta_{0n}. \tag{17}$$

The first few modified spherical harmonics are

$$C_{00}(\beta\gamma) = 1,$$

$$C_{10}(\beta\gamma) = \cos\beta,$$

$$C_{1\pm1}(\beta\gamma) = \sqrt{\frac{1}{2}}\sin\beta\exp(\mp i\gamma),$$

$$C_{20}(\beta\gamma) = (3\cos^2\beta - 1)/2,$$

$$C_{2\pm1}(\beta\gamma) = \pm\sqrt{\frac{3}{2}}\sin\beta\cos\beta\exp(\mp i\gamma),$$

$$C_{2\pm2}(\beta\gamma) = \sqrt{\frac{3}{8}}\sin^2\beta\exp(\mp i2\gamma). \tag{18}$$

As seen previously, the expansion coefficients can be obtained from general results in Equation (4) by setting $m = 0$ and integrating out the dependence on $\alpha$; this gives the expansion coefficients, $f_{Ln}$ as

$$f_{Ln} = \frac{2L+1}{4\pi}\overline{C}^*_{Ln}. \tag{19}$$

The averages of the modified spherical harmonics, $\overline{C}^*_{Ln}$ which are equal to that of the Wigner rotation, $\overline{D}^{L*}_{0n}$, allow a complete set of orientational order parameters to be defined. Hence, rewriting Equation (16) we have

$$f(\omega) = \sum_{Ln}\frac{2L+1}{4\pi}\overline{C}^*_{Ln}C_{Ln}(\omega). \tag{20}$$

In addition, it is important to note the limiting values for the order parameters. In the isotropic phase, all of the order parameters, $\overline{C}_{Ln}$ vanish, while in uniaxial liquid crystals, only the even values of L remain for apolar phases. At the other extreme in the limit of complete order, in which the molecular z axis is perfectly ordered (parallel to the laboratory Z axis), but with the x and y axes random in the XY plane to preserve the uniaxiality of the phase, we get

$$\overline{C}_{Ln} = \delta_{0n}. \tag{21}$$

For example, for perfect order where the molecular axis z is aligned parallel to the director, $\overline{C}_{20} = 1$ . The other components with n not equal to zero, vanish ($\overline{C}_{2\pm1} = \overline{C}_{2\pm2} = 0$) because they are all proportional to sinβ, as seen in Equation (18). The molecular field theory prediction of the variation of $\overline{C}_{22} (\equiv \overline{C}_{2-2})$ with $\overline{C}_{20}$ for a molecule with $D_{2h}$ or $C_{2v}$ symmetry is shown in Figure 5. The figure shows that the biaxial order parameter $\overline{C}_{22}$ vanishes when the major order parameter $\overline{C}_{20}$ is zero or unity. In between these limiting values, the $\overline{C}_{22}$ increases, passes through a maximum, and then decreases again. The molecular field theory predicts that these curves terminate at the N-I transition as indicated by the dotted lines in the figure [1].

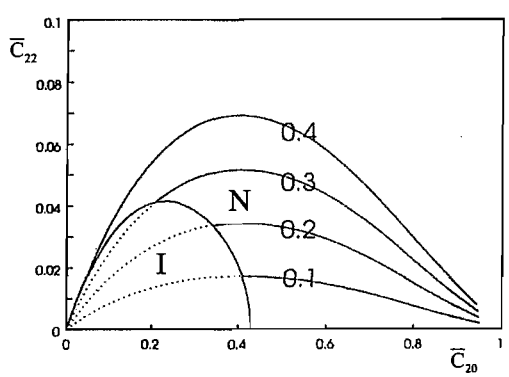


**Figure 5** The dependence of the biaxial order parameter $\overline{C}_{22}$ on the major order parameter $\overline{C}_{20}$ predicted for different values of the molecular biaxiality parameter, λ. The solid lines end at the N-I transition [1].

*Relationship of the Modified Spherical Harmonics to the Saupe Ordering Matrix*

Sometimes a Cartesian representation of the ordering tensor is preferred because it is relatively easier to understand the physical significance of the various components of this tensor as compared to the irreducible spherical tensor approach [1]. The second-rank quantities, $\overline{C}_{2n}$, are the spherical tensor analogues of the definition of the order parameters introduced by Saupe [7], $S_{ab}$, which simply differs in the language used to define the molecular orientations. The Saupe ordering matrix which represents the orientational ordering at the second-rank level is defined by

$$S_{ab} = \left( \frac{3\overline{\ell_a \ell_b} - \delta_{ab}}{2} \right), \tag{22}$$

where a,b denote general molecular axes, and $\ell_a$ is the direction cosine between the a axis and the director. Since there are three axes, the Saupe ordering matrix contains nine elements which are not independent from its definition (see Equation (22)); the matrix is symmetric and traceless, *i.e.*,

$$S_{ab} = S_{ba}, \tag{23}$$

and

$$\sum_a S_{aa} = 0. \tag{24}$$

This reduces the number of independent elements of the Saupe ordering matrix to five. Their relationship with the second-rank modified spherical harmonics is

$$S_{zz} = \overline{C}_{20},$$

$$S_{xx} - S_{yy} = \sqrt{\frac{3}{2}}\left(\overline{C}_{22} + \overline{C}_{2-2}\right),$$

$$S_{xy} = i\sqrt{\frac{3}{8}}\left(\overline{C}_{2-2} - \overline{C}_{22}\right), \tag{25}$$

$$S_{xz} = \sqrt{\frac{3}{8}}\left(\overline{C}_{2-1} - \overline{C}_{21}\right),$$

$$S_{yz} = i\sqrt{\frac{3}{8}}\left(\overline{C}_{21} + \overline{C}_{2-1}\right).$$

Since the ordering matrix is real and symmetric (see Equation (22)) , a principal axis system can be found in which the off-diagonal elements vanish, leaving only two independent elements; these are taken to be the major order parameter, $S_{zz}$ and the biaxial order parameter, $\left(S_{xx} - S_{yy}\right)$. The convention for labelling the axes is such that $\left(S_{xx} - S_{yy}\right) > 0$, and $|S_{zz}| > \left(S_{xx} - S_{yy}\right)$, *i.e.*, z is near the symmetry axis for **S**. In the high order limit, when the z-axis is parallel to the director **n**, $S_{zz}$ is unity and the biaxial order parameter, $\left(S_{xx} - S_{yy}\right)$, is zero.

In this Thesis, we are mainly concerned with measuring these two independent order parameters for solutes dissolved in liquid crystals. By employing the deuterium NMR technique, we can measure $S_{zz}$ and $\left(S_{xx} - S_{yy}\right)$ through the quadrupolar interactions of each deuterium atom in the molecule. In Chapter 4, we shall make use of the two order parameters when we discuss the orientational ordering of iptycenes.

## 2.5 Biaxial Molecules in a Biaxial Phase

We now discuss the general case of a biaxial, rigid molecule confined in a biaxial mesophase such as a biaxial nematic, biaxial smectic A or a crystal E. In a biaxial phase, at the macroscopic level, the three principal components of a second rank

tensor denoted by $\tilde{Q}_n, \tilde{Q}_m, \tilde{Q}_l$ would all be different. The three directors, **l**, **m**, and **n**, correspond to the symmetry axes of the phase and hence, the principal axes for tensorial properties, such as the dielectric susceptibility. Unlike the situation for the uniaxial nematic where the director is uniquely associated with the symmetry axis of any second-rank property, the labelling of the axes in a biaxial nematic is a matter of convention [1] as for the labelling of the principal axes for a biaxial molecule. For example, the Z axis could be identified as that about which $\tilde{\mathbf{Q}}$ approximates to cylindrical symmetry, *i.e.*, $\left|\tilde{Q}_{ZZ}\right| > \left(\tilde{Q}_{XX} - \tilde{Q}_{YY}\right)$, where X and Y are chosen such that the biaxiality in $\tilde{\mathbf{Q}}$ is positive. With this convention, **n** would be identified with Z, **m** with X, and **l** with Y. However, we should note that this assignment of the principal axes may vary with the choice of the tensorial property used to determine the principal axes.

The orientation of a molecule with respect to an axis system fixed in a biaxial phase now depends on all three Euler angles, $\alpha$, $\beta$, and $\gamma$, collectively denoted as $\Omega$, as we have seen in Section 2.2. The singlet orientational distribution function can be expanded in terms of the Wigner rotation matrix elements. This expansion is given in Equation (5) as

$$f(\Omega) = \sum_{Lmn} \left( \frac{2L+1}{8\pi^2} \right) \overline{D}^{L*}_{mn} D^{L}_{mn}(\Omega).$$

The complete set of orientational order parameters is given by the average quantities, $\overline{D}^{L*}_{mn}$. $\overline{D}^{L}_{00}$ describes the orientational order of the molecular z axis with respect to the director **n**; it is non-zero in both the uniaxial and biaxial nematic phases. Similarly, the order parameters, $\overline{D}^{L}_{0n}$, which measures the biaxiality in the ordering of the molecule with respect to the director **n**, are also non-zero in both uniaxial and biaxial nematic phases. This occurs because they are independent of the Euler angle, $\alpha$, which is the azimuthal angle for the molecular z axis in the director frame. On the other hand, the order parameters $\overline{D}^{L}_{m0}$ $(m \neq 0)$ which measure the biaxial ordering of the molecular z axis in the director frame, vanish in the uniaxial nematic phase but are

non-zero in the biaxial nematic. The order parameters, $\overline{D}^{L}_{mn}$, where both m and n are non-zero, vanish in the uniaxial nematic but not in the biaxial nematic. The characteristics of these order parameters for the uniaxial and biaxial phases are summarised in Table 1.

| Order Parameters | Uniaxial Phase | Biaxial Phase |
|---|---|---|
| $\overline{D}^{L}_{00}$ | $\neq 0$ | $\neq 0$ |
| $\overline{D}^{L}_{0n}$ $(n \neq 0)$ | $\neq 0$ | $\neq 0$ |
| $\overline{D}^{L}_{m0}$ $(m \neq 0)$ | 0 | $\neq 0$ |
| $\overline{D}^{L}_{mn}$ $(m \neq 0, n \neq 0)$ | 0 | $\neq 0$ |

**Table 1** A summary of the behaviour of the order parameters $\overline{D}^{L}_{mn}$ based on the Wigner rotation matrices in the uniaxial and biaxial nematics.

To understand further the order parameters, we take the example of a second-rank ordering tensor, $\overline{D}^{2}_{mn}$, because unlike the higher rank order parameter, they are available experimentally. In principle, $\overline{D}^{2}_{mn}$ has twenty-five independent components because both n and m take values from 2 to -2 in steps of unity. However, if the principal axes for both the molecule and the nematic phase are known, the number of the independent components can be reduced to four. The four principal second rank order parameters are $\overline{D}^{2}_{00}, \overline{D}^{2}_{02}, \overline{D}^{2}_{20}$, and $\overline{D}^{2}_{22}$, where $\overline{D}^{2}_{00}$, and $\overline{D}^{2}_{02}$ are non-zero in both the uniaxial and biaxial nematic phases (see Table 1); they are essentially equivalent to those for a biaxial molecule in a uniaxial phase as discussed in Section 2.4. In the high order limit when the molecular z axis is parallel to the director **n**, the major order parameter, $\overline{D}^{2}_{00}$, is unity while the molecular biaxial order parameter, $\overline{D}^{2}_{02}$, vanishes, as we have seen. The other two order parameters, $\overline{D}^{2}_{20}$, and $\overline{D}^{2}_{22}$, vanish in the uniaxial phase, but not in the biaxial phase. In the limit of complete order, $\overline{D}^{2}_{20}$ is zero, while $\overline{D}^{2}_{22}$ takes the value of unity. These results follow from the fact that the three Euler angles relating xyz and XYZ are zero in the high order limit and from the

definition of the Wigner rotation matrices [2]. Since the major order parameter is expected to be high in a biaxial nematic phase because the phase is expected to occur at a low reduced temperature, it would seem that a property with a strong dependence on $\overline{D}^2_{22}$ is needed in order to observe the phase biaxiality [1].

*Saupe Representation of Ordering for a Biaxial Nematic Phase*

The orientational order in a biaxial nematic can also be described with a second-rank Cartesian supermatrix, $S^{AB}_{ab}$, *i.e.*, a matrix of the matrices. The elements of the supermatrix are defined by

$$S^{AB}_{ab} = \frac{\left(3\overline{\ell_{aA}\ell_{bB}} - \delta_{ab}\delta_{AB}\right)}{2}, \tag{26}$$

in which the capital and the lower case letters represent the laboratory and the molecular axes, respectively [8]. This supermatrix contains eighty-one elements, but this number can be reduced in the phase and molecular principal axes, in which the only surviving elements are the nine diagonal elements, $S^{AA}_{aa}$. These nine diagonal elements are not independent because $\sum_a S^{AA}_{aa}$ and $\sum_A S^{AA}_{aa}$ are both zero, which, thus, leaves us with just four independent elements of the ordering supermatrix [9]. These four independent elements of $S^{AA}_{aa}$ used to describe the second rank orientational ordering of a biaxial molecule within a biaxial nematic phase are

$$S_{zz}^{ZZ} = \frac{3\overline{\ell_{zZ}^2} - 1}{2},$$

$$S_{xx}^{ZZ} - S_{yy}^{ZZ} = \frac{3\left(\overline{\ell_{xZ}^2} - \overline{\ell_{yZ}^2}\right)}{2},$$

$$S_{zz}^{XX} - S_{zz}^{YY} = \frac{3\left(\overline{\ell_{zX}^2} - \overline{\ell_{zY}^2}\right)}{2}, \tag{27}$$

and

$$\left(S_{xx}^{XX} - S_{xx}^{YY}\right) - \left(S_{yy}^{XX} - S_{yy}^{YY}\right) = \frac{3\left(\left(\overline{\ell_{xX}^2} - \overline{\ell_{xY}^2}\right) - \left(\overline{\ell_{yX}^2} - \overline{\ell_{yY}^2}\right)\right)}{2}.$$

$S_{zz}^{ZZ}$ and $\left(S_{xx}^{ZZ} - S_{yy}^{ZZ}\right)$ which are the major and biaxial order parameters, respectively, are the order parameters for the molecule measured with respect to the director **n**. In both the uniaxial and biaxial nematic phases, these values are non-zero. The remaining two order parameters vanish in the uniaxial nematic phase but are non-zero in the biaxial nematic. The order parameter, $\left(S_{zz}^{XX} - S_{zz}^{YY}\right)$, which measures the biaxiality in the ordering of the molecular z axis with respect to the laboratory X and Y axes, is zero in the uniaxial nematic phase, but not in the biaxial nematic phase. The same is true for the final order parameter, $\left(S_{xx}^{XX} - S_{xx}^{YY}\right) - \left(S_{yy}^{XX} - S_{yy}^{YY}\right)$, which measures the difference in the phase biaxial order parameter for the molecular x and y axes. In the limit of high order where the system is completely ordered with the molecular axes x, y and z parallel to the laboratory axes X, Y and Z, respectively, the order parameters are

$$S_{zz}^{ZZ} = 1,$$

$$S_{xx}^{ZZ} - S_{yy}^{ZZ} = 0,$$

$$S_{zz}^{XX} - S_{zz}^{YY} = 0, \tag{28}$$

$$\left(S_{xx}^{XX} - S_{xx}^{YY}\right) - \left(S_{yy}^{XX} - S_{yy}^{YY}\right) = 3.$$

Finally, we shall end this Chapter by giving the relationship between the principal components of the ordering matrix $S_{aa}^{AA}$ and the ordering tensor $\overline{D}_{mn}^{2}$. They are

$$
\begin{aligned}
&S_{zz}^{ZZ} = \overline{D}_{00}^{2}, \\
&S_{xx}^{ZZ} - S_{yy}^{ZZ} = \sqrt{6}\,\mathrm{Re}\,\overline{D}_{02}^{2}, \\
&S_{zz}^{XX} - S_{zz}^{YY} = \sqrt{6}\,\mathrm{Re}\,\overline{D}_{20}^{2}, \\
&\left(S_{xx}^{XX} - S_{xx}^{YY}\right) - \left(S_{yy}^{XX} - S_{yy}^{YY}\right) = 3\,\mathrm{Re}\left(\overline{D}_{22}^{2} + \overline{D}_{-22}^{2}\right).
\end{aligned}
\tag{29}
$$

## 2.6 References


[1] G. R. Luckhurst, in *Physical Properties of Liquid Crystals: Nematics*, (Eds. D. A. Dunmur, A. Fukuda, G. R. Luckhurst), INSPEC, London (2001), Chap. 2.1.

[2] C. Zannoni, *The Molecular Physics of Liquid Crystals*, (Eds. G.R. Luckhurst, G. W. Gray), Academic Press, London (1979), Chap. 3.

[3] C. Zannoni, *The Molecular Dynamics of Liquid Crystals*, (Eds. G.R. Luckhurst, C. A. Veracini), Kluwer Academic Publishers, Dordrecht (1994), Chap. 2.

[4] V. Tsvetkov, *Acta Physicoch. U.S.S.R*, **10**, 557 (1939).

[5] C. Zannoni, *Nuclear Magnetic Resonance of Liquid Crystals*, *NATO ASI Series*, (Ed. J. W. Emsley), D. Reidel Publishing Co., Dordrecht (1985), Chap. 1.

[6] D. Sandström, *PhD Thesis: Nuclear Magnetic Resonance Studies of Thermotropic Liquid Crystals*, Stockholm University (1996), Chap. 3.

[7] A. Saupe, *Angew. Chem. Int. Ed.*, **7**, 97 (1968).

[8] P. G. de Gennes, *The Physics of Liquid Crystals*, Clarendon Press, Oxford (1974), p. 27.

[9] M. A. Bates, G. R. Luckhurst, *Phys. Rev. E*, **72**, 051702 (2005).

# Chapter 3

# NMR Spectroscopy: The Informative Tool

## 3.1 Introduction

While Chapter 1 provides an overview of the liquid crystal systems which we are studying and Chapter 2 discusses their long-range orientational order, the key characteristic of liquid crystals, this Chapter will address the technique we use in order to obtain important information such as the orientational order, director dynamics and phase symmetry of the systems we are investigating. Our most valuable investigative tool is nuclear magnetic resonance spectroscopy (NMR), whose impact on the field of liquid crystals has been significant [1]. The rapid growth in its applications to study both liquid crystals and solutes dissolved in them has made NMR an unrivaled technique as a mean of probing the behaviour of the molecules in mesophases as well as the macroscopic properties. This Thesis will explore various aspects of liquid crystal behaviour, particularly concerning orientational order, phase symmetry, and field-induced dynamics of the director using deuterium NMR spectroscopy. The objective of this Chapter is, therefore, to provide an overview of the importance of NMR in the investigation of liquid crystals, and so allow us to appreciate why this technique is one of the most valuable tools for such research.

## 3.2 NMR Spectroscopy of Liquid Crystals

In general, NMR spectroscopy is a very useful tool to extract information on the static and dynamic properties of the systems being studied, and so, we have been able to explore both of these properties of liquid crystals. For example, for the static property, we will discuss the orientational order of iptycenes in Chapter 4, and for the dynamic property we will describe the field-induced reorientational process of the director in the SmA phase of 8CB-$d_2$ in Chapter 6. Although there are other techniques such as Raman [2] and fluorescence [3] spectroscopies which can also be employed in the

investigation of liquid crystals, they, however, only measure a single averaged component of a tensor, $\tilde{A}_{ZZ}$. This, however, is not sufficient to characterise the orientational order of the mesogenic molecules as these molecules are neither rigid nor are they highly symmetrical. In contrast, NMR has been proven to be particularly useful as it allows the investigations of not only the ordering along different molecular axes such as the major order parameter $S_{ZZ}$ and the biaxial order parameter $(S_{XX} - S_{YY})$ of the major and minor molecular axes, but for the case of non-rigid molecules also the order of different rigid subunits, like the order of the methylene groups along the alkyl chains of flexible molecules [4]. In addition to the microscopic properties, NMR spectroscopy can also be used to study the macroscopic properties such as the phase symmetry of the liquid crystals, and this topic will be discussed in detail in Chapter 7 which deals with the crystal E phase. Despite its many contribution in the liquid crystal research, NMR spectroscopy has the disadvantage of measuring only partially averaged second-rank tensor, and therefore only provides information on second-rank order parameters. For higher rank order parameters, it is necessary to employ other technique such as the fluorescence [3] and ESR spectroscopies [5].

### *3.2.1 Interactions in NMR Spectroscopy*

The nuclear magnetic resonance spectra of molecule in a partially oriented liquid crystal phase are dominated by the second-rank tensorial properties such as the dipolar couplings, $\tilde{\mathbf{D}}_{ij}$ and quadrupolar interactions, $\tilde{\mathbf{q}}_{ij}$. These properties are partially averaged by the anisotropic molecular tumbling to an extent which depends on the orientational order. Thus information about the orientational order in a liquid crystal phase can be obtained by measurement of such second-rank properties from the splittings occurring in the NMR spectra.

We shall take the applied magnetic field, **B**, to define the Z direction of an XYZ laboratory axis system; the component of a second-rank tensor $\tilde{\mathbf{A}}$ measured by NMR is $\tilde{A}_{ZZ}$, which can be expressed in terms of the components of **A** in an arbitrary molecular fixed axis system, x′y′z′:

$$\tilde{A}_{ZZ} = \sum_{\alpha\beta}^{x'y'z'} A\alpha\beta\langle \ell_{\alpha Z}\ell_{\beta Z}\rangle, \tag{1}$$

where $\ell_{\alpha Z}$ is the direction cosine between α and Z, and $\ell_{\beta Z}$ is that between β and Z. According to the definition of the Saupe ordering matrix given in the previous Chapter,

$$S_{\alpha\beta} = \frac{1}{2}\langle 3\ell_{\alpha Z}\ell_{\beta Z} - \delta_{\alpha\beta}\rangle, \tag{2}$$

we can express $\tilde{A}_{ZZ}$ as

$$\tilde{A}_{ZZ} = A_0 + \frac{2}{3}\sum_{\alpha\beta}^{x'y'z'} A_{\alpha\beta}S_{\alpha\beta}, \tag{3}$$

where

$$A_0 = \frac{1}{3}(A_{xx} + A_{yy} + A_{zz}) \tag{4}$$

is the isotropic average of **A** with $A_{xx}$, $A_{yy}$, and $A_{zz}$ being the three diagonal components of **A**. For purely anisotropic interaction tensors such as the dipolar and quadrupolar interactions, $A_0$ is zero. Equation (3) is generally only valid for rigid molecules. For flexible molecules [4], in addition to the ensemble average of the rotational motion of the molecule as a whole, a further average of the internal molecular motion is needed.

In order to understand the form of the NMR spectra, it is important to highlight the various interactions involved between a magnetic nucleus and the static magnetic field. Nuclei with a spin quantum number, I, larger than zero possess magnetic moments, and various interactions arise when an external magnetic field is applied.

The static spin Hamiltonian, $\hat{H}$, can be expressed as a sum of Hamiltonians corresponding to the various spin interactions

$$\hat{H} = \hat{H}_Z + \hat{H}_S + \hat{H}_J + \hat{H}_D + \hat{H}_Q, \tag{5}$$

where $\hat{H}_Z$, $\hat{H}_S$, $\hat{H}_J$, $\hat{H}_D$, and $\hat{H}_Q$ are the Hamiltonians for the Zeeman interaction, the shielding effect, the indirect spin-spin coupling (J-coupling), the direct spin-spin coupling, and the quadrupolar interaction, respectively. The hats on the Hamiltonians show that they are operators, usually involving nuclear spin operators. The majority of the NMR experiments are conducted by employing a high magnetic field and consequently the Zeeman term which represents the interaction between the magnetic dipole moment, $\mu$, and the magnetic field, **B**, is dominant. Other interactions such as the shielding effect, the indirect spin-spin coupling, the direct spin-spin coupling, and the quadrupolar interaction arise from different electric and magnetic interactions and are treated as perturbations to the Zeeman interaction. This is certainly the case for deuterium with which we shall be primarily concerned. The chemical shielding is the result of the screening effect from the electrons surrounding the nucleus which generate a local field that counteracts the applied magnetic field. The indirect spin-spin coupling is the interaction between nuclei whose coupling mechanism is influenced by the bonding electrons on the magnetic fields running between the nuclear spins. However, in the orientational study of liquid crystals, the two most useful anisotropic interactions are the dipolar and quadrupolar interactions. Hence, in the next subsections we shall focus on the Zeeman interaction followed by the dipolar and quadrupolar interactions.

### *3.2.2 Zeeman Interaction*

The Zeeman interaction is the interaction between the magnetic dipole moment, $\mu$, of a nucleus and the external magnetic field with magnetic flux density, **B**. Taking the magnetic field to be along the Z direction of the laboratory frame, then, classically, the interaction energy between the magnetic moment and the magnetic field can be expressed as

$$E = -\mu_Z B_Z. \tag{6}$$

The magnetic moment of a nucleus is related to its spin angular momentum, $I_Z$, as

$$\mu_Z = -\gamma I_Z, \tag{7}$$

where $\gamma$ is the gyromagnetic ratio, a constant for a given nucleus.

The Hamiltonian for the system is obtained by replacing $I_Z$ with its operator equivalent $\hbar\hat{I}_Z$,

$$\hat{H} = -\gamma\hbar B\hat{I}_Z, \tag{8}$$

where $\hat{I}_Z$ is the Z component of the spin operator $\hat{\mathbf{I}}$. The spin energy is now obtained from the time independent Schrodinger equation

$$\hat{H}|I,m\rangle = E|I,m\rangle, \tag{9}$$

where $|I,m\rangle$ is the spin wavefunction. As the Z component of the spin operator $\hat{I}_Z$ commutes [6] with $I^2$, it is possible to specify the eigenvalues of both $\hat{I}_Z$ and $I^2$ simultaneously.

$$I^2|I,m\rangle = I(I+1)|I,m\rangle, \tag{10}$$

$$\hat{I}_Z|I,m\rangle = m|I,m\rangle, \quad m = I, I-1, I-2, \ldots -I. \tag{11}$$

There are $(2I+1)$ spin states for a nucleus with a nuclear spin number I. In the absence of the external magnetic field, **B**, these spin states are *degenerate*, meaning that they have the same energy. On the other hand, the application of an external

magnetic field breaks this degeneracy, causing each of the $(2I+1)$ spin states to have a slightly different energy. The energy separation between the m sublevels in a magnetic field is called the *Zeeman splitting*. This energy separation is obtained from the Zeeman spin Hamiltonian

$$\begin{aligned}\hat{H}|I,m\rangle &= -\gamma\hbar B\hat{I}_Z|I,m\rangle, \\ &= -(\gamma\hbar B)m|I,m\rangle.\end{aligned} \tag{12}$$

This gives the Zeeman energy, $E_m$, as

$$E_m = -(\gamma\hbar B)m, \tag{13}$$

which means that adjacent energy levels are separated in energy by $\gamma B/2\pi$. In NMR spectroscopy, the selection rule is $\Delta m = \pm 1$, and so

$$\Delta E = \gamma\hbar B = h\nu. \tag{14}$$

The allowed transitions between these energy levels will therefore give a single line at the frequency, $\nu$, given by $\gamma B/2\pi$, which is known as the *Larmor frequency*.

### *3.2.3 Dipolar Interaction*

The dipolar interaction or the direct dipolar spin-spin coupling represents the direct magnetic interactions of the nuclear spins with each other (see Figure 1). The Hamiltonian of the second rank dipolar spin coupling between a pair of nuclei with gyromagnetic ratios, $\gamma_i$ and $\gamma_j$, can be written as

$$\hat{H}_D = \hat{\mathbf{I}}_i \cdot \mathbf{D}_{ij} \cdot \hat{\mathbf{I}}_j, \tag{15}$$

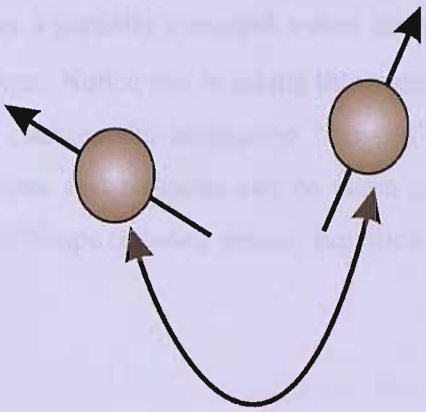

**Figure 1** Schematic representation of the direct dipolar spin-spin coupling.

where $\mathbf{D}_{ij}$ is a second-rank tensor for a fixed orientation of the nuclear pair defined by

$$D_{ij}^{\alpha\beta} = \left(\frac{\gamma_i \gamma_j h}{4\pi^2 r_{ij}^3}\right)\left(\delta_{\alpha\beta} - 3\ell_\alpha \ell_\beta\right) \tag{16}$$

Here, $r_{ij}$ is the internuclear distance and $\ell_\alpha$ is the direction cosine between the internuclear vector $r_{ij}$ and the $\alpha$ axis of the laboratory frame. According to this definition, $\mathbf{D}_{ij}$ is both symmetric and traceless. In a strong magnetic field, the dipolar interaction is small compared to the Zeeman interaction, and so the spins are quantised along the magnetic field direction, Z. This means that the off-diagonal terms in the spin Hamiltonian are negligible; this is known as the *high field approximation*. So far we have been considering a system in which the molecular orientation is fixed. However, in the liquid crystal phase the molecules move on a timescale which is fast in comparison with that of the NMR experiment. Under these conditions, it is necessary to average the dipolar tensor in Equation (16) over all orientations but weighted with the singlet orientational distribution function. Using the result given in Equation (16) for a uniaxial phase, this gives the Z component of $\mathbf{D}_{ij}$ as

$$\tilde{D}_{ij}^{ZZ} = \left(\frac{\gamma_i \gamma_j h}{4\pi^2}\right)\left\langle \frac{1 - 3\ell_Z^2}{r_{ij}^3} \right\rangle, \tag{17}$$

where the tilde ~ indicates a partially averaged value, and the angular brackets, $\langle\ \rangle$, implies an ensemble average. Notice that in taking this average, we have also allowed for the vibration which changes the separation between the nuclei. To a good approximation, the vibrations and rotations can be taken as independent. Then, by employing the definition of Saupe ordering matrix, Equation (17) can be rewritten as

$$\tilde{D}_{ij}^{zz} = -\left(\frac{\gamma_i \gamma_j h}{2\pi^2}\right)\frac{S_{ij}}{\left\langle r_{ij}^3 \right\rangle}, \tag{18}$$

in which

$$S_{ij} = \left\langle \frac{3\ell_z^2 - 1}{2} \right\rangle. \tag{19}$$

$S_{ij}$ is the Saupe order parameter for the ij vector and $\left\langle r_{ij}^3 \right\rangle$ is the vibrational averaged distance between nuclei i and j. Here we have taken the diamagnetic anisotropy to be positive so that the director is aligned parallel to the magnetic field, *i.e.*, to the Z axis. It is seen that from the measurement of the dipolar splittings, it is possible to obtain $S_{ij}$. Given that $r_{ij}$ is known from the molecular geometry, the measurement of $\tilde{D}_{ij}^{zz}$ will provide information on the second-rank orientational order parameters for the molecule.

### *3.2.4 Quadrupolar Interaction*

The most common NMR spectra are the proton NMR. However, as a result of the extensive dipolar interactions between protons, the proton NMR spectra of liquid crystals are extremely complicated and so can severely impede the interpretation of the results. For this reason, deuterium NMR spectroscopy is commonly employed due to its spectra simplicity which results from the dominance of the quadrupolar interactions.

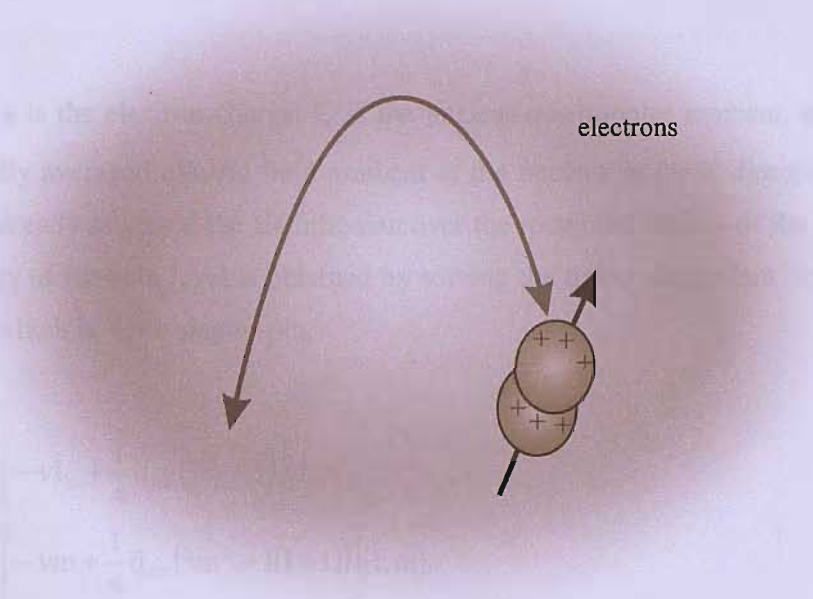


**Figure 2** Schematic representation of the quadrupolar coupling interaction; the electrons are depicted by a grey cloud.

For nuclei with spin, I, greater than $1/2$, aside from the dipolar interaction, they also experience an electrical quadrupolar interaction *via* the electric field gradient tensor at the nuclear site (see Figure 2). For deuterons attached to a carbon atom, the quadrupolar interaction is significantly larger than the dipolar interaction between a pair of deuterons. In fact in this Thesis, we shall only consider deuterium which has a spin quantum number of 1. In the high field approximation, the total spin Hamiltonian for the Zeeman and quadrupolar interaction in a uniaxial liquid crystal phase is given as [4]

$$\hat{H} = -\nu\hat{I}_Z + \frac{1}{4}\tilde{q}_{ZZ}\left(3\hat{I}_Z^2 - \hat{\mathbf{I}}\right), \tag{20}$$

where $\nu$ is the Larmor frequency, $\hat{I}_Z$ is the Z component of the spin operator $\hat{\mathbf{I}}$ and $\tilde{q}_{ZZ}$ is defined as

$$\tilde{q}_{ZZ} = \frac{e^2 Q \tilde{V}_{ZZ}}{h}, \tag{21}$$

in which e is the electron charge, Q is the nuclear quadrupolar moment, and $\tilde{V}_{ZZ}$ is the partially averaged electric field gradient at the nucleus in the Z direction. Here, we have already averaged the Hamiltonian over the rotational motion of the molecule. The energy of the spin level is obtained by solving the time-independent Schrodinger equation which is, for a single spin,

$$\begin{aligned} \hat{H}|I,m\rangle &= \left[-\nu\hat{I}_Z + \frac{1}{4}\tilde{q}_{ZZ}\left(3\hat{I}_Z^2 - \hat{I}\right)\right]|I,m\rangle \\ &= \left[-\nu m + \frac{1}{4}\tilde{q}_{ZZ}\left(3m^2 - I(I+1)\right)\right]|I,m\rangle. \end{aligned} \tag{22}$$

This gives the energy, $E_m$, as

$$E_m = -\nu m + \frac{1}{4}\tilde{q}_{ZZ}\left(3m^2 - I(I+1)\right). \tag{23}$$

For deuterium, I = 1, and so Equation (23) can be reduced to

$$E_m = -\nu m + \frac{1}{4}\tilde{q}_{ZZ}\left(3m^2 - 2\right). \tag{24}$$

Substituting the three possible values of m, *i.e.*, 1, 0, and -1, into Equation (24), the corresponding energies of the three levels are given as

$$E = -\nu + \frac{1}{4}\tilde{q}_{ZZ} \tag{25}$$

$$E = -\frac{1}{2}\tilde{q}_{ZZ} \tag{26}$$

$$E = \nu + \frac{1}{4}\tilde{q}_{ZZ} \tag{27}$$

Equations (25) – (27) show that the quadrupolar interaction affects the Zeeman levels such that the energy levels are no longer equally spaced as depicted in Figure 3.

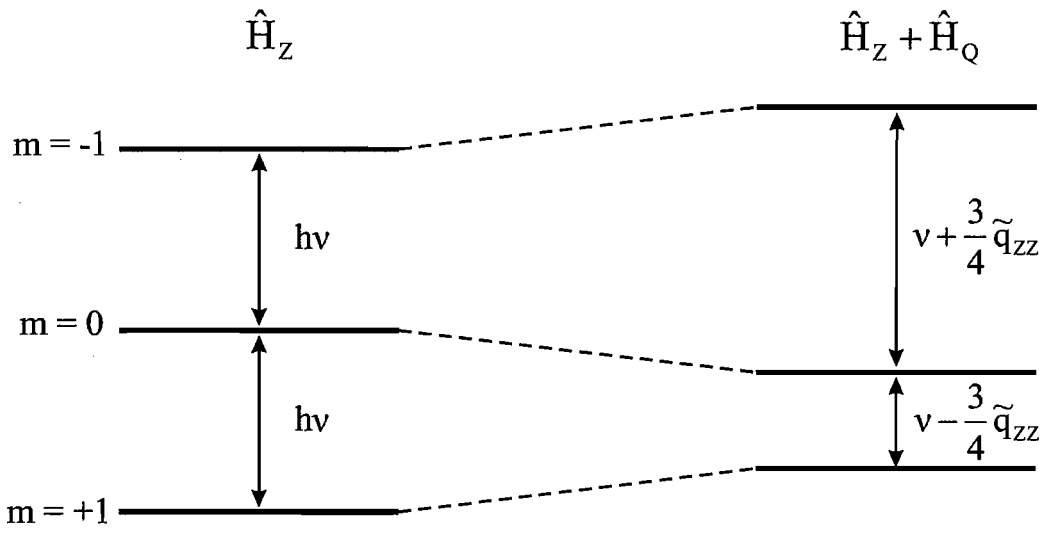


**Figure 3** The effect of the quadrupolar interaction on the Zeeman energy levels for spin-1 nucleus like deuterium.

According to the selection rule $\Delta m = \pm 1$, the deuterium NMR spectrum of a single deuteron in a uniaxial liquid crystal phase contains a doublet centred at $\nu$ and separated by

$$\Delta\nu = \frac{3}{2}\tilde{q}_{zz}. \tag{28}$$

The partially averaged component of the quadrupolar interaction tensor along the director which, for $\Delta\chi > 0$, is parallel to the magnetic field direction can be written as

$$\tilde{q}_{zz} = \frac{2}{3}\sum_{\alpha\beta}^{x'y'z'} q_{\alpha\beta} S_{\alpha\beta}, \tag{29}$$

where x′y′z′ is an arbitrary molecular frame. In the principal axis system, xyz, of **S**, Equation (29) reduces to

$$\tilde{q}_{ZZ} = \frac{2}{3}\left(q_{xx}S_{xx} + q_{yy}S_{yy} + q_{zz}S_{zz}\right) \tag{30}$$

The diagonal quadrupolar components $q_{xx}$, $q_{yy}$, $q_{zz}$ can be expressed in terms of the principal components $q_{aa}$, $q_{bb}$, $q_{cc}$ by

$$q_{xx} = q_{aa}\ell^2_{xa} + q_{bb}\ell^2_{xb} + q_{cc}\ell^2_{xc}, \tag{31}$$

$$q_{yy} = q_{aa}\ell^2_{ya} + q_{bb}\ell^2_{yb} + q_{cc}\ell^2_{yc}, \tag{32}$$

and

$$q_{zz} = q_{aa}\ell^2_{za} + q_{bb}\ell^2_{zb} + q_{cc}\ell^2_{zc}, \tag{33}$$

where abc are the principal axes of the quadrupolar tensor, and $\ell_{xa}$ is the direction cosine of axis x with a.

Since the quadrupole tensor is traceless, it is convenient to write the two independent components of **q** as $q_{bb}$ and the asymmetry parameter, $\eta$, defined by

$$\eta = \frac{q_{aa} - q_{cc}}{q_{bb}}, \tag{34}$$

which necessarily vanishes when the quadrupolar tensor has true rotational symmetry. Substituting these relations into Equation (30), the component of the quadrupolar tensor along the laboratory Z axis is given by

$$\tilde{q}_{ZZ} = \frac{3q_{bb}}{2}\left[\begin{array}{l} S_{zz}\left(\ell^2_{zb} + \frac{\eta}{3}\left(\ell^2_{za} - \ell^2_{zc}\right)\right) + S_{xx}\left(\ell^2_{xb} + \frac{\eta}{3}\left(\ell^2_{xa} - \ell^2_{xc}\right)\right) \\ + S_{yy}\left(\ell^2_{yb} + \frac{\eta}{3}\left(\ell^2_{ya} - \ell^2_{yc}\right)\right) \end{array}\right]. \tag{35}$$

Given the molecular geometry and measurements of $\tilde{q}_{ZZ}$ for different deuterons in the same molecule, we can obtain the complete description of the second-rank

orientational ordering matrix of the molecule. Finally, we note that for deuterons attached to carbon atoms, both aliphatic and aromatic, the quadrupolar tensor approximates to cylindrical symmetry about the C – D bond which becomes the b axis. Indeed, it is usually a good approximation to ignore the biaxiality, $\eta$, which simplifies the result for $\tilde{q}_{zz}$ considerably.

## 3.3 Experimental Set-Up

In this Thesis, we have employed Fourier Transform (FT) NMR spectroscopy. In an FT NMR, all frequencies in a spectrum are irradiated simultaneously with a radiofrequency pulse. A time domain emission signal, which is the free induction decay (FID) is then recorded by the spectrometer. This signal is then Fourier transformed to produce the more conventional frequency domain spectrum.

The spectrometer used was a *Varian Infinity Plus 300* with a magnetic field of 7.05T. NMR spectrometer names usually refer to the proton frequency, and so "300" indicates that for this field, the proton frequency is 300MHz.

*Quadrupolar Echo Pulse Sequence*

In our experiments, we have employed the quadrupolar echo pulse sequence which is shown schematically in Figure 4.

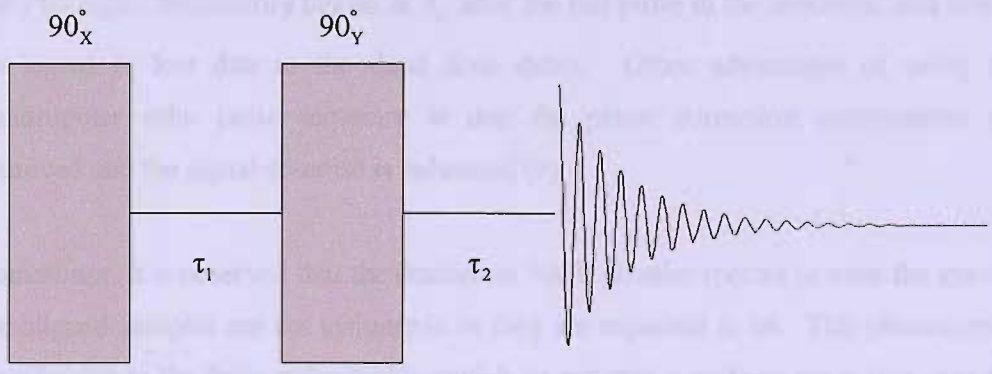


**Figure 4** Schematic representation of the quadrupolar echo pulse sequence used in our experiments.

The angle 90° is called the *flip angle* of the radiofrequency pulse, and is a specialized notation for the time duration of the pulse [7]. The time interval between the first and the second pulse is denoted by $\tau_1$ and the time interval between the second pulse and before the signal acquisition starts is denoted by $\tau_2$. The quadrupolar echo pulse sequence is commonly used in deuterium NMR to avoid lineshape distortion which may be caused if using a single pulse sequence. A single pulse sequence is essentially the most basic FT NMR pulse sequence which consists of a single pulse followed by the acquisition of the FID. The distortion caused by the single pulse is the result from the *probe ringing* which results from the radiofrequency pulse in the NMR coil in the magnetic field; the ringing prevents the measurement of the signal until a short time (or dead time) after a pulse [8]. This is especially damaging when the FID decays rapidly, *i.e.*, for broad NMR spectrum.

The quadrupolar echo is, thus, used to suppress the ringing. In this pulse sequence, the magnetisation components dephase under the effects of quadrupolar coupling or homonuclear dipolar coupling during the first period, $\tau_1$. Subsequently, a 90° pulse rotates the magnetisation components 90° about the pulse axis so that the components refocus after a further period, $\tau_2$. In the quadrupolar echo sequence, $\tau_1$ is approximately equal to $\tau_2$, although in practice, $\tau_2$ is adjusted so that the data acquisition begins exactly at the echo maximum; this is achieved in practice by doing an array experiment with different values of $\tau_2$, and then choose the value which gives the FID that starts at the echo maximum. Using this sequence, acquisition of the FID signal necessarily begins at $\tau_2$ after the last pulse in the sequence, and hence, no signal is lost due to the dead time delay. Other advantages of using the quadrupolar echo pulse sequence is that the phase correction uncertainties are removed and the signal-to-noise is enhanced [9].

Sometimes, it is observed that the deuterium NMR powder spectra or even the spectra for aligned samples are not symmetric as they are expected to be. This phenomenon may be due to the finite pulse widths which do not give a uniform excitation over the whole powder pattern. The other cause may arise from the spectrometer probe electronics which may not be symmetric, and so the match setting on the probe needs

to be adjusted to ensure that the impedence of the probe and the transmitter are matched for maximum power transfer to occur.

## 3.4 References


[1] J. W. Emsley (Ed.), *Nuclear Magnetic Resonance of Liquid Crystals, NATO ASI Series*, D. Reidel Publishing Co., Dordrecht (1985).

[2] P. S. Pershan, *The Molecular Physics of Liquid Crystals*, (Eds. G. R. Luckhurst, G. W. Gray), Academic Press Inc., London (1979), Chap. 17.

[3] Y. K. Levine, G. Van Ginkel, *The Molecular Dynamics of Liquid Crystals*, (Eds. G. R. Luckhurst, C. A. Veracini), Kluwer Academic Publisher, Dordrecht (1994), Chap. 22.

[4] S. Fan, *PhD. Thesis: An Experimental and Theoretical Study of Liquid Crystal Phenomena*, University of Southampton (1992).

[5] P. L. Nordio, U. Segre, *The Molecular Physics of Liquid Crystals*, (Eds. G. R. Luckhurst, G. W. Gray), Academic Press Inc., London (1979), Chap. 16.

[6] M. H. Levitt, *Spin Dynamics: Basics of Nuclear Magnetic Resonance*, John Wiley & Sons Ltd., West Sussex (2001), Chap. 6.

[7] M. H. Levitt, *ibid.*, Chap. 5.

[8] M. J. Duer, *Solid State NMR Spectroscopy: Principles and Applications*, (Ed. M. J. Duer), Blackwell Science, Oxford (2002), Chap. 2 and 6.

[9] J. H. Davis, K. R. Jeffrey, M. Bloom, M. I. Valic, T. P. Higgs, *Chem. Phys. Lett.*, **42**, 390 (1976).

# Chapter 4

## The Orientational Order of Triptycenes

### 4.1 Introduction

A *triptych* (from the Greek *tri-*"three" + *-ptychos* "fold") is a set of three panels hinged together to form a complete artwork. Triptychs were especially popular embellishments during the period of the Renaissance, an era which marked the vibrant activities and passion of the great revival of art, literature and knowledge in Europe. A contemporary example of a triptych is shown in Figure 1; this collage artwork is entitled *Gypsy Music* [1].

**Figure 1** *Gypsy Music* [1], an example of a contemporary triptych artwork.

Inspired by the profile of the triptych artwork, the name *triptycene* (see Figure 2) was proposed for this phenomenal new class of molecules when it was first synthesized [2 ]. The shape and the structure of triptycenes contribute to their unique physical properties in which the nature of the ring fusion maintains the overall molecular shape, making them very rigid and shape persistent, which is important when they are being used as solutes in some liquid crystal solvents [3]. Building on this, the

motivation of this Chapter is to introduce triptycene and its derivatives called *iptycenes*, as a new class of probe molecules in liquid crystal studies and to discuss their orientational ordering as solutes in some selected liquid crystal hosts. These beautiful molecules which are rigid and highly symmetrical are certainly good choices to serve as probe molecules, giving us fantastic sets of NMR results, as we shall see later. Our extensive exploration of how the orientational order of these unique solutes varies with different liquid crystal hosts should allow us to enhance our understanding of the nature of the anisotropic interactions responsible for both the existence of liquid crystals and their behaviour.

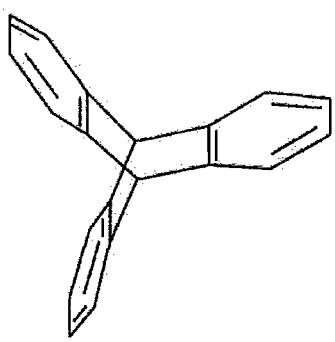

**Figure 2** The molecular structure of triptycene.

## 4.2 Solute Ordering

Since most molecules known to give liquid crystalline phases are non-rigid and have a low symmetry, the use of probe molecules has been very common in NMR studies of liquid crystals. In addition, due to the limited number of deuteriated liquid crystals available commercially, using a deuteriated probe molecule offers an appropriate solution to this problem. One of the marked advantages of using a dopant is that it can be chosen to be rigid and highly symmetric in order to identify the principal axes so that the principal elements of the Saupe ordering matrix can be determined readily *via* deuterium NMR spectroscopy. The same solute can also be used as a probe to investigate the anisotropic intermolecular interactions in different liquid crystal solvents. Alternatively, systematic variations in the structure of the solute may be employed to understand the possible contributions to the solute-solvent interactions for a given liquid crystal [4].

The Saupe ordering matrix is defined by

$$S_{ab} = \frac{\left(3\overline{\ell_a \ell_b} - \delta_{ab}\right)}{2}, \qquad (1)$$

where $\ell_a$ is the direction cosine between the director of a uniaxial liquid crystal and an axis, a, set in the molecule; the bar denotes an ensemble average over molecular orientations. There are five independent elements of **S** because the ordering matrix is symmetric and traceless (see Chapter 2), but for molecules with $C_{2v}$ or $D_{2h}$ symmetry or higher, a principal axis system can be found in which the off-diagonal elements vanish, leaving only two independent elements defined as the major order parameter, $S_{zz}$ and the biaxial order parameter, $\left(S_{xx} - S_{yy}\right)$. The principal axes, xyz, are selected, by convention such that $\left(S_{xx} - S_{yy}\right)$ is positive and $\left|S_{zz}\right| > \left(S_{xx} - S_{yy}\right)$. Deuterium NMR spectroscopy is a powerful technique which is capable of yielding these two independent pieces of information. For each non-equivalent deuteron, the deuterium NMR of a deuteriated solute gives a quadrupolar splitting, $\Delta\tilde{\nu}$, which results directly from the orientational order of the solute. The quadrupolar splitting is related to the principal elements of **S** by

$$\Delta\tilde{\nu} = \frac{3}{2} q_{zz} S_{zz} + \frac{1}{2}\left(S_{xx} - S_{yy}\right)\left(q_{xx} - q_{yy}\right), \qquad (2)$$

where $q_{\alpha\alpha}$ are the diagonal elements of the quadrupolar tensor in the principal axis system of the ordering matrix, and we assume that contributions to the electric field gradients at each deuteron which arise from the surrounding molecules are negligibly small [4]. We need to highlight here that Equation (2) applies to a liquid crystal with a positive magnetic anisotropy, $\Delta\tilde{\chi}$, and hence, its director is aligned parallel to the magnetic field. The equation can also be applied to liquid crystals with negative $\Delta\tilde{\chi}$ where the director is aligned orthogonal to the magnetic field by multiplying the observed splittings by $-2$. Provided the solute contains at least two deuterons with significantly different principal axes for their quadrupolar tensors, then it is possible to determine both $S_{zz}$ and $\left(S_{xx} - S_{yy}\right)$ from their quadrupolar splittings. Details of the

molecular geometry, the orientation of the C – D bond and the calculation of the order parameters can be found in the Appendix in Section 4.8 and in Chapter 7 in Section 7.7.

## 4.3 Anthracene-$d_{10}$ as a Benchmark

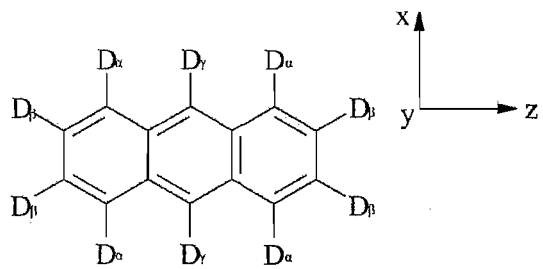


**Figure 3** The molecular structure of anthracene-$d_{10}$ with its atomic labelling and its symmetry axes.

We shall briefly discuss the use of anthracene (see Figure 3) which serves as a benchmark for our studies of orientational order mainly due to its extensive usage as a probe molecule in liquid crystal hosts [4, 5, 6]. Anthracene is a rigid molecule with $D_{2h}$ symmetry; hence, the principal axes are known and so the elements of the Saupe ordering matrix can be easily determined from deuterium NMR. The choice of anthracene has other advantages, for example, its structure has been characterised by X-ray diffraction and the quadrupolar tensors for the deuterons in anthracene-$d_{10}$ have been determined from a single crystal study [7]. Such information is important in order to extract the principal elements of the Saupe ordering matrix from the observed quadrupolar splittings of the deuterium NMR spectra. In addition, a variety of liquid crystals was chosen to represent a range of chemical types and properties, with wide mesomorphic ranges which are found to result in a large variation in the orientational order of the solute.

Figure 4 shows the molecular structures of the liquid crystal hosts used in our studies. The dielectric anisotropies, $\Delta\tilde{\varepsilon}$, for these liquid crystals vary from being positive for 5CB and PCH5, zero for I22 and I35, and negative for CCN47 and EBBA. The sign of the dielectric anisotropy depends on the orientation of the dipole moment, $\mu$, with respect to the molecular long axis and is given as

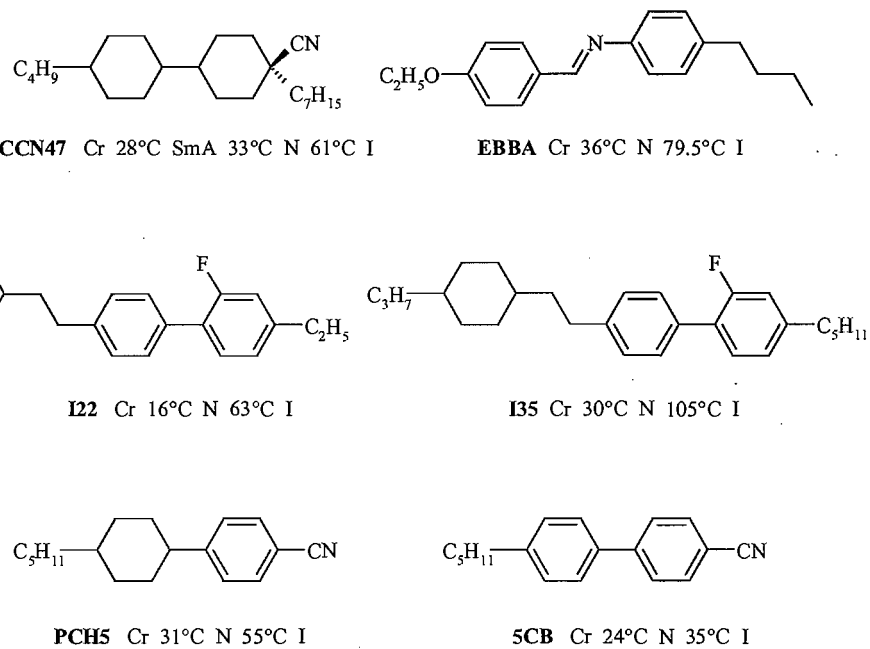


**Figure 4** The molecular structures of the liquid crystal solvents used and their phase transitions. The dielectric anisotropies, $\Delta\tilde{\varepsilon}$, are 16 (5CB), 18 (PCH5), 0 (I22 and I35), -3.0 (EBBA), and -6.4 (CCN47), at room temperature.

$$\Delta\varepsilon = \frac{nhF}{\varepsilon_0}\left(\alpha_l - \alpha_t + F\left(\frac{\mu^2}{k_B T}\right)P_2(\cos\theta)\right)S, \qquad (3)$$

where $k_B$ is the Boltzmann factor and T is the absolute temperature. $P_2(\cos\theta)$ is the second Legendre polynomial and S is the orientational order parameter. The number density, *i.e.*, the number of molecules divided by the volume is denoted by n, while h and F are related to the differences between the applied field and the field experienced by the molecules. $\varepsilon_0$ is the permittivity of a vacuum, $\alpha_l$ is the molecular polarizability along the long axis of the molecule and $\alpha_\perp$ is that at right angles to this axis. Depending on $\Delta\alpha$, which is $(\alpha_l - \alpha_t)$, the value of $\Delta\tilde{\varepsilon}$ is either positive or negative. For the study of anthracene-$d_{10}$, we have used 5CB, PCH5, and I35 as the hosts. Approximately 1wt% of anthracene-$d_{10}$ was dissolved in these liquid crystal solvents. The details of the preparation of the sample in this research and the experimental methodology are described in Section 4.6.1.

From Figure 3, we assume that the six αγ-deuterons of anthracene-$d_{10}$ have their $C-D$ bonds parallel to the x-axis and the remaining four deuterons have their bonds in the xz plane. The deuterium NMR spectra for anthracene-$d_{10}$ in 5CB, PCH5 and I35 are shown in Figure 5. The outer pair of lines is assigned to the β-deuterons on the grounds of their smaller relative intensity. The central group of lines originate from the αγ-deuterons. The fine splitting observed in the inner peaks for the spectrum of anthracene-$d_{10}$ in 5CB is caused by the dipolar couplings between the deuterons and also because the α-deuterons have a slightly different quadrupolar splitting from that of the γ-deuterons. The weak peaks observed in anthracene-$d_{10}$ in PCH5 and I35 are from the impurities. The calculations for the major order parameter and the biaxial order parameter from the splittings can be found in the Appendix in Section 4.8.

Figure 6 shows the shifted temperature dependence of the quadrupolar splittings for anthracene-$d_{10}$ in 5CB, PCH5 and I35. The open squares are for the β-deuterons and the closed squares are for the αγ-deuterons. The quadrupolar splitting for the β-deuterons is larger than that for the αγ-deuterons. As expected the splitting increase with increasing shifted temperature. The splitting for the β-deuterons is the largest for 5CB while that for PCH5 and I35 are almost similar. However, for the αγ-deuterons, while the splitting is still the largest for 5CB, it is not the same for PCH5 and I35; the splitting is slightly larger for I35.

Figure 7 shows the shifted temperature dependence of the major order parameter, $S_{zz}$, for anthracene-$d_{10}$ dissolved in the three liquid crystal solvents. Unfortunately, due to the unavailability of nitrogen gas at the time of the experiment, we did not heat the sample into the isotropic phase because of its high clearing point (105°C), and so, we do not have the complete results for I35. However, it is clear from Figure 7 that the z-axis of anthracene-$d_{10}$ is the most ordered in 5CB, and in PCH5 and I35, its major order parameter is comparable.

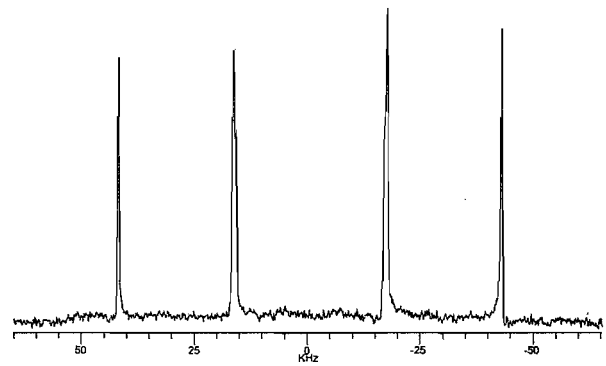


anthracene-$d_{10}$ in 5CB

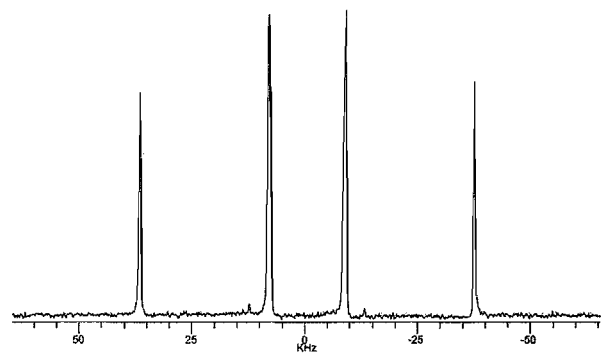


anthracene-$d_{10}$ in PCH5

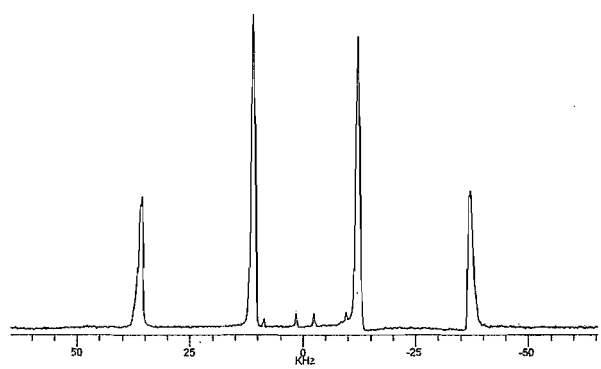


anthracene-$d_{10}$ in I35

**Figure 5** The deuterium NMR spectra of anthracene-$d_{10}$ dissolved in 5CB, PCH5, and I35 at a shifted temperature, $(T_{NI} - T)$, of 10°C. The outer splitting is attributed to the β-deuterons and the inner splittings are originated from the αγ-deuterons.

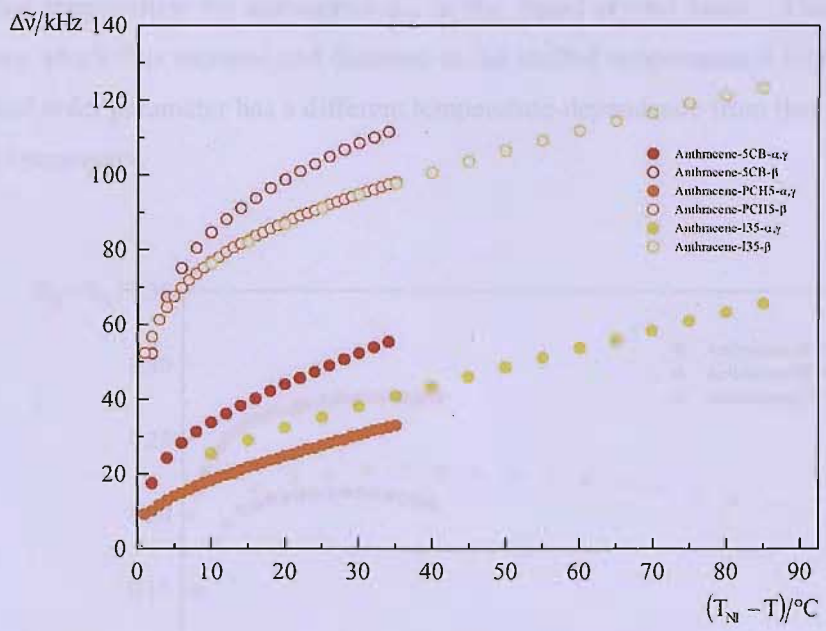


**Figure 6** The quadrupolar splittings, $\Delta\tilde{\nu}$, plotted against the shifted temperature for anthracene-$d_{10}$ dissolved in 5CB, PCH5, and I35.

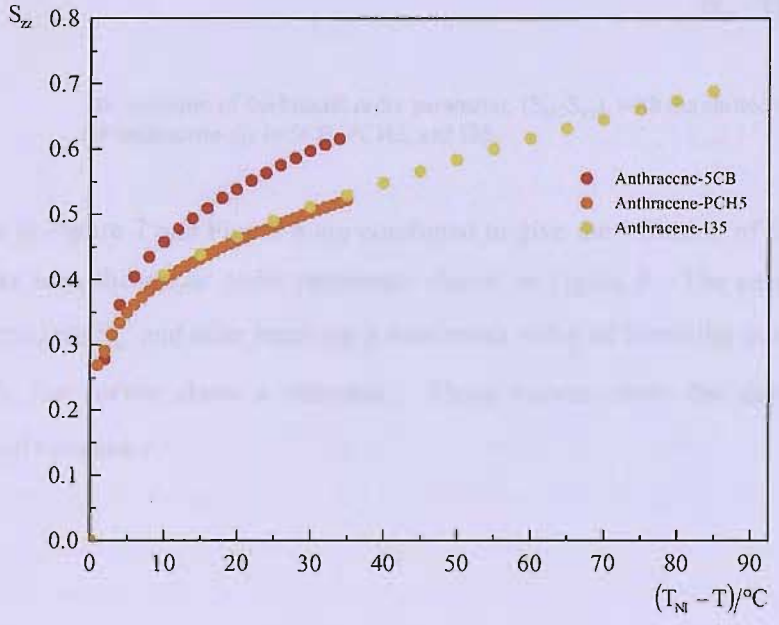


**Figure 7** The variation of the major order parameter, $S_{zz}$, with the shifted temperature for anthracene-$d_{10}$ in 5CB, PCH5, and I35.

Figure 8 shows the variation of the biaxial order parameter, $(S_{xx} - S_{yy})$, with the shifted temperature for anthracene-$d_{10}$ in the liquid crystal hosts. The plot shows curves which first increase and decrease as the shifted temperature is increased. This biaxial order parameter has a different temperature-dependence from that of the major order parameter.

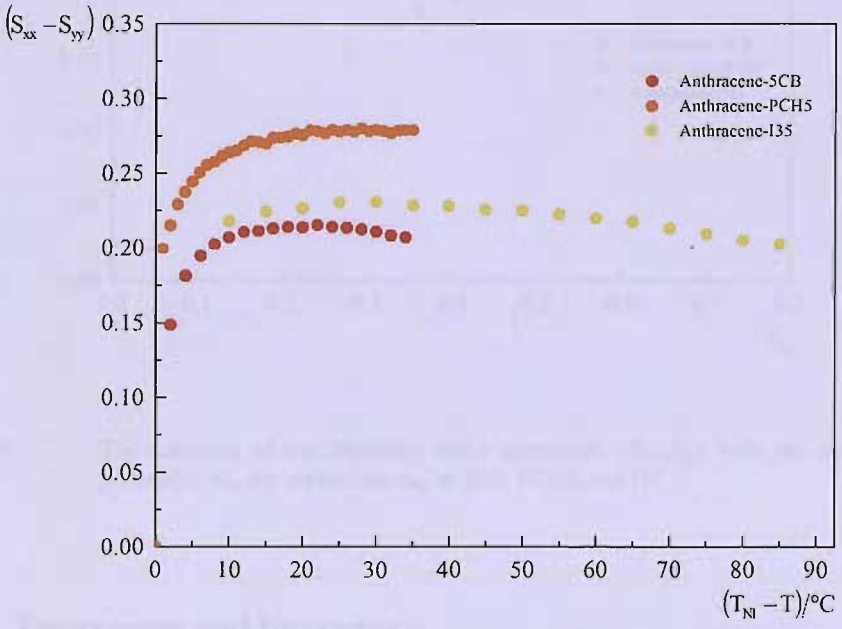


**Figure 8** The variation of the biaxial order parameter, ($S_{xx}$-$S_{yy}$), with the shifted temperature for anthracene-$d_{10}$ in 5CB, PCH5, and I35.

The data in Figure 7 and Figure 8 are combined to give the variation of the biaxiality parameter with the major order parameter shown in Figure 9. The curves increase with increasing $S_{zz}$ and after reaching a maximum value of biaxiality parameter near $S_{zz} = 0.5$, the curves show a decrease. These curves show the deviation from cylindrical symmetry.

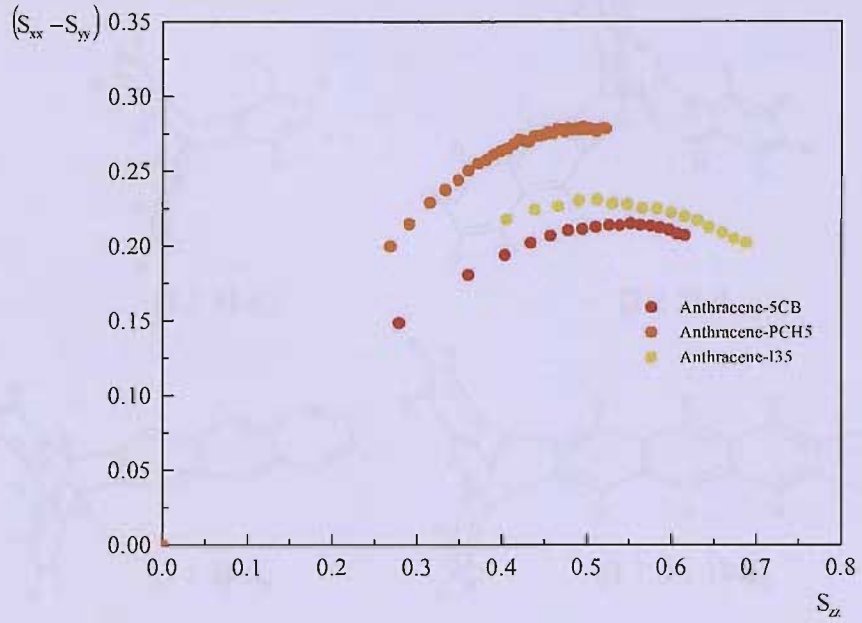


**Figure 9** The variation of the biaxiality order parameter, $(S_{xx}-S_{yy})$ with the major order parameter, $S_{zz}$, for anthracene-$d_{10}$ in 5CB, PCH5, and I35.

## 4.4 Triptycenes and Iptycenes

Figure 10 shows triptycene [111] and its derivatives, [113], [222] and [11311]. These iptycenes are so labelled to indicate the number of aromatic rings, and so hypothetically, anthracene can be labelled as [00300]! ☺ The symmetry for [111], [113], [222] and [11311] are $D_{3h}$, $C_{2v}$, $D_{3h}$, and $D_{2h}$ respectively, and so the principal elements of the Saupe ordering matrix can be determined from deuterium NMR experiment for the temperature range of the liquid crystal solution. Except for [113], the protonated iptycenes were kindly given to us by the Massachusetts Institute of Technology (MIT) research group led by Professor Tim Swager. These iptycenes were all deuteriated *via* catalytic exchange at Merck in Chilworth, Southampton, except for deuteriated [113] which was synthesized from perdeuteriated anthracene at Merck.

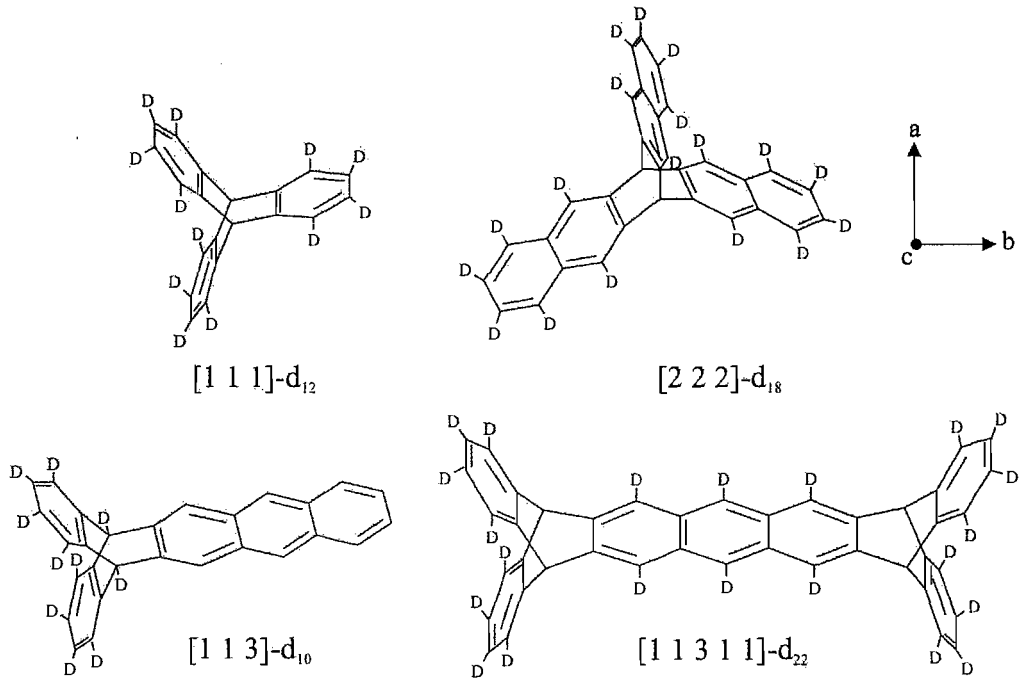


**Figure 10** The molecular structures of the deuteriated iptycenes studied. The numbers in the bracket denote the number of aromatic rings.

Before we proceed to the deuterium NMR results of the iptycenes, we shall begin with a discussion of the orientational order studies of these iptycenes carried out by our collaborators in MIT and Merck using UV-vis spectroscopy. This technique has the advantage of providing us with the sign of the order parameter for certain ordering matrix elements to determine the complete matrix when it comes using deuterium NMR spectroscopy. This makes the UV-vis spectroscopy an important complementary tool in determining the orientational order parameters of the iptycenes in the liquid crystal hosts.

## 4.5 Orientational Order Studies of Iptycenes *via* UV-vis Spectroscopy

### *4.5.1 About UV-vis Spectroscopy*

This technique determines the degree of order of the molecular axis with the transition dipole relative to the director. The UV polariser is rotated so that its transmission

direction is either perpendicular or parallel to the liquid crystal director. The measured absorptions are labelled as $A_{\parallel}$ when the measurement is made with the transmission direction parallel to the director and $A_{\perp}$ when perpendicular. With the determination of the direction of the electronic transition moment, the order parameter can be obtained in terms of the *dichroism ratio*, R, in which [8]

$$R = \frac{A_{\parallel}}{A_{\perp}}. \tag{4}$$

If the electronic transition moment is parallel to the molecular long axis, the order parameter is

$$\begin{aligned} S &= \frac{A_{\parallel} - A_{\perp}}{A_{\parallel} + 2A_{\perp}} \\ &= \frac{R-1}{R+2}. \end{aligned} \tag{5}$$

On the other hand, if the electronic transition moment is perpendicular to the long axis, the order parameter for the long axis is

$$\begin{aligned} S &= \frac{A_{\perp} - 2A_{\parallel}}{A_{\parallel} + A_{\perp}} \\ &= \frac{1-2R}{R+1}. \end{aligned} \tag{6}$$

In general, Equation (5) gives the order parameter for the axis parallel to the transition moment.

### *4.5.2 The Orientational Order Studies by the MIT Research Group*

Our collaborators in MIT had conducted some orientational order studies of iptycenes in the nematic liquid crystal host, 4-(trans-4-pentylcyclohexyl)benzonitrile, better known as PCH5 [9]. Homeotropic alignment of 1wt.% mixtures of anthracene, [113]

and [333] in PCH5 was achieved using surface rubbed test cells to give a uniaxial alignment. The determination for this order with respect to the director was made using UV-vis spectroscopy. Polarised UV-vis spectra of the iptycenes were compared with that of anthracene, whose order according to its aspect ratio, defined by the ratio of the longest to the shortest axis, is well-established. The aspect ratio order means that the alignment of the long axis of each molecule will be, on average, parallel to the liquid crystal director. However, their results showed that this aspect ratio consideration only holds true for anthracene, but not for the iptycenes. Using the short axis absorbances (across the molecules), the order parameters at room temperature are $-0.13$, 0.14, and 0.31 for anthracene, [113] and [333], respectively.

In their earlier studies, the MIT research team was involved in manipulating the unique structure of iptycenes for the creation of novel organisations such as in a highly fluorescent chemosensor to detect TNT vapours [10]. This manipulation was made possible by the existence of the internal free volumes, swept out by their aromatic faces, which is due to the inability of the iptycene structure to obtain any fully co-planar molecular orientation [9]. In other words, the aromatic faces are not able to exist in the same plane because of the rigid molecular structure. In their investigation of the alignment of iptycene in a nematic liquid crystal host, they have shown that iptycenes align normal to the director, in contrast with the aspect ratio order. In order to fill in the volume efficiently and not disrupt the nematic liquid crystal, the long axes of the iptycene guests were found to align normal to the liquid crystal host *via* a so-called"threading" mechanism (see Figure 11) in which the mesogenic molecules pack within the iptycene voids. This observed solvation should fill the empty spaces created by the iptycenes while minimally disrupting the alignment of the host [9]. On the contrary, when the liquid crystals are packed in the aspect ratio order, they do not fill the voids efficiently and hence would cause a greater disruption to the nematic phase.

We, however, propose that the aspect ratio is not defined in [113] because of the "wings", and so the concept of the aspect ratio order is not applicable for the iptycenes. A more reasonable model is the surface tensor approach [11], in which the basic idea is that the probe molecule tries to align itself so that as much of the surface

is parallel to the director. In other words, the alignment of the probe is such that as many of the surface normals are orthogonal to the director as possible.

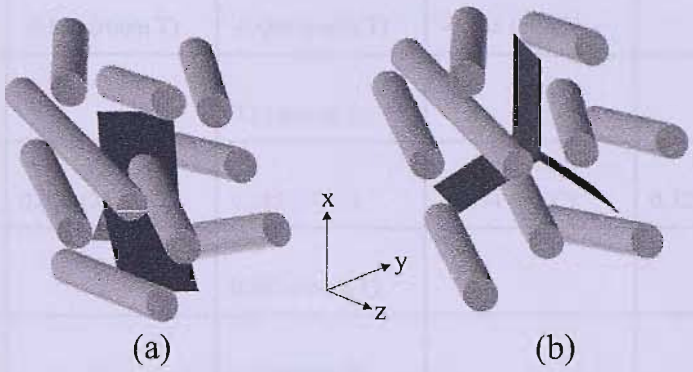


**Figure 11** (a) The aspect ratio order of triptycenes in liquid crystals. (b) The proposed minimisation of free volume guided alignment of triptycenes in liquid crystals [9].

### *4.5.3 The Orientational Order Studies by the Merck Research Group*

To extend these investigations, UV-vis spectroscopy experiments were also conducted by our collaborators in Merck [12]. The liquid crystal hosts used by the group in Merck were PCH5, 5CB, I22 and CCN47 (see Figure 4). The iptycene guest molecules used were anthracene, [113] and [11311] (see Figure 10). Table 1 compares the results obtained from MIT and Merck. For both measurements carried out by the groups in MIT and Merck, the order parameters for anthracene and [113] in PCH5 are comparable. The order parameter across the molecule for anthracene in PCH5 is negative while for [113] in PCH5, the order parameter across the molecule is positive. Interestingly, while we expect the order parameters to be comparable for [113] in 5CB and PCH5 because of the close similarity in their molecular structures (see Figure 4), they are not. In fact, the order parameter for [113] in 5CB is so small, close to zero, while that for PCH5 is 0.245. In contrast, the ordering for anthracene in the nematic hosts are, however, about the same. We shall now compare the results for these systems using deuterium NMR spectroscopy.

| LC Solvent / Solute | 5CB | PCH5 | I22 | CCN47 |
|---|---|---|---|---|
| Anthracene (MIT) | | -0.13 (room T) | | |
| Anthracene (Merck) | -0.136 (room T) | -0.099 (room T) | -0.158 (30°C) | |
| [113] (MIT) | | 0.14 (room T) | | |
| [113] (Merck) | 0.004 (35°C) | 0.245 (30°C) | -0.034 (30°C) | 0.325 (35°C) |
| [11311] (Merck) | | 0.262 (room T) | | |
| [333] (MIT) | | 0.31 (room T) | | |

**Table 1** Comparison of order parameters from UV-vis studies by the research group in MIT [9] and the group in Merck [12].

## 4.6 Orientational Order Studies *via* Deuterium NMR Spectroscopy

### *4.6.1 Experimental*

Approximately 2wt.% of the solute (iptycene) was added to a 3.5cm length of a 5mm o.d. 4mm i.d. NMR glass tube followed by the selected liquid crystal solvent. The sample was mixed mechanically and heated using a hot air gun to ensure the homogeneity of the sample. The sample was prevented from escaping from the bottom of the tube by securing the tube with some PTFE tape. This was used due to the unavailability of a Teflon vortex plug, which does the job more effectively. Following this, the sample tube was inserted into the NMR probe.

The deuterium NMR measurements were performed on a *Varian Infinity Plus 300* spectrometer with *Spinsight* software for data acquisition and processing, using the *Solaris Operating Environment* on a SUN *Microsystem* workstation. The spectra were recorded using a quadrupolar echo sequence $(\pi/2-\tau_1-\pi/2-\tau_2)$, where $\tau_1$ and $\tau_2$ varied with different experiments; these two parameters were determined through

the optimization of each value to achieve a signal at the maximum echo. The length of the $\pi/2$ pulse was fixed at 5μs. The temperature was controlled *via* a thermocouple in the probe head connected to a *Varian* temperature control unit with a stability of 0.1 K. Using the procedure described, the sample was heated into the isotropic phase, and later cooled to room temperature to begin the temperature variation experiment.

### *4.6.2 [113]-$d_{10}$ in 5CB, PCH5, I22, CCN47 and Magic Mixture (5CB:EBBA, 7:3 wt.%)*

From the UV-vis spectroscopy results shown in Table 1, we know that the order parameter across the [113] molecule is positive for both PCH5 and CCN47, but negative for I22. Using this as our starting point in the analysis of the deuterium NMR experiment, we calculated the major and biaxial order parameters. Since we know the principal axes of the molecule, we label them as a, b and c first as shown in Figure 10. The axis a is for the deuterons across the molecule, b being the axis along the anthracene's molecular long axis, and c is normal to both the axes a and b. In [113]-$d_{10}$, there are six deuterons across the molecule and two of them are aliphatic as shown in Figure 10. These deuterons make up the larger of the two quadrupolar splittings in the deuterium NMR spectra. The quadrupolar splitting for the aliphatic deuterons is slightly smaller than that of the aromatic and this distinction can be seen in some of the spectra. However, in calculating the order parameter, $S_{aa}$, we have chosen the quadrupolar splitting for the aromatic deuterons across the molecule. We then use the smaller of the two quadrupolar splittings to calculate $S_{bb}$ and since the ordering tensor is traceless, $S_{cc}$ is simply $(-S_{aa}-S_{bb})$.

We have just described the basic routine we use in calculating the order parameters in our iptycenes experiments including that of anthracene. We then relabel the abc axes to xyz axes system according to the convention such that $|S_{zz}|>|S_{xx}-S_{yy}|$ and that $|S_{xx}-S_{yy}|\geq 0$. Once these axes are relabelled, we then plot the major and biaxial order parameters, $S_{zz}$ and $(S_{xx}-S_{yy})$, respectively, against the shifted temperature. It is important to note here that since the UV-vis spectroscopy results only provide us

with the sign of the splitting for the deuterons parallel to the z-axis, we have to choose the sign of the other splitting such that the set of order parameters will generate a reasonable model of the order of the probe molecule in the liquid crystal host. The equations used to calculate the order parameters in all our experiments can be found in the Appendix in Section 4.8.

Figure 12 shows the deuterium NMR spectra for [113]-$d_{10}$ in 5CB, PCH5, I22, CCN47 and the magic mixture which is made up of 5CB and EBBA in the ratio of 7:3 wt.%. The name *magic mixture* was coined for liquid crystal solvents designed in making the solutes experience essentially zero long-range electrostatic interactions [13, 14]. If the composition of the liquid crystals and temperature are carefully chosen, the degree of orientational order could be zero [13, 14]. However, there is also the shape anisotropy which contributes to the orientational order. We shall discuss the concept of the so-called magic mixture further shortly.

The spectra in Figure 12 clearly show that the quadrupolar splittings for [113]-$d_{10}$ in 5CB, I22 and the magic mixture is relatively small in comparison with that in PCH5 and CCN47. Interestingly, 5CB, which has almost similar molecular structure with PCH5, has different results; the quadrupolar splittings for [113]-$d_{10}$ are about twice as large as that for 5CB. In Figure 5, the spectra for anthracene-$d_{10}$ in 5CB and PCH5 are, however, comparable. In addition, we can observe the fine splitting in the outer peaks in the spectra of [113]-$d_{10}$ in PCH5 and in CCN47 originate from the aromatic and aliphatic deuterons across the molecule, as mentioned earlier. The smaller of the two splitting comes from the aliphatic deuterons because its quadrupolar coupling constant is smaller than that for the aromatic deuterons. Except for the magic mixture, the outer splitting for [113]-$d_{10}$ in all the hosts are coming from the deuterons across the molecule while the inner splittings originate from the deuterons with the $C-D$ bond tilted with respect to the principle axes. The reverse assignment is true for the spectrum of [113]-$d_{10}$ in the magic mixture. This is based on the inner peaks which look broader than the outer peaks because of the two sources of deuterons, the aromatic and the aliphatic, for the $C-D$ parallel to the z axis.

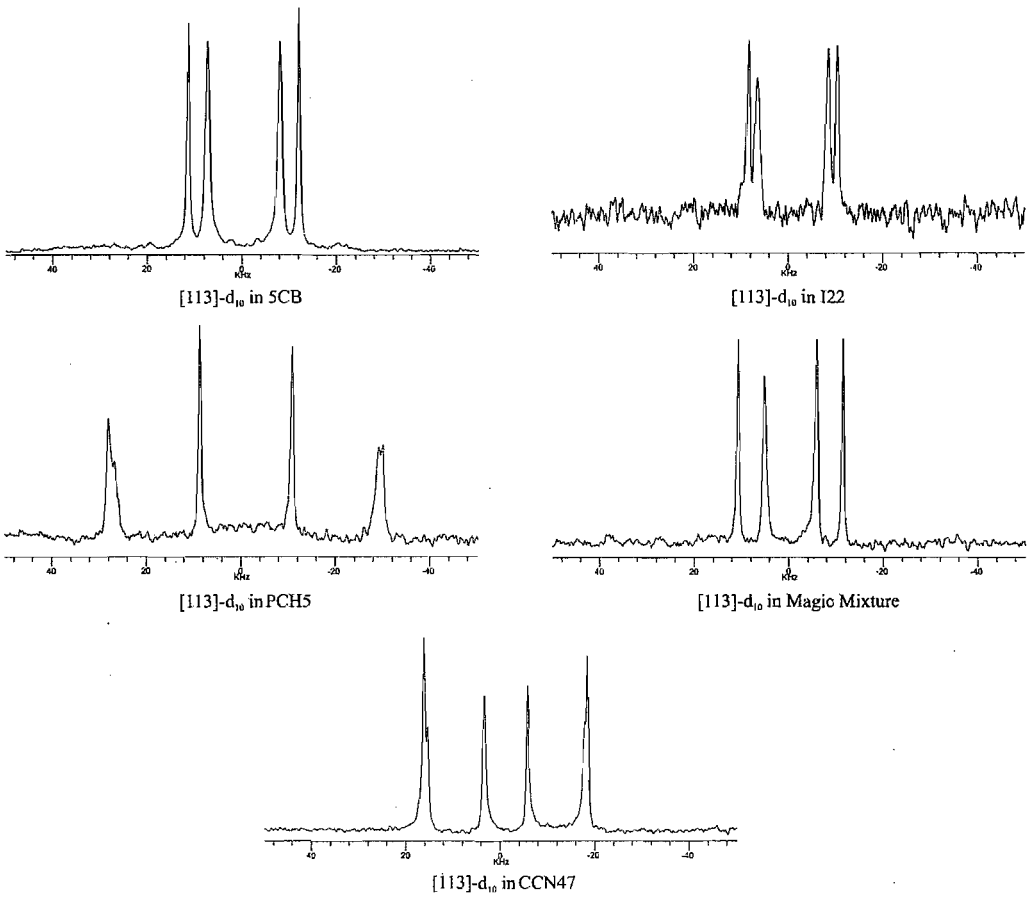


**Figure 12** The deuterium NMR spectra of [113]-$d_{10}$ dissolved in 5CB, PCH5, CCN47, I22 and the so-called magic mixture (5CB:EBBA, 7:3 wt.%) at a shifted temperature, $(T_{NI} - T)$, of 12°C.

Figure 13 shows the shifted temperature dependence of the quadrupolar splittings, $\Delta\tilde{\nu}$, for [113]-$d_{10}$ in 5CB, PCH5, I22, CCN47 and the magic mixture. The filled circle represents the quadrupolar splitting from the aromatic deuterons across the molecule and is labelled $\Delta\tilde{\nu}_1$. On the other hand, the open circle represents $\Delta\tilde{\nu}_2$ from the four deuterons that are winged out at 30° to the x-axis in Figure 33. Note that all of the liquid crystal samples that we use have positive diamagnetic anisotropy, $\Delta\tilde{\chi}$, except for CCN47 which has a negative $\Delta\tilde{\chi}$. Hence, the quadrupolar splittings measured in the deuterium NMR experiments for CCN47 are doubled when doing this analysis. In addition, the plot for CCN47 shows a kink and this is due to its phase transition from the nematic phase into the SmA phase.

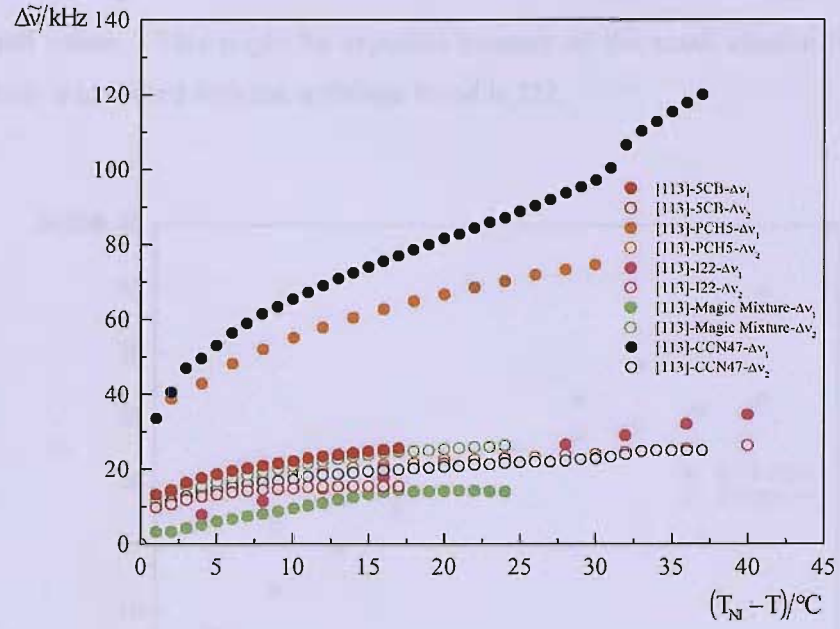


**Figure 13** The quadrupolar splittings, $\Delta\tilde{\nu}$, plotted against the shifted temperature for [113]-$d_{10}$ in 5CB, PCH5, I22, CCN47 and magic mixture (5CB:EBBA, 7:3 wt.%).

The plot in Figure 13 shows that CCN47 has the largest $\Delta\tilde{\nu}_1$ followed by PCH5, 5CB, I22 and the magic mixture. Interestingly, $\Delta\tilde{\nu}_1$ and $\Delta\tilde{\nu}_2$ for I22 from both the deuterons across the molecule and the deuterons that make an angle at the wings, respectively, are comparable. What is more fascinating is that as the temperature is increased, $\Delta\tilde{\nu}_1$ for I22 reduces at a faster rate than that for $\Delta\tilde{\nu}_2$, and so, at a shifted temperature of 24°C, both $\Delta\tilde{\nu}_1$ and $\Delta\tilde{\nu}_2$ overlap each other as shown in the plot in Figure 14. In other words, their quadrupolar splittings are the same. Further increase in temperature causes the two quadrupolar splittings to cross each other, and so now $\Delta\tilde{\nu}_1$ has a smaller value than $\Delta\tilde{\nu}_2$, as can been seen in Figure 13. This is the first time we have observed such phenomenon in deuterium NMR and as we shall see later for another iptycene probe, the results are more dramatic and fascinating. Another key observation is that the quadrupolar splittings for the probe PCH are more than twice as large as than that of 5CB, and this can also be clearly observed from the deuterium NMR in Figure 12. This observation seems to be in agreement with the UV-vis results shown earlier that the ordering of [113] in PCH5 is larger than that in 5CB. In

addition, Figure 13 also shows that both $\Delta\tilde{\nu}_1$ and $\Delta\tilde{\nu}_2$ for the magic mixture have small values. This might be expected because of the small electric field gradient which is in accord with the splittings found in I22.

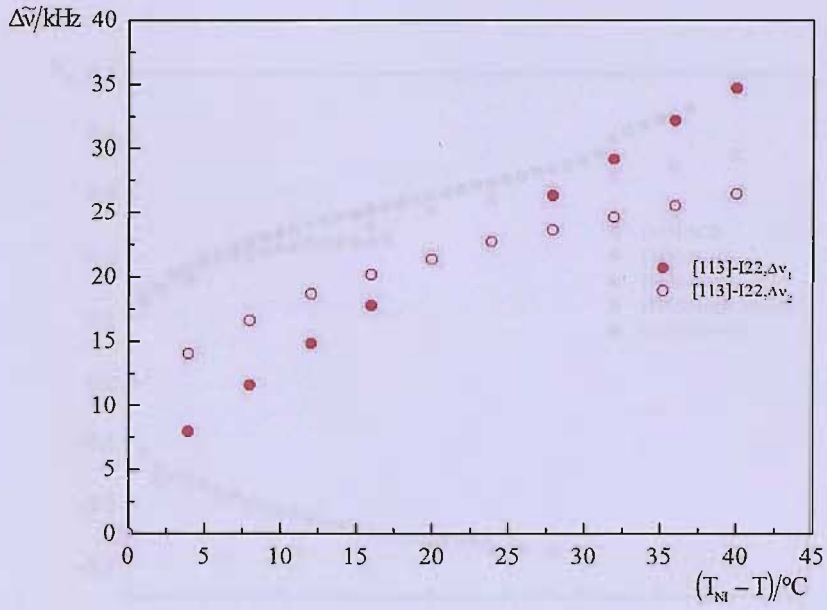


**Figure 14** The quadrupolar splittings, $\Delta\tilde{\nu}$, plotted against the shifted temperature for [113]-$d_{10}$ in I22.

The shifted temperature dependence of the major order parameter, $S_{zz}$, is shown in Figure 15. While the $S_{zz}$ for 5CB, I22 and CCN47 are positive, it is negative for both PCH5 and the magic mixture, which suggests that the molecule is acting almost like a disc in the two latter solvents.

Figure 16 shows the biaxial order parameter, $(S_{xx} - S_{yy})$, plotted against the shifted temperature, and PCH5 gives the largest value followed by CCN47, the magic mixture and I22; the smallest value comes from 5CB. The relationship between the major and biaxial order parameters are shown in Figure 17. In the extreme case when $S_{zz}$ is zero, $(S_{xx} - S_{yy})$ is zero too. In the limit of perfect order, $S_{zz}$ is a unity, and so $(S_{xx} - S_{yy})$ is zero. For a disc, $S_{zz} = -1/2$, and so $S_{xx} = 1$, and $S_{yy} = -1/2$, making the biaxial order parameter, $(S_{xx} - S_{yy}) = 3/2$. Hence for these limiting cases,

a curve is obtained on the right-hand side of the plot in Figure 17, and a straight line on the left-hand side. Figure 17 shows that 5CB, I22 and CCN47 give a curve as we normally expect for molecules that act like a rod, but both PCH5 and the magic mixture give a negative value for $S_{zz}$.

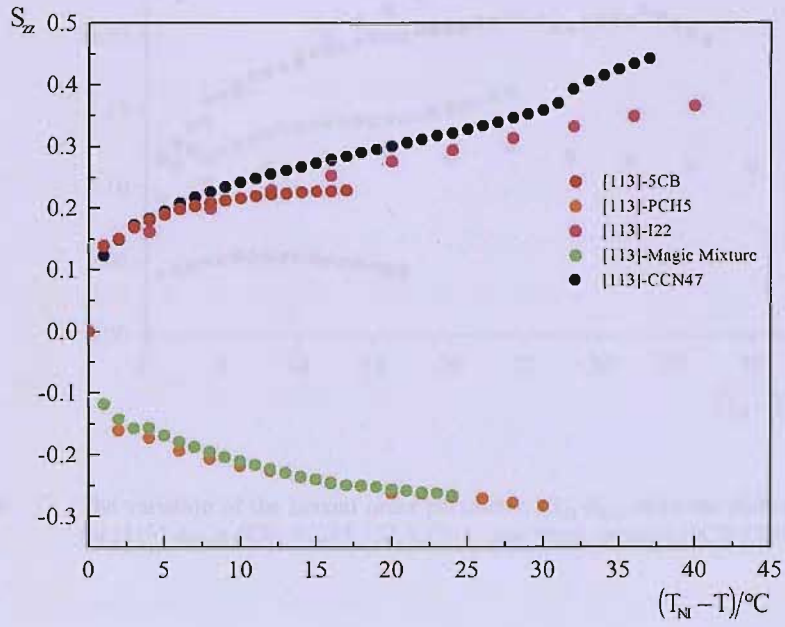


**Figure 15** The variation of the major order parameter, $S_{zz}$, with the shifted temperature for [113]-$d_{10}$ in 5CB, PCH5, I22, CCN47 and magic mixture (5CB:EBBA, 7:3 wt. %).

As promised earlier, we shall now discuss the *magic mixture* in more detail. The mean electric field gradient (EFG), which is temperature and concentration dependent is a property of the liquid crystal solvent and can have a positive or negative sign depending on the particular liquid crystal chosen. To obtain a zero EFG in a liquid crystal solvent would require a mixture of two liquid crystals with opposing signs for the dielectric anisotropies, $\Delta\tilde{\varepsilon}$ [13]. In essence, this means that the orientational order which partly depends on the average EFG of the resulting nematic liquid crystal and its interaction with a solute's quadrupole moment, can be tailored when the appropriate amounts of the liquid crystals are mixed. The other contributor to the orientational order originates from the short-range repulsive interactions which depend on the size and shape anisotropy of the solute.

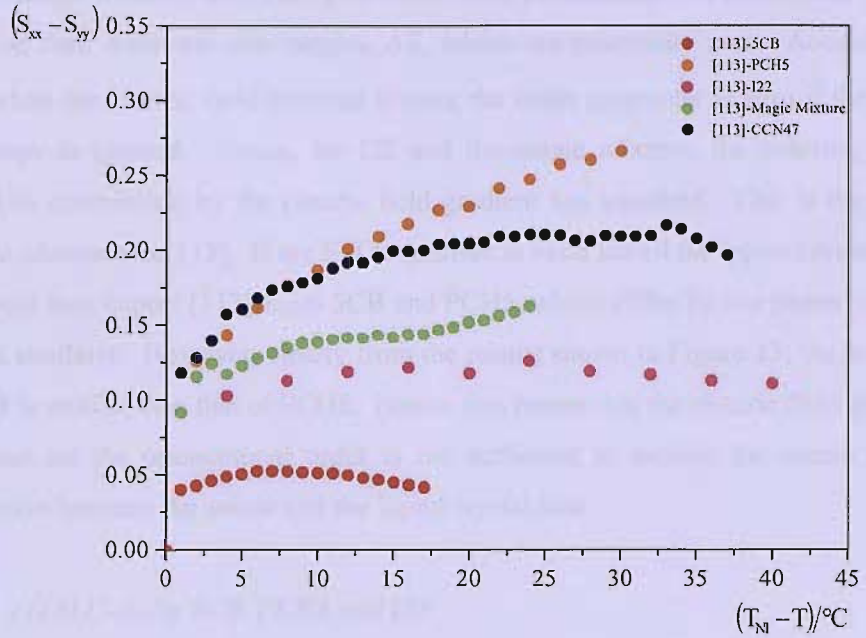


**Figure 16** The variation of the biaxial order parameter, $(S_{xx}-S_{yy})$, with the shifted temperature for [113]-$d_{10}$ in 5CB, PCH5, I22, CCN47 and magic mixture (5CB:EBBA, 7:3 wt. %).

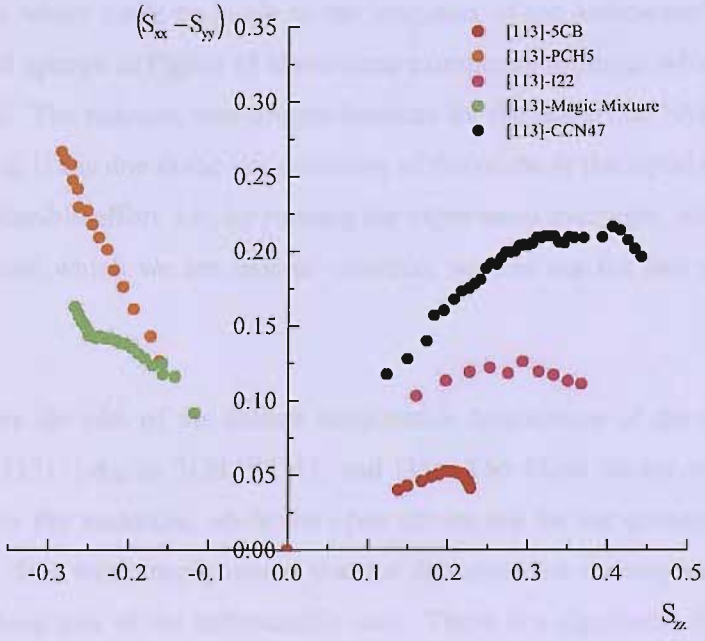


**Figure 17** The variation of the biaxial order parameter, $(S_{xx}-S_{yy})$, with the major order parameter, $S_{zz}$, for [113]-$d_{10}$ in 5CB, PCH5, I22, CCN47 and magic mixture (5CB:EBBA, 7:3 wt. %).

The most striking discovery in these series of experiments is that for [113]-$d_{10}$ in I22 and the magic mixture, they both give small order parameters. We reason this finding based on their dielectric anisotropies, $\Delta\tilde{\varepsilon}$, which are essentially zero. According to [13], when the electric field gradient is zero, the order parameter is zero if the shape anisotropy is ignored. Hence, for I22 and the magic mixture, the ordering which should be contributed by the electric field gradient has vanished. This is the *magic mixture phenomenon* [13]. If the EFG argument is valid for all the liquid crystal hosts, we would then expect [113]-$d_{10}$ in 5CB and PCH5, which differ by one phenyl ring, to behave similarly. However, clearly from the results shown in Figure 13, the ordering of 5CB is smaller than that of PCH5. Hence, this means that the electric field gradient argument on the orientational order is not sufficient to explain the nature of the interaction between the solute and the liquid crystal host.

### *4.6.3 [11311]-$d_{22}$ in 5CB, PCH5 and I35*

Figure 18 shows the deuterium NMR spectra of [11311]-$d_{22}$ (see Figure 10) in some selected liquid crystal hosts. The outer quadrupolar splitting corresponds to the fourteen deuterons across the molecule, while the inner splitting originates from the eight deuterons which make an angle to the long axis of the anthracene's unit. The deuterium NMR spectra in Figure 18 show some extraneous splittings which originate from impurities. The hideous, non-straight baseline for the deuterium NMR spectrum of [11311]-$d_{22}$ in I35 is due to the low solubility of the probe in the liquid crystal host. But after considerable effort, *i.e.*, by running the experiment overnight, we are able to obtain a spectrum which we are able to construe; we can see the two pairs of the major peaks.

Figure 19 shows the plot of the shifted temperature dependence of the quadrupolar splittings for [11311]-$d_{22}$ in 5CB, PCH5, and I35. The filled circles represent the deuterons across the molecule, while the open circles are for the deuterons that are "winged" out. This term simply means that the deuterons are making an angle with respect to the long axis of the anthracene's unit. There is a significant difference in the splittings corresponding to the deuterons across the molecules, but not for those that correspond for the deuterons that is "winged" out. PCH5 gives almost twice the

quadrupolar splitting of that of 5CB despite the only difference in their structure being the existence of an extra phenyl ring in 5CB replacing the cyclohexyl in PCH5. The probe in I35 gives the smallest splittings of the three liquid crystal hosts.

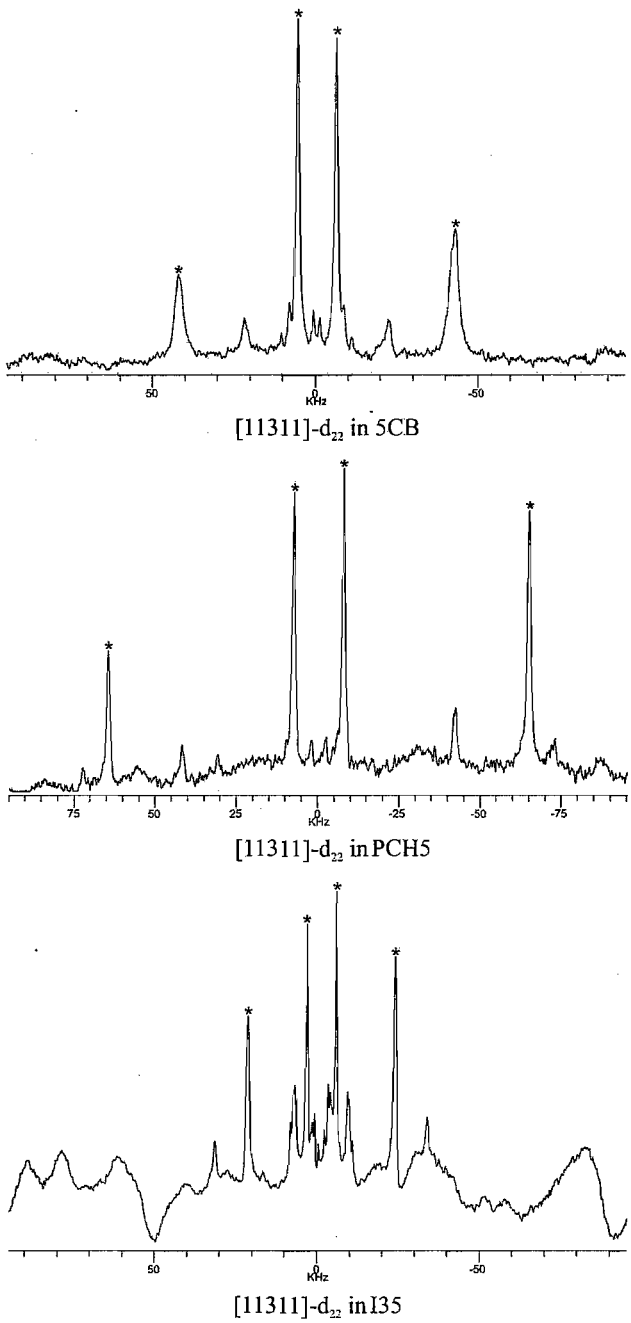


**Figure 18** The deuterium NMR spectra of [11311]-$d_{22}$ dissolved in 5CB, PCH5 and I35 at a shifted temperature, ($T_{NI} - T$), of 10°C. The peaks coming from [11311]-$d_{22}$ are marked with asterisks.

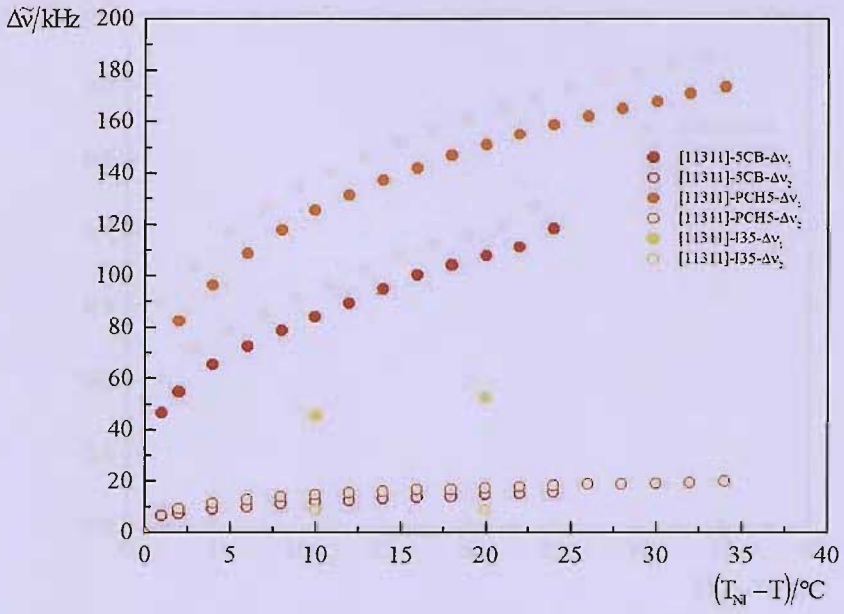


**Figure 19** The quadrupolar splittings, $\Delta\tilde{\nu}$, plotted against the shifted temperature for [11311]-$d_{22}$ in 5CB, PCH5 and I35.

The shifted temperature dependence of major order parameter, $S_{zz}$, for [11311]-$d_{22}$ in the liquid crystals hosts is shown in Figure 20 and it increases with increasing shifted temperatures, as expected. Of the three solvents, PCH5 gives the largest order for the probe. The smallest orientational order is for the I35. The shifted temperature dependence of the biaxial order parameter, $(S_{xx} - S_{yy})$, for [11311]-$d_{22}$ dissolved in 5CB, PCH5, and I35 is shown in Figure 21. Here, 5CB and PCH5 appear to give comparable values. However, the most significant observation is that the biaxiality for [11311]-$d_{22}$ is almost zero. The two hosts also give comparable values for the variation of the biaxial order parameter with the major order parameter as shown in Figure 22. However, we do not observe the curve we normally expect for this plot.

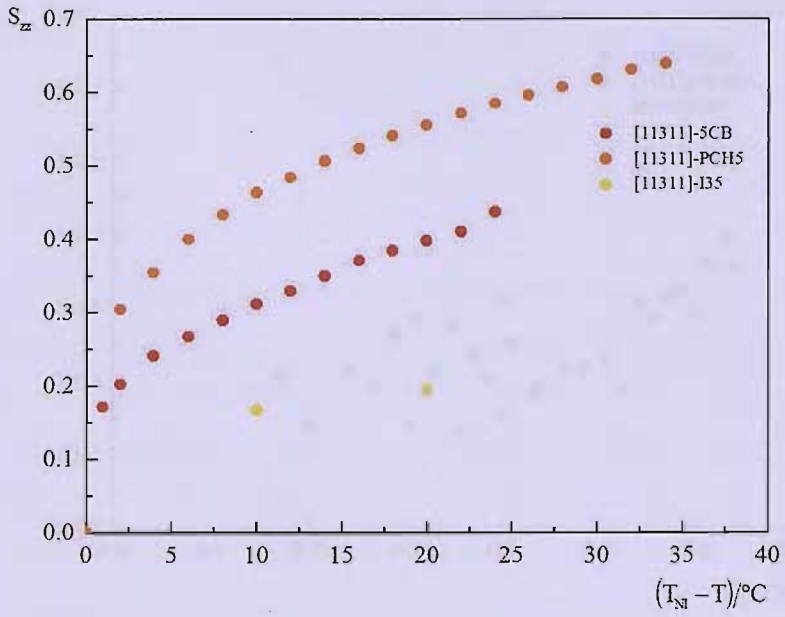


**Figure 20** The variation of the major order parameter, $S_{zz}$, with the shifted temperature for [11311]-$d_{22}$ in 5CB, PCH5, and I35.

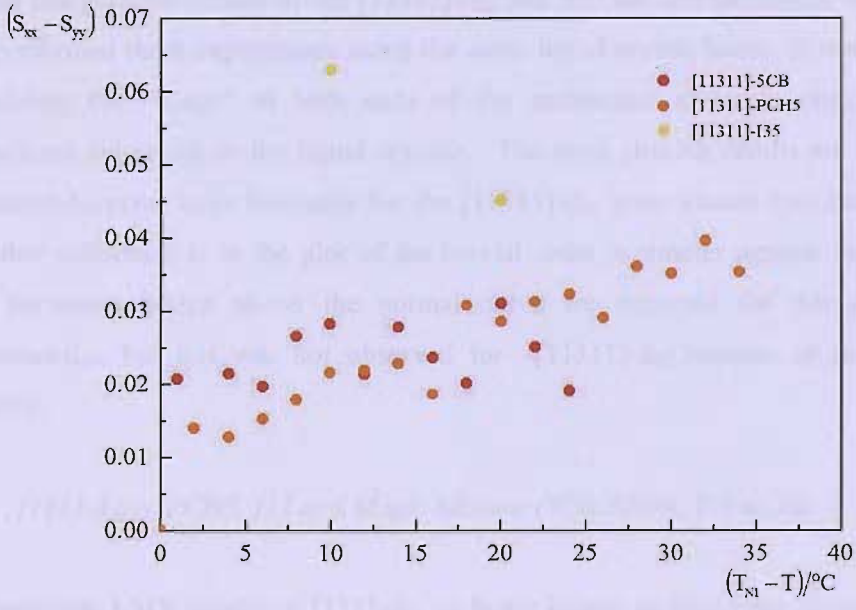


**Figure 21** The variation of the biaxiality order parameter, ($S_{xx}$-$S_{yy}$), with the shifted temperature for [11311]-$d_{22}$ in 5CB, PCH5, and I35.

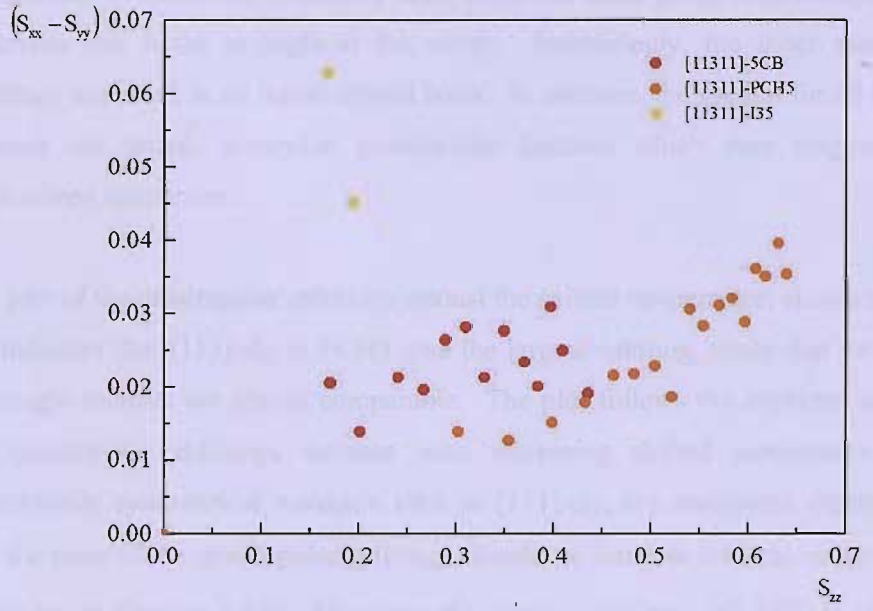


**Figure 22** The variation of the biaxial order parameter, $(S_{xx}-S_{yy})$ with the major order parameter, $S_{zz}$, for [11311]-$d_{22}$ in 5CB, PCH5,and I35.

We can compare the results of the [11311]-$d_{22}$ and that for anthracene-$d_{10}$ since we have performed these experiments using the same liquid crystal hosts. It is apparent that adding the "wings" at both ends of the anthracene molecule changes the orientational behaviour in the liquid crystals. The most striking results are that the anthracene-$d_{10}$ gives large biaxiality but the [11311]-$d_{22}$ gives almost zero biaxiality. The other difference is in the plot of the biaxial order parameter against the major order parameter which shows the normal curve we expected for this plot for anthracene-$d_{10}$, but this was not observed for [11311]-$d_{22}$ because of the small biaxiality.

### *4.6.4 [111]-$d_{12}$ in PCH5, I22 and Magic Mixture (5CB:EBBA, 7:3 wt.%)*

The deuterium NMR spectra of [111]-$d_{12}$, or better known as triptycene, dissolved in various liquid crystal solvents are shown in Figure 23. Despite the noise caused by the low solubility of this highly symmetric probe, we can see the two prominent

quadrupolar doublets, the outer coming from the deuterons across the probe molecule, *i.e.*, parallel to three-fold symmetry axis, while the inner peaks originating from the deuterons that make at angle at the wings. Interestingly, the inner quadrupolar splittings are small in all liquid crystal hosts. In addition, the spectra for all the three solvents are broad, somewhat powder-like features which may originate from undissolved spin probe.

The plot of the quadrupolar splittings against the shifted temperature, shown in Figure 24, indicates that [1 1 1]-$d_{12}$ in PCH5 give the largest splitting, while that for I22 and the magic mixture are almost comparable. The plot follows the expected trend that the quadrupolar splittings increase with increasing shifted temperature. For a cylindrically symmetrical molecule such as [1 1 1]-$d_{12}$, the traditional expectation is that the ratio of the quadrupolar splittings should be constant with the value 8/1 (see Appendix in Section 4.8.4). However, the plots of the ratio $\Delta\tilde{\nu}_1/\Delta\tilde{\nu}_2$ in Figure 25 clearly show that the ratios are not constant. Of course, the range for the scales for the ratio plot is small for PCH5 but not so for I22 and the magic mixture. Hence, in our analyses, we have adopted the $D_{2h}$ symmetry assumption for the [1 1 1]-$d_{12}$ in all the liquid crystal hosts. The result for ratio $\Delta\tilde{\nu}_1/\Delta\tilde{\nu}_2$ for I22 is inconsistent; this could be caused by the experimental error in the splittings which might result from the accuracy with which they are quoted. It is also important to note that the expected ratio 8/1 is for 60°, *i.e.*, the angle the deuterons make to the z-axis. Small deviations from this angle can cause a significant variation in the ratio.

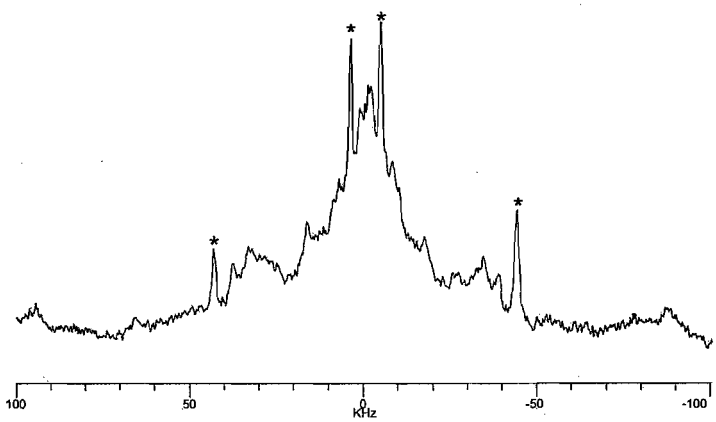


[111]-$d_{12}$ in PCH5

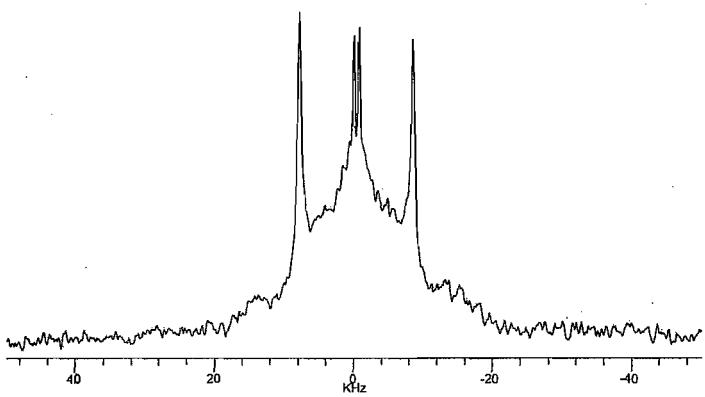


[111]-$d_{12}$ in I22

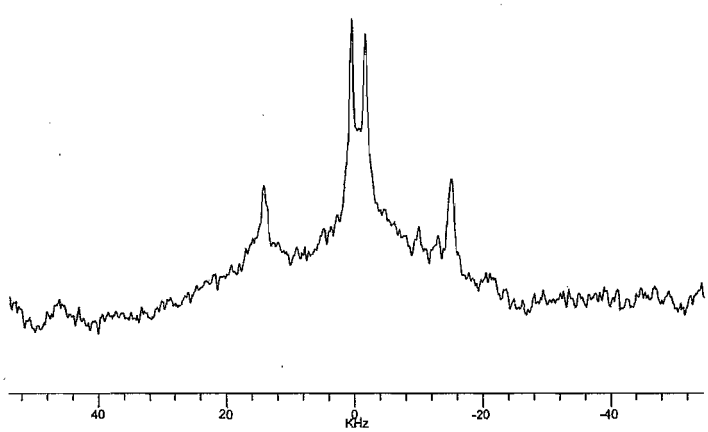


[111]-$d_{12}$ in Magic Mixture

**Figure 23** The deuterium NMR spectra for [111]-$d_{12}$ dissolved in some selected liquid crystal hosts at the shifted temperature, $(T_{NI} - T)$, of 12°C. The asterisks on the peaks for [111]-$d_{12}$ in PCH5 are to indicate the relevant peaks for the probe.

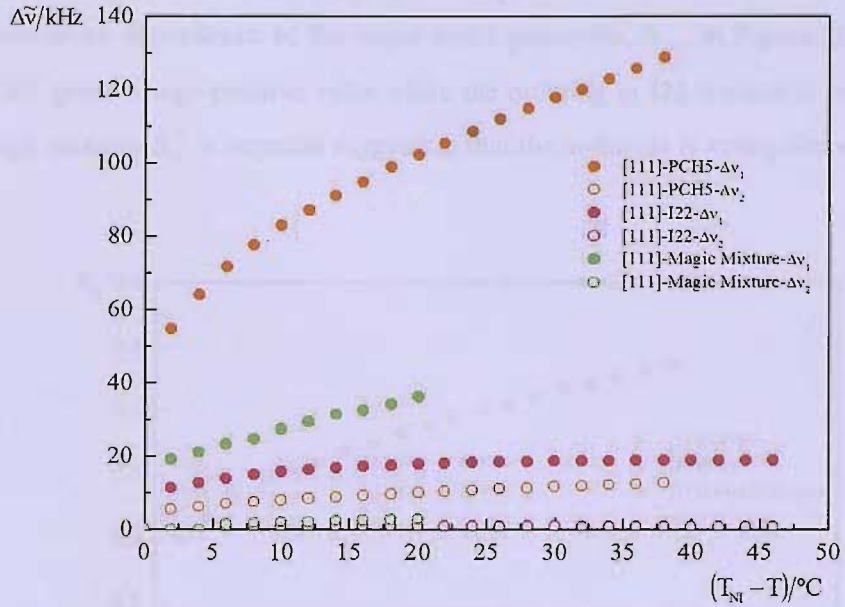


**Figure 24** The quadrupolar splittings, $\Delta\tilde{\nu}$, against the shifted temperature for [111]-$d_{12}$ in PCH5, I22, and the magic mixture (5CB:EBBA, 7:3 wt. %).

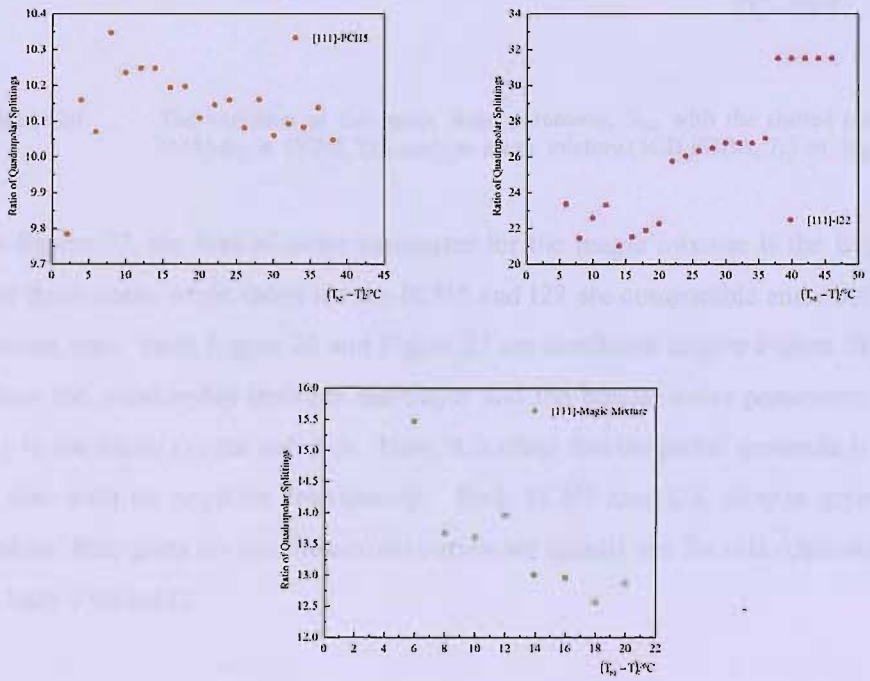


**Figure 25** The shifted temperature dependence of the ratio of the quadrupolar splittings for [111]-$d_{12}$ in PCH5, I22, and magic mixture (5CB:EBBA, 7:3 wt.%).

Since we do not have supported data from UV-vis spectroscopy to assign the sign of the splittings we choose an appropriate sign for a reasonable model. The shifted temperature dependence of the major order parameter, $S_{zz}$, in Figure 26 shows that PCH5 gives a huge positive value while the ordering in I22 is close to zero. For the magic mixture $S_{zz}$ is negative suggesting that the molecule is acting almost like a disc.

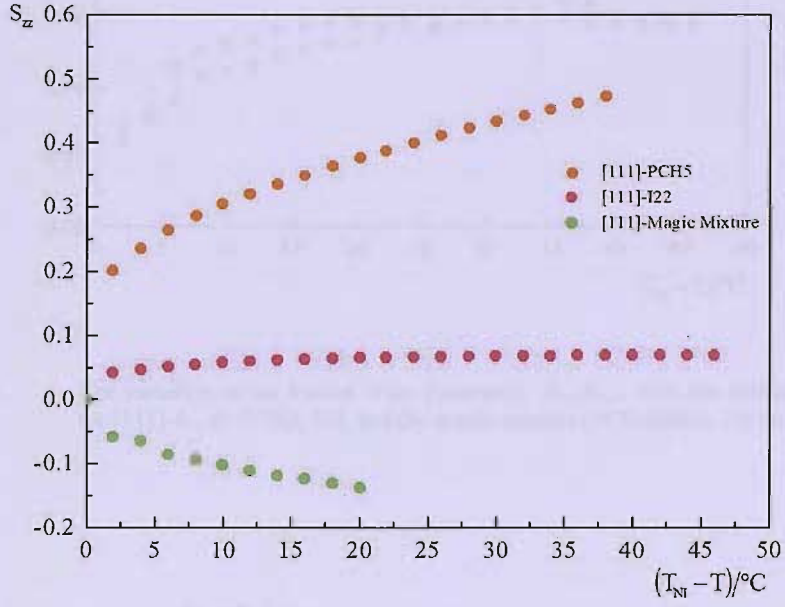


**Figure 26** The variation of the major order parameter, $S_{zz}$, with the shifted temperature for [111]-$d_{12}$ in PCH5, I22, and the magic mixture (5CB:EBBA; 7:3 wt. %).

In Figure 27, the biaxial order parameter for the magic mixture is the largest among the three hosts, while those for the PCH5 and I22 are comparable and small in values, almost zero. Both Figure 26 and Figure 27 are combined to give Figure 28 in order to show the relationship between the major and the biaxial order parameters for [111]-$d_{12}$ in the liquid crystal solvents. Here, it is clear that the probe molecule is acting like a disc with its negative relationship. Both PCH5 and I22, despite giving positive values, their plots are not the normal curves we usually see for this relationship, which is truly a curiosity.

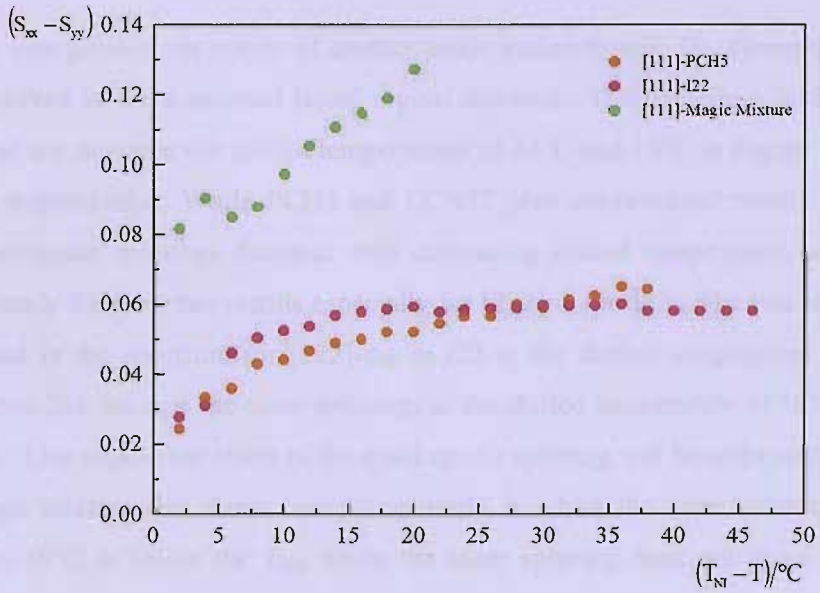


**Figure 27** The variation of the biaxial order parameter, $(S_{xx}-S_{yy})$, with the shifted temperature for [111]-$d_{12}$ in PCH5, I22, and the magic mixture (5CB:EBBA, 7:3 wt. %).

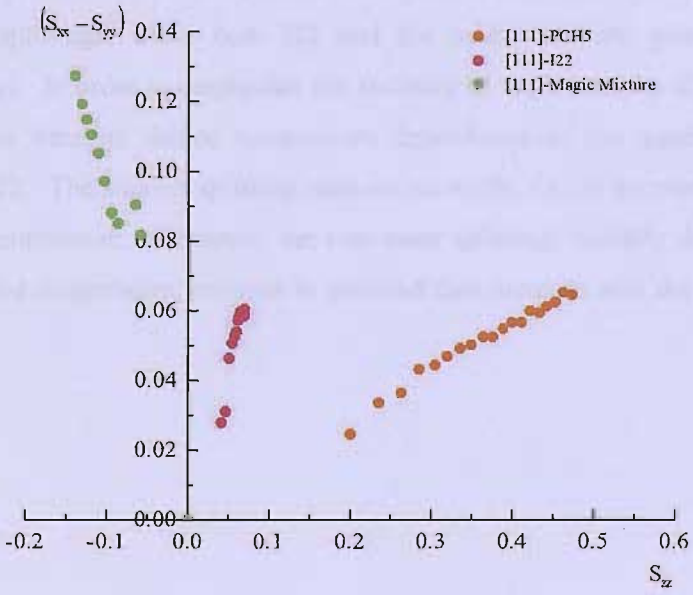


**Figure 28** The variation of the biaxiality order parameter, $(S_{xx}-S_{yy})$ with the major order parameter, $S_{zz}$, for [111]-$d_{12}$ in PCH5, I22, and the magic mixture (5CB:EBBA, 7:3 wt. %).

### *4.6.5 [222]-$d_{18}$ in PCH5, I22, CCN47 and Magic Mixture (5CB:EBBA, 7:3 wt.%)*

We now present our results of another probe molecule with $D_{3h}$ symmetry, [222]-$d_{18}$, dissolved in some selected liquid crystal solvents. The deuterium NMR spectra for these are shown at the shifted temperatures of 34°C and 10°C in Figure 29 and Figure 30, respectively. While PCH5 and CCN47 give conventional results such that the quadrupolar splittings decrease with decreasing shifted temperature, we observe an anomaly for the other results especially for [222]-$d_{18}$ in I22. The two inner splittings found in the spectrum for [222]-$d_{18}$ in I22 at the shifted temperature of 34°C (see Figure 29), become the outer splittings at the shifted temperature of 10°C (see Figure 30). This cross-over effect of the quadrupolar splitting will be addressed shortly. The magic mixture also shows interesting results in which the inner splitting collapses to zero 16°C at below the $T_{NI}$, while the outer splitting does not show this dramatic behaviour.

The shifted temperature dependence of the quadrupolar splittings is shown in Figure 31. The deuterons across the molecule are represented by the filled circles, while the deuterons that make an angle with the naphthalene long axis are represented by the open circles. From Figure 31, it is apparent that both PCH5 and CCN47 give significantly large splittings, while both I22 and the magic mixture give small quadrupolar splittings. In order to emphasize the anomaly of the behaviour of [222]-$d_{18}$ in I22, we show here its shifted temperature dependence of the quadrupolar splittings in Figure 32. The smaller splitting behaves normally, *i.e.*, it increases with increasing shifted temperature. However, the two outer splittings initially decrease with increasing shifted temperature, collapse to zero and then increase with the shifted temperature.

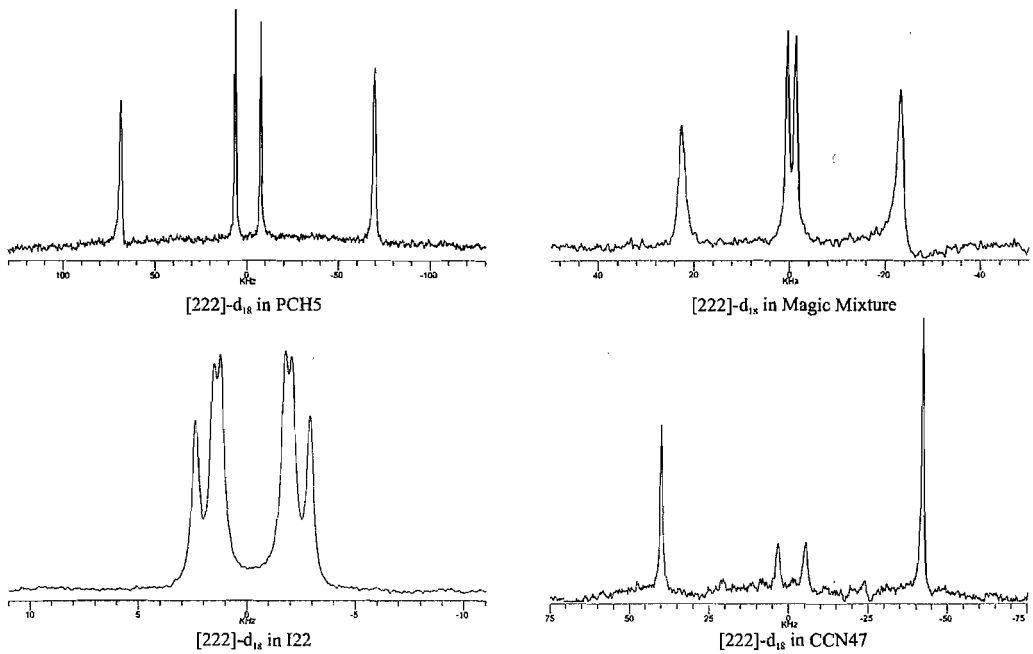


**Figure 29** The deuterium NMR spectra for [222]-$d_{18}$ dissolved in some selected liquid crystal hosts at the shifted temperature, $(T_{NI} - T)$, of 34°C.

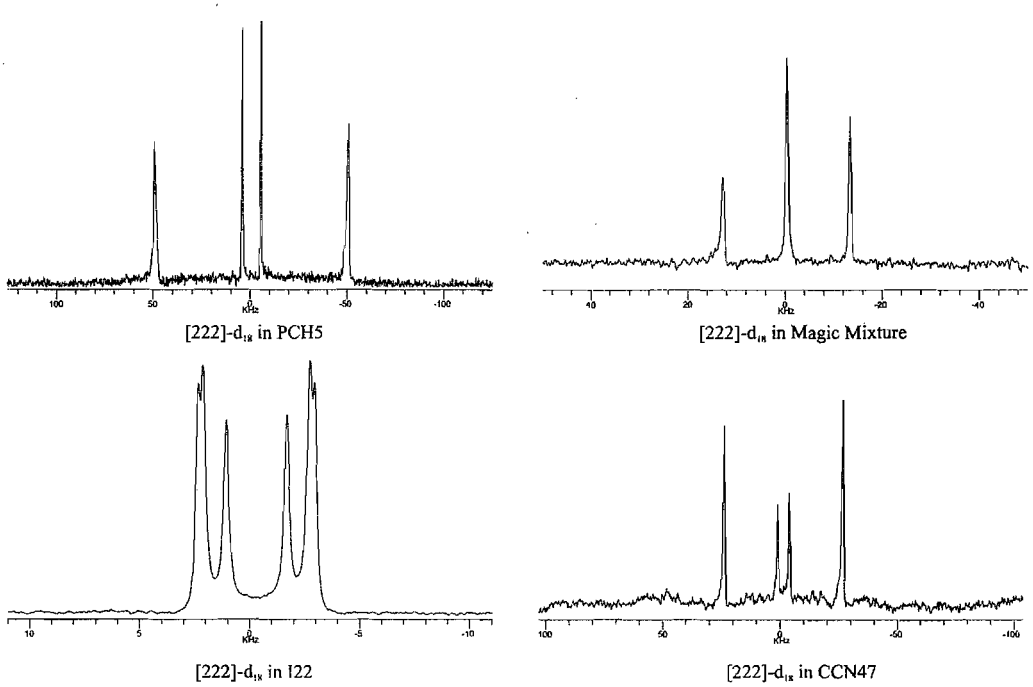


**Figure 30** The deuterium NMR spectra for [222]-$d_{18}$ dissolved in some selected liquid crystal hosts at the shifted temperature, $(T_{NI} - T)$, of 10°C.

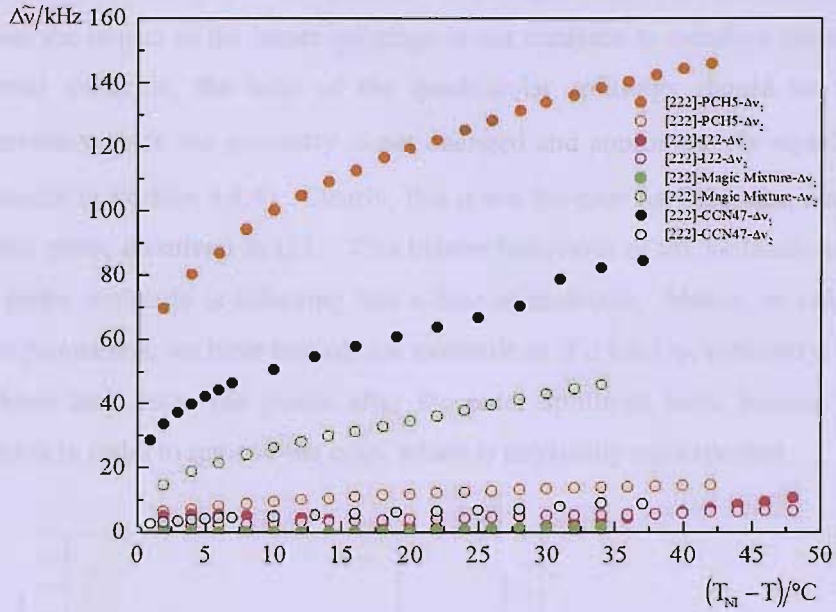


**Figure 31** The quadrupolar splittings, $\Delta\tilde{\nu}$, plotted against the shifted temperature for [222]-$d_{18}$ in PCH5, I22, CCN47, and the magic mixture (5CB:EBBA, 7:3 wt. %).

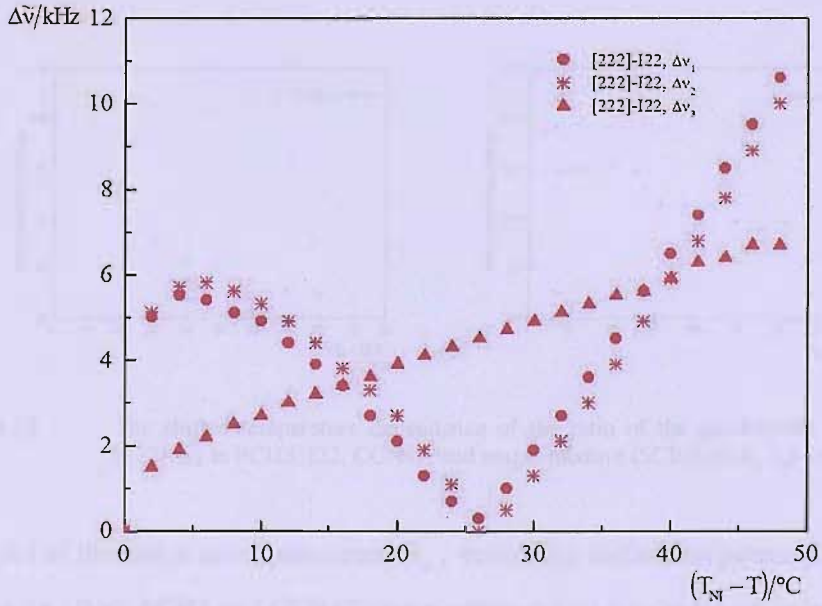


**Figure 32** The quadrupolar splittings, $\Delta\tilde{\nu}$, plotted against the shifted temperature for [222]-$d_{18}$ in I22.

The ratios of the quadrupolar splittings are calculated and the plots against the shifted temperature for all of the hosts are given in Figure 33. For the host I22, we have chosen the largest of the larger splittings in our analyses to calculate the ratios. For a uniaxial molecule, the ratio of the quadrupolar splittings should be temperature independent since the geometry is not changed and approximately equal to 8/1 (see Appendix in Section 4.8.4). Clearly, this is not the case for [222]-$d_{18}$, and especially for this probe dissolved in I22. This bizarre behaviour of the molecule suggests that this probe molecule is behaving like a biaxial molecule. Hence, in calculating the order parameters, we have treated this molecule as if it has $D_{2h}$ symmetry. In addition, we have also taken the points after the outer splittings have become zero to be negative in order to remove the cusp, which is physically not expected.

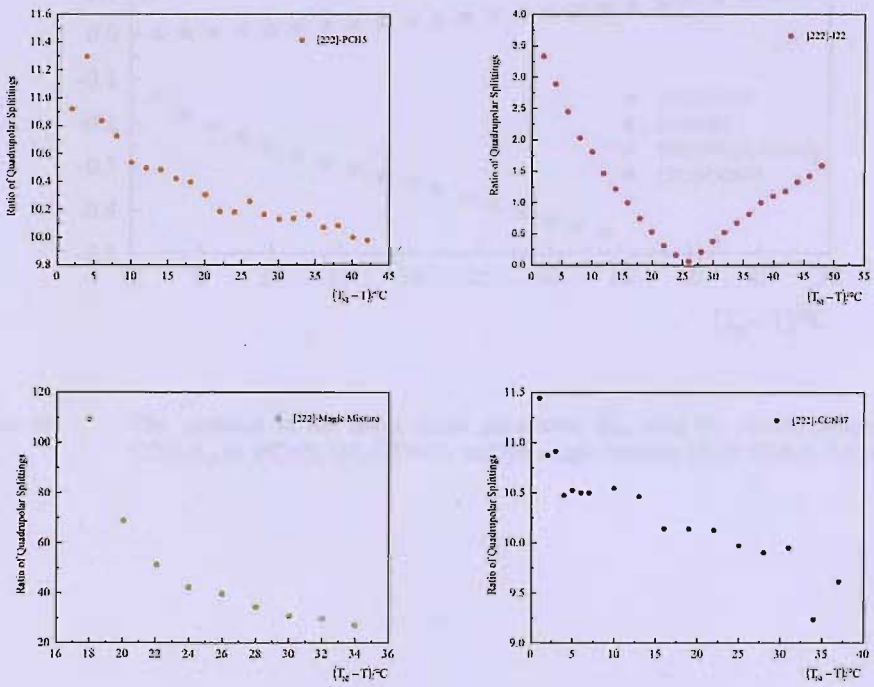


**Figure 33** The shifted temperature dependence of the ratio of the quadrupolar splittings for [222]-$d_{18}$ in PCH5, I22, CCN47, and magic mixture (5CB:EBBA, 7:3 wt.%).

The plot of the major order parameter, $S_{zz}$, versus the shifted temperature is shown in Figure 34. Both PCH5 and CCN47 give positive values for the major order parameter, while I22 give almost zero order. On the other hand, the magic mixture gives a large negative value indicating that the molecule is aligned almost perfectly orthogonal to the z-axis.

The biaxial order parameter, $(S_{xx} - S_{yy})$, shows a high biaxiality for [222]-$d_{18}$ in the magic mixture in comparison with PCH5, I22 and CCN47 (see Figure 30). Further, the relationship of $(S_{xx} - S_{yy})$ with $S_{zz}$ clearly shows [222]-$d_{18}$ in the magic mixture is behaving like a disc as shown in Figure 36.

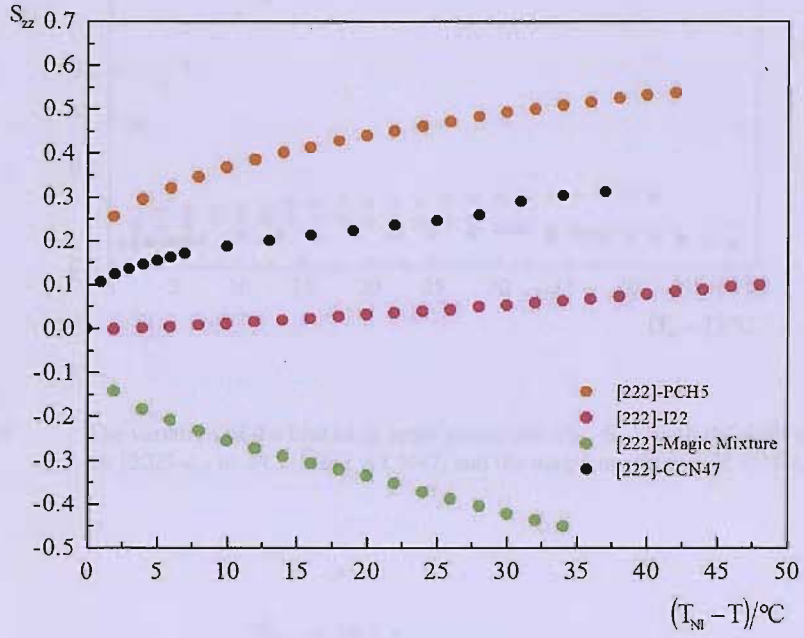


**Figure 34** The variation of the major order parameter, $S_{zz}$, with the shifted temperature for [222]-$d_{18}$ in PCH5, I22, CCN47, and the magic mixture (5CB:EBBA, 7:3 wt. %).

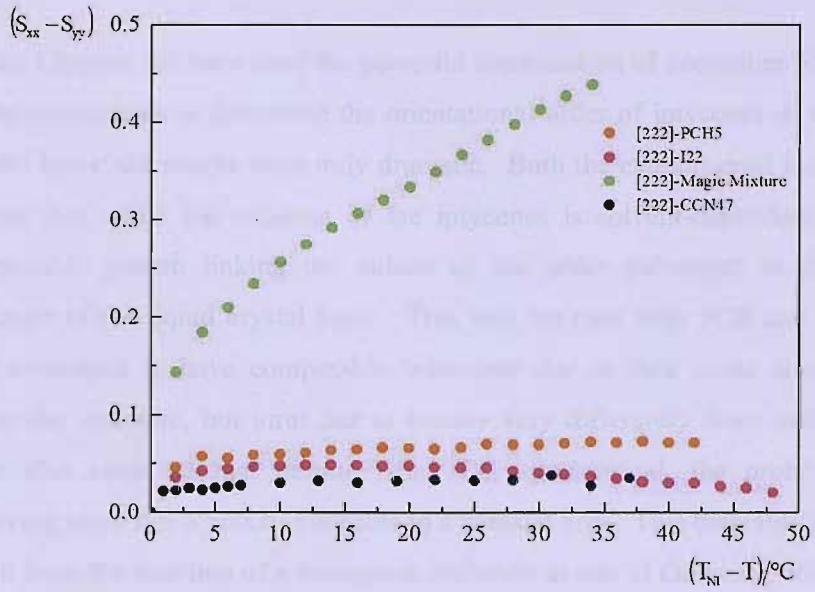


**Figure 35** The variation of the biaxiality order parameter, $(S_{xx}-S_{yy})$, with the shifted temperature for [222]-$d_{18}$ in PCH5, I22, CCN47, and the magic mixture (5CB:EBBA, 7:3 wt. %).

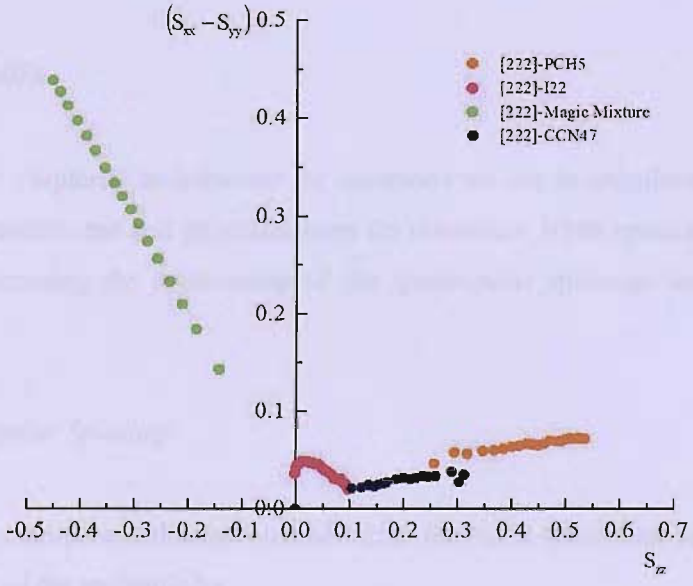


**Figure 36** The variation of the biaxiality order parameter, $(S_{xx}-S_{yy})$, with the major order parameter, $S_{zz}$, for [222]-$d_{18}$ in PCH5, I22, CCN47, and the magic mixture (5CB:EBBA, 7:3 wt. %).

## 4.7 Conclusions

In this Chapter, we have used the powerful combination of deuterium NMR and UV-vis spectroscopies to determine the orientational order of iptycenes in various liquid crystal hosts; the results were truly dramatic. Both the experimental techniques have shown that while the ordering of the iptycenes is solvent-dependent, there is no appreciable pattern linking the values of the order parameter to the molecular structure of the liquid crystal hosts. This was the case with 5CB and PCH5 which was envisaged to have comparable behaviour due to their close similarity in the molecular structure, but turns out to behave very differently from each other. We have also observed that despite being $D_{3h}$ symmetrical, the probe [222]-$d_{18}$ is behaving more like a biaxial molecule in a nematic host. This biaxiality is assumed to result from the insertion of a mesogenic molecule in one of the voids, allowing for the exchange between the three voids in order to get the precise calculation of the biaxiality. In addition, we have also introduced the magic mixture which has essentially, zero $\Delta\varepsilon$ like the I-series of the liquid crystal hosts, but not necessarily behaves similarly.

## 4.8 Appendix

This part of the chapter is to introduce the equations we use in calculating the order parameters for anthracene and iptycenes from the deuterium NMR spectra. We begin this section discussing the relationship of the quadrupolar splittings and the order parameters.

### *4.8.1 Quadrupolar Splittings*

The observed quadrupolar splittings obtained from the NMR spectra are related to the ordering matrix of the molecule by

$$\Delta\tilde{\nu} = \sum_{\alpha} q_{\alpha\alpha} S_{\alpha\alpha}, \qquad (7)$$

where α denotes a principal axis for the ordering matrix, **S**, in which

$$S_{\alpha\alpha} = \frac{3\overline{\ell_\alpha^2} - 1}{2}, \tag{8}$$

where $\ell_\alpha$ is the direction cosine between α and the director (see Equation (1)). It is convenient and realistic to take the quadrupolar tensor to be cylindrically symmetric about the C – D bond with a major component $q_{CD}$. If the bond is parallel to one of the principal axes, say z, then,

$$\Delta\tilde{\nu} = q_{CD}S_{zz} - \left(\frac{q_{CD}}{2}\right)\left(S_{xx} + S_{yy}\right). \tag{9}$$

But since the ordering matrix is traceless, then,

$$S_{xx} + S_{yy} = -S_{zz}, \tag{10}$$

and so,

$$\Delta\tilde{\nu} = \frac{3}{2}q_{CD}S_{zz}, \tag{11}$$

which is a standard result.

### *4.8.2 Anthracene*

Since the C – D bonds for the six deuterons are parallel to the x-axis (see Figure 37 and Figure 3), the quadrupolar splittings for these give the $S_{xx}$ element of the ordering matrix, *i.e.*,

$$\Delta\tilde{\nu}_1 = \frac{3}{2}q_{CD}S_{xx}. \tag{12}$$

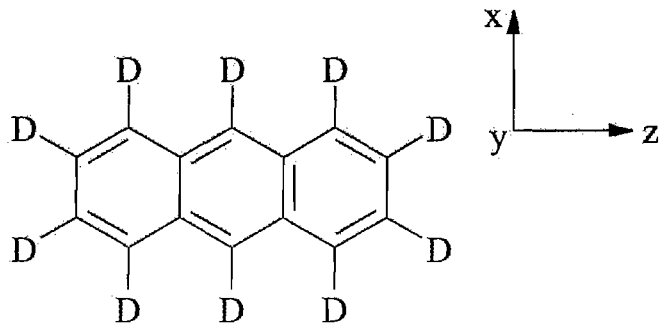


**Figure 37** The molecular structure of anthracene-$d_{10}$ and its principal axes.

The quadrupolar coupling constant for aromatic deuterons varies slightly from compound to compound, but is in the order of 181kHz, a value found for solid anthracene [7]. The remaining four deuterons are inclined with respect to the principal axes. Hence, we need to transform from the local C – D frame to the principal axis system. This is achieved using the general result

$$Q_{ab} = \sum_{\alpha\beta} \ell_{\alpha a} \ell_{\beta b} Q_{\alpha\beta}, \tag{13}$$

where $\ell_{\alpha a}$ is the direction cosine for the axes $\alpha$ and a. In the case of anthracene, the C – D bond is in the xz plane so that the transformation involves a single angle.

For simplicity, we take the C – D bond to be in the xz plane with the bond at an angle 30° to the z-axis. The value of $q_{zz}$ is then,

$$\begin{aligned} q_{zz} &= q_{CD} \cos^2 30° - \frac{q_{CD}}{2} \cos^2 120° \\ &= \frac{5}{8} q_{CD}, \end{aligned} \tag{14}$$

$$\begin{aligned} q_{xx} &= q_{CD} \cos^2 300° - \frac{q_{CD}}{2} \cos^2 30° \\ &= -\frac{q_{CD}}{8}, \end{aligned} \tag{15}$$

$$q_{yy} = -\frac{q_{CD}}{2}, \tag{16}$$

in which the sum of the diagonal elements necessarily vanishes.

The observed quadrupolar splitting for the β deuterons is then,

$$\Delta\tilde{\nu}_2 = q_{CD}\left(\frac{5}{8}S_{zz} - \frac{1}{8}S_{xx} - \frac{1}{2}S_{yy}\right). \tag{17}$$

Since we only know $S_{xx}$ from the quadrupolar splittings for the αγ deuterons (see Equation 12), it is desirable to replace $S_{yy}$ with $-S_{zz} - S_{xx}$; this gives

$$\Delta\tilde{\nu}_2 = q_{CD}\left(\frac{9}{8}S_{zz} + \frac{3}{8}S_{xx}\right). \tag{18}$$

From the relationship in Equation (10), $S_{yy}$ is obtained. Hence, both the major and biaxial order parameters, $S_{zz}$ and $(S_{xx} - S_{yy})$, respectively, are known.

### *4.8.3 Iptycene (with $C_{2v}$ symmetry like [113])*

We change the axis labels with respect to anthracene such that the new z axis (see Figure 38) tends to be parallel to the director. There are six deuterons whose $C-D$ bonds are parallel to the z-axis for [113]-$d_{10}$ (see Figure 38) whose symmetry gives as a principal axis so that

$$\Delta\tilde{\nu}_1 = \frac{3}{2}q_{CD}S_{zz}. \tag{19}$$

However, it is important to recognise that two of the deuterons are aliphatic and that $q_{CD}$ is smaller than for aromatic deuterons; typically $q_{CD}$ is about 168kHz. This difference could explain the difference in quadrupolar splittings observed within the group of six deuterons. Here, we take $\Delta\tilde{\nu}_1$ as for the aromatic deuterons. To determine the other elements of the ordering matrix, we use the splitting for the remaining group of four deuterons. To achieve this, we need to transform from the local $C-D$ frame to the principal abc frame. This transformation is performed in

two steps; first from the local C – D frame to the phenyl ring, and then from this to the principal axes of the molecule. We have already performed the first transformation, but it is convenient to relabel the axes so that they fit it better with the molecular axes; thus z becomes x, x becomes z, and y is unchanged.

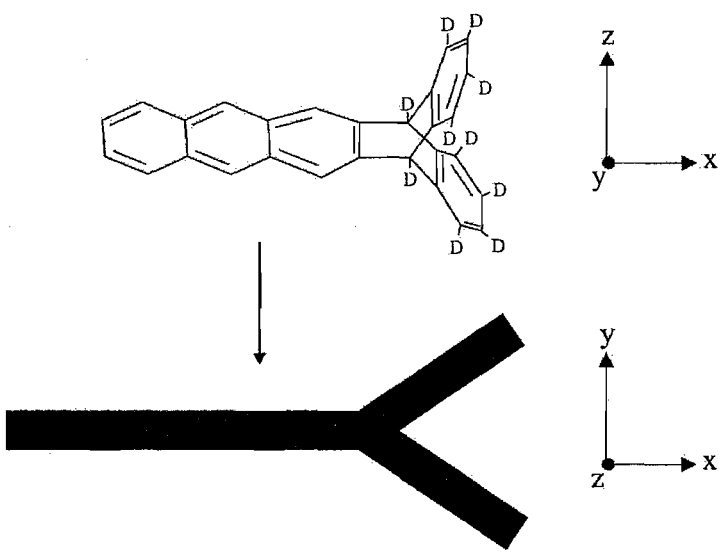


**Figure 38** The molecular structure of [113]-$d_{10}$ and its schematic model with its principal axes.

Thus,

$$q_{zz} = -\frac{1}{8} q_{CD}, \tag{20}$$

$$q_{yy} = -\frac{1}{2} q_{CD}, \tag{21}$$

$$q_{xx} = -\frac{5}{8} q_{CD}; \tag{22}$$

there is, in addition, an off-diagonal element, $q_{xz}$. However, this is not involved in transforming to the molecular frame which involves a rotation about the z axis. Thus,

$$q_{xx} = \frac{5}{8} q_{CD} \cos^2 60° - \frac{1}{2} q_{CD} \cos^2 150°$$
$$= \frac{5}{32} q_{CD} - \frac{3}{8} q_{CD} \qquad (23)$$
$$= -\frac{7}{32} q_{CD},$$

$$q_{yy} = -\frac{1}{2} q_{CD} \cos^2 60° - \frac{5}{8} q_{CD} \cos^2 330°$$
$$= -\frac{1}{8} q_{CD} + \frac{15}{32} q_{CD} \qquad (24)$$
$$= \frac{11}{32} q_{CD},$$

$$q_{zz} = -\frac{1}{8} q_{CD}. \qquad (25)$$

Hence, the quadrupolar splitting for the four remaining aromatic deuterons are given by

$$\Delta\tilde{\nu}_2 = q_{CD}\left(-\frac{1}{8} S_{zz} + \frac{11}{32} S_{yy} + \frac{7}{32} S_{xx}\right), \qquad (26)$$

and replacing $S_{yy}$ by $-S_{zz} - S_{xx}$ gives

$$\Delta\tilde{\nu}_2 = -q_{CD}\left(-\frac{15}{32} S_{zz} + \frac{18}{32} S_{xx}\right). \qquad (27)$$

*4.8.4 Iptycene (with $D_{3h}$ symmetry like [111] and [222])*

For this uniaxial molecule, we only expect one order parameter, *i.e.*, $S_{zz}$. Hence, we have for deuterons parallel to the symmetry axis,

$$\Delta\tilde{\nu}_1 = \frac{3}{2} q_{CD} S_{zz}. \tag{28}$$

For deuterons that make an angle θ to the z-axis (see Figure 39), the quadrupolar splitting is given as

$$\Delta\tilde{\nu}_2 = \frac{3}{2} q_{CD} S_{zz} P_2(\cos\theta), \tag{29}$$

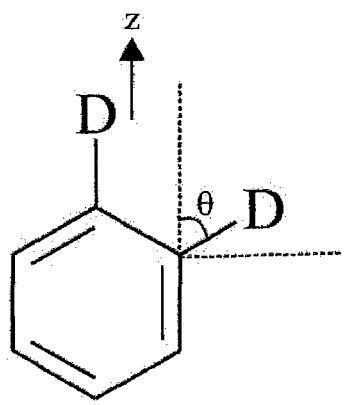


**Figure 39** The molecular structure of one of the wings of the iptycenes with $D_{3h}$ symmetry; typically θ is approximately 60°.

where $P_2(\cos\theta)$ is the second Legendre polynomial.

If we take the ratio of the quadrupolar splittings, $\Delta\tilde{\nu}_1/\Delta\tilde{\nu}_2$, then $S_{zz}$ cancels out leaving $1/P_2(\cos\theta)$, and so this means that the ratio is temperature-independent since $S_{zz}$ is a temperature-dependent entity while $P_2(\cos\theta)$ is temperature independent. Therefore, we expect the ratio $\Delta\tilde{\nu}_1/\Delta\tilde{\nu}_2$ to be constant and equal to 8/1 throughout the temperature if θ is 60°.

## 4.9 References

[1] http://www.artchixstudio.com

[2 ] P. D. Bartlett, M. J. Ryan, and S. G. Cohen, *J. Am. Chem. Soc.*, **64**, 2649 (1942).

[3] T. M. Long, PhD. Thesis: *Triptycenes as a Molecular Building Block to Introduce Internal Free Volume in Organic Materials*, Massachusettes Institute of Technology, USA (2002).

[4] J. W. Emsley, R. Hashim, G. R. Luckhurst, and G. N. Shilstone, *Liq. Cryst.*, **1**, 437 (1986).

[5] G. N. Shilstone, *PhD. Thesis: A Study of Liquid Crystalline Systems by Deuterium Magnetic Resonance*, University of Southampton, United Kingdom (1986).

[6] S. Fan, *PhD Thesis*: *An Experimental and Theoretical Study of Liquid Crystal Phenomena*, University of Southampton, United Kingdom (1992).

[7] D. M. Ellis, and J. L. Bjorkstam, *J. Chem. Phys.*, **46**, 4460 (1967).

[8] V. D. Neff, *Liquid Crystals & Plastic Crystals Vol. 2: Physico-Chemical Properties and Methods of Investigation*, (Eds. G. W. Gray, P. A. Winsor), Ellis Horwood Limited, Chichester (1974).

[9] T. M. Long, and T. M. Swager, *Adv. Mater.*, **13**, 601 (2001).

[10] J.-S. Yang, T. M. Swager, *J. Am. Chem. Soc.*, **120**, 5321 (1998); *J. Am. Chem. Soc.*, **120**, 11864 (1998).

[11] A. Ferrarini, G. J. Moro, P. L. Nordio, G. R. Luckhurst, *Mol. Phys.*, **77**, 1 (1992).

[12] C. Hague, *MChem Replacement Report,* School of Chemistry, University of Southampton, and Merck Chemicals, Southampton (2004).

[13] J. B. S. Barnhoorn, C. A. de Lange, E. E. Burnell, *Liq. Cryst.*, **13**, 319 (1993).

[14] E. E. Burnell, C. A. de Lange, *Chem. Rev.*, **98**, 2359 (1998).

# Chapter 5

# Liquid Crystal Gels

## 5.1 Introduction

Underneath the tropical sun of Malaysia, indulging in a nice cold dessert is almost heaven. My mother, who enjoys making desserts, has her very own favourite called *agar-agar*, a *Jell-O*-like dessert, only tastier. The main raw ingredient, which is also called agar-agar, is a carbohydrate polymer obtained from a particular form of seaweed; this uncooked agar-agar purchased from the shops usually comes in strips. To make the agar-agar, she would first boil some water before putting the agar-agar strips in it. One must be very careful about putting the right amount of agar-agar, if put too much, one will get a stiff dessert, while too little agar-agar will result in a wobbly dessert! Once the agar-agar strips have dissolved in the boiling water, my mother would stir in some sugar, rose flavouring and red colouring, and sometimes even fruit cocktail and evaporated milk for a relish. Subsequently, she would pour the mixture into a container and set it aside to cool. After some time, in between tending to her other chores, the dessert eventually hardened (or more scientifically, "gelled"). Then, she would chill it in the fridge for a while until it is nice and cold, and serve the agar-agar for our dessert. Apparently, agar-agar is a very simple dessert to a bourgeois family. To put into perspective: the cost of making an agar-agar with fruit cocktail – £2, the cost of writing a PhD Thesis on gels – £ 11, 205 per annum and countless sleepless nights. But the cost of a mother's affection to make her children feel cool and happy – priceless.

The agar-agar dessert is just one of many examples of normal gels. Other household gels include jam, glue, facial cleansing gel and hair styling gel. This Chapter, however, focuses on another dimension of gels, in which we combine liquid crystalline materials with a gelator to form a liquid crystal gel. With the application of deuterium NMR spectroscopy, our aim is to observe how the synergetic coupling of the liquid crystal and the gelator would affect the director alignment. In other

words, we are interested to know whether the gelator does change the properties of the liquid crystal. Our investigation is the first of its kind to be performed *via* deuterium NMR although analogous studies have been made using proton NMR [1].

## 5.2 Gels

### *5.2.1 Normal Gels*

Gels are defined as a two-component system of a semi-solid nature rich in liquid, and have a distinctive property of being highly viscous [2]. They are formed from colloidal suspensions by reducing the solubility of the colloidal material sufficiently so as to enable the particles to link together, forming a weakly solid mass which is distributed uniformly within a dispersion medium [2]. The different modes of reducing the solubility, hence, gelation, are (i) by varying the temperature (commonly cooling), (ii) by the addition of a precipitating liquid, and (iii) by the addition of salts. The first method of gelation *via* cooling is the same process used to prepare the agar-agar dessert. In fact, the process of gelation investigated in this Chapter also falls into this category. The second method of gelation involves a rapid mixing of sufficient precipitant to the sol (shortened from the word *hydrosol*, a colloidal suspension in water), as in the preparation of 'solid alcohol' by rapidly mixing saturated aqueous calcium acetate with a ten-fold excess of alcohol. The third gelation procedure essentially takes place by the addition of one-half of the amount of salts needed for complete precipitation forming thixotropic gels, in which the sol-gel transition occurs *via* mechanical agitation. Although reducing the solubility of the solution will lead to gel formation, it is equally important to ensure that the gelator does not crystallise on cooling in order for the gelation to occur. One way to inhibit the formation of crystals is to introduce chirality in the gelator [3].

Gels can be broadly classified as *chemical gels* and *physical gels*. Chemical gels are formed by the dispersion of covalently cross-linked networks. On the other hand, physical gels are formed *via* non-covalent interactions such as hydrogen bonding.

### 5.2.2 *Liquid Crystal Gels*

So, why is there an interest in liquid crystal gels? The recent upsurge in interest is mainly due to the fact that the phase segregation occurring in liquid crystal gels has led to the formation of materials potentially suitable for electro-optic displays [4]. A well-known example of a phase-segregated structure is polymer-dispersed liquid crystals (PDLCs), in which micron- or submicron-scale droplets of a nematic liquid crystal are dispersed in polymer matrices (20-70wt% of the polymer). However, there are many drawbacks in displays based on PDLCs which include slow reorientation dynamics, lack of homogeneity, and lack of optical clarity displayed by the materials [5]. One way to preserve the fluid nature of the liquid crystal in a single-phase liquid crystal-polymer material is to create a gel [6, 7]. Liquid crystal chemical gels are formed by the dispersion of covalently cross-linked polymeric networks in calamitic liquid crystals. In contrast to PDLCs, the liquid crystal chemical gels have a lower concentration of polymers (< 10wt%). Unfortunately, the liquid crystal chemical gels still do not solve the reorientation dynamics problem caused by the resistance of the polymeric network [7].

The first example of a new class of liquid crystal physical gels was developed by the gelation of a nematic liquid crystal by self-aggregation of low molecular weight molecules such as *trans*-(1*R*,2*R*)-bis(dodecanoylamino)cyclohexane (see Figure 1) as

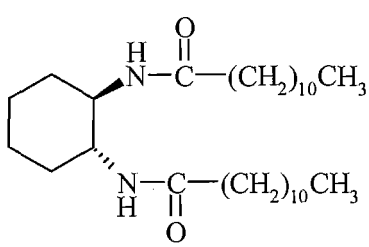

**Figure 1** The molecular structure of the first example of a liquid crystal gelator, *trans*-(1*R*,2*R*)-bis(dodecanoylamino)cyclohexane [8].

the gelator which acts through hydrogen bonding [8]. So far, the gelators used by Kato *et al.* in their studies [8, 9, 10, 11, 12, 13] are amino acid derivatives which are able to form the hydrogen bonds necessary to lower the solubility and to create the fibrous network which traps the liquid crystal host. The surface of the fibrous

network can then pin the director, and this pinning will compete with an applied electric field or magnetic field for the director alignment [14]. It was recently discovered that liquid crystal physical gels have potential applications in display devices [15]. One of the most important phenomena is that the liquid crystalline physical gels exhibit faster electro-optic responses (turn-off) than liquid crystalline components in twisted nematic (TN) cells [15]. In contrast to liquid crystal chemical gels, these physical gels are fabricated by self-assembly processes of hydrogen bonded molecules and they exhibit thermo-reversible structural changes between anisotropic gels and isotropic liquid states. The self-assembled liquid crystalline physical gels consist of low molecular weight liquid crystals and a hydrogen-bonded gelator developed for the gelation of common organic solvents [15]. The resulting anisotropic gels are dynamic soft-solid materials possessing both the properties of liquid crystals and organic physical gels, which do not flow. In these gels, three dimensional fibrous network aggregates of the hydrogen-bonded molecules are formed and dispersed in the liquid crystal. These microphase-separated composite structures contribute to the electro-optic properties of the liquid crystal physical gels.

For the liquid crystal physical gels, there are two types of transitions which occur independently. The first is the liquid crystal gel – normal gel transition induced by the phase transition of the liquid crystals, whereas the second is the sol – gel transition induced by the association and dissociation of the gelator [16]. These two types of phase transitions are observed when they have different transition temperatures. Figure 2 shows the two types of structural changes of liquid crystal physical gels. When the fibrous assembly of a gelator occurs at a temperature higher than the isotropic-anisotropic transition temperature of a liquid crystal, a randomly dispersed fibrous network is formed in the isotropic medium. This phenomenon is depicted in Type I of the phase transition. On the other hand, association of a gelator in a liquid crystalline phase induces the formation of an oriented liquid crystal gel as observed in Type II of the phase transition, whereupon, the liquid crystal serves as a template. The morphologies of the fibres, such as the thickness and the growing directions in liquid crystals, are highly dependent on the combination of the gelators and the liquid crystals [16]. Our gel system falls into the Type I gel.

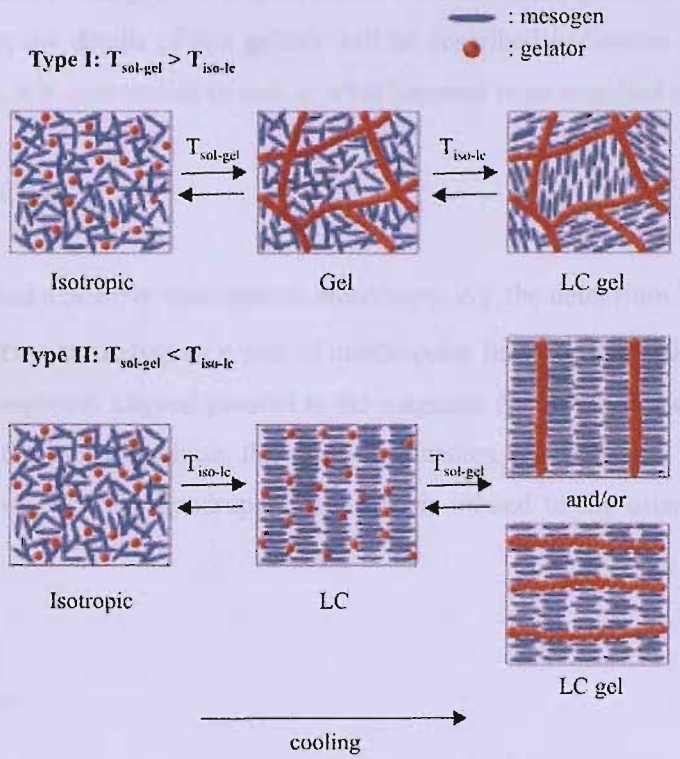


**Figure 2** The two types of structural changes of liquid crystal physical gels [16].

In this research, we wish to investigate whether the gelator can change the orientational order of the liquid crystal, and whether an applied magnetic field can align the director in the gelled liquid crystal. In order to answer these questions, we have employed deuterium NMR spectroscopy as our primary tool of investigation.

## 5.3 Selected Examples

Deuterium NMR spectroscopy is a powerful tool with which to study the orientational order of liquid crystals and their phase transitions. The quadrupolar splitting from deuterons observed in the liquid crystal phase is directly related to the orientational order parameter, $\overline{P}_2$, for the C – D bond. In addition, the quadrupolar splitting is also determined by the angle the director makes with the magnetic field, which is important to investigate the director distribution, and hence the director orientational order. Our investigation involves the gelation of a room temperature nematic liquid crystal, 4-cyano-4′-pentyl-biphenyl (5CB-$d_2$), deuteriated at the α-position of the

hydrocarbon chain. The gelator is of an amino acid derivative given to us by the Kato research group; the details of this gelator will be described in Section 5.4. To begin our discussion, it is appropriate to look at what happens in an ungelled system.

### *5.3.1 Pure 5CB-$d_2$*

Since 5CB-$d_2$ has a positive diamagnetic anisotropy, $\Delta\tilde{\chi}$, the deuterium NMR shows a typical spectrum consisting of a pair of quadrupolar lines for the bulk nematic with the director completely aligned parallel to the magnetic field. When the liquid crystal is heated into the isotropic phase, the splitting vanishes, resulting in a single, narrow peak (see Figure 3). The quadrupolar splitting is related to the orientational order parameter, by

$$\Delta\tilde{\nu}_0 = \frac{3}{2} q_{CD} S_{CD}, \qquad (1)$$

where $q_{CD}$ is the quadrupolar coupling constant, and $S_{CD}$ is the order parameter for the $C-D$ bond. A plot of the temperature dependence of the quadrupolar splitting

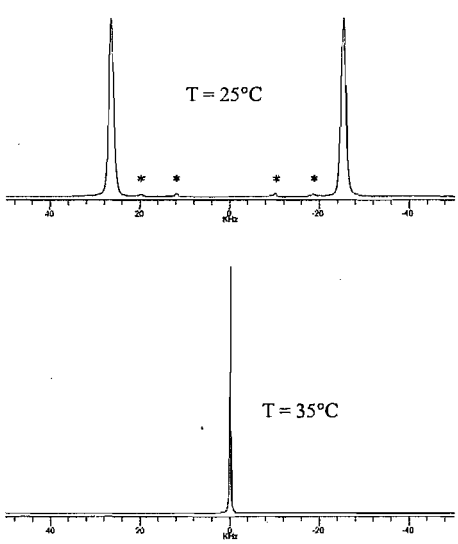


**Figure 3** The deuterium NMR spectra for 5CB-$d_2$ in the nematic phase at 25°C, and in the isotropic phase at 35°C.

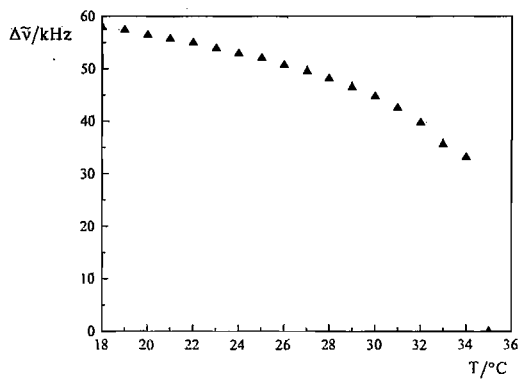


**Figure 4** The dependence of the quadrupolar splitting on temperature for 5CB-$d_2$.

for 5CB-$d_2$ in Figure 4 shows that the splitting decreases with increasing temperature, and vanishes discontinuously at the transition into the isotropic phase. Hence, the N-I transition is a first order phase transition.

On a side note, careful examination of the spectrum in Figure 3 reveals two pairs of extraneous small peaks (marked by the asterisks). In order to discover the origin of these extraneous peaks, we can compare their quadrupolar splittings with that of a perdeuteriated 5CB (*i.e.*, 5CB-$d_{19}$) at 20°C, since these values are available from the study of the deuterium NMR spectrum of 5CB-$d_{19}$ by Luckhurst *et al.* [17]. At 20°C, the quadrupolar splittings for the first extraneous pair in the 5CB-$d_2$ sample is 41.8kHz, while that for the second pair is 24.7kHz. We then compare these values found for 5CB-$d_{19}$. Figure 5 shows the molecular structure and the deuterium NMR spectrum of the 5CB-$d_{19}$ in the nematic phase at 20°C. The seven quadrupolar splittings observed have been assigned to the groups of deuterons of 5CB-$d_{19}$, and this assignment is shown on the peaks according to the labelling indicated on the molecular structure, as seen in Figure 5. Presumably, the outer extraneous pair of peaks existing in our 5CB-$d_2$ spectrum should originate from the C2/C3 deuterons of the 5CB-$d_{19}$ since, in addition, to a comparable quadrupolar splitting, the peaks found in our spectrum appear to be broad indicating that the peaks come from the C2 and C3 deuterons. The inner extraneous pair appears to originate from the C4 deuterons since their quadrupolar splittings are comparable. This phenomenon occurs, presumably, due to the leakage *via* the reduction of the keto – enol isomers.

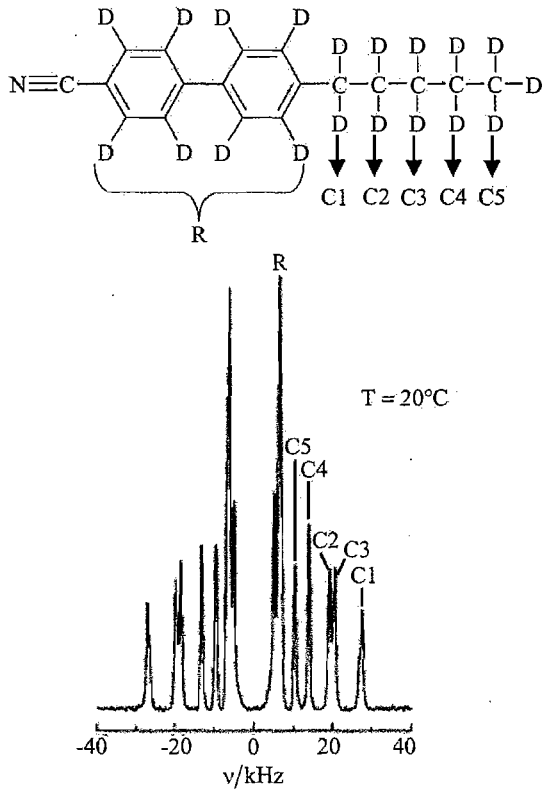


**Figure 5** The molecular structure of 5CB-$d_{19}$ with its deuterium NMR spectrum at 20°C [17].

### *5.3.2 Cylindrically Confined Nematics*

With that as our starting point, we shall look at a well-studied system which will help us understand our results in the gelled 5CB-$d_2$ later in Section 5.5. The system that we shall discuss first is a cylindrically confined nematic. When a liquid crystal is confined to a volume with sub-micron dimensions, a specific director field configuration is obtained, which is the result of the competition between the elastic forces, the strength of the surface interactions, and the size and shape of the confining volume [18]. While the study of the director distribution is crucial, information on the surface roughness of the cavity walls is also important because the molecular orientational order parameter has been shown to depend on surface roughness [19] . It was shown that the degree of orientational order at the surface decreases with increasing surface roughness [19]. In addition, the NMR spectrum is particularly useful in determining the surface-induced liquid crystal alignment within a pore. In

pores where the director is everywhere parallel to the magnetic field, the NMR spectrum shows a pair of lines with a quadrupolar splitting of $\Delta\tilde{\nu}_0$. This would be the case for the cylindrical confinement where the pore axes are oriented parallel to the field and the liquid crystal director is axially (parallel) oriented. If on the other hand, the director is everywhere perpendicular to the magnetic field (a radial director alignment in a cylinder), the spectrum will also consist of two lines, but now separated by $-(1/2)\Delta\tilde{\nu}_0$. If the director is randomly distributed in space, the NMR spectrum is a Pake-type powder pattern with two horns at $\pm(1/4)\Delta\tilde{\nu}_0$ and two shoulders at $\pm(1/2)\Delta\tilde{\nu}_0$. The shoulders are due to those directors that are aligned parallel to the magnetic field, while the horns are due to the regions where the liquid crystal director is perpendicular to the magnetic field. Some examples of liquid crystal director configurations found in cylindrical pores are planar-radial (PR), planar-polar (PP), escaped-radial (ER), and escaped-radial with point defects (ERPD) (see Figure 6). Configurational transitions from one configuration to another can be achieved by changing the surface-liquid crystal interaction, by varying the confining size, or through changes in the elastic constants [20].

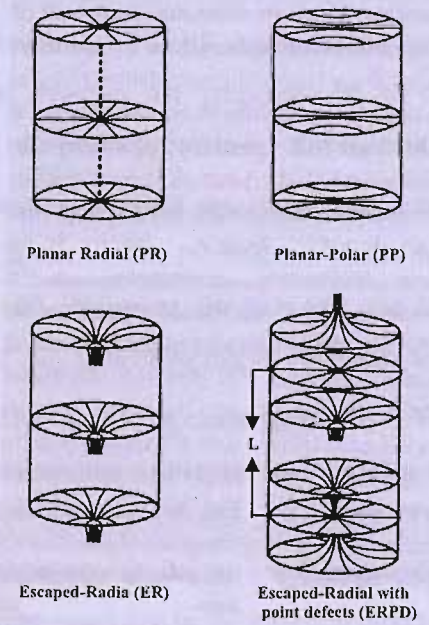


**Figure 6** Examples of the liquid crystal director configurations found in a cylindrical geometry [20].

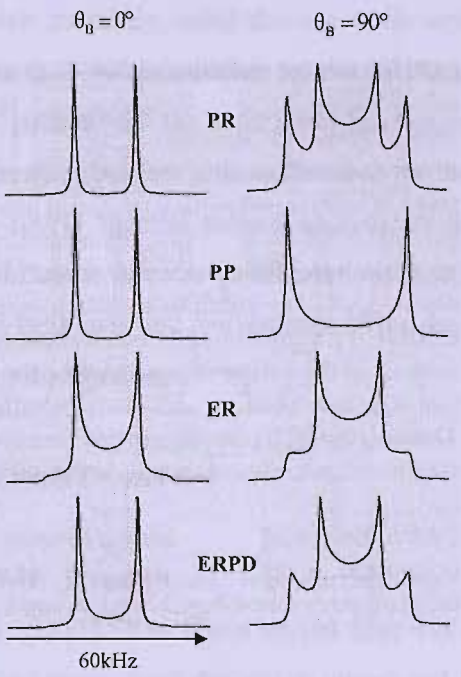


**Figure 7** The deuterium NMR spectra associated with the liquid crystal director configurations depicted in Figure 6. $\theta_B$ represents the angle between the cylindrical pore axis and the applied magnetic field [20].

The deuterium NMR spectra associated with each configuration are shown in Figure 7 for the field parallel and perpendicular to the cylinder axis; the angle between the field and the pore axis is denoted $\theta_B$. The PR configuration for $\theta_B = 0°$ corresponds to a situation where all the directors are perpendicular to the magnetic field. The separation between the two peaks is $(1/2)\Delta\tilde{\nu}_0$. For $\theta_B = 90°$, the result obtained is a classic uniaxial 2D deuterium NMR spectrum indicating that the directors are randomly distributed in a plane. The PP structure yields the same spectral pattern as that of the PR for $\theta_B = 0°$. However, for $\theta_B = 90°$, the NMR obtained is a pair of peaks with a splitting of $\Delta\tilde{\nu}_0$ indicating that the directors are parallel to the magnetic field. The ER structure for $\theta_B = 0°$ is characterized by a 3D uniaxial powder pattern with the shoulders corresponding to the directors parallel to the field and the horns corresponding to the directors perpendicular to the field. The $\theta_B = 90°$ orientation for ER results in a spectral pattern similar to a cylindrical distribution, except for the outer peaks which are suppressed due to the escaping directors along the cylinder axis [21]. The NMR spectra for ERPD are almost like those of the ER structure. However, for $\theta_B = 0°$, the shoulders for the NMR spectrum for ERPD are suppressed due to the

presence of defects which introduce radial domain walls separated by a distance L (see Figure 6) [21]. The $\theta_B = 90°$ orientation for the ERPD yields a spectral pattern similar to the cylindrical pattern with the outer peaks having greater intensity than that found for the ER configuration but less intense than that for the PR configuration. As L becomes larger, the ERPD spectral pattern approaches that of the ER spectral pattern. With these different director configurations producing unique spectral patterns, they emphasize the power and convenience of the deuterium NMR technique to investigate the director distribution.

### *5.3.3 Proton NMR of Liquid Crystal Gel*

Recently, a proton NMR investigation was carried out to study the director distribution in a nematic gel [1]. The liquid crystal host was 8CB, while the gelator was that of the gelator of amino acid derivative introduced by Kato *et al.* [8], the molecular structure of which is shown in Figure 1. Three different concentrations of the gelator were prepared namely 1wt%, 3wt%, and 5wt%. The NMR spectra were measured on a *Bruker MSL 100* spectrometer with a magnetic field of 2.3T.

*Order Parameter Calculation via Variable Temperature Experiment*

*Pure 8CB*

The first set of experiments performed by Li *et al.* [1] was simply a temperature variation run from the isotropic phase into the nematic phase. The dipolar splittings observed are directly related to the molecular orientational order parameters. To begin with, they first carried out a proton NMR experiment on ungelled 8CB. In the isotropic phase, two narrow peaks corresponding to the aromatic and the aliphatic protons were observed. When the temperature was reduced just close to the $T_{NI}$, the spectra showed a sharp central line corresponding to the coexisting isotropic phase and a doublet of broad lines corresponding to the nematic phase. Further cooling of 8CB into the nematic phase and then the smectic A phase resulted in the broader lines with larger splitting. The central part observed (see Figure 8) corresponds to the alkyl chain protons with partially motion-averaged dipolar interactions which are small,

whereas the outer peaks which are approximated by two doublets, weakly resolved, come from the aromatic protons. The order parameter determined is in agreement with known literature data for the pure 8CB [22].

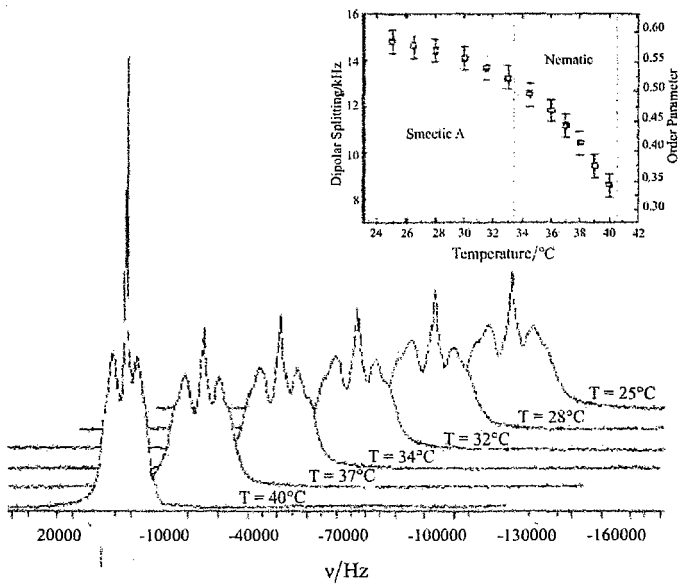


**Figure 8** The proton NMR spectra of pure 8CB at selected temperatures. The inset shows the temperature dependence of the dipolar splitting and the order parameter for the molecular long axis [1].

*Gelled 8CB*

Next, the sample of 8CB was gelled with 5wt% of the amino derivative gelator (see Figure 1). Figure 9 shows the proton NMR at some selected temperatures. The line shape observed indicates a powder pattern corresponding to a random distribution for the director. It was observed that the line shape of the spectra can be fitted extremely well using the same order parameter as for pure 8CB. This suggests that the order parameter changes due to the addition of the gelator are negligibly small at least for the NMR line shape analysis. It was thought that most of the gelator was contained in the network strands after gelation, so that the material contained in the meshes of the network was close to being pure 8CB [1].

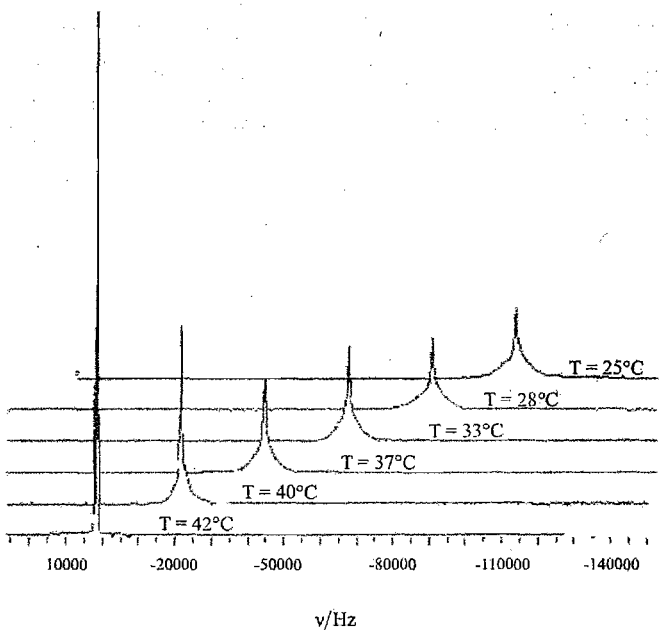


**Figure 9** The proton NMR of 8CB with 5wt% gelator at selected temperatures. The line shape corresponds to a random powder pattern, with the width scaling with the order parameter of pure 8CB [1].

*Director Orientation for the Rotated Sample*

*Pure 8CB*

For pure 8CB, the director alignment in the magnetic field was complete. In addition, the sample was rotated into another orientation away from the magnetic field, the director realigned immediately parallel to the magnetic field of 2.3T.

*Gelled 8CB*

In the gelled system, the experiments were conducted by rotating the sample by different angles, β, away from the magnetic field. For low concentration of the gelator (1wt%), the director tends to align with respect to the magnetic field (since $\Delta\tilde{\chi}$ is positive). Since the coherence length, $\xi_{mag}$, the distance from the surface over which order is maintained by a magnetic field, was smaller than the average dimension of the hydrogen-bonded network meshes, the influence of the network was

insufficient to fix the director over the entire sample, that is far from the network strands. The line shape and splitting corresponds to the director orientation close to $\beta = 0°$, independent of the sample rotation. In other words, although some of the directors were pinned at the surface, most of the directors were actually aligned parallel to the magnetic field as sketched in Figure 10.

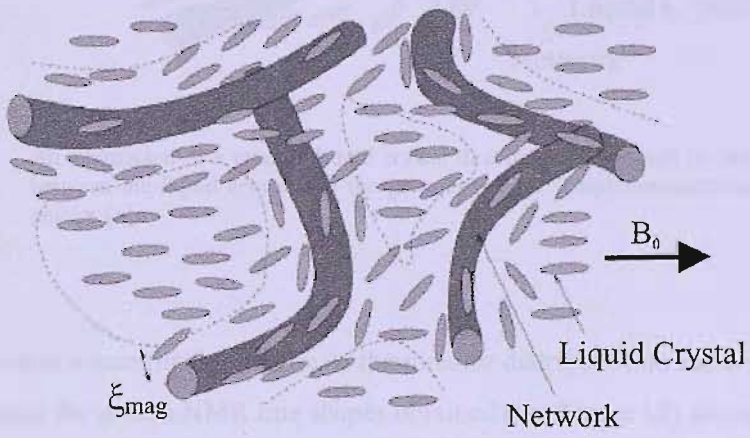


**Figure 10** An illustration of a partially aligned liquid crystal director field in a sufficiently strong applied magnetic field for a low concentration (1wt%) of gelator. The tubes represent aggregates of the gelator fibrils. Close to the network strands, the director orientation remains unaffected by the magnetic field [1].

At a concentration of 3wt% of the gelator, the surface effect seemed to win, causing the alignment of the director parallel to the magnetic field to be incomplete. Now when the sample was rotated at a particular orientation away from the magnetic field, part of the director field realigned, but most remain unchanged. At 5wt% concentration of the gelator, the effect of the network was further strengthened. In this case, the gel network mesh size had become smaller than the magnetic coherence length which caused the director to be almost unaffected by the magnetic field (see Figure 11).

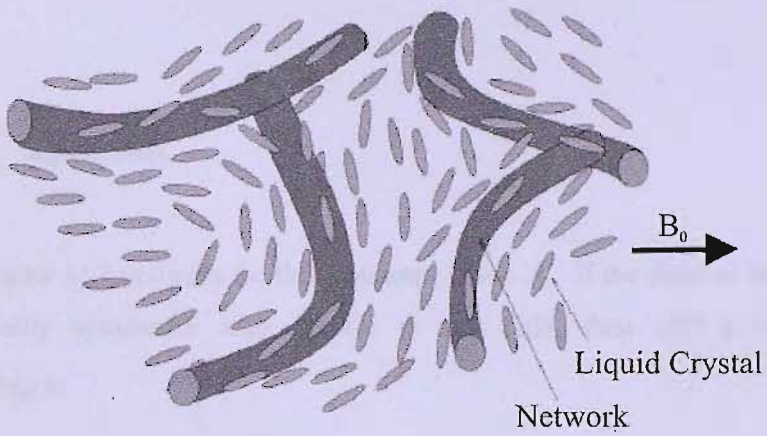


**Figure 11** An illustration of a random liquid crystal director field imposed by the interactions between the liquid crystal and the gel network for a high concentration (5wt%) of gelator [1].

In order to obtain a quantitative picture of the director distribution in the system, Li *et al.* [1] simulated the proton NMR line shapes obtained (see Figure 12) according to

$$F(\nu)=\frac{1}{4\pi}\int_0^{\pi} f_\beta(\nu)\tilde{n}(\beta)\sin\beta d\beta, \qquad (2)$$

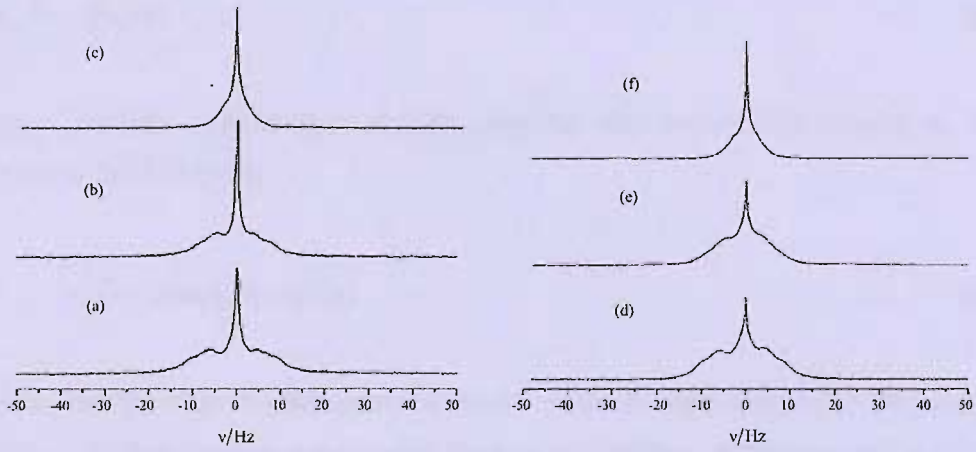


**Figure 12** The measured proton NMR for the orientation, $\beta = 0°$, of the gelled 8CB at 37°C for the concentration of the gelator of (a) 1wt%, (b) 3wt%, and (c) 5wt%. The simulated spectra are given in (d-f) corresponding to the experimental spectra of (a-c) [1].

where $\tilde{n}(\beta)$ is the orientational distribution function for the director in the sample. In addition,

$$n(\beta)=\frac{2}{4\pi}\int_0^{\pi}\tilde{n}(\beta)\sin\beta d\beta, \tag{3}$$

where the factor of 2 accounts for the symmetry $n \leftrightarrow -n$. If the director distribution is cylindrically symmetric with respect to the field, then $n(\beta)$ is related to $\tilde{n}(\beta)$ according to

$$n(\beta)=\sin(\beta)\tilde{n}(\beta). \tag{4}$$

Essentially, the simulation of the line shape was performed by varying the distribution, $n(\beta)$, and by using the lineshape function $f_0(\nu)$ which corresponds to the completely aligned sample when the director order parameter is a unity. Since the influence of $n(\beta)$ was not quite specific to extract $n(\beta)$ unambiguously from a deconvolution of the spectra, some supplementary model distributions [1] were constructed. It was assumed that, the director field consisted of a randomly disordered part

$$n_{dis}=n_{dis}^{(0)}\sin\beta, \tag{5}$$

and a partially ordered part, a Boltzmann-like distribution with respect to the magnetic field direction

$$n_{ord}=n_{ord}^{(0)}\sin\beta\exp\left(-A\cos^2\beta\right), \tag{6}$$

where the parameter A determines the degree of macroscopic alignment. Physically, this distribution function is misleading because for a random distribution this function does not give a constant. Hence, we propose a more appropriate distribution function, given as

$$f(\beta) = Z^{-1} \exp(-A\cos^2\beta), \tag{7}$$

where the normalisation is

$$Z = \int \exp(-A\cos\beta)\sin\beta\, d\beta. \tag{8}$$

The director distributions for the different concentration of the gelator are shown in Figure 13. For A = 0, the distribution function is constant, and for larger A, the distribution function has a maximum at $\beta = 0$, *i.e.*, with the director parallel to the magnetic field. From the experimental spectra and the director distribution determined from them, it is apparent that the concentration of the gelator does affect the liquid crystal director distribution in the samples. The magnetic field distorts the random director distribution, though the director remained fixed close to the network surface. For low concentrations of the gelator (1wt%), the magnetic field seems to win over the surface alignment of the director, that is most of the director moved towards the direction of the field. As the concentration was increased above a critical concentration (~3wt%), the average distance between neighbouring network strings became smaller than the magnetic coherence length and so the influence of the network was strengthened. When the concentration of the gelator was increased to 5wt%, the director orientation was found to be close to the random distribution, as depicted in Figure 13.

### *5.3.4 Deuterium NMR of Liquid Crystal Dispersed Polymer*

For our last example of a gelled system and its study by NMR, we now briefly refer to an investigation of a liquid crystal dispersed polymer (LCDP) performed by Stannarius *et al.* [23]. They have employed deuterium NMR to determine the director distributions in LCDP cells in the presence of a magnetic field of 4.7T. The samples consisted of a nematic liquid crystal mixed with a small amount of a monomer which was then polymerised by UV irradiation. The nematic liquid crystal was a mixture of

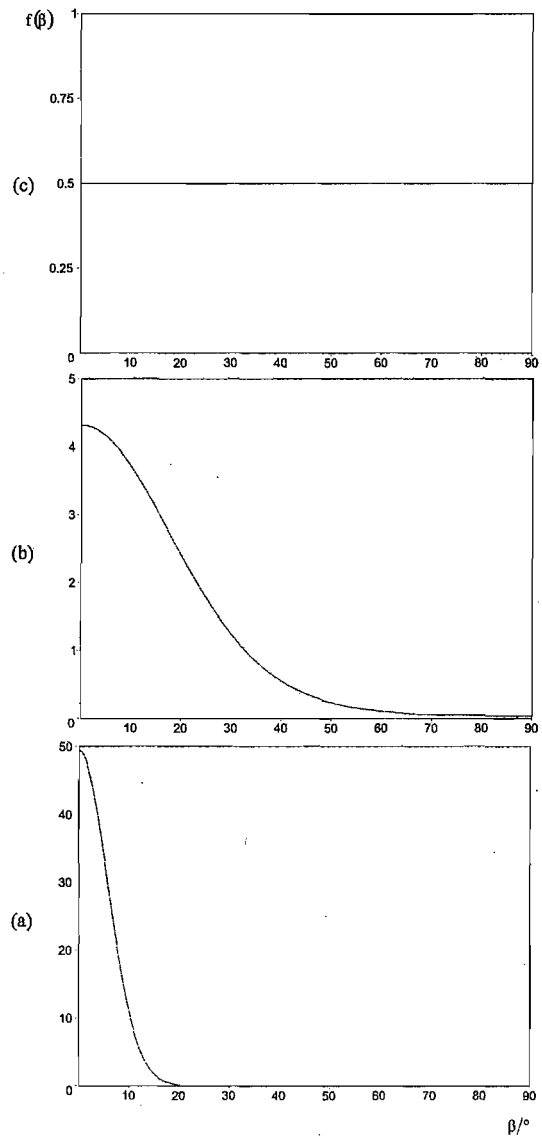


**Figure 13** The distribution function used in the simulation of the proton NMR spectra shown in Figure 12 (a-c). The distributions were calculated using equations (7) and (8) with A as (a) 50, (b) 5, and (c) 0.

50% 5CB and 50% 5OCB-$d_2$ (4-pentyloxy-4′-cyanobiphenyl) deuteriated at the α-position of the pentyl chain. Three different concentrations of the starting monomer were used to prepare the polymer gelled samples, *i.e.*, 1.28wt%, 2.16wt%, and 3.00wt%. The monomer of BAB type (4,4′-bisacryloylbiphenyl, see Figure 14) was used together with 0.5wt% photoinitiator of benzoin methyl ether.

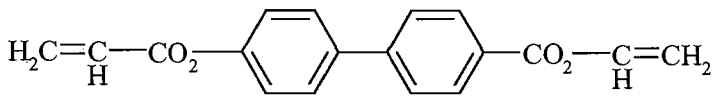

**Figure 14** The molecular structure of 4,4'-bisacryloylbiphenyl.

To summarise their results, they found that the critical amount of the polymer skeleton necessary to pin the director orientations was just ~1wt%. A random distribution of the director could be achieved with ~3wt% of the polymer. For low concentrations of the polymer, the magnetic field seemed to win over the surface effect as expected, while the polymer structure at least retained a random orientation memory in which it is not influenced by the magnetic field. Interestingly, the phase transition was shifted to lower temperatures after the polymerisation for the three concentrations of the samples, in which the measured phase transition shifts were -0.75K, -1.55K, and -2.20K for the 1.28wt%, 2.16wt%, and 3.00wt%, respectively.

With the four selected examples already discussed to provide us some useful background, we will proceed with our experimental study of the gelled 5CB-$d_2$ with deuterium NMR spectroscopy.

## 5.4 Experimental

4-pentyl-4'-cyano-biphenyl, deuteriated at the α-position of the pentyl chain (5CB-$d_2$), was chosen as the liquid crystal host, while the gelator dodecamethylenediamide of N-benzyloxycarbonyl-L-valine ($(ZV)_2$12) (see Figure 15), was used for the preparation of the anisotropic gel. The $(ZV)_2$12 was kindly given to us by Professor Takashi Kato, from the Department of Chemistry and Biotechnology, School of Engineering, University of Tokyo, Japan. The synthesis of $(ZV)_2$12 is described in [24]. The phase transition for the mixture as a function of the concentration of gelator, on cooling, is shown in Figure 16 [11]. From the phase diagram, it is apparent that the transition temperature between the isotropic gel and the nematic gel is almost constant with increasing concentration of the gelator, suggesting that the inherent transition temperature of the liquid crystal does not vary greatly [11]. In contrast, the isotropic-isotropic gel (or sol – gel) transition temperatures increase with increasing concentration of the gelator.

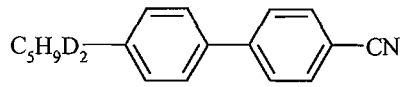


**5CB-$d_2$**

Cr 22.5°C N 35.0°C I

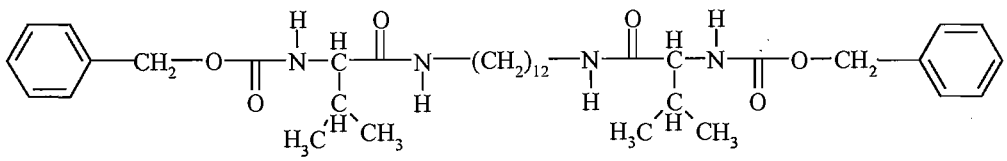

**$(ZV)_2$12**

**Figure 15** The molecular structure of 5CB-$d_2$ and the gelator, $(ZV)_2$12.

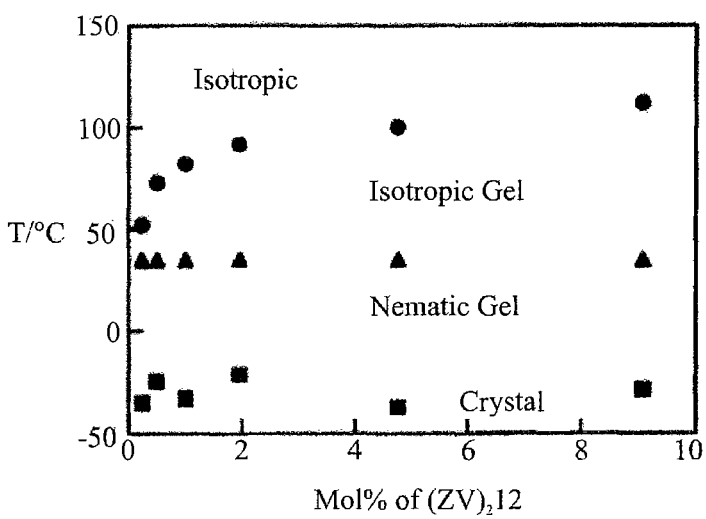


**Figure 16** The phase diagram of 5CB-$d_2$ and the gelator $(ZV)_2$12 [11].

The liquid crystal physical gels were prepared by mixing 5CB-$d_2$ and $(ZV)_2$12 in an NMR tube (5mm in diameter), heating the mixture into the isotropic phase, stirring it mechanically, and subsequently cooling it to the desired temperatures. Three samples with different concentrations of the gelator were prepared, *i.e.*, 0.27mol%, 0.73mol%, and 2.5mol%.

The measurements for the effect of the gelator on the director distribution in the nematic 5CB-$d_2$ were conducted with deuterium NMR spectroscopy using a 300MHz

*Varian Infinity Plus* spectrometer (magnetic strength of 7.5T) with *SPINSIGHT* software for data acquisition and spectral processing. The spectra were recorded using a quadrupolar echo sequence $(\pi/2-\tau_1-\pi/2-\tau_2)$, where $\tau_1$ was 30μs and $\tau_2$ was 42μs, while the length of the $\pi/2$ pulse was 5 $\mu s$ . The temperature was controlled by a thermocouple in the probe head connected to a *Varian* temperature control unit with a stability of 0.1 K over the time needed to obtain a spectrum.

In addition, we also performed an optical study on the gelled systems using optical polarising microscopy in order to complement the NMR results. The phase behaviour of the gelled systems was studied with an *Olympus BH-2* polarising microscope equipped with a *TMS Linkam 90* heating stage using a heating rate of 5°C/min. A thin sample for each concentration of the gel was sandwiched between a glass plate and a glass cover slip. The microscope slide was then mounted on the heating stage between polarisers which are crossed at 90° to each other. Each sample was heated from room temperature up to the desired temperature, and cooled back to room temperature. The snapshots of the optical textures were taken using a *Canon G3 Powershot* digital camera.

## 5.5 Results and Discussion

### *5.5.1 Deuterium NMR Spectroscopy*

Figure 17 shows an overview of the spectra obtained at different temperature for the three different concentrations of the gelator in 5CB-$d_2$. It is apparent from the deuterium NMR spectra that each concentration of the gelator gives a different NMR line shape corresponding to different director distributions. For the lowest concentration of the gelator of 0.27mol%, the deuterium NMR spectral lineshape resembles that for pure 5CB-$d_2$ (see Figure 3), except for the existence of the inner pair of peaks found in the gelled 5CB-$d_2$. In essence, the outer splitting corresponds to the sample with the director parallel to the magnetic field, whereas the inner peaks correspond to the director perpendicular to the field. The ratio of these splittings is found not to be 2:1 as might be expected for a uniaxial nematic and this phenomenon will be addressed shortly. The outer peaks are more pronounced than the inner peaks

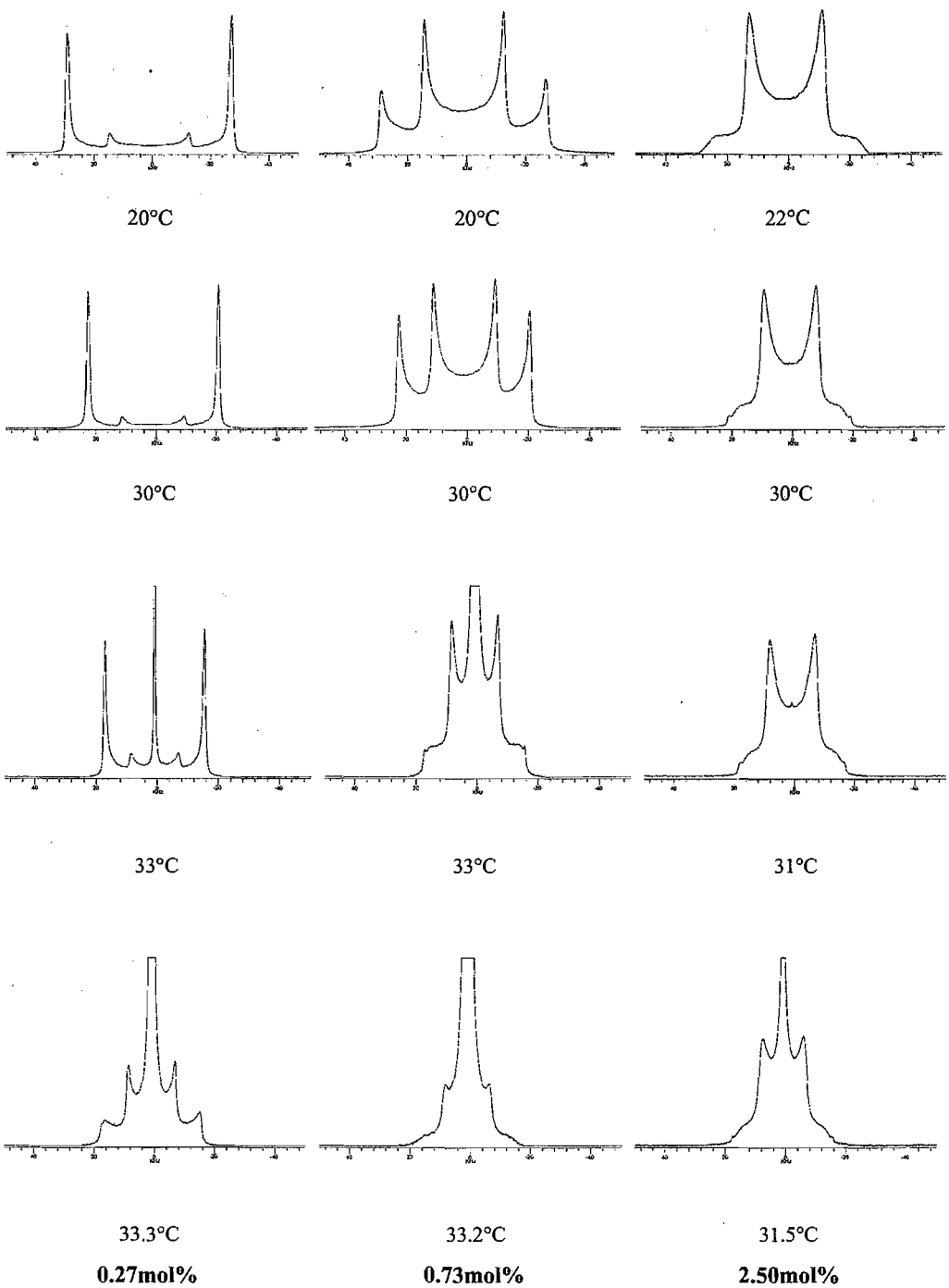


**Figure 17** An overview of the deuterium NMR spectra for the three different concentrations of the $(ZV)_2 12$ gelator in 5CB-$d_2$.

indicating the alignment of the director by the magnetic field. As the temperature is increased, the quadrupolar splittings are reduced, in keeping with the reduction in the orientational order, as seen at 30°C. The spectrum at 33°C shows a central peak from the coexisting isotropic gel present in the nematic gel. At 33.3°C, the intensity of the inner quadrupolar doublet has increased with respect to the outer peaks and the spectrum shows a powder-like feature. In addition, there exists a new pair of peaks at the tip of the outer peaks close to the transition temperature. The origin of these peaks will be discussed later.

The central column in Figure 17 shows the deuterium NMR spectra for an intermediate concentration, of 0.73mol%, gelator in 5CB-$d_2$. The spectral lineshape at 20°C seems to show a powder pattern consistent with a two dimensional director distribution. As we have seen the outer peaks relate to the directors parallel to the magnetic field, the inner peaks correspond to the directors perpendicular by the field. As found in the 0.27mol% gel, the ratio of the quadrupolar splittings for the 0.73mol% gel is also not exactly 2:1. The quadrupolar splitting decreases with increasing temperature. However, in contrast with that for the 0.27mol% concentration of the gel, the spectra from the 0.73mol% gel shows that the inner peaks are more intense than the outer peaks as expected with more of the existence of the gelled nematic. In other words, the director orientation is now more influenced by the surface than by the field interactions. At 33°C, a biphasic region of the isotropic gel phase and the nematic gel phase is observed and there is a major change in the spectral lineshape in which the spectrum now looks more like a powder pattern with a three dimensional distribution of the director. More interestingly, an extra sharp feature is observed at the tip of the outer shoulder of the spectrum, which suggests that the directors corresponding to these new peaks may originate from the bulk nematic aligned parallel to the magnetic field.

For the highest concentration of the gelator, 2.5mol%, the spectral lineshape obtained is a three dimensional powder pattern, with the inner peaks more prominent than the outer shoulders. As observed for the two lower concentrations of the gelators, an increase in temperature results in the reduction of the quadrupolar splittings corresponding to a reduction in the molecular orientational order. At 30°C, a new pair

of peaks appears by the shoulders of the spectrum again as we have seen for the other two samples. This feature is more prominent one degree above at 31°C, where the biphasic region also begins to form. Then at 31.5°C, the isotropic peak becomes dominant, the spectral shoulders become less pronounced and relatively the sharp outer lines are less prominent.

The influence of the magnetic field on the orientation of the liquid crystal dispersed polymer (LCDP) samples by Stannarius *et al.* [23] mentioned earlier in Section 5.3 suggests the assumption of a behaviour similar to a *Fréedericksz transition*, which occurs when there is a competition between the surface elastic and the magnetic forces on the liquid crystal director. In the case of the LCDP, the director orientation is elastically distorted by the magnetic field but remains fixed at the polymer skeleton. While for low concentrations of the polymer, an applied field can easily align the nematic director, above a critical concentration, the average distance between neighbouring polymer strings or clusters becomes smaller than the coherence length corresponding to the field strength. This Fréedericksz-like transition phenomenon seems to also occur in our gelled systems.

We shall consider a highly idealised system, namely, a nematic liquid crystal, confined between two planar surfaces with a spacing, d. In order for the magnetic field to win over the surface alignment, then

$$d > \frac{\pi}{B}\sqrt{\frac{\mu_0 K}{\Delta\tilde{\chi}}}, \tag{9}$$

where B is the magnetic field strength, $\mu_0$ is the permeability of vacuum, K is an average elastic constant, and $\Delta\tilde{\chi}$ is the diamagnetic anisotropy.

On the other hand, for the surface alignment to be dominant over the magnetic field alignment, then

$$d < \frac{\pi}{B}\sqrt{\frac{\mu_0 K}{\Delta\tilde{\chi}}}. \tag{10}$$

Figure 18 shows the temperature dependence of the quadrupolar splittings for the outer peaks for the three different concentrations of the gelled 5CB-$d_2$. For comparison, we have also included the data points for the ungelled 5CB-$d_2$. The first observation from the plots in Figure 18 is that the nematic gel-isotropic gel transition for all the three gels is a first order phase transition in that there is a discontinuous change in the splittings at the transition. In addition, the nematic gel-isotropic gel transition temperature is reduced with increasing concentration of the gelator. The N-I transition temperature for the pure system is 35°C, but this transition is reduced by 1.5°C, 1.6°C and 3.0°C for the gel concentration of 0.27mol%, 0.73mol% and 2.50mol%, respectively. This phenomenon is in accord with that found in the study of liquid crystal dispersed polymer by Stannarius *et al.* [23] as discussed earlier. Our NMR results are also in agreement with our observation from the optical polarising microscopy as we shall discuss later. However, our results are not in accord with the findings by Kato *et al.* as shown in the phase diagram in Figure 16 where the transition temperature from the nematic gel to the isotropic gel is almost constant with increasing concentration of the gelator.

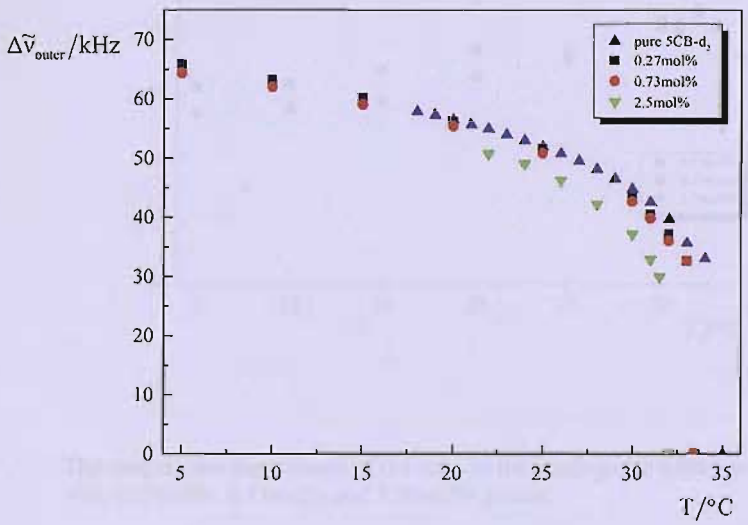


**Figure 18** Temperature dependence of the quadrupolar splittings for the outer peaks in the NMR spectra of 5CB-$d_2$, gelled and ungelled.

For all three different concentrations of the gelator, we observe that on increasing the concentration of the gelator, we observe a change in the spectral pattern showing a

changing director distribution. The results contained in the three dimensional powder pattern spectra found with increasing concentration of the gelator are to be expected. However, what we did not expect is the existence of the new peaks especially apparent close to the transition temperature, *i.e.*, on going from the nematic gel to the isotropic gel. These sharp peaks which gave the largest quadrupolar splitting in the spectra suggest that they correspond to the ungelled bulk nematic in which the director is readily aligned by the magnetic field. This means that for each concentration of the gel, the system actually consists of regions of ungelled nematic, gelled nematic, and near the phase transition, the isotropic gel which is shown by the central single peak shown in Figure 17. Perhaps, this is the fact that the ratio of the quadrupolar splittings is not associated with 2:1 as expected for the uniaxial nematic. The temperature dependence of the ratio of the splittings is shown in Figure 19 and from this it is apparent that the ratio is larger than 2:1.

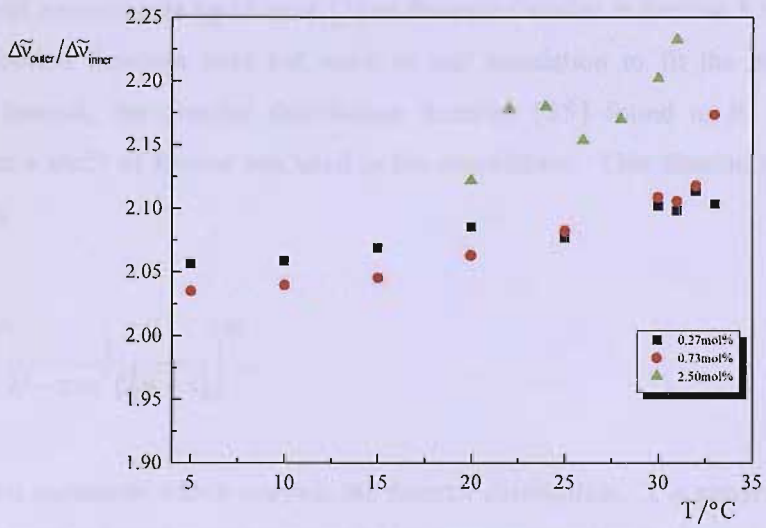


**Figure 19** The temperature dependence of the ratio of the quadrupolar splittings for the systems with 0.27mol%, 0.73mol% and 2.50mol% gelator.

### *5.5.2 Spectral Simulations*

The spectral simulations described in this section were kindly performed by Angela Downing from the University of Southampton.

In order to obtain a quantitative picture of the spectral features that we have observed for the gelled 5CB-$d_2$ samples, that is the director distribution, the unusual ratio of splittings and the sharp spectral features, our experimental spectra have been simulated. To undertake these spectral simulations, we require a functional form for the director distribution function. The molecular distribution function derived in the Maier-Saupe theory of nematics might be assumed to be a good starting point for the director distribution. This would allow us to write the distribution function as

$$f(\beta) = Z^{-1} \exp(-aP_2(\cos\beta)), \tag{11}$$

where Z is the normalisation parameter, $P_2(\cos\beta)$ is the second-rank Legendre polynomial, $\beta$ is the angle between the director and the magnetic field and $a$ is a constant. This distribution function is identical to that used for the spectra in the proton NMR experiments by Li *et al.* [1] as discussed earlier in Section 5.3. However, this distribution function does not work in our simulation to fit the experimental spectra. Instead, the director distribution function [25] found to fit the spectra obtained in a study of Kevlar was used in the simulations. This distribution function is given by

$$f(\beta) = \frac{\lambda^2}{2}\left(\frac{1}{\lambda^2 - \cos^2\beta(\lambda^2 - 1)}\right)^{3/2}, \tag{12}$$

where $\lambda$ is a parameter which controls the director distribution. $\lambda$ is equal to unity for a three dimensional random distribution (zero director order) and at the other extreme, as $\lambda$ tends to infinity, the director is aligned parallel to the magnetic field with $\beta$ tending to zero, and the probability of finding the director orthogonal to the field tends to zero [26]. The director orientational distribution function calculated from Equation (12) for various values of $\lambda$ is shown in Figure 20. In addition, the director order parameter is related to the distribution function by

$$\overline{P}_2^d = \int_0^{\pi} P_2(\cos\beta) f(\beta) \sin\beta \, d\beta, \tag{13}$$

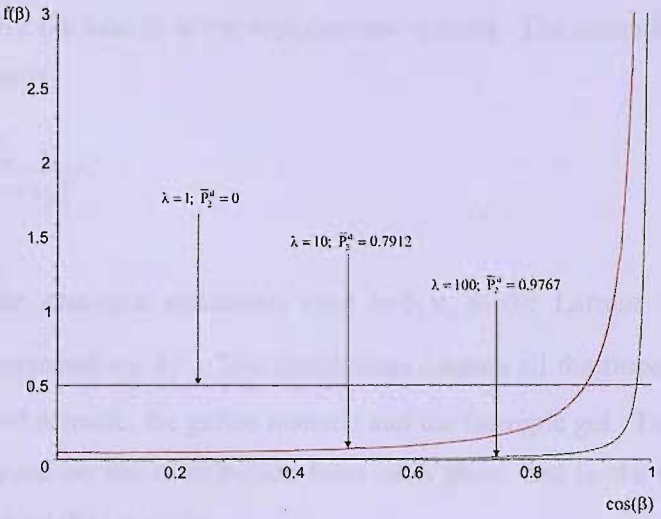


**Figure 20** The director distribution function for a selection of values for λ; associated with each curve is the value of the director orientational order parameter, $\overline{P}_2^d$.

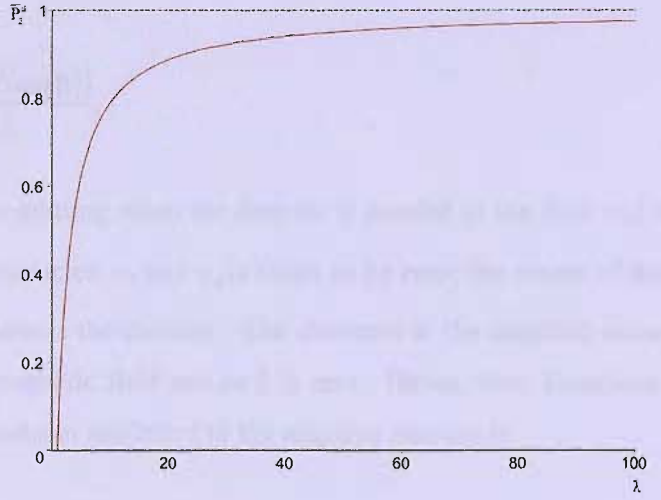


**Figure 21** The relationship between the director orientational order parameter, $\overline{P}_d^2$, and the distribution parameter, λ.

and can be obtained analytically as

$$\overline{P}_2^d = \frac{\lambda^2}{2}\left\{\left(\frac{2\lambda^2+1}{\lambda^2(\lambda^2-1)}\right)-\left(\frac{3arctan(\lambda^2-1)^{1/2}}{(\lambda^2-1)^{3/2}}\right)\right\}. \qquad (14)$$

The influence of λ on the director orientational order parameter, $\overline{P}_2^d$, is featured in Figure 21.

The lineshape employed in our spectral simulations is taken to be Lorentzian because it is found to give the best fit to the experimental spectra. The normalised Lorentzian function is given as

$$L(\nu)=\frac{2T_2}{1+T_2^2(\nu-\nu_0)^2}, \tag{15}$$

where $T_2$ is the spin-spin relaxation time and $\nu_0$ is the Larmor frequency; the linewidth is determined by $T_2^{-1}$. The simulations contain all the three peaks coming from the ungelled nematic, the gelled nematic and the isotropic gel. The intensities of these peaks depend on the contribution from each phase and in the simulation, the contributions are totalled to unity.

The positions of the peaks for the ungelled nematic phase are given by

$$\tilde{\nu}=\nu_0\pm\frac{\Delta\tilde{\nu}_0\left(P_2^d(\cos\beta)\right)}{2}, \tag{16}$$

where $\Delta\tilde{\nu}_0$ is the splitting when the director is parallel to the field and is used to scale the spectral frequencies, $\nu$, and $\nu_0$ is taken to be zero, the centre of the spectrum; the superscript d denotes the director. The directors in the ungelled nematic are aligned parallel to the magnetic field and so $\beta$ is zero. Hence, from Equations (15) and (16), the observed spectrum attributed to the ungelled nematic is

$$U(\nu)=\frac{2\varepsilon}{1+\varepsilon^2(\nu\pm 0.5)^2}, \tag{17}$$

where $\varepsilon$ is the spin-spin relaxation time for the ungelled nematic and the reciprocal of the linewidth of the peaks. This function gives a pair of peaks.

The gelled nematic is represented by

$$G(\nu)=\frac{1}{2}\int_0^{\pi}\frac{2\tau}{1+\tau^2\left(\nu\pm\frac{\left(P_2^d(\cos\beta)\right)}{2}\right)^2}d\cos\beta, \tag{18}$$

where $\tau$ is the spin-spin relaxation time for the gelled nematic and hence, the reciprocal of the linewidth. The factor 1/2 in Equation (18) comes from the distribution function in Equation (12), where $\lambda$ is taken to be 1 to indicate that the distribution of the directors in the gelled nematic is independent of $\beta$ that is the director is randomly distributed in three dimensions.

Finally, the single isotropic peak is given by

$$I(\nu)=\frac{\kappa}{1+\kappa^2\nu^2}, \tag{19}$$

where $\kappa$ is the spin-spin relaxation time and hence, the reciprocal of the linewidth of the isotropic peak.

The simulation is performed by adding these three functions given in Equations (17-19) using the appropriate scaling factor for the contributions from each phase. These scaling factors are $u$ for the ungelled nematic, $g$ for the gelled nematic and $(1-g-u)$ for the isotropic gel, the total of which for the scaling factor is unity, as mentioned earlier. The peaks from each phase do not necessarily have the same linewidths, and from Equations (17-19), we are able to vary these. In addition, since only the gelled nematic changes with $\lambda$, then only Equation (18) will be multiplied by the distribution function given in Equation (12). Earlier, from Figure 19, we found that the ratio of the outer splitting to the inner splitting is not necessarily 2:1; most of the time it is larger. To cater this in our simulation, we have used a value slightly larger than 0.5 used in Equation (17). For example, if the ratio is to be 2.1:1, we would use the value 0.525 instead of 0.5 in Equation (17).

The effect of the gelator on the gelled system can also be observed through the linewidth of the isotropic phase. To demonstrate this phenomenon, Figure 22 shows

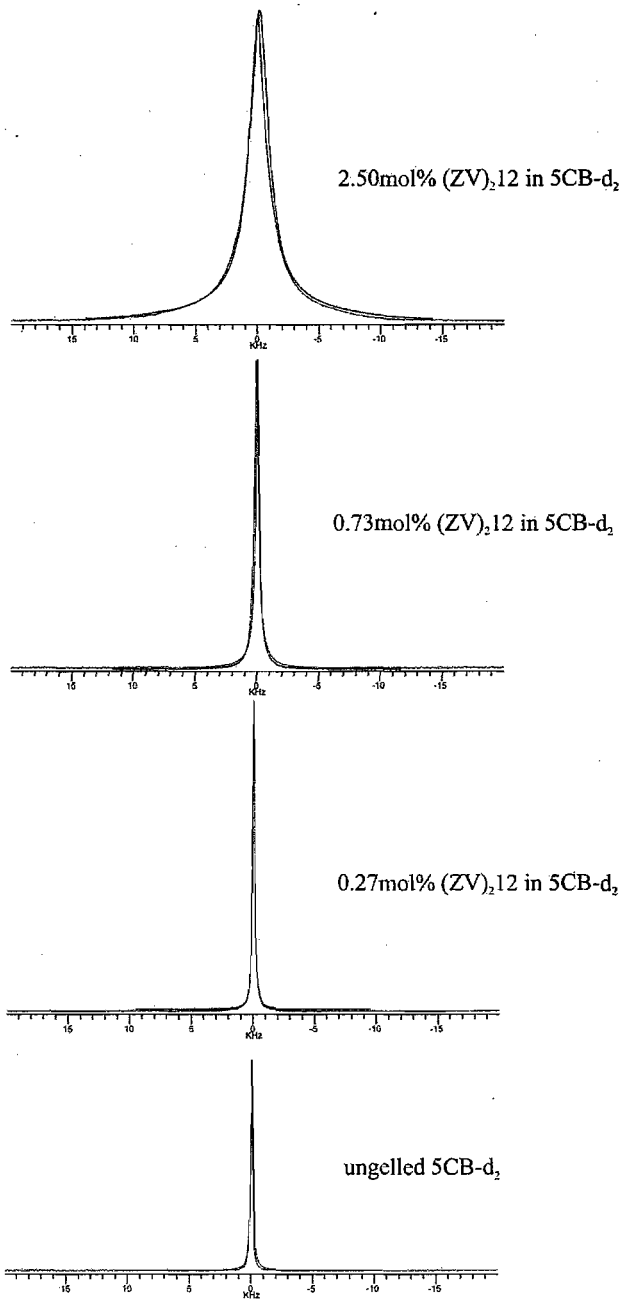


**Figure 22** The deuterium NMR spectra of the isotropic phase for the ungelled 5CB-$d_2$ and for the gelled 5CB-$d_2$. The simulated spectra are shown in blue.

the isotropic spectra for the ungelled 5CB-$d_2$ and the three gelled systems with different concentrations of the gelator together with the simulated spectra. The spectrum for each sample was taken when the system was just in the isotropic phase,

and so, for the gelled systems, this means that the samples were in the isotropic gel phase. The temperatures are 35°C, 33.5°C, 33.4°C and 32°C for the ungelled 5CB-$d_2$, 0.27mol%, 0.73mol% and 2.50mol% concentration of the gel respectively. Clearly, increasing the concentration of the gelator in the system increases the linewidth. In the simulation, the values used for $\kappa$, which is the reciprocal of the linewidth of the isotropic peaks are 95, 90 and 55 for the ungelled 5CB-$d_2$, the 0.27mol% concentration gel and the 0.73mol%, respectively. For the 2.50mol% concentration, the simulation consists not only of the isotropic gel ($\kappa$ =15), but also the ungelled nematic ($u$ = 0.02, $\varepsilon$ = 5) and the gelled nematic ($g$ = 0.2, $\tau$ = 5). This result means that the transition of the isotropic gel to the isotropic phase also increases with the concentration of the gelator, as supported by the phase diagram of Kato *et al.* in Figure 16.

The experimental spectra for the three concentrations of the gel when they are close to the nematic gel-isotropic gel transition were then fitted in order to have a quantitative picture of the director distribution in the gelled systems, in addition to understanding the nature of the new peaks that emerge near the transition temperature. We began with the lowest concentration of the gel, that is 0.27mol% $(ZV)_2 12$ in 5CB-$d_2$. Figure 23 shows the experimental deuterium NMR at some selected temperatures close to the nematic-isotropic transition temperature. The corresponding spectra simulated using the director distribution given by Equation (12) and the appropriate scaling factor for the ungelled nematic, gelled nematic, and isotropic gel, are shown in red. The spectrum at 30°C shows two pairs of peaks, the outer pair represents the ungelled nematic and the inner pair is of the gelled nematic. In fact, the spectrum from the gelled nematic also contains shoulders as well as the inner pair of horns; whereas the horns are readily observed, the shoulders are not. The scaling factor, $g$, attributed to the gelled nematic is slightly higher than that of the ungelled nematic, represented by $u$. This similarity in the weighting factors may appear to be somewhat surprising given that the spectrum is dominated by the outer quadrupolar doublet; however, the area of the powder patter is considerably greater than that for a single quadrupolar doublet. At 32.8°C, the isotropic peak appears in the spectrum, the amount of the

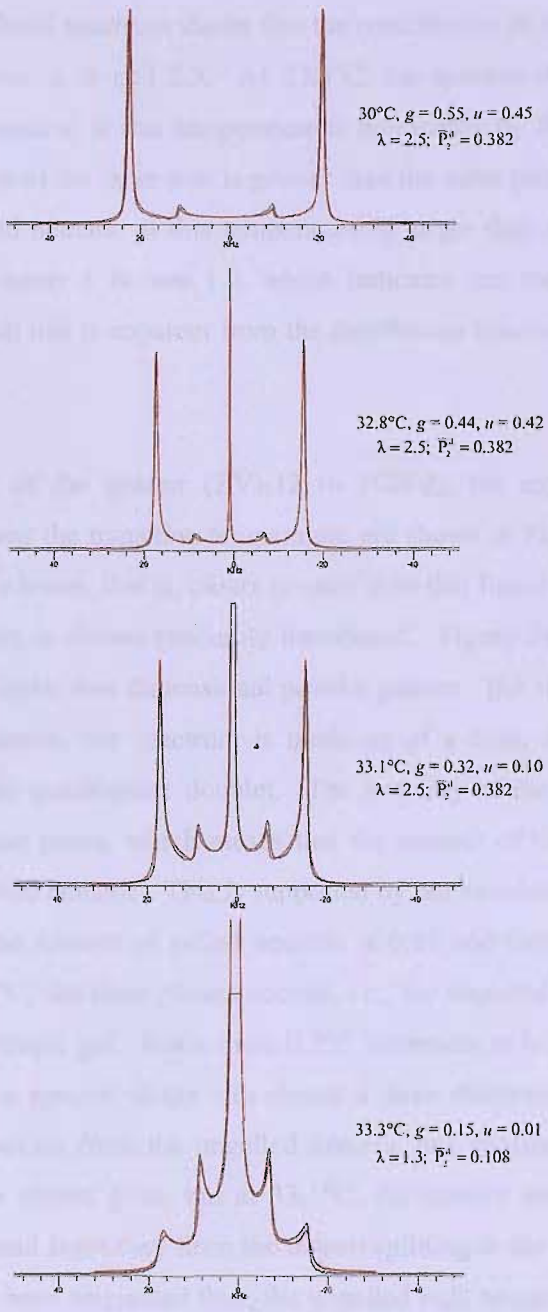


**Figure 23** The deuterium NMR spectra for the system with 0.27mol% $(ZV)_2 12$ in 5CB-$d_2$. The simulated spectra are indicated in red; $g$ represents the scaling factor for the amount of the gelled nematic, $u$ the amount for the ungelled nematic, while $\lambda$ controls the director distribution in the gelled nematic.

ungelled and gelled nematic is almost comparable and the director distribution stays they same as that found at 30°C, where $\lambda$ is 2.5 for the gelled nematic. Increasing the temperature to 33.1°C caused the intensity of the isotropic peak and the inner pair to

increase. The simulated spectrum shows that the contribution of the ungelled nematic is reduced. However, $\lambda$ is still 2.5. At 33.3°C, the spectral shape changes to be powder-like. The system at this temperature is dominated by the isotropic gel. In addition the intensity of the inner pair is greater than the outer pair suggesting that the amount of the gelled nematic at this temperature is larger than that of the ungelled nematic. The parameter $\lambda$ is now 1.3, which indicates that the director is almost randomly distributed; this is apparent from the distribution functions shown in Figure 20.

For the 0.73mol% of the gelator $(ZV)_212$ in 5CB-$d_2$, the experimental and the simulated spectra near the transition temperature are shown in Figure 24. The value of $\lambda$ in this system is lower, that is, closer to unity than that found in the 0.27mol% so that the director here is almost randomly distributed. Figure 24 at 30°C shows an apparently almost classic two dimensional powder pattern. But this is an illusion for as the simulation shows, the spectrum is made up of a three dimensional powder pattern and a simple quadrupolar doublet. The intensity of the inner pair is more intense than the outer peaks, which means that the amount of the gelled nematic is more than the ungelled nematic. This is supported by our simulation, in blue, and the scaling factor for the amount of gelled nematic is 0.91 and that for the ungelled is only 0.09. At 32.7°C, the three phases coexist, *i.e.*, the ungelled nematic, the gelled nematic and the isotropic gel. Just a mere 0.2°C increment in temperature causes an abrupt change in the spectral shape into almost a three dimensional powder pattern because the contribution from the ungelled nematic has vanished. At 32.9°C, the ungelled nematic is almost gone, but at 33.1°C, the relative intensity of the sharp outer peaks grows, and since they form the largest splitting in the spectrum, we argue that the peaks must have originated from the ungelled bulk nematic. The appearance of these sharp outer peaks near the nematic gel-isotropic gel transition was unexpected although may result from a decrease in the intensity of the powder spectrum from the gelled nematic.

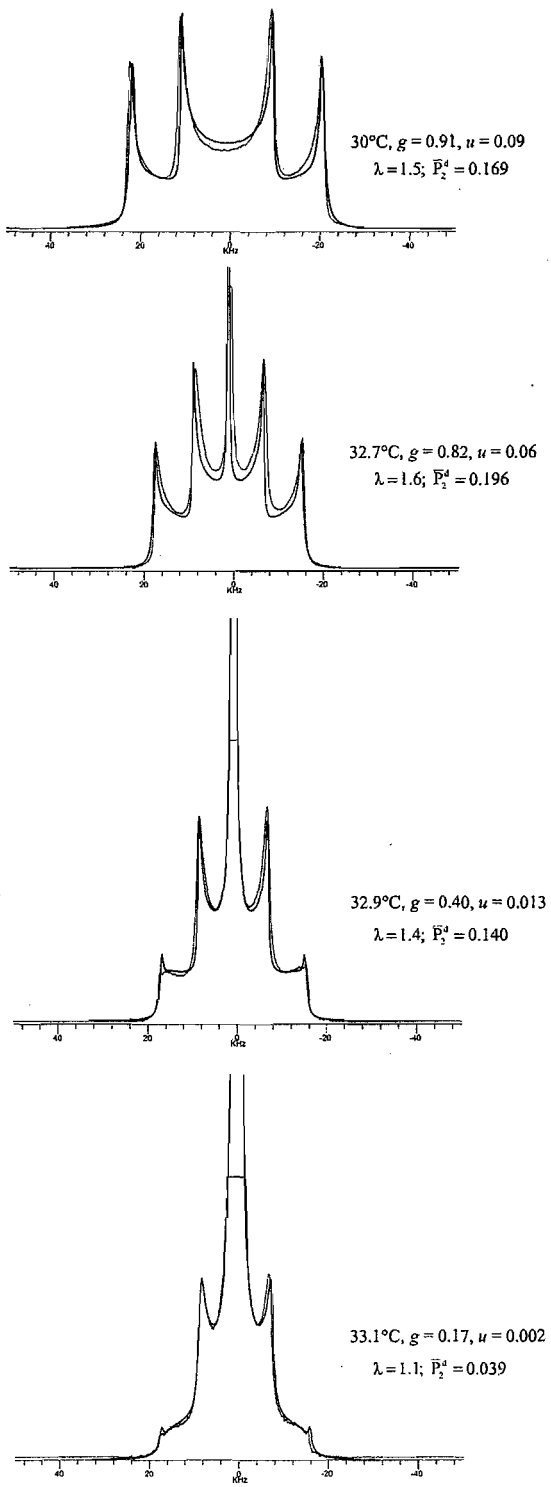


**Figure 24** The deuterium NMR spectra for the system with 0.73mol% $(ZV)_2 12$ in 5CB-$d_2$. The simulated spectra are indicated in blue; $g$ represents the scaling factor for the amount of gelled nematic, $u$ is that for the ungelled nematic, while $\lambda$ controls the director distribution in the gelled nematic.

Figure 25 shows the deuterium NMR spectra for the mixture of 2.50mol% $(ZV)_2 12$ in 5CB-$d_2$ together with the simulated spectra which are shown in green. The value of $\lambda$ used in the simulation is 1.0, suggesting that the director is now randomly distributed

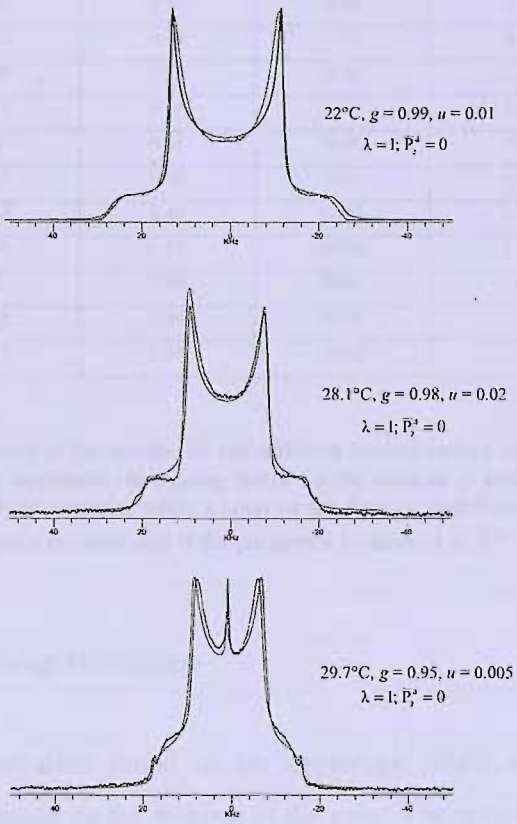


**Figure 25** The deuterium NMR spectra for the system with 2.50mol% $(ZV)_2 12$ in 5CB-$d_2$. The simulated spectra are indicated in green; $g$ represents the scaling factor for the amount of gelled nematic, $u$ is that for the ungelled nematic, while $\lambda$ controls the director distribution in the gelled nematic.

in three dimensions. This is certainly apparent from the spectrum observed at 22°C which shows a three dimensional powder pattern. As expected, the amount of the gelled nematic is more than that of the ungelled nematic and is confirmed by the simulation at the two lower temperatures of 22°C and 28.1°C. At 29.7°C, the isotropic peak begins to appear and the sharp peaks from the bulk nematic also emerge. Interestingly, the appearance of these outer peaks near the phase transition is consistent for the three different concentrations of the gels that we studied.

The results for the three different concentrations of the gelators are summarised in Table 1.

| | Temperature/°C | $g$ | $u$ | $\lambda$ | $\overline{P}_2^d$ |
|---|---|---|---|---|---|
| **0.27mol%** | 30 | 0.55 | 0.45 | 2.5 | 0.382 |
| | 32.8 | 0.44 | 0.42 | 2.5 | 0.382 |
| | 33.1 | 0.32 | 0.10 | 2.5 | 0.382 |
| | 33.3 | 0.15 | 0.01 | 1.3 | 0.108 |
| **0.73mol%** | 30 | 0.91 | 0.09 | 1.5 | 0.169 |
| | 32.7 | 0.82 | 0.06 | 1.6 | 0.196 |
| | 32.9 | 0.40 | 0.013 | 1.4 | 0.140 |
| | 33.1 | 0.17 | 0.002 | 1.1 | 0.039 |
| **2.50mol%** | 22 | 0.99 | 0.01 | 1 | 0 |
| | 28.1 | 0.98 | 0.02 | 1 | 0 |
| | 29.7 | 0.95 | 0.005 | 1 | 0 |

**Table 1** A summary of the results for the different concentrations of the gelator, $(ZV)_2 12$, in which $g$ represents the scaling factor for the amount of gelled nematic, $u$ is that for the ungelled nematic, while $\lambda$ controls the director distribution in the gelled nematic. The director orientational order parameter is denoted as $\overline{P}_2^d$.

### *5.5.3 Optical Polarising Microscopy*

To support our observation found in the deuterium NMR study, we have also conducted an optical study on the textures of the gels. The optical study is important, for example, to support the NMR results of the disappearance of the ungelled nematic before the gelled nematic. We begin our discussion with a brief background on this technique and on the textures and defects shown by a nematic phase, since 5CB-$d_2$ shows only a nematic phase.

The manner in which the directors are arranged within the phase can be detected by careful analysis of the macroscopic "defect" texture. Since the polarisers in the microscope are crossed at 90° to each other, then with no sample in place, light is extinguished and so the sample is black. Similarly, if an isotropic liquid is studied, the polarised light remains unaffected by the isotropic sample, and so no light passes through the analyser. However, when an anisotropic, birefringent sample is present, light is not extinguished, and an optical texture appears which gives information

relating to the arrangement of the directors within the sample. When studying mesophases by this optical technique, the texture observed depends upon how the sample is aligned, in addition to being dependent upon the phase structure of the sample [27].

There are two extreme forms of alignment for liquid crystals: *homeotropic* and *uniform planar*. Homeotropic alignment is where the directors that constitute the phase structure are oriented such that they are normal to the supporting substrate. When the director is so oriented, polarised light is unaffected by the material, hence light cannot pass through the analyser, resulting in complete blackness. In a uniform planar alignment, the constituent directors of the liquid crystal phase are oriented parallel to the supporting substrates. A thin film of liquid crystal phase exhibits birefringence and a coloured texture results when viewed between the crossed polarisers. However, where the director is in line with either polariser, light is extinguished.

A defect is a region where the director abruptly changes direction in which no specific director can be identified. This line defect is known as a *disclination* and results in a black thread-like feature in the optical texture. They appear black because of the optical extinction caused by the crossed polarisers. For optical extinction to occur, the directors must be aligned in the direction of either the two crossed polarisers. When these disclinations meet at a point, they give rise to *brush defects*, and the most common of which is the four-brush defect [27]. A thin sample of a material in the nematic phase when viewed by optical polarising microscopy is often seen in the homeotropic texture which is optically extinct, and so appears black. However, there may be small areas of a birefringent texture with dark disclinations if the sample is quite thick. Displacement of the cover slip (shearing) induces uniform planar alignment, and produces a temporary birefringent flash. On heating the sample, uniform planar alignment is often induced close to the clearing point, just before the isotropic liquid produces a completely optically extinct texture. It is at this point that the colourful birefringence of the *Schlieren texture* appears.

When cooling from the isotropic liquid, birefringent droplets appear against a black background as the nematic phase is generated in the isotropic matrix. If the sample is

thick enough, these droplets coalesce to give a Schlieren texture which may contain the thread-like defects described earlier. On cooling, the nematic phase comes from the isotropic liquid, and so the texture that results is called a *natural texture*, as opposed to a *paramorphotic texture* which results from the heating or cooling of another anisotropic phase, and often takes characteristics from that preceding phase [27].

*Optical Textures of Pure 5CB-$d_2$*

Figure 26 shows the optical texture of the ungelled 5CB-$d_2$. At 26.9°C, the sample shows regions of homeotropic and uniform planar alignment, although most of the region is actually homeotropic, *i.e.*, the sample should be black. This is because the cyano group of 5CB-$d_2$ prefers to be aligned perpendicular to the glass surface which is made up of the $SiO_2$ chain. As the sample is heated to 33.9°C, we observed the reticulated structure caused by the co-existence of the isotropic and nematic phases. The sample was then heated into the isotropic phase at 35.0°C and then cooled back to room temperature. The Schlieren texture is apparent at 33.3°C and some regions of the sample show Maltese crosses inside some of the droplets while in others there is a circle at the centre of the cross. As the sample was cooled further, most of the sample appeared dark due to the homeotropic director alignment.

26.9°C [N]

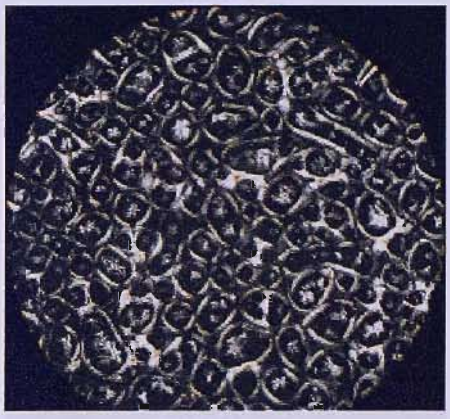

33.9°C [N + I]

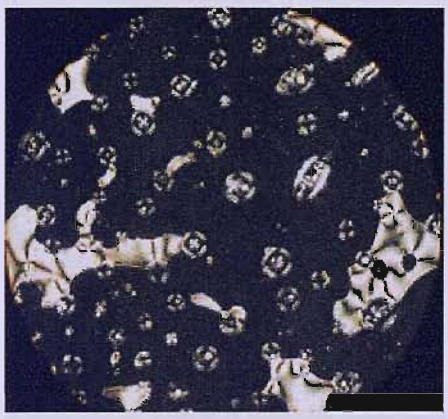

33.3°C [N + I; cooling]

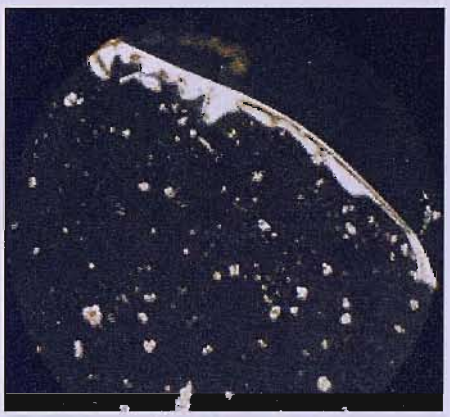

25.4°C [N; cooling]

**Figure 26** The optical textures of 5CB-$d_2$ [x100].

*Optical Textures of 0.27mol% $(ZV)_2 12$ in 5CB-$d_2$*

Figure 27 shows the phase textures of 0.27mol% of $(ZV)_2 12$ in 5CB$d_2$. At 30.1°C, the sample consists of the gel with some pockets of nematic region identified by the coloured region and the black thread-like feature of the Schlieren texture. The Schlieren texture of the nematic phase becomes more apparent when the sample is heated to 31.6°C. At 32.1°C, the nematic phase has gone into the isotropic phase, leaving only the gelled nematic and the isotropic. The gelled nematic looks bright due to the liquid crystal host. At 38.1°C, the isotropic gel also looks bright although less brighter than that found for the gelled nematic; we attribute this birefringence to the fibres that hold the gel together. At 56.1°C, the fibres of the gel begin to melt. The sample is heated further, and at 94.9°C, the isotropic gel melts into the isotropic

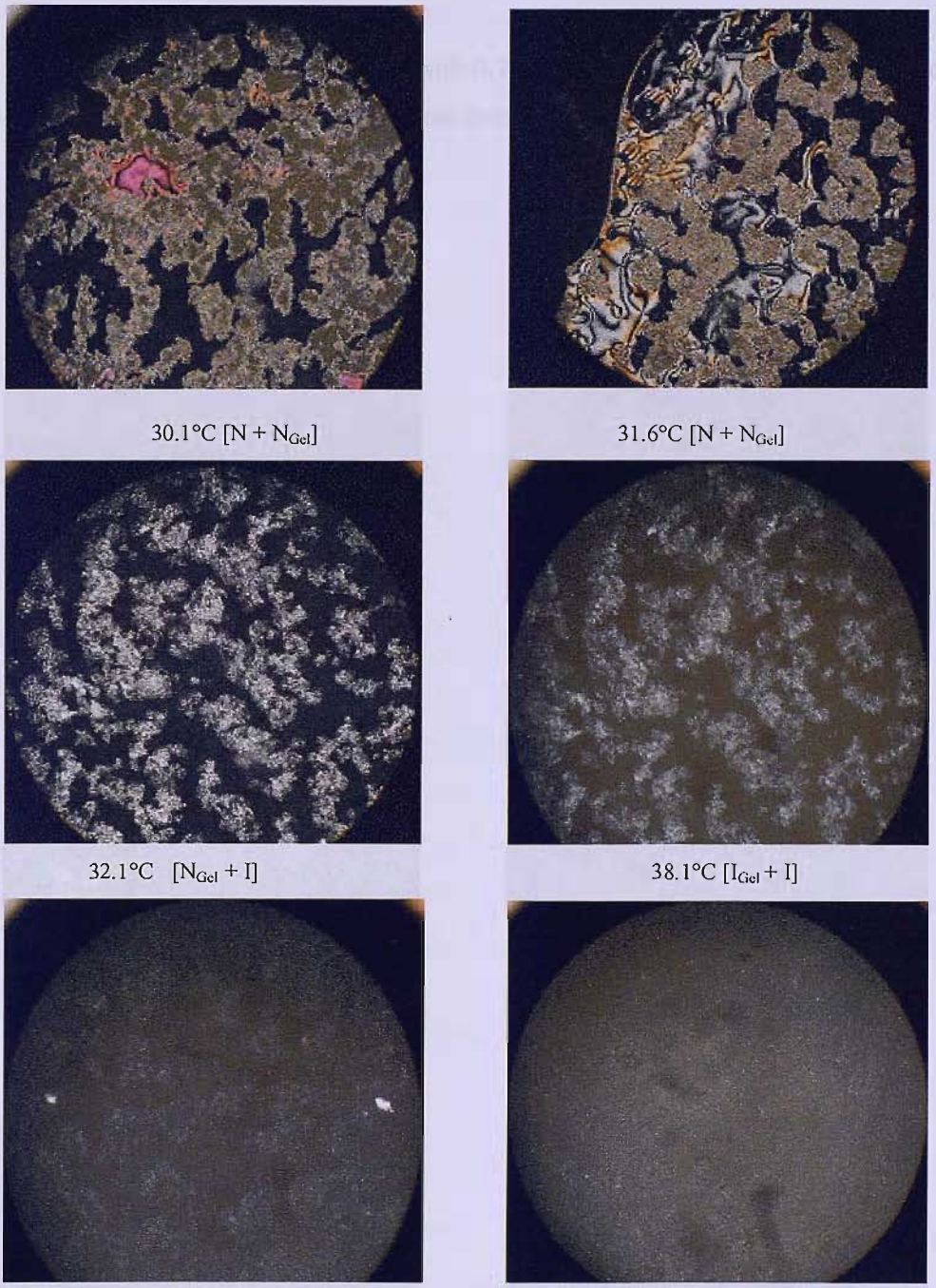


**Figure 27** The optical textures of 0.27mol% of $(ZV)_2 12$ in 5CB-$d_2$ [x100].

phase. This results tally with the NMR results in which we observe that the ungelled nematic melts first into the isotropic before the gelled nematic.

*Optical textures of 0.73mol% $(ZV)_2$12 in 5CB-$d_2$*

The optical textures for the sample with 0.73mol% of $(ZV)_2$12 in 5CB-$d_2$ are shown in Figure 28. At 24.1°C, the gel is more dominant than the nematic; there are only a

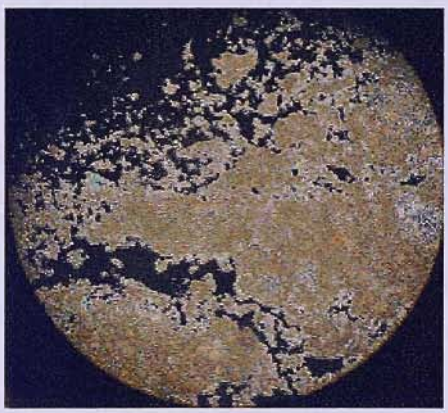

24.1°C [N + $N_{Gel}$]

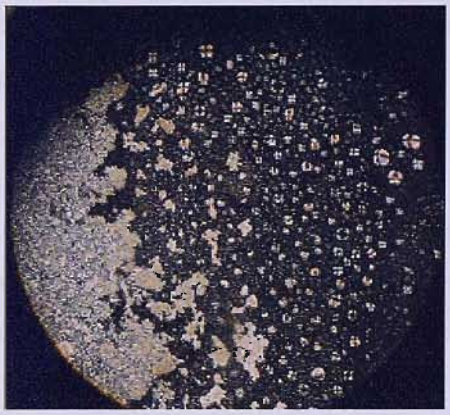

31.8°C [N + I + $N_{Gel}$]

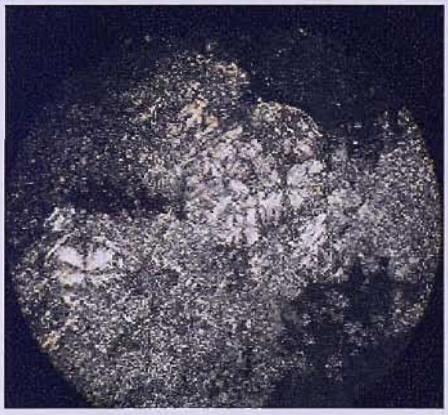

32.4°C [$N_{Gel}$ + I]

75.1°C [$I_{Gel}$]

110°C [$I_{Gel}$]

132.1°C [I]

**Figure 28** The optical textures of 0.73mol% of $(ZV)_2$12 in 5CB-$d_2$ [x100].

small number of nematic pockets in the sample as shown by the coloured regions. At 31.8°C, we can see the four-brush defect of the nematic texture before the sample melts into the isotropic phase. At 32.4°C, the ungelled nematic has melted leaving only the gelled nematic and the isotropic. Further heating to 75.1°C causes the gelled nematic to melt into the isotropic gel. As mentioned earlier, the brightness of the isotropic gel texture could be caused by the fibres that hold the gel together. Heating the sample further to 132.1°C melts the isotropic gel into the isotropic phase.

As observed for the 0.27mol% of the gelator, the same trend is observed for this 0.73mol% gelator in which the ungelled nematic goes into the isotropic first before the gelled nematic. The results are comparable with that for the deuterium NMR spectroscopy in which the ungelled nematic peaks disappear first before the gelled nematic peaks.

*Optical Textures of 2.50mol% $(ZV)_2$12 in 5CB-$d_2$*

Figure 29 shows the optical texture of 2.50mol% $(ZV)_2$12 in 5CB-$d_2$. At 25.4°C, the gel is more dominant than the nematic phase. When the sample is heated, the Schlieren texture from the nematic phase appears as observed at 30.9°C, just before it goes into the isotropic phase. At 35.8°C, what remain are the gelled nematic and the isotropic. Heating the sample further causes the gelled nematic to melt into the isotropic gel. At 115.1°C, the sample is still in the isotropic gel phase due to the fibrous texture. Once again, these optical results are comparable with that for the deuterium NMR spectroscopy in which the ungelled nematic peaks vanish before the gelled nematic peaks.

From these optical studies, we observe that each concentration of the $(ZV)_2$12 gelator in 5CB-$d_2$ shows a different $T_{NI}$ for the ungelled nematic. The lowest concentration of $(ZV)_2$12 at 0.27mol% gives a $T_{NI}$ of just above 31.6°C. For the intermediate concentration of $(ZV)_2$12 at 0.73mol%, the $T_{NI}$ is just before 31.8°C (*i.e.* lower than 31.6°C), and for the highest concentration of 2.50mol% of $(ZV)_2$12, $T_{NI}$ occurs just after 30.9°C. Hence, the $T_{NI}$ for all the three gels are shifted from that of the ungelled 5CB-$d_2$, *i.e.*, 33.9°C, from the optical studies shown in Figure 26. The $T_{NI}$ reduces with the increase of the concentration of the $(ZV)_2$12 gelator. This phenomenon is in

accord with that observed by Stannarius *et al.* in the LCDP study [23], as we have discussed earlier in Section 5.3 .

25.4°C [N + $N_{Gel}$]

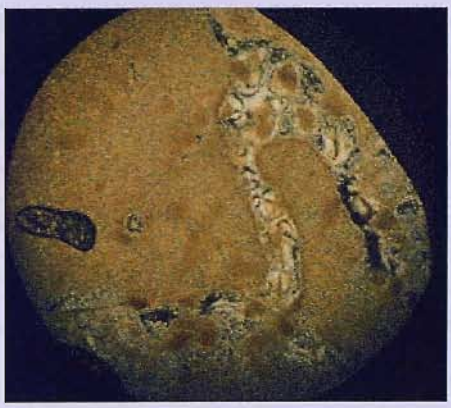

30.9°C [N + $N_{Gel}$]

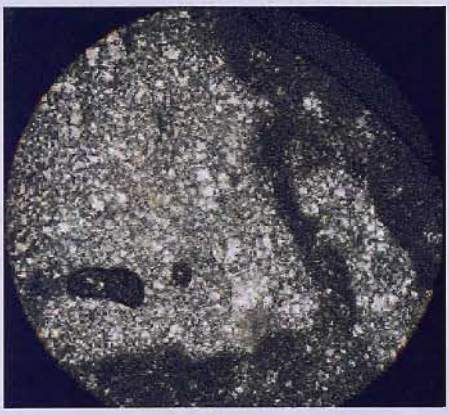

35.8°C [$N_{Gel}$ + I]

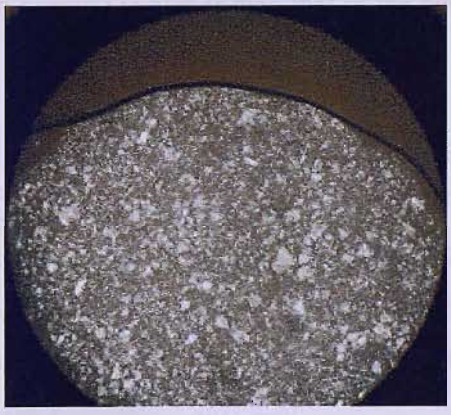

68.3°C [$I_{Gel}$]

104.3°C [$I_{Gel}$]

115.1°C [$I_{Gel}$]

Figure 29 The optical textures of 2.50mol% of $(ZV)_2 12$ in 5CB-$d_2$ [x100].

## 5.6 Conclusions

The deuterium NMR results and spectral simulations have shown that the gelator has affected the director distribution of the liquid crystal host in a magnetic field, and hence the director order parameter. We have observed that at low concentrations of the gelator, the magnetic field and not the surface controls the director alignment, and so the director is aligned essentially parallel to the field. Increasing the concentration of the gelator, with its random surface, causes a random distribution of the director, as we had expected. In addition, we also observed from the NMR spectra that, on increasing the temperature, the peaks attributed to the ungelled nematic disappeared before that of the gelled nematic, and this is consistent with our optical polarising microscopy results. These results are apparently in contrast with the fact that the molecular orientational order for the ungelled nematic is higher than that of the gelled nematic.

We also conclude that the effect of gelation on the director order parameter increases as the concentration of the gelator increases which suggests that the spacing between the fibres decreases. Secondly, with the gelled nematic, the effect of the surface field is to increase the molecular orientational order but just slightly. The deformation of the director in the gelled state with the associated increase in the elastic energy seems to decrease the nematic – isotropic transition temperature.

## 5.7 References


[1] J. Li, D. Geschke, R. Stannarius, *Liq. Cryst.*, **31**, 21 (2004).

[2] A. E. Alexander, P. Johnson, *Colloid Science*, Clarendon Press, Oxford (1949).

[3] A. Aggeli, I. A. Nyrkova, M. Bell, R. Harding, L. Carrick, T. C. B. McLeish, A. N. Semenov, N. Boden, *PNAS*, **98**, 11857 (2001).

[4] T. Kato, *Science*, **295**, 2414 (2002).

[5] M. D. Kempe, N. R. Scruggs, R. Verduzco, J. Lal, J. A. Kornfield, *Nature*, **3**, 177 (2004).

[6] E. M. Terentjev, M. Warner, R. B. Meyer, J. Yamamoto, *Phys. Rev. E*, **60**, 1872 (1999).

[7] C. C. Chang, L. C. Chien, R. B. Meyer, *Phys. Rev. E*, **56**, 595 (1997).

[8] T. Kato, T. Kutsuna, K. Hanabusa, M. Ukon, *Adv. Mater.*, **10**, 606 (1998).

[9] T. Kato, G. Kondo, K. Hanabusa, *Chem. Lett.*, 193 (1998).

[10] N. Mizoshita, T. Kutsuna, K. Hanabusa, T. Kato, *Chem. Commun.*, 781 (1999).

[11] N. Mizoshita, K. Hanabusa, T. Kato, *Adv. Mater.*, **11**, 392 (1999).

[12] N. Mizoshita, T. Kutsuna, K. Hanabusa, T. Kato, *J. Photopol. Sci. and Tech.*, **13**, 307 (2000).

[13] N. Mizoshita, H. Monobe, M. Inoue, M. Ukon, T. Watanabe, Y. Shimizu, K. Hanabusa, T. Kato, *Chem. Commun.*, 428 (2002).

[14] S. Marchant-Lane, *PhD. Thesis: Low Viscosity Nematics: Design of Dopants*, University of Southampton (2004).

[15] N. Mizoshita, K. Hanabusa, T. Kato, *Displays*, **22**, 33 (2001).

[16] T. Kato, N. Mizoshita, K. Kishimoto, *Angew. Chem. Int. Ed.*, **45**, 38 (2006).

[17] G. R. Luckhurst, T. Miyamoto, A. Sugimura, B. A. Timimi, *J. Chem. Phys.*, **116**, 5099 (2002).

[18] G. P. Crawford, L. M. Steele, R. Ondris-Crawford, G. S. Iannacchione, C. J. Yeager, J. W. Doane, D. Finotello, *J. Chem. Phys.*, **96**, 7788 (1992).

[19] R. Barberi, G. Durand, *Phys. Rev. A*, **41**, 2207 (1990).

[20] P. Ukleja, D. Finotello, *Liquid Crystals: Experimental Study of Physical Properties and Phase Transitions*, (Ed. S. Kumar), Cambridge University Press, United Kingdom (2001).

[21] G. P. Crawford, D. W. Allender, J. W. Doane, *Phys. Rev. A*, **45**, 8693 (1992).

[22] P. L. Sherrell, D. A. Crellin, *J. Physique*, **40**, 211 (1979).

[23] R. Stannarius, G. P. Crawford, L. C. Chien, J. W. Doane, *J. Appl. Phys.*, **70**, 135 (1991).

[24] K. Hanabusa, R. Tanaka, M. Suzuki, M. Kimura, H. Shirai, *Adv. Mater.*, **9**, 1095 (1997).

[25] S. M. Fan, G. R. Luckhurst, and S. J. Picken, *J. Chem. Phys.*, **101**, 3255 (1994).

[26] G. R. Luckhurst, *Thin Solid Films*, **509**, 36 (2006).

[27] P. J. Collings, M. Hird, *Introduction to Liquid Crystals: Chemistry and Physics*, Taylor & Francis, London (1997).

# Chapter 6

## Field-Induced Director Alignment in the SmA phase of 8CB

### 6.1 Introduction

Liquid crystal alignment technology, the reorientational behaviour of the director in a nematic phase in response to an electric field, is very important especially for the successful application in electro-optical display devices. One of the key parameters for the selection of a liquid crystal for an electro-optical device is the response time to the switching between states, *i.e.*, from on to off, which is controlled by the electric field, or *vice versa*, determined by the elastic energy and surface alignment, when the liquid crystal is subjected to the new torque [1]. The paramount importance for understanding the molecular and macroscopic origins of the response time has led to a vast amount of research, both theoretical and experimental, concerning the field-induced alignment of the director in a nematic phase [see for example, 2, 3, 4]. In comparison, the field-induced alignment of a smectic A phase is almost like an untold story. The field-induced alignment process of the director in a smectic A phase is more complicated than that in the nematic phase because the coupling between the translational and orientational coordinates of the molecules play a role in the process. The rotation of the director by the field must also induce a flow in the sample if the layers of the smectic A phase are to be retained with the director parallel to the layer normal. This is because the alignment field is not directly involved in the orientation of the layer normal. The alignment of the smectic A phase results directly from the interactions between the molecules which are responsible for the existence of the phase.

This small amount of knowledge concerning the alignment of a smectic A phase by a magnetic field has prompted us to conduct studies on it using time-resolved deuterium NMR spectroscopy. This technique is particularly relevant and useful because it is able to provide the director orientation for a monodomain sample and the director

distribution if the sample is not uniformly aligned. Presented in the following sections, are results and discussions on our NMR experiments for the smectic A phase of 4-octyl-4'-cyanobiphenyl (8CB-$d_2$), which is specifically deuteriated at the α-position of the chain (see Figure 1).

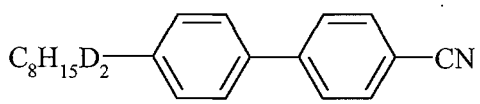


Cr 21.5°C SmA 33.5°C N 40.5°C I

**Figure 1** The molecular structure, phase behaviour and transition temperatures of 8CB-$d_2$.

Since 8CB-$d_2$ has a positive diamagnetic anisotropy, $\Delta\tilde{\chi}$, and a nematic phase, so the directors can first be uniformly aligned in the nematic phase along the magnetic field of the NMR spectrometer. By cooling the nematic phase slowly into the smectic A phase, the alignment produced by the field remains intact so that a monodomain smectic A is produced [5]. The sample is then rotated about an axis perpendicular to field, causing the director to adopt a new orientation, $\beta_0$, and time-resolved deuterium NMR is employed to monitor how the director is aligned back parallel to the field.

The layout for this Chapter is as follows. The next section starts with the objectives of the research. The explanation of the basic theory of deuterium NMR spectroscopy and its important features for the study of field-induced director dynamics are featured in Section 6.3. In Section 6.4, we will review on the previous work on the alignment of smectic A phase related to ours. Section 6.5 describes the experimental set-up for this study. The results and discussion are contained in Section 6.6, while Section 6.7 summarises the research presented.

## 6.2 Objectives

Our experiments and the new results obtained are built on earlier NMR studies and are made possible by the technological advances in the instrumentation, in our case, by using a more advanced spectrometer. Our objective is to extend the previous studies of the field-induced director realignment of the smectic A phase of 8CB-$d_2$

conducted by Emsley *et al.* [5,6]; in their experiments, the deuterium NMR spectra were recorded on a *Bruker MSL200* spectrometer, corresponding to a magnetic field of 4.67T. However, due to the limitation of their spectrometer, the spectral resolution and sensitivity was not good which caused some features of the director dynamics not to be apparent in the spectra. With our state-of-the-art *Varian Infinity Plus 300* NMR spectrometer with its higher field of 7.05T, we are able to observe some significant features in the spectra which were not observed before, presumably because of the higher sensitivity of the present spectrometer. This enables us to investigate the field-induced behaviour of the directors in the realignment process and the temperature dependence of the director dynamics, more convincingly.

A series of experiments at different temperatures and initial angles, $\beta_0$, between the director of the sample and the magnetic field, was conducted in order to characterise the dynamics of how the smectic A director is aligned by the field. In addition, the effects of surfaces on the director realignment, *i.e.*, the effect of using a conventional NMR glass tube versus a PTFE tube capped with Kapton discs, which simulates that used in the X-ray experiments [7], are studied. The objective is to compare the results of the surface effect qualitatively.

## 6.3 Theoretical Background

For a set of equivalent deuterons, the deuterium NMR spectrum exhibits a single line in the isotropic phase because the two allowed transitions are degenerate [8]. In a liquid crystal phase, this degeneracy is removed because of the intrinsic long-range orientational order combined with the quadrupolar interaction of the deuterium nuclei (see Chapter 3). For a monodomain sample, where the director is uniformly aligned, the NMR spectrum consists of a single doublet, provided the dipolar interaction is negligible in comparison with the linewidth. When the director makes an angle, $\beta$, with the magnetic field, the quadrupolar splitting, $\Delta\tilde{\nu}$, is given by

$$\Delta\tilde{\nu}_\beta = \Delta\tilde{\nu}_0 P_2(\cos\beta), \qquad (1)$$

where $\Delta\tilde{\nu}_0$ is the splitting when the director is parallel to the magnetic field, and $P_2(\cos\beta)$ is the second Legendre polynomial, that is

$$P_2(\cos\beta)=\frac{3\cos^2\beta-1}{2}. \qquad (2)$$

According to Equations (1) and (2), as the director moves away from being parallel to the field, the splitting should decrease, pass through zero at the magic angle, 54.74°, and then decrease to minus one half of the original splitting, $\Delta\tilde{\nu}_0$, when the director is orthogonal to the magnetic field. Although the quadrupolar splitting changes sign after passing through the magic angle, the sign of the splitting is not directly available from the spectrum. Figure 2 shows the changes in the quadrupolar splitting as a result of the different orientations of the director with respect to the magnetic field [8].

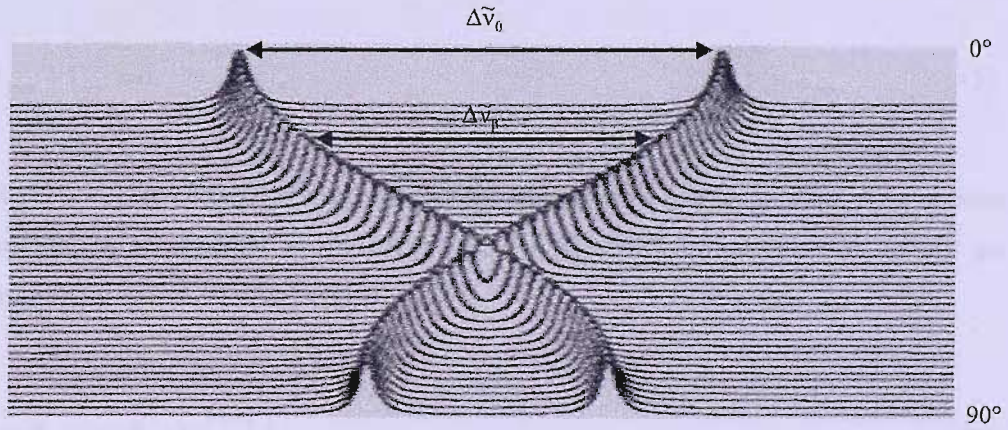


**Figure 2** The simulated dependence of the deuterium NMR spectrum for a single deuteron on β, the angle between the director and the magnetic field [8].

As mentioned in the Section 6.1, the field-induced dynamics for a nematic phase are well-known both theoretically and experimentally, and so, we shall outline the major outcomes of the studies of the nematic phase in order to provide a framework for our investigation on the SmA phase. The behaviour of the director in the nematic phase and the SmA is expected to be comparable since the SmA-N transition for 8CB is second order, at least within the vicinity of the transition [7]. In the monodomain

nematic, if the director is at an angle, $\beta$, to the magnetic field, provided that $\Delta\tilde{\chi}$ is positive and there are no surface effects, the directors are pulled towards the field by the magnetic torque, $\Gamma_{mag}$,

$$\Gamma_{mag} = -\frac{1}{2}\Delta\tilde{\chi}B^2\mu_0^{-1}\sin 2\beta, \tag{3}$$

which is resisted by the viscous torque, $\Gamma_{vis}$,

$$\Gamma_{vis} = \gamma_1\frac{d\beta}{dt}. \tag{4}$$

Here, B is the magnetic flux density, $\mu_0$ is the magnetic constant, and $\gamma_1$ is the rotational viscosity coefficient. When the torques are balanced [9, 10],

$$\Gamma_{mag} + \Gamma_{vis} = 0. \tag{5}$$

Here, it is assumed that the inertial and the elastic terms can be ignored. The director orientation is obtained by the integration of this differential equation giving the solution

$$\tan\beta_t = \tan\beta_0 \exp\left(\frac{-t}{\tau}\right), \tag{6}$$

where the field-induced relaxation time, $\tau$, is

$$\tau = \frac{\mu_0\gamma_1}{\Delta\tilde{\chi}B^2}. \tag{7}$$

The scaled time, $t^*(\equiv t/\tau)$, dependence predicted by the theory for the director dynamics is shown in Figure 3 for a selection of initial director orientations.

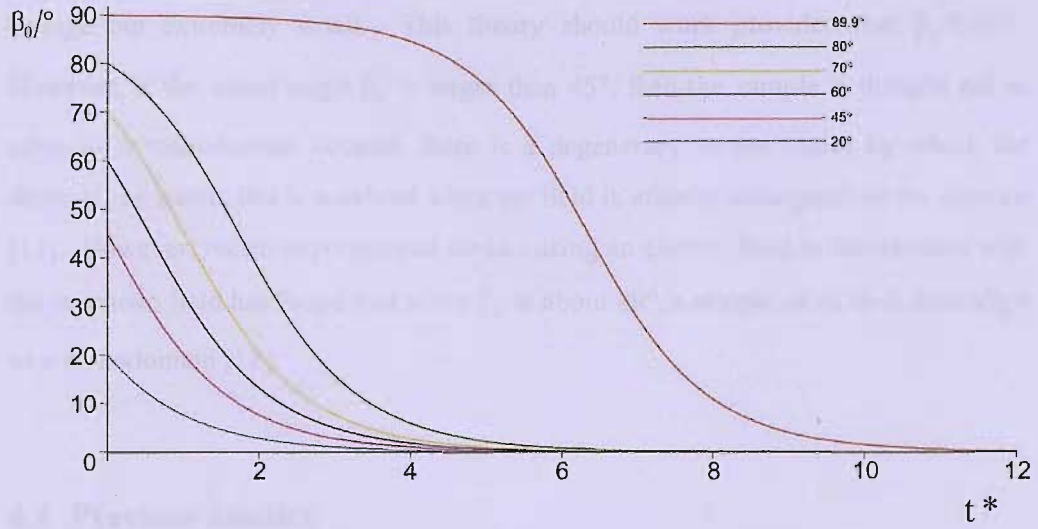


**Figure 3** The time dependence of the director orientation predicted for a nematic phase, where the scaled time, $t^* \equiv t/\tau$, for different initial director orientations, $\beta_0$.

Figure 3 shows that when the initial angle of the director is 20° from the magnetic field, the director reorientation to its equilibrium position, *i.e.*, parallel to the magnetic field, is predicted to start immediately. When the initial angle is 45°, the director also starts to align immediately parallel to the magnetic field, but with a greater initial rate. This change in the rate is given by the general expression for the initial rate obtained from the torque-balance equation in Equation (5) as

$$\left(\frac{d\beta}{dt^*}\right)_{t^*=0} = -\frac{1}{2}\sin 2\beta_0. \qquad (8)$$

Equation (8) shows that the rate has its maximum value when the initial angle, $\beta_0$, is 45°. For larger $\beta_0$, the rate decreases as evidence from the plot in Figure 3, for example for the initial angle of 89.9°. The value of 90° cannot be used as the initial angle because for this orientation, the magnetic torque vanishes (see Equation (3)), and so the integration of the torque-balance equation is no longer valid. Since the magnetic torque tends to zero as $\beta_0$ tends to 90°, the director orientation changes extremely slowly. This gives the impression that there is an induction period during which the director does not change its orientation but as we have seen, there is a

change but extremely small. This theory should work provided that $\beta_0 \leq 45°$. However, if the initial angle $\beta_0$ is larger than 45°, then the sample is thought not to align as a monodomain because there is a degeneracy in the routes by which the director can move; this is maximal when the field is initially orthogonal to the director [11]. However, recent experimental studies using an electric field in competition with the magnetic field has found that when $\beta_0$ is about 89°, a sample of 8CB-$d_2$ does align as a monodomain [12].

## 6.4 Previous Studies

### *6.4.1 Field-Induced Director Dynamics of SmA for $\beta_0 \leq 45°$ and $\beta_0 \approx 90°$*

As mentioned in Section 6.2, the initial investigation of the field-induced alignment of the director in the smectic A phase of 8CB-$d_2$ by Emsley *et al.* [5,6] were carried out on a *Bruker MSL 200* spectrometer, with a magnetic field of 4.67T. In these earlier studies [5], a sample of pure 8CB-$d_2$ was first prepared as a monodomain by cooling it slowly from the nematic phase into the smectic A phase. The sample was then rotated mechanically through an angle, $\beta_0$ using a stepper motor. In one experiment, $\beta_0$ was 41°, and in another, $\beta_0$ was 88° (see Figure 4). The field-induced alignment process was then monitored *via* the time-resolved deuterium NMR spectra and it was observed whether the directors had returned to the equilibrium state, *i.e.,* when the directors are parallel to the magnetic field or not. To contribute to the understanding of the alignment process, experiments on the added solute p-xylene-$d_{10}$ in pure 8CB were also carried out and compared with that of the pure 8CB-$d_2$. Doping 8CB with a deuteriated solute and measuring its deuterium NMR spectrum provides an alternative way to monitor the director alignment. Their investigation showed that although qualitatively the behaviour of the solute and the solvent molecules can be described by the same director alignment, using the probe molecule slowed down the alignment process [5]. In their case for the 38° rotation using the probe, even after 15h, the director orientation was still at 15°. On the other hand for the pure system with the

rotation at 41°, after 15h, the director orientation is at 4.6°, suggesting that the alignment process when using the probe was slower [5].

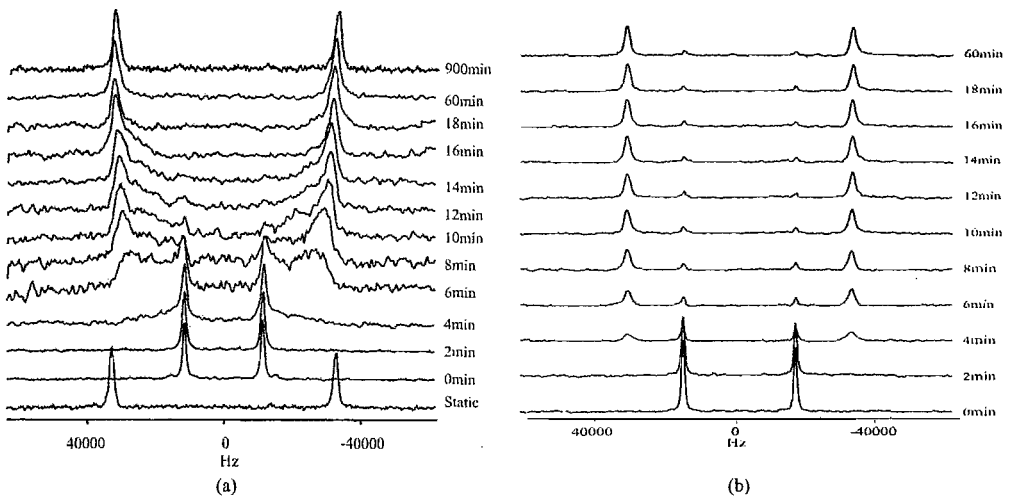


**Figure 4** Deuterium NMR spectra of the smectic A phase of 8CB-$d_2$ at T = 23°C with initial rotation $\beta_0$ of (a) 41° and (b) 88° on the *Bruker MSL 200* spectrometer [5].

Since our experiments only deal with the undoped system, we shall focus only on the results obtained by Emsley *et al.* for pure 8CB-$d_2$ which are relevant to our research. Figure 4 shows the results for the director alignment of the SmA phase of 8CB-$d_2$ when the sample was rotated through 41° and 88° in order to study the dynamics when $\beta_0 \leq 45°$ and when $\beta_0 \approx 90°$. Figure 4a shows that for the 41° rotation experiment, there was an induction period followed by a complex alignment process during which the director adopted a range of orientations before being aligned almost parallel to the field after approximately 1h. It showed that in the alignment process, the directors did not remain parallel, but moved at different rates towards the field direction. However, the sensitivity of the spectrum to a spread in the director orientations was least when $\beta_t$ was close to 0°, and so the values of the quadrupolar splittings and the linewidth alone close to this orientation did not reveal the nature of the distribution with great accuracy. In contrast, the spectrum for the 88° rotation experiment, seen in Figure 4b, showed no intermediate director orientation in between 88° and 0° orientation. Initially, there was an induction period of about 2min before a rapid alignment of a part of the sample having $\beta_t$ close to 0°. After 1h, the alignment process was still incomplete in that not all directors were aligned back to the

equilibrium state; some of the directors remained fixed at the initial 88° orientation, although the intensity of the peaks became weaker with time. The deuterium NMR spectra consisted only of the 0° and 88° orientations and not anything in between, probably because some of the sample had a very broad distribution of directors so that the deuterium signal was dispersed approximately evenly over a frequency range of 65kHz, the splitting close to 0° orientation, and so was too weak to be detected.

### *6.4.2 Surface Effects in the Field-Induced Director Dynamics of SmA Phase*

In another study [6], it was conjectured that some of the features of the director dynamics observed might be caused by the coupling of the smectic phase to the glass surface. As a result, this coupling could cause a frictional torque which could retard the rotation of the SmA sample as a solid body. Hence, the nature of the interface was changed by suspending the smectic A phase as a droplet in an isotropic fluid, in this case glycerol. A single droplet, about 3mm in diameter, was suspended in glycerol contained in a 4mm i.d. NMR tube. This particular medium was chosen because the solubility of 8CB in it is essentially zero and because the difference in density between 8CB and glycerol is small so that the droplet stays suspended.

Just as in the previous experiment, a monodomain SmA sample is also prepared, in this case at 27°C. The sample of the 8CB-$d_2$/glycerol suspension was rotated through 90° by a stepper motor. Due to the high viscosity of glycerol, the smectic droplet rotated through the same angle as the tube. After the sample had been rotated, acquisition of the FID *via* a quadrupolar echo sequence was triggered. The deuterium NMR spectra shown in Figure 5a indicated that the director of the smectic A droplet was aligned by the magnetic field almost as a monodomain, and the time taken to realign the director from orthogonal to parallel to the field was relatively rapid, *i.e.*, 60s. The spectrum also contained a weak central feature which may come from the small quantity of 8CB-$d_2$ dissolved in glycerol. This behaviour was found to be in contrast both quantitatively and qualitatively with that observed when the sample of the SmA was contained in a conventional NMR tube [5]. The time taken for the director for the sample in the tube to be realigned parallel to the magnetic field was ~ 60min (see Figure 5b), which is much longer than the time taken for that when the SmA phase was suspended in glycerol. In addition, the nature of the alignment

process was also different between the two surfaces. For the sample in the tube, there was an induction period of 2min, followed by the realignment process. However, only two sets of doublet were apparent, *i.e.*, that from the 90° orientation, and that of the 0° orientation. Unlike the suspended SmA spectra, the spectra for the SmA sample in the tube did not show any director distribution between the 90° and the 0°. It had been proposed that the intermediate state was not observed in the NMR spectra because there is a broad director distribution [5].

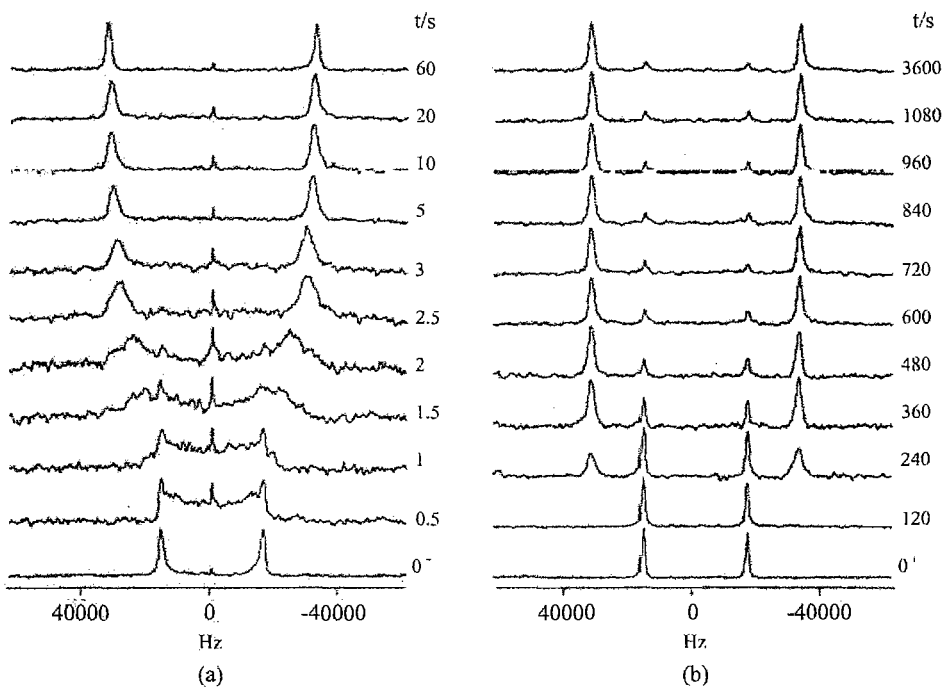


**Figure 5** Deuterium NMR spectra of the smectic A phase of 8CB-$d_2$ following a rotation of $\beta_0 = 90°$ (a) a 3mm droplet suspended in glycerol and (b) a sample contained in a 4mm i.d. glass tube. Both sets of spectra were measured on the *Bruker MSL 200* spectrometer [6].

### *6.4.3 X-ray Diffraction Studies* of *Field-Induced Director Dynamics of SmA Phase*

X-ray experiments to monitor the field-induced alignment of the SmA phase of 8CB [7], were performed to complement the NMR experiments because the NMR technique cannot provide information on the motion of the smectic layers only for the director. This information is important because the alignment process in the SmA

phase involves the director rotation *via* the interaction of the magnetic field and the layer rotation *via* the molecular interactions. Thus a time-resolved X-ray experiment had been conducted using synchrotron radiation to capture the diffraction pattern during the alignment of the smectic layers. The experiment consisted of preparing a monodomain SmA sample by slow cooling from the nematic phase in a magnetic field of 7T as in the NMR experiments. The sample was then turned through an angle about an axis parallel to the X-ray beam direction, but orthogonal to the field. A sequence of 2D small angle X-ray diffraction patterns were then collected at short time intervals. Figure 6 shows a schematic representation of the scattering geometry.

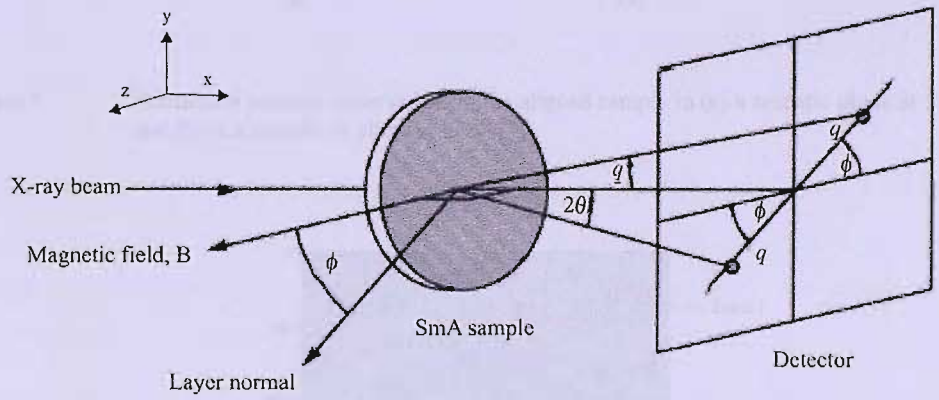


**Figure 6** Schematic representation of the scattering geometry. The X-ray beam is incident along the x-axis and the magnetic field is along the z-axis. $q$ denotes the radial distance on the detector [7].

Typical small-angle scattering patterns obtained from the sample in the nematic and the SmA phases is shown in Figure 7. The figure features the starting point of the rotation experiment with the angle $\phi = 0$. The diffraction patterns of the SmA phase exhibit narrower diffraction maxima than the nematic phase and its diffraction peaks are about six times more intense [7]. We shall only discuss briefly on one experiment from the X-ray work and that is the 66.6° rotation experiment. Figure 8 shows a typical example of a gray-scale plot of the time course of the angle-resolved scattering patterns at a shifted temperature of $\Delta T_{SmA-N} = 2.7°C$, and individual diffraction patterns 50s and 100s following rotation. The plot shows that a brief induction period is followed by an alignment process which involves a return to equilibrium by two pathways, *i.e.*, one corresponding to a decrease in $\phi$, and the other an increase towards

180°. We shall see later that such aligning phenomenon is also observed in our experiments.

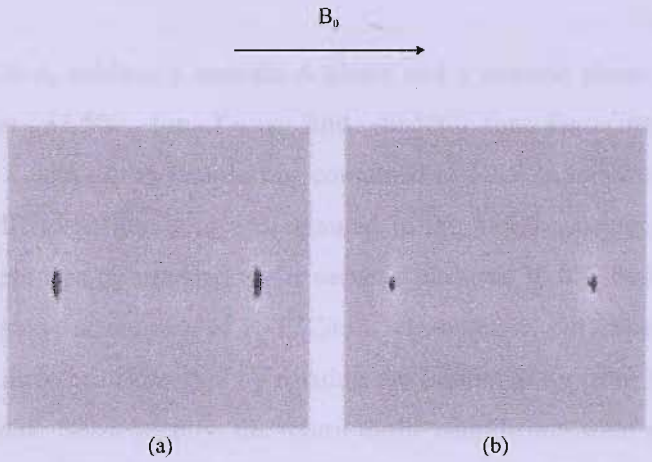


**Figure 7** Diffraction patterns observed from the aligned sample in (a) a nematic phase at 35°C and (b) in a smectic A phase at 32°C [7].

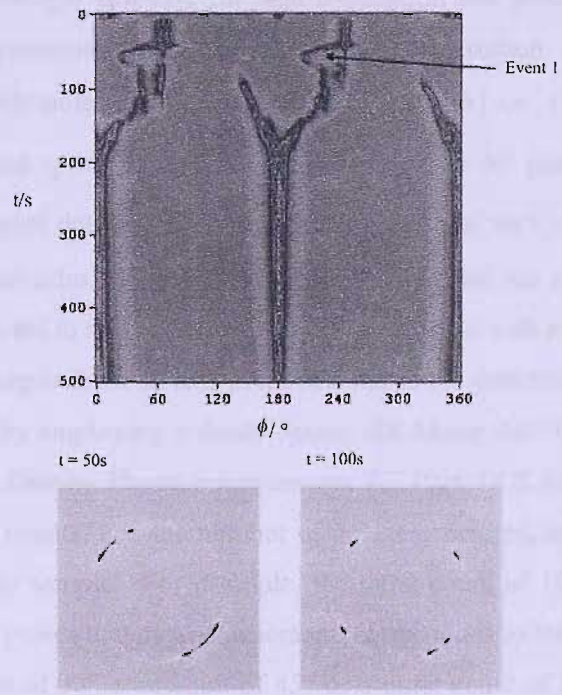


**Figure 8** The time dependence of the angle-resolved intensity of the diffraction maxima during the 66.6° rotation experiment at $\Delta T_{SmA-N} = 2.7°C$. Also shown are the diffraction patterns acquired at 50s and 100s following the rotation. Event 1 indicates the point when the sample reforms after the sample was disordered during the induction period [7].

## 6.5 Experimental

The sample 8CB-$d_2$ exhibits a smectic A phase and a nematic phase, with transition temperatures at 33.5°C for $T_{SmAN}$ and 40.5°C for $T_{NI}$ (literature values). Approximately 1.0cm of the sample was contained in a 3.5cm length of a 5.0mm o.d. 4.0mm i.d. NMR glass tube and was retained in the tube by using a Teflon vortex plug. The sample was first heated to the nematic phase at 36.0°C before cooling it to the smectic A phase at the rate of 10.0°C/min. In essence, our experiment involves creating a new director orientation by rotating the sample away from being parallel to the magnetic field. Subsequently, the return to the equilibrium state with the director uniformly aligned along the field is monitored by recording spectra at discrete time intervals during the director relaxation process.

The deuterium NMR measurements were performed on a *Varian Infinity Plus 300* spectrometer with *Spinsight* software for data acquisition and processing, using the Solaris Operating Environment on a SUN *Microsystem* workstation. The spectra were recorded using a quadrupolar echo sequence [13, 14, 15, 16] *i.e.*, ($90°-\tau_1-90°-\tau_2$), where $\tau_1$ was 48μs and $\tau_2$ was 55μs, while the length of the 90° pulse was 5μs. The values of $\tau_1$ and $\tau_2$ were determined through optimization of each value to achieve a signal at the maximum echo. The temperature was controlled *via* a thermocouple in the probe head connected to a *Varian* temperature control unit with a stability of 0.1K. The rotation of the sample about an axis perpendicular to the direction of the magnetic field was automated by employing a *Radio Spares RS Motor 440-458* stepper motor driver, operated by a *Thurlby Thandar Instruments TG 1010 DDS* function generator. The number of burst counts, *i.e.*, the number of pulses generated, corresponds to the angular rotation of the sample. For example, the burst count of 1000, which is the maximum number of pulses that can be generated, corresponds to the angular rotation of 60°. For a rotation of 90°, a rotation of 45° or a burst count of 750 is performed twice. Hence, the desired rotation is calculated using the direct relationship between the rotation and the number of burst counts. The total time taken for the sample to rotate is within 50-100ms. Subsequently, in our results, we will determine the angle of rotation from the quadrupolar splitting using the relationship in Equation (1). In

order to minimise the difference between the angles through which the director turns and the angle calculated, it is important to ensure that the gears connecting the drive shaft to the NMR sample tube were fully engaged at the start of the experiment. Throughout our analyses of the results, we will also use the quadrupolar splitting to determine the director orientation as the alignment towards the magnetic field progresses.

Using the procedure described, the sample was cooled from the nematic to the smectic A phase and the FID was recorded for different values of $\beta_0$, the initial angle between the director and the direction of the magnetic field. The FIDs were recorded in two arrays, which is a set of experiments, run subsequently one after another, in which each array contained 40 spectra, the maximum value allowed by *Spinsight*. The second array of FIDs was recorded immediately after the first to monitor the final stage of the relaxation process of the directors in the SmA phase. The experiment was repeated for each value of $\beta_0$ to ensure that the results obtained were reproducible, and qualitatively, the spectra and the nature of the alignment were found to be so.

In general, the selected angles are within the range of $45° \leq \beta_0 \leq 90°$. These angles were chosen systematically so as to have a good overview and a wealth of detailed information on the dynamics of how the SmA samples are aligned by the magnetic field, especially when the director is not expected to be uniformly aligned during this process.

As discussed earlier, in the nematic phase, the time dependence predicted for the director dynamics is straightforward, and the field-induced alignment conforms with the Leslie-Ericksen prediction for $\beta_0 \leq 45°$ [3,11]. On the other hand, the analysis of the spectra of a smectic A phase offers a greater challenge because the spectra almost always display an orientational distribution of the directors. This distribution results in line broadening (although there may be other reasons that can contribute to the linewidth [17]) which makes it difficult to determine the quadrupolar splitting. To resolve this, we have set some rules of thumb on how to analyse the spectra, at least semi-quantitatively. We are looking at:

§ the quality of the monodomain (if it is a monodomain) before and after rotation by determining the linewidths of the spectrum;

§ the *induction period* - the time after the rotation of the sample, in which the director does not move.

§ whether, after a long time, the director alignment is complete or not.

§ the effects of the surface on the director realignment, *i.e.*, the effect of using a glass surface versus a PTFE tube capped with Kapton discs [7]. The objective is to compare the results of the surface effect but only qualitatively.

## 6.6 Results and Discussion

### *6.6.1 Rotation by 45°*

*45° rotation at 25°C*

The first set of experiments was a 45° rotation of the sample. At 25°C, prior to the rotation of the sample, $\Delta\tilde{\nu}_0$, the quadrupolar splitting of the initial NMR spectrum was 67.61kHz and the linewidth at half-height was 1.47kHz. The first spectrum recorded after rotation had a quadrupolar splitting of 18.11kHz with a linewidth of 1.05kHz; this reduction in the linewidth was due to the reduction in the dipolar couplings between the deuteron and neighbouring protons. The director orientation determined from the splitting was 44.3° (see Equation (1)). With time, the quadrupolar splitting and hence the angle, β, became smaller signifying that the director had begun to move towards the magnetic field. The spectral changes resulting from the realignment process can be observed in Figure 9. There was an induction period of 37.2s in which the director did not move, and only after this period did the alignment process took place. Some of the directors remained within the vicinity of the 45° orientation. At 102.3s, another quadrupolar doublet of 31.43kHz seemed to be apparent, corresponding to 36.7°. Then at 176.7s, another pair of lines appeared; these had a quadrupolar splitting of 56.64kHz, corresponding to a director orientation with respect to the magnetic field of 17.3°. This observation of several quadrupolar doublets in the NMR spectra at the same time suggests that the

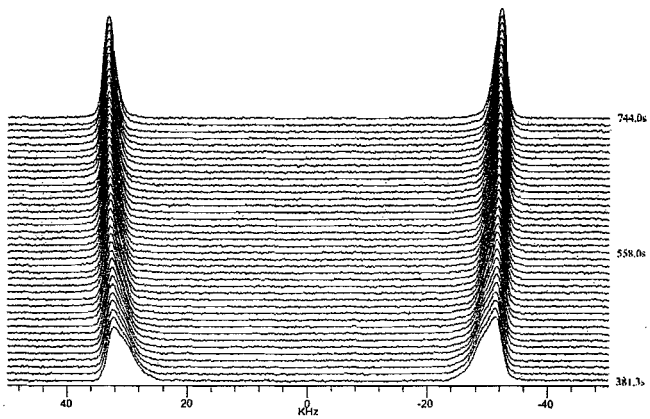


The second array

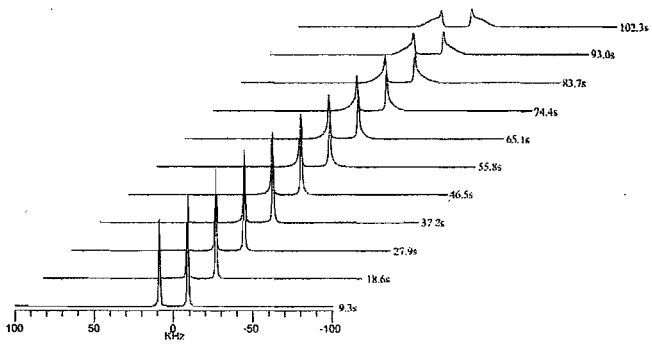


The first eleven spectra

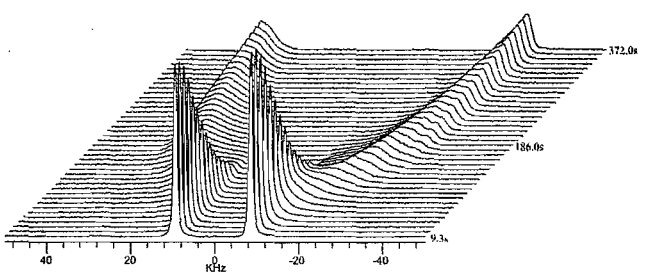


The first array from a different perspective

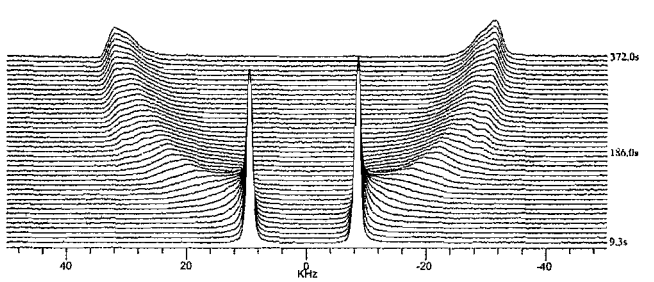


The first array

**Figure 9** Time-resolved deuterium NMR spectra obtained with the array acquisition for a rotation through 45° for 8CB-$d_2$ at 25°C with a time interval of 9.3s between scans.

directors are moving at different rates towards the magnetic field. Ultimately, after the first array of experiments is complete at 372s, the quadrupolar splitting was 63.45kHz, corresponding to a director orientation of 11.7°. The linewidth was 4.87kHz, suggesting the director was spread out. After the second array experiment was complete at 744.0s, the quadrupolar splitting was 65.29kHz, and the linewidth was 2.24kHz. This corresponded to the angle of 8.7° with the magnetic field, and so with time, more of the directors had aligned parallel to the field, although there were still some directors which had not reached their equilibrium state even after 744s. The additional peaks and the increase in the linewidths suggest that the sample does not align strictly as a monodomain. Nonetheless the director distribution is not so broad that it is not possible to determine an average director orientation from the spectra. We shall discuss the time dependence of this later.

*45° rotation at 28°C*

Qualitatively, the alignment process of the director at 28°C was the same as that at 25°C. The difference was that the field-induced director dynamics are faster at 28°C, which is to be expected. Before the rotation of the sample, the quadrupolar splitting was 66.11kHz with a linewidth of 1.38kHz. Upon rotation, the splitting of the first spectrum acquired was 15.57kHz, corresponding to a director orientation with respect to the magnetic field of 45.5°, with a linewidth of 0.86kHz. The induction period was 27.9s, shorter than that found at 25°C. After this time, the director began moving towards the magnetic field, as observed from the spectra shown in Figure 10. Some of the directors remained within the vicinity of the 45° orientation until 102.3s. However, at 83.7s, another quadrupolar doublet was apparent in the spectrum with a splitting of 26.21kHz, corresponding to a director orientation of 34.4°. From this orientation, the director continued moving towards equilibrium position parallel to the magnetic field. For the last spectrum of the first set of array experiments at 372s, the quadrupolar splitting was 64.18kHz, corresponding to a director orientation of 8.0°. The linewidth was 1.56kHz which is close to that observed prior to rotation of the sample. After the second array was completed at 744s, the quadrupolar splitting of the last spectrum was slightly larger at 65.51kHz, corresponding to 4.0°; the linewidth remained at 1.56kHz. Clearly, these values suggest that the director alignment process was faster at 28°C than that at 25°C and so the director was able to approach

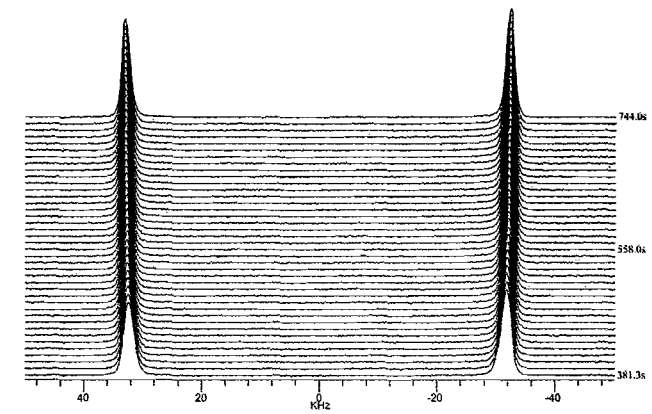


The second array

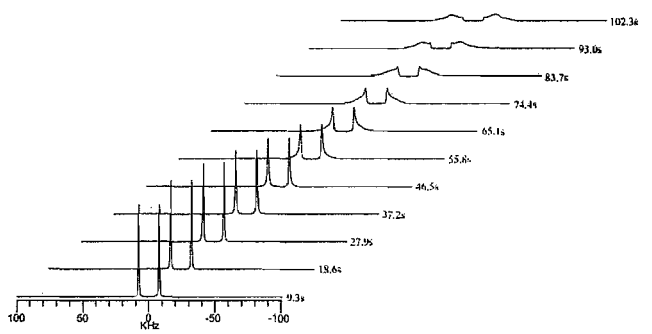


The first eleven spectra

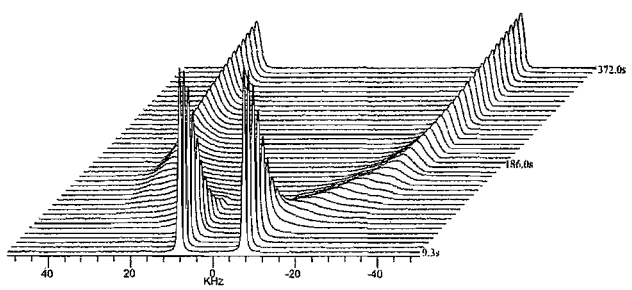


The first array from a different perspective

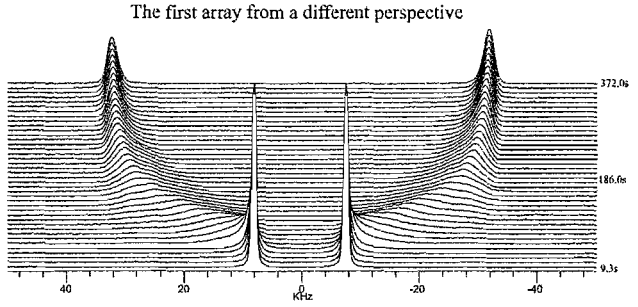


The first array

**Figure 10** Time-resolved deuterium NMR spectra obtained from the array acquisition for a rotation through 45° for 8CB-$d_2$ at 28°C with a time interval of 9.3s between scans.

closer to its equilibrium orientation.

*45° rotation at 30°C*

The same trend of the alignment process was found at 30°C, but with an even faster field-induced director dynamics than that found for the two previous lower temperatures; this increase in the rate of alignment is apparent from the spectra shown in Figure 11. Compared to the two lower temperatures, there was no induction period at 30°C which is perhaps surprising. At the end of the second array of experiments, the quadrupolar splitting was 64.80kHz, corresponding to a director orientation of 1.3°, with a linewidth of 1.41kHz which is comparable to that found prior to the rotation of the sample.

To obtain a more quantitative view of the changes that occur during the field-induced alignment of the director in the SmA of 8CB-$d_2$, we have plotted in Figure 12 the reduced quadrupolar splittings, $\Delta\tilde{\nu}/\Delta\tilde{\nu}_0$, and the director orientation determined from them. The different symbols on the plot represent the different director orientations in the sample. We start with the behaviour observed at the lowest temperature studied, namely 25°C (see Figure 12a). First, there is a period when the director orientation changes by an extremely small amount, suggestive of an induction period which lasts for about 160s. Then a second quadrupolar doublet appears with a splitting which increases with time as the director returns to being parallel to the magnetic field. However, before this can occur, another quadrupolar doublet appears which is closer to being parallel to the field, as indicated by the larger splitting. This behaviour is apparent from the time dependence of the director orientation in a more direct manner from the director orientation. Initially the director is at 45° to the magnetic field and this angle changes slowly. Then the director associated with another part of the sample changes its orientation relatively rapidly and approaches an angle of about 20°. At the same time, the director associated with another region adopts a smaller angle to the field which decreases with increasing time. The angle reaches a value of 10° and it would seem that it would decrease but only very slowly before reaching the limiting value of 0°. Clearly, the director dynamics at this low temperature is somewhat complex.

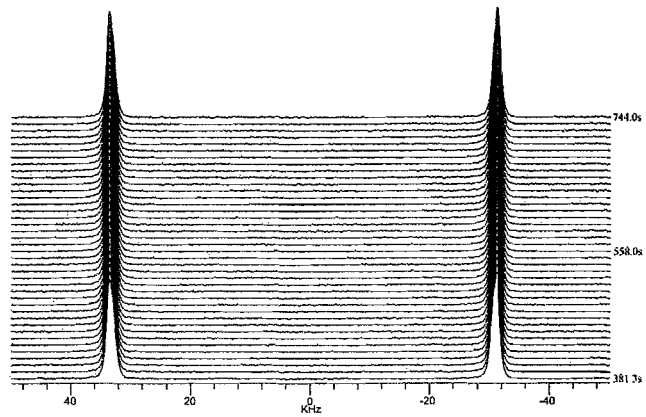


The second array

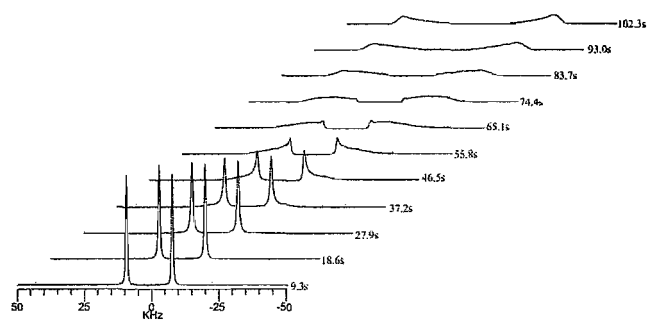


The first eleven spectra

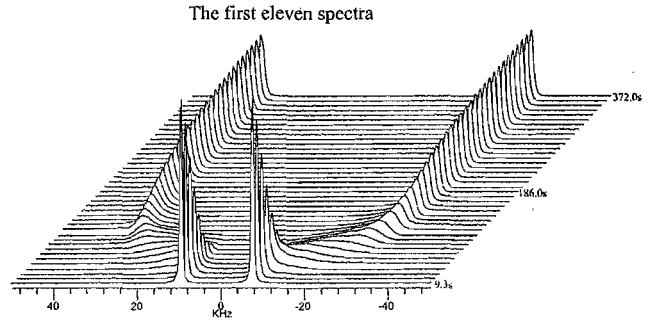


The first array from a different perspective

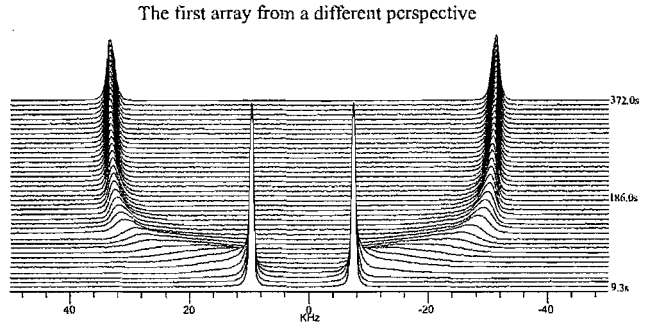


The first array

**Figure 11** Time-resolved deuterium NMR spectra obtained by the array acquisition for a rotation through 45° for 8CB-$d_2$ at 30°C with a time interval of 9.3s between scans.

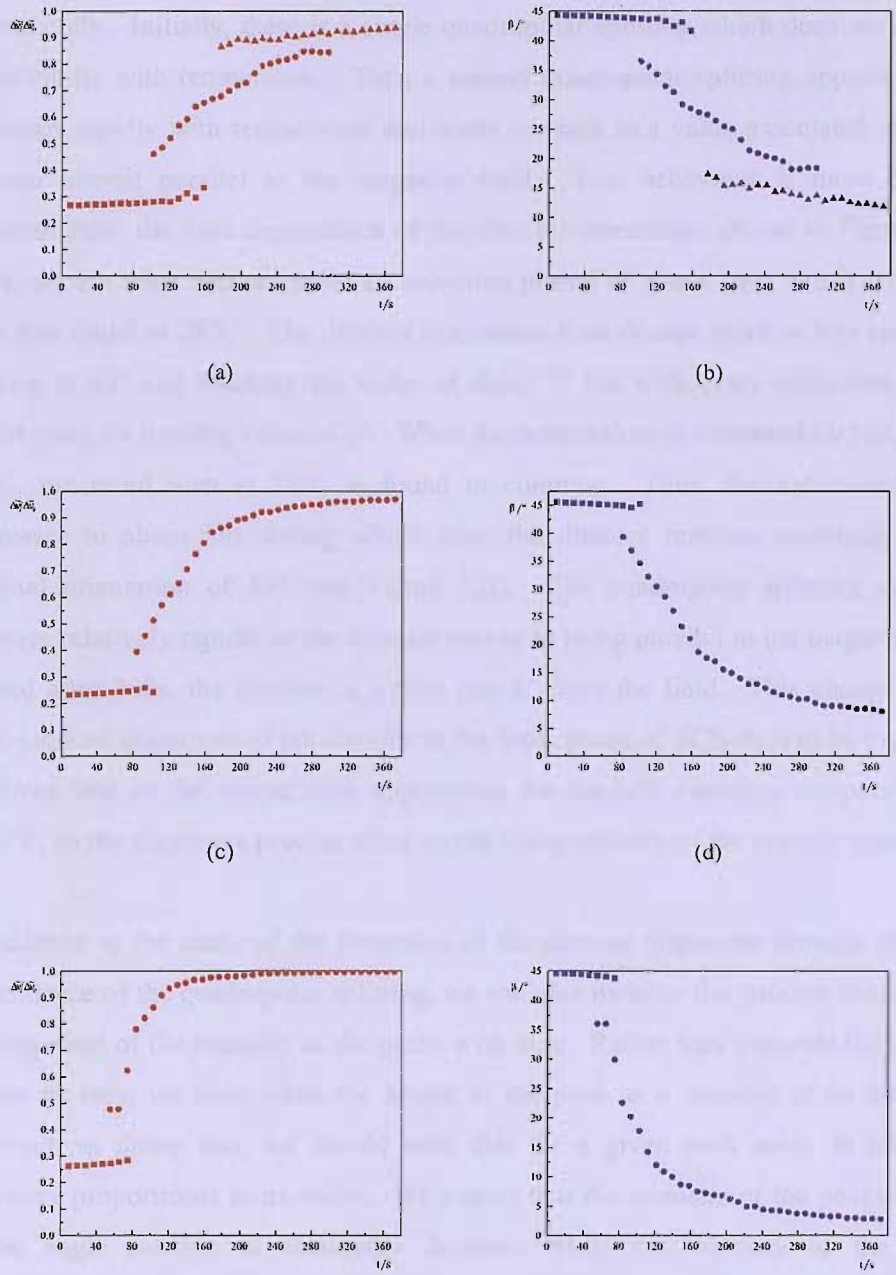


**Figure 12** The time dependence of $\Delta\tilde{\nu}/\Delta\tilde{\nu}_0$ for the SmA phase of 8CB-$d_2$ determined at (a) 25°C, (c) 28°C and (e) 30°C and the corresponding angle, β, made by the director with the magnetic field in (b), (d) and (f), respectively for the 45° rotation experiments. The different symbols represent different director orientations in the sample.

At the slightly higher temperature of 28°C, the behaviour appears to change dramatically. Initially, there is a single quadrupolar splitting which does not change significantly with temperature. Then a second quadrupolar splitting appears which increases rapidly with temperature and tends towards to a value associated with the director almost parallel to the magnetic field. This behaviour is more directly apparent from the time dependence of the director orientation shown in Figure 12d. Here, we see what appears to be an induction period of about 100s which is shorter than that found at 25°C. The director orientation then decays more or less smoothly starting at 40° and reaching the value of about 7° but with every indication that it might reach its limiting value of 0°. When the temperature is increased by just 2°C to 30°C, the trend seen at 28°C is found to continue. Thus, the induction period decreases to about 80s during which time the director remains essentially at its original orientation of 45° (see Figure 12f). The quadrupolar splitting starts to increase relatively rapidly as the director moves to being parallel to the magnetic field. Indeed after 360s, the director is within just 2° from the field. This change in the field-induced alignment of the director in the SmA phase of 8CB-$d_2$ is to be expected. It shows that as the temperature approaches the SmA-N transition temperature of 33.5°C, so the alignment process takes on the characteristics of the nematic phase.

In addition to the study of the dynamics of the director alignment through the time dependence of the quadrupolar splitting, we can also monitor this process through the development of the intensity of the peaks with time. Rather than integrate the peak to obtain its area, we have taken the height of the peak as a measure of its intensity; however, in doing this, we should note that for a given peak area, its height is inversely proportional to its width. We expect that the intensity of the peaks for the initial angle rotation to eventually decrease while the intensity of the peaks corresponding to the director parallel to the magnetic field to increase with time. Figure 13 shows the plots of the intensity of the peaks with time for the 45° rotation experiments at 25°C, 28°C and 30°C. For all three temperatures, we observe that the intensity for corresponding to initial 45° rotations decreased with time. Then we observe the growth of the new peaks with time, and these new peaks correspond to the director moving towards the magnetic field. As expected, the peak intensities change more rapidly with increasing temperature showing that the dynamics is faster at 30°C

compared to 25°C and 28°C, both in the decreasing of the intensity of the peaks for the 45° rotation and in the growth of the intensity for the 0° orientation. In addition, at all temperatures, the spectral heights for the initial director orientation start to decrease immediately with no indication of an induction period, as expected from theory.

To have a quantitative comparison in the dynamics for the three different temperatures, we compare the time taken for the height of the peaks immediately following the initial rotation (■ symbol) to decay to half its height. For the growth of the height corresponding to the director parallel to the magnetic field (● symbol), we will also take the time taken at half-height of the plot before it reaches its limiting value, indicating that the director is close to parallel to the magnetic field. Figure 13a shows the results for the 45° rotation experiment at 25°C. The ▲ symbol in the plot indicates that the deuterium NMR spectra show that parts of the sample adopt another director orientation during the alignment process. The time taken for the height of the 45° peaks to reduce to half of their original value, after being rotated, is 65s. The plot also shows that the height of the new peak was still slowly growing as it is aligned towards the magnetic field. Figure 13b shows a steep decay in the height of the peaks for the 45° rotation at 28°C. The time taken for the height of the peaks to be reduced to half its height is approximately 50s, which is 15s faster or a factor of 23% than that found at 25°C. The plot also indicates that the rate of the growth of the new peaks towards the equilibrium state is faster than that observed at 25°C as might be expected. It only takes 37s for the height of the peaks to be reduced to half their value at 30°C as shown in Figure 13c corresponding to a reduction of 13s, *i.e.*, 26% reduction compared to that for 28°C. The dynamic of the director orientation process was very fast in that after 150s, the intensity of the new peaks for the director moving towards the magnetic field has already become half of their final height. After 240s, the intensity began to grow very slowly and the plot looks plateau-like, suggesting that the director is close to parallel to the magnetic field. At the lower temperatures of 25°C and 28°C, the data is not available for longer enough periods to see the heights of the peaks corresponding to the director parallel to the magnetic field to reach their limiting values.

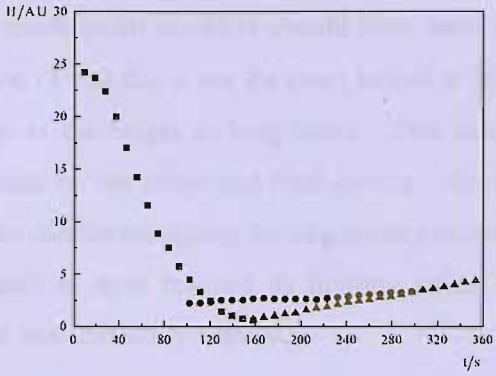


(a)

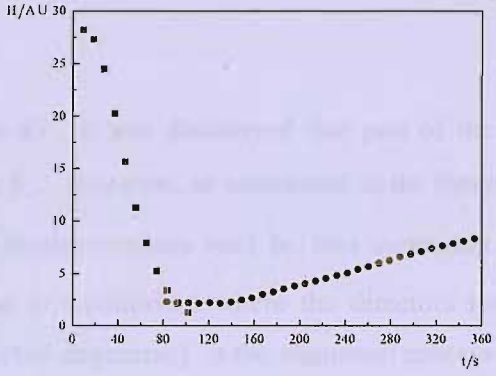


(b)

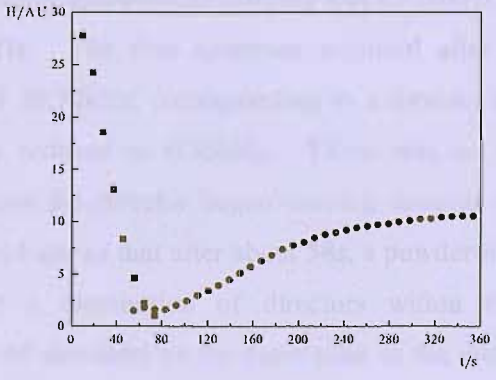


(c)

**Figure 13** The time-dependence of the intensity for the peaks in the NMR spectrum of SmA phase of 8CB-$d_2$ determined at (a) 25°C, (b) 28°C and (c) 30 °C for the 45° rotation experiments; here H denotes heights of the peak, and AU is arbitrary units. The different symbols represent different director orientations in the sample.

Finally, for the 45° rotation experiments, it might have been expected that the sum of the heights of the two quadrupolar doublets should have been constant. It is clear from the results in Figure 13 that this is not the case; indeed at 30°C, the initial height is significantly different to the height at long times. This could be caused by the difference in the linewidths for the initial and final spectra. Alternatively, it might be that the director is widely distributed during the alignment process and that even when the peak intensity appears to have reached its limiting value, there are still some regions with the director non-uniformly aligned.

### *6.6.2 Rotation by 75°*

*75° rotation at 25°C*

For angles greater than 45°, it was discovered that part of the directors realign as expected by decreasing $\beta_t$. However, as mentioned in the theoretical background, a smaller fraction of the directors moves back by first increasing $\beta_t$, passing through 90°, and then returning to equilibrium where the directors realign parallel to the magnetic field. This partial degeneracy in the alignment process was observed in the 75° rotation experiments.

At 25°C, before rotation, the quadrupolar splitting was 67.70kHz and the linewidth at half-height was 1.41kHz. The first spectrum acquired after the rotation had a quadrupolar splitting of 26.70kHz, corresponding to a director orientation of 74.6°, and the linewidth was reduced to 0.85kHz. There was an induction period of approximately 48s before the director began moving towards the direction of the magnetic field. Figure 14 shows that after about 58s, a powder-like spectrum seemed to develop suggesting a distribution of directors within the sample. More interestingly, we observed shoulders on the outer sides of the intense inner peaks. At 58s, the quadrupolar splitting for the humps was 33.00kHz, corresponding to a director orientation of 84.7°. This suggests that some of the directors have actually passed through 90° before being aligned back towards 0°. The partial degeneracy in the alignment process can be observed more clearly through the two selected spectra shown in Figure 15. The spectrum recorded after 76.8s corresponds to a director

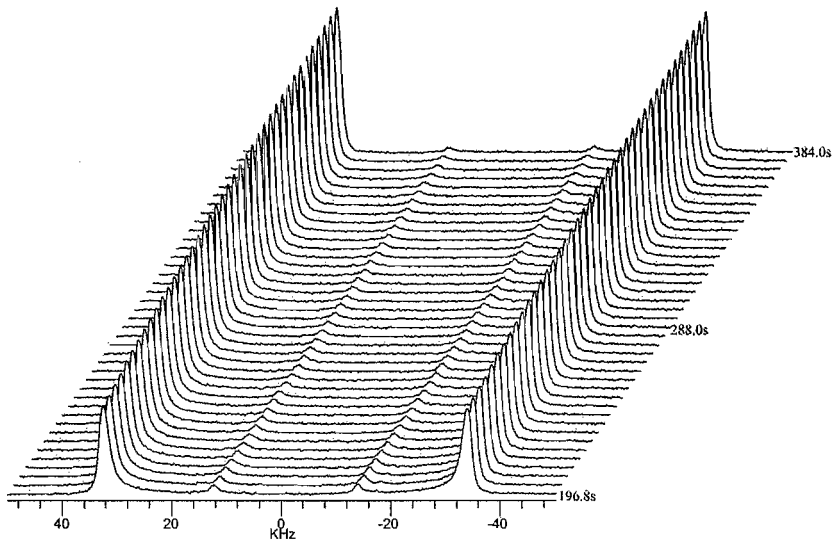


The second array

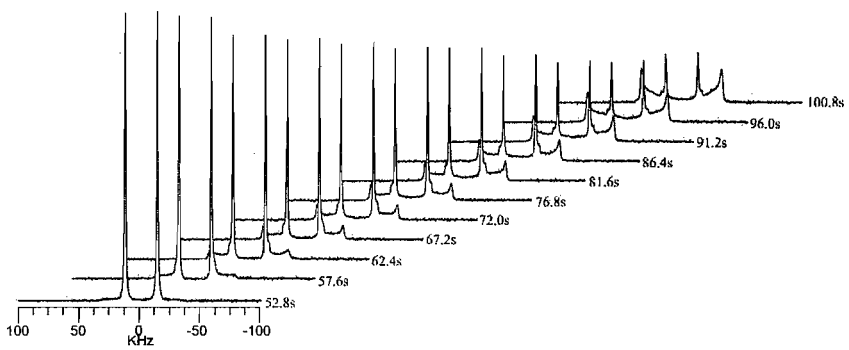


The spectra after the induction period

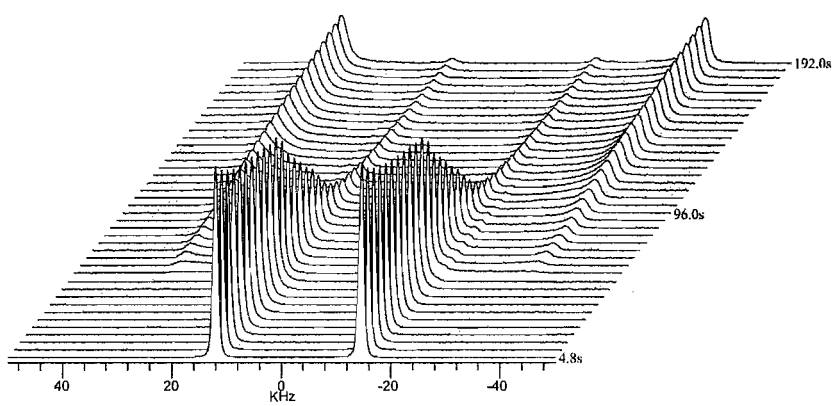


The first array

**Figure 14** Time-resolved deuterium NMR spectra of the array acquisition for a sample rotation of 75° for 8CB-$d_2$ at 25°C with an interval time of 4.8s between the spectra.

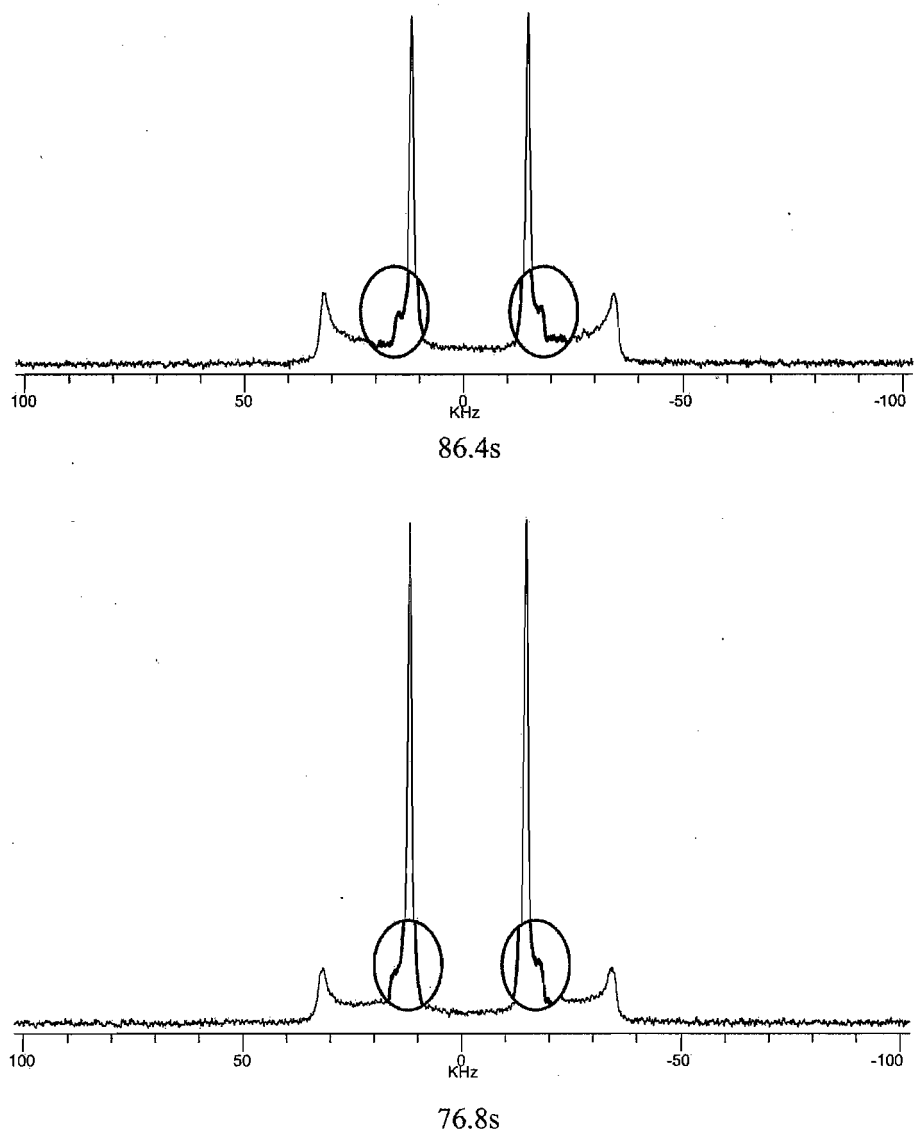


**Figure 15** Two of the selected spectra in the first array for a sample rotation of 75° for 8CB-$d_2$ at 25°C; the ellipses enclose shows the peaks which come from the directors increasing first to 90°, before returning to equilibrium.

orientation of 84.4° for the shoulders, while the spectrum after 86.4s, showed a director orientation of 83.9° from the director moving in the counterclockwise direction. The outer peaks of the spectra are the other part of the director which has moved clockwise by decreasing the director orientation, β, directly towards 0°. After the first array of experiments at 192s, the quadrupolar splitting of the outer peak was 66.60kHz, corresponding to a director orientation of 5.9°. The linewidth was 2.23kHz.

After the second array, at 384s, the last spectrum showed a splitting of 67.2kHz, corresponding to an orientation of 4.0°, with a linewidth of 1.46kHz. Even after the second array of experiments there were still some directors within the 75° orientation, although the intensity of the peaks was reduced. We should note that the director at an angle close to 90° tends to move very slowly because the magnetic torque acting on it is so small (see Equation (3)).

*75° rotation at 28°C*

As observed for the 45° rotation experiments, the rate of the field-induced director alignment increases with increasing temperature. This was also the case with the 75° rotation experiments performed at 28°C. Qualitatively, the alignment process was the same as that at 25°C and the spectra showing this are given in Figure 16. The effect of the partial degeneracy in the director alignment was also observed. However, at 28°C, the induction period was shorter, *i.e.*, 9.0s, after which the director began moving towards its equilibrium orientation. At the end of the first array of experiments at 180s, the quadrupolar splitting of the outer peaks was 65.93kHz, corresponding to the director orientation of just 2.7° with respect to the magnetic field. The linewidth was 1.48kHz. The last spectrum in the second array after 360s, had a quadrupolar splitting of 66.15kHz, corresponding to the angle of just 0.6° with respect to the field in the spectrometer. The linewidth was 1.26kHz. At this time, there were still some directors remaining at the 75° orientation, although the intensity of the NMR peaks corresponding to this was very weak.

*75° rotation at 30°C*

At 30°C, the alignment process was more rapid than that at 25°C and 28°C, as expected. However, the trend in the alignment did not differ from that at the two lower temperatures, although at 30°C, there was no induction period. The partial degeneracy in the alignment process could also be observed as shown in the spectrum after 13.5s in Figure 17. It can be seen that after about 90s, there was no director remaining at the 75° orientation in that the peak intensity is very weak. At the end of the second array, the quadrupolar splitting was 64.96kHz, corresponding to an angle

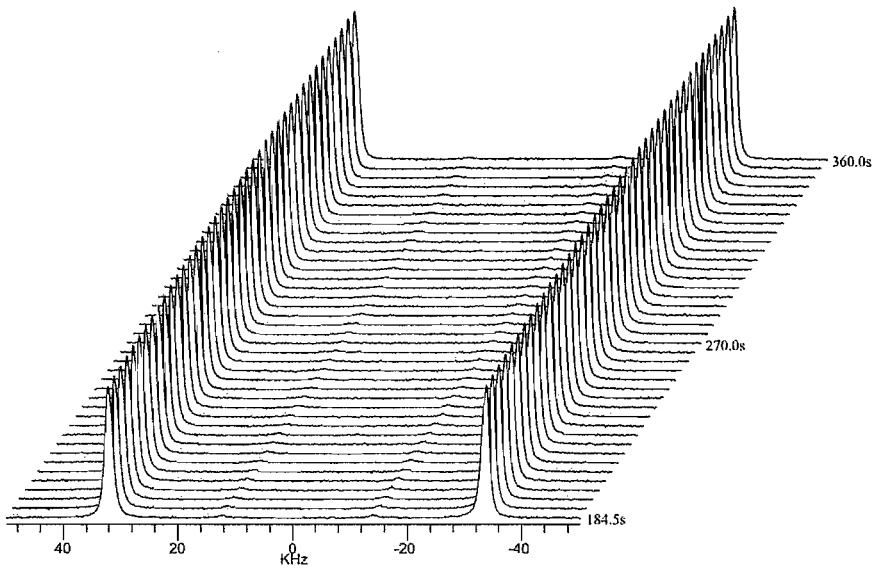


The second array

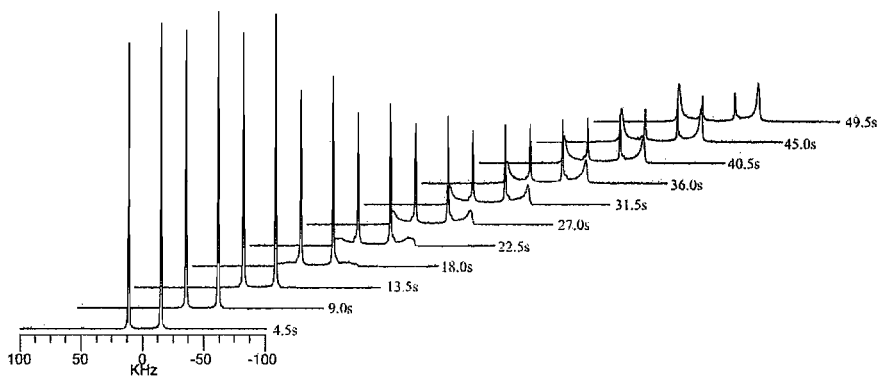


The first eleven spectra

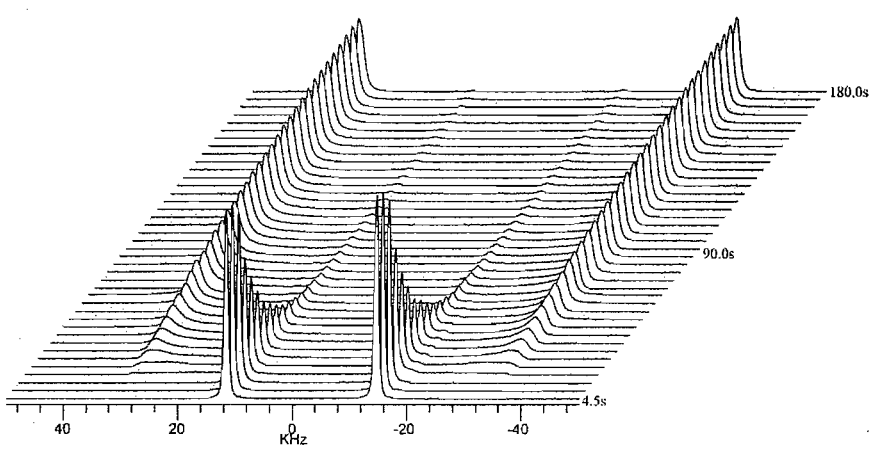


The first array

**Figure 16** Time-resolved deuterium NMR spectra of the array acquisition for an initial sample rotation of 75° for 8CB-$d_2$ at 28°C with the time interval of 4.5s between the spectra.

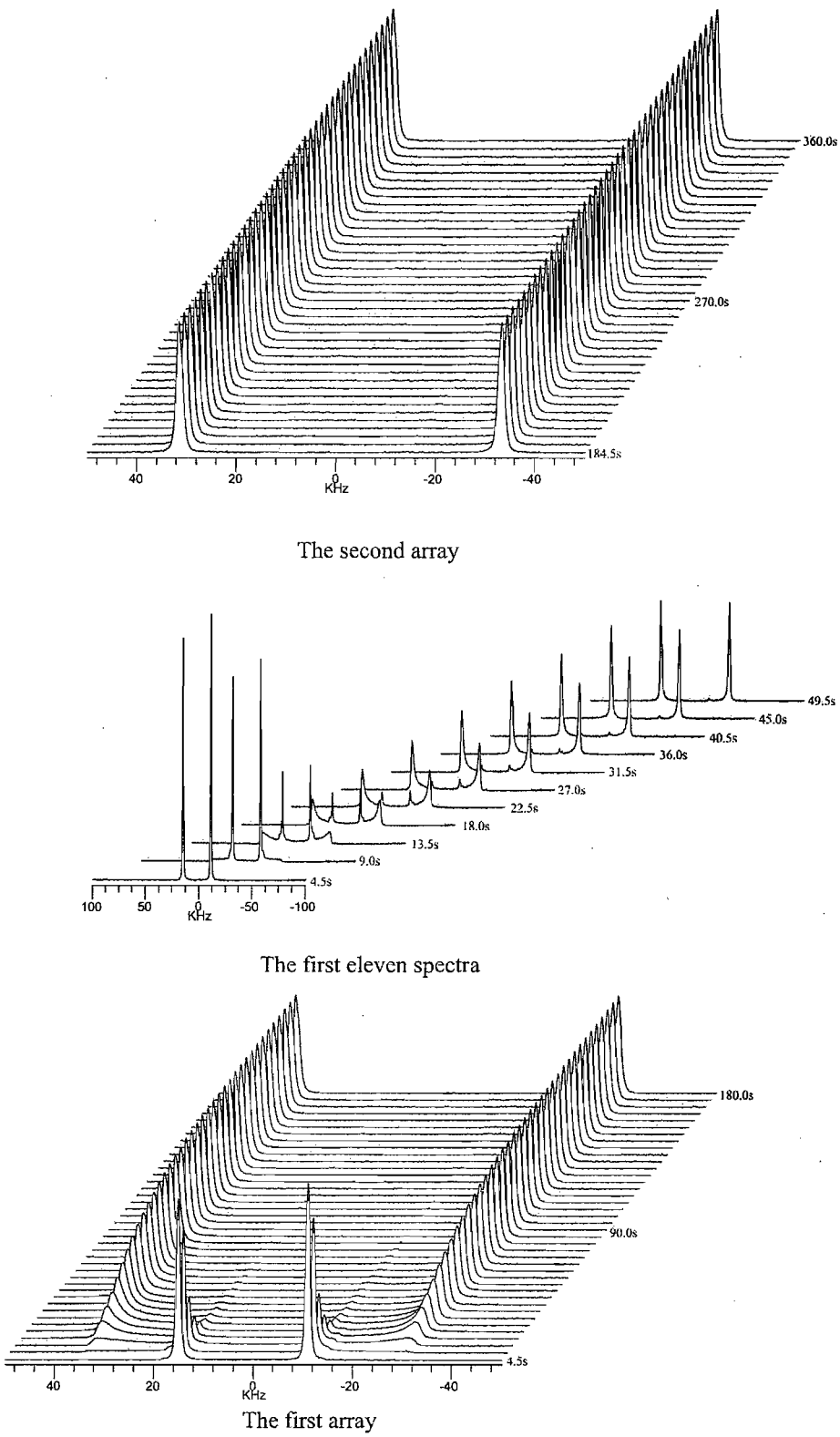


**Figure 17** Time-resolved deuterium NMR spectra of the array acquisition for a sample rotation of 75° for 8CB-$d_2$ at 30°C with the time interval of 4.5s between the spectra.

of 1.7° made by the director with the magnetic field. The linewidth of this spectrum was 1.21kHz.

Figure 18 shows the time dependence of the ratio of the quadrupolar splitting and the quadrupolar splitting before rotation, and the corresponding angle for the 75° rotation at 25°C, 28°C and 30°C. The plots refer to the first array of the experiments and the different symbols represent different director orientations in the sample. The dynamics are clearly faster at higher temperature. As mentioned earlier, at 30°C, there were no directors remaining at the 75° orientation after about 90.0s. This, however, was not the case at 25°C and 28°C, in which some of the directors remained in place within the vicinity of the 75° and the 90° orientations throughout the array.

As we have seen, the dynamic director behaviour is quite different for the 75° rotation experiment with the director orientations being widely distributed at just few peaks corresponding to particular director orientations being apparent. The plots of the time-dependence of the heights of the peaks for these rotation experiments shows three peaks where the ■ symbolises the peaks for the director at the initial 75° rotation, the ● indicates the orthogonal to the magnetic field and the ▲ signifies the peaks for the director close to parallel to the magnetic field. Figure 19a for the 25°C experiment shows that initially, the heights of the peaks associated with the 75° orientation decreased slowly but that after 60s, the height began to drop quickly. The time taken for the intensity of the peaks to be half its initial height after the sample was rotated through 75° was approximately 70s. At this temperature, the director distribution was still nowhere near the equilibrium state because the peaks for the 0° orientation indicate that their heights were still increasing. It seems that the director distribution for much of the sample is still widely distributed although the intensity of the resultant powder pattern is too weak to be apparent. Indeed, the different relaxation times for the decay and growth in the heights of the peaks associated with different director orientations is consistent with the model in which the director moves to a random state and then is refocused at its final equilibrium state parallel to the magnetic field. At 28°C, the time taken for the heights of the spectral peaks for the director at the 75° orientation to be reduced to half their value was just 23s, as shown

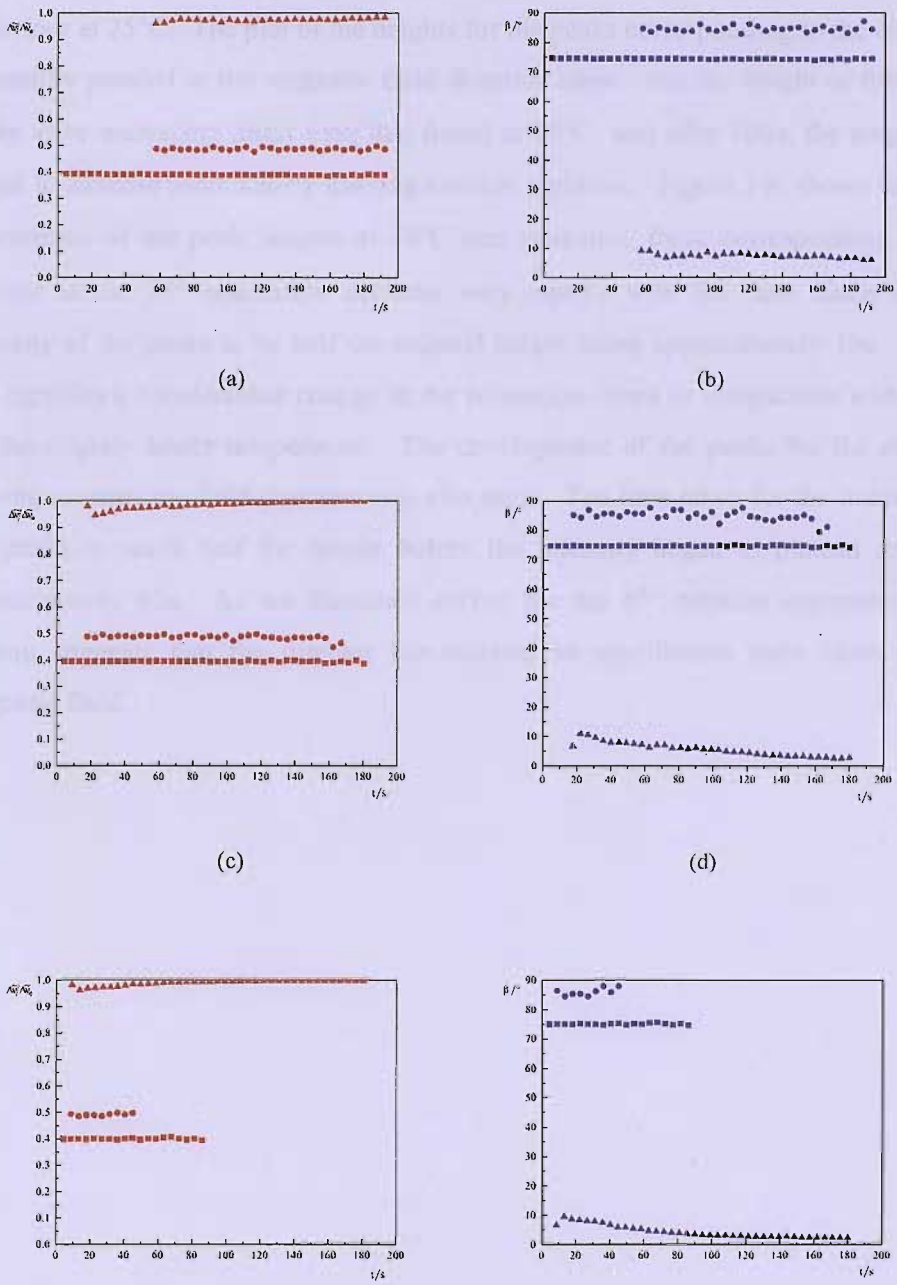


**Figure 18** The time dependence of $\Delta\tilde{\nu}/\Delta\tilde{\nu}_0$ for the SmA phase of 8CB-$d_2$ determined at (a) 25°C, (c) 28°C and (e) 30°C and the corresponding angle, β, made by the director with the magnetic field in (b), (d) and (f), respectively for the 75° rotation experiments. The different symbols represent different director orientations in the sample.

in Figure 19b which represents a significant reduction in comparison with the behaviour at 25°C. The plot of the heights for the peaks corresponding to the director essentially parallel to the magnetic field direction shows that the height of the NMR peaks were increasing faster than that found at 25°C, and after 100s, the height has begun to increase more slowly moving towards a plateau. Figure 19c shows the time dependence of the peak heights at 30°C and evidently, these corresponding to the director at the 75° orientation decrease very rapidly with the time taken for the intensity of the peaks to be half the original height being approximately 10s. Again this signifies a considerable change in the relaxation times in comparison with those for the slightly lower temperature. The development of the peaks for the director moving towards the field direction was also rapid. The time taken for the intensity of the peaks to reach half the height before the intensity began to plateau out was approximately 40s. As we discussed earlier for the 45° rotation experiment, the plateau suggests that the director has reached an equilibrium state close to the magnetic field.

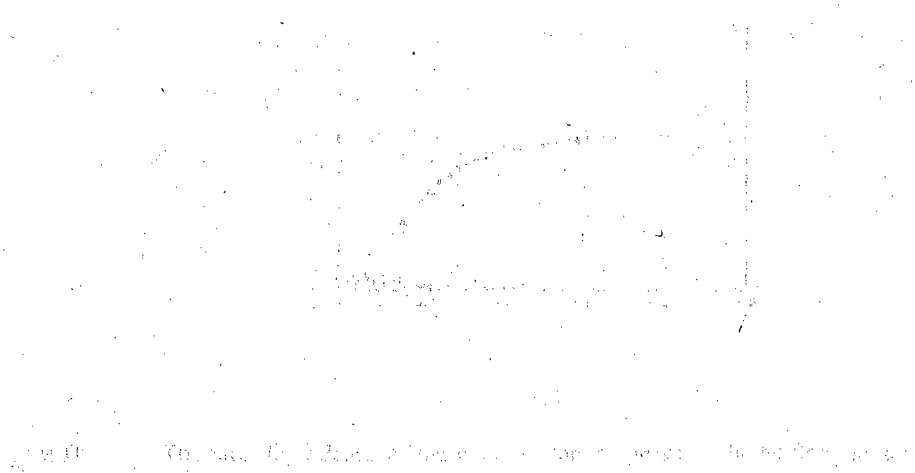

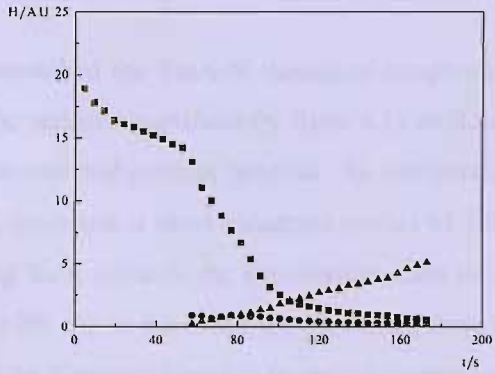


(a)

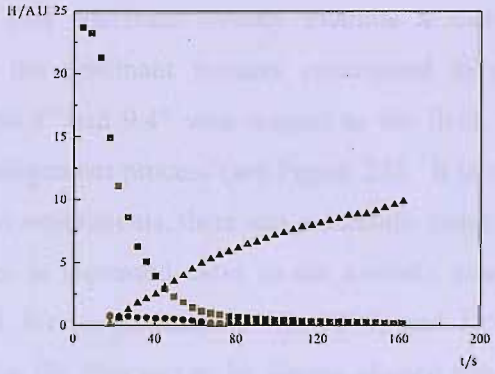


(b)

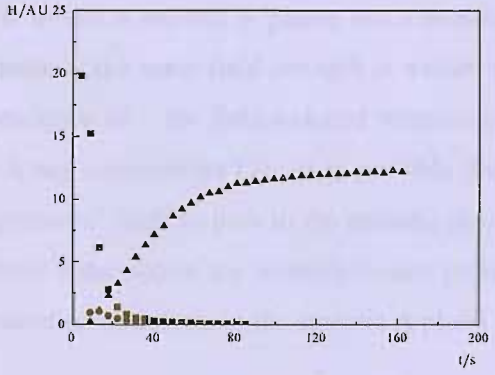


(c)

**Figure 19** The time-dependence of the intensity for the peaks in the NMR spectrum of SmA phase of 8CB-$d_2$ determined at (a) 25°C, (b) 28°C and (c) 30 °C for the 75° rotation experiments; here H denotes height of the peak, and AU is arbitrary units. The different symbols represent different director orientations in the sample.

*75° rotation near the SmA-N phase transition*

As the temperature approached the SmA-N transition temperature, 33.5°C, the time between scans had to be reduced significantly from 4.5s to 0.3s in order to monitor the dynamics of the director realignment process. In comparing the experiments at 31°C, 32°C, and 33°C, there was a short induction period of 1.8s at 31°C before the directors started moving back towards the equilibrium state as is apparent from the spectra shown in Figure 20. As at the lower temperatures, there are powder-like with peaks corresponding to the director aligned at its initial orientation and also at 90° and 0°. At 32°C, there was no induction period as can be seen in Figure 21. In addition, the intensity of the peaks decreases significantly faster than at 31°C. At 33°C, upon rotation by 75°, the first spectrum already exhibits a distribution of director orientations in which the dominant features correspond to the directors at the orientations of 74.1°, 84.8° and 9.4° with respect to the field, in keeping with the rapid dynamics of the alignment process (see Figure 22). It is especially interesting that in these 75° rotation experiments, there was a dramatic reduction in the relaxation time as the temperature is increased close to the nematic phase. As observed in Figures 11, 13 and 14 for temperatures 25°C, 28°C, and 30°C, respectively, the relaxation time taken for the directors to be almost aligned parallel to the magnetic field was within 90s. On going from 30°C to 31°C, a mere increase in a temperature of 1°C, the time taken for the directors to relax was within 5s. It is important to note that the phase at 31°C is in fact a smectic A phase, not a nematic phase because the relaxation time in a nematic at the same field strength is within ms. This large effect in the temperature dependence of the field-induced relaxation time is comparable with that found by the X-ray experiments [7]. It is possible that as the temperature increases, the sample "prepares" itself to pass to the nematic phase, and this results in a significant pretransitional reduction in the relaxation time probably associated with an increase in the concentration of defects in the smectic A phase.

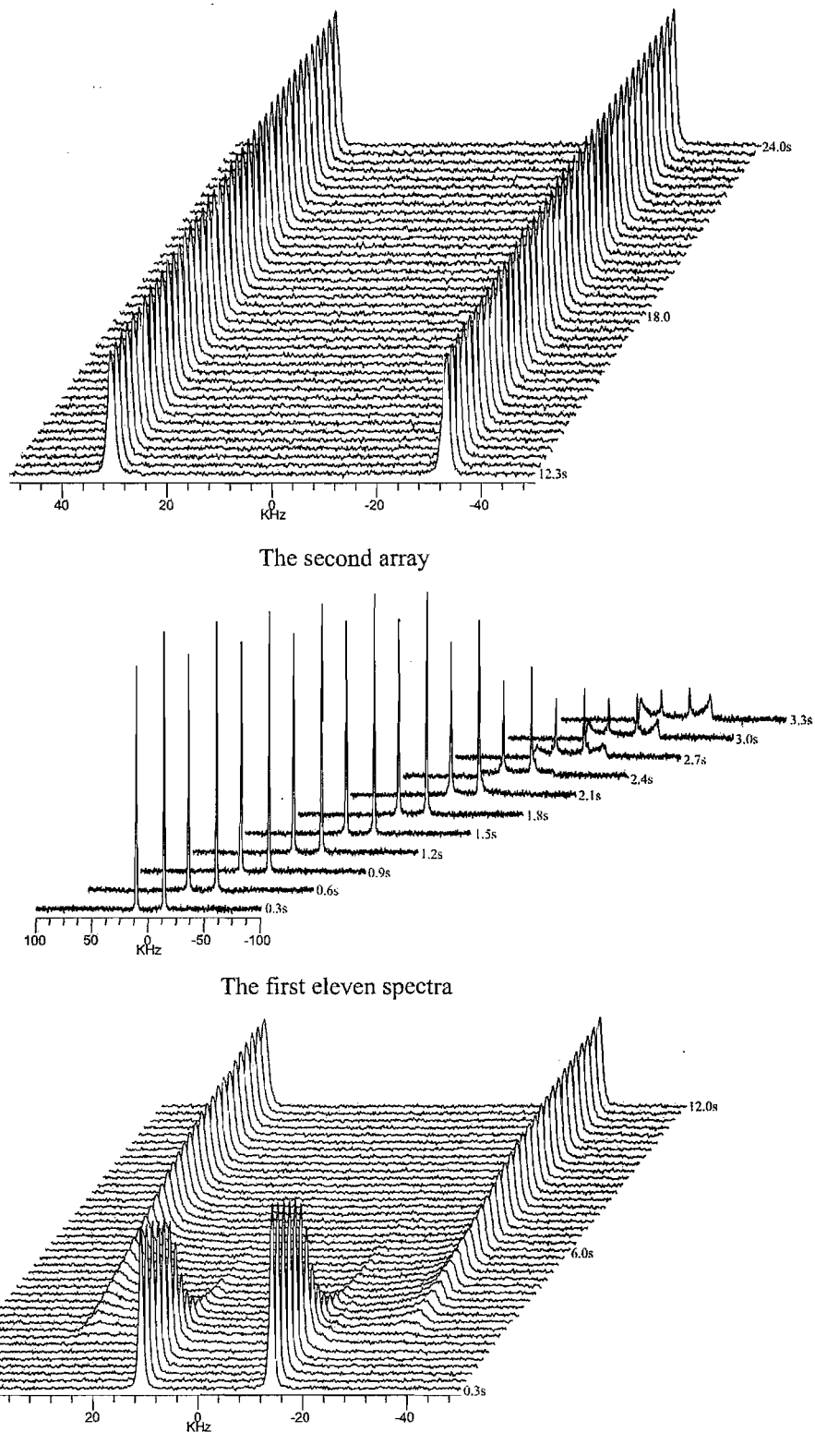


**Figure 20** Time-resolved deuterium NMR spectra of the array acquisition for a sample rotation of 75° for 8CB-$d_2$ at 31°C with 0.3s between the spectra.

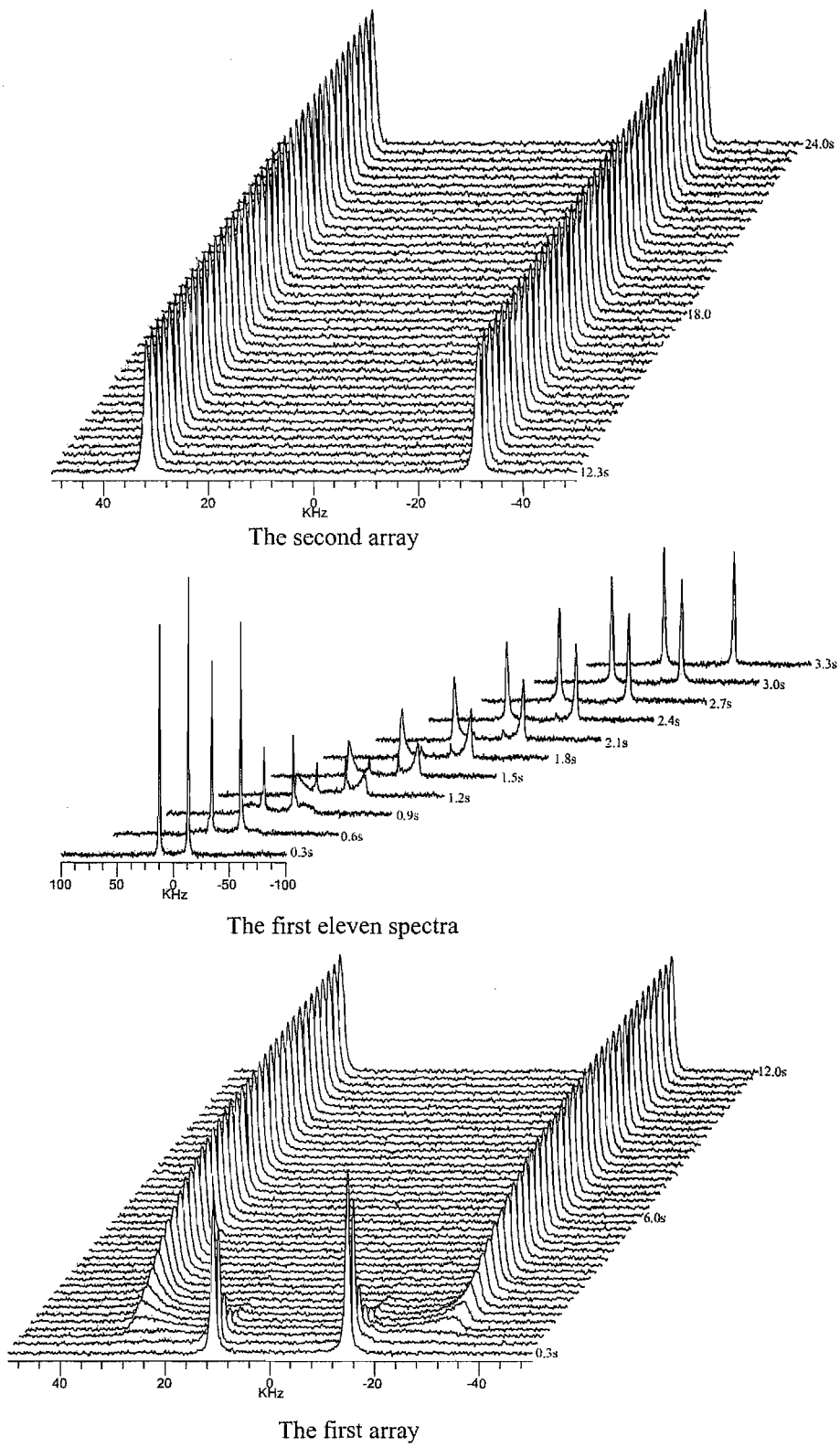


**Figure 21** Time-resolved deuterium NMR spectra of the array acquisition for a sample rotation of 75° for 8CB-$d_2$ at 32°C with 0.3s between the spectra.

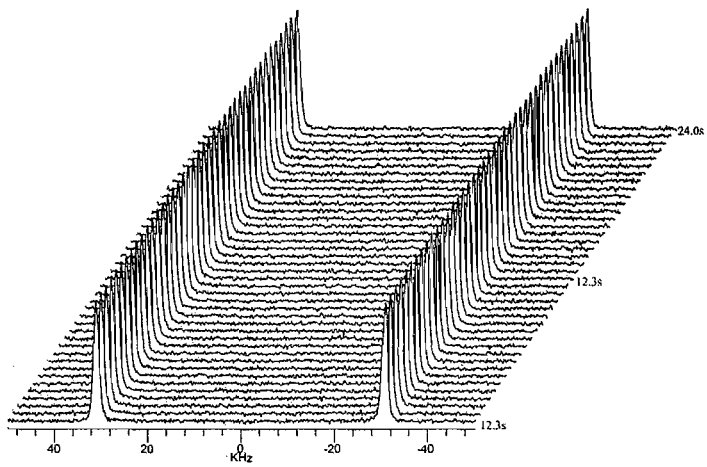


The second array

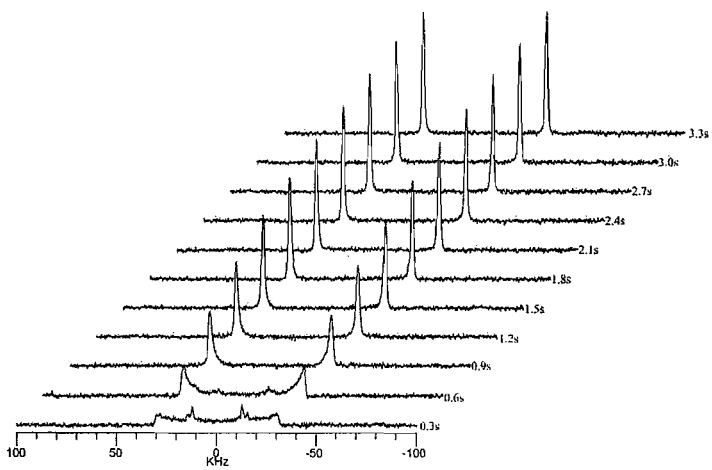


The first eleven spectra

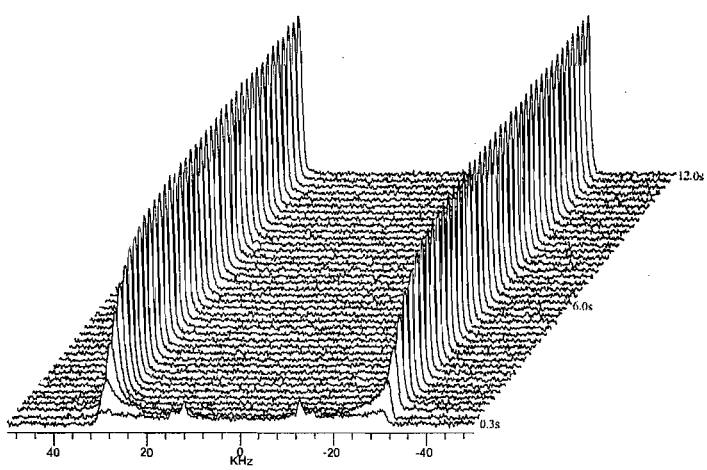


The first array

**Figure 22** Time-resolved deuterium NMR spectra of the array acquisition for a sample rotation of 75° for 8CB-$d_2$ at 33°C with 0.3s between the spectra.

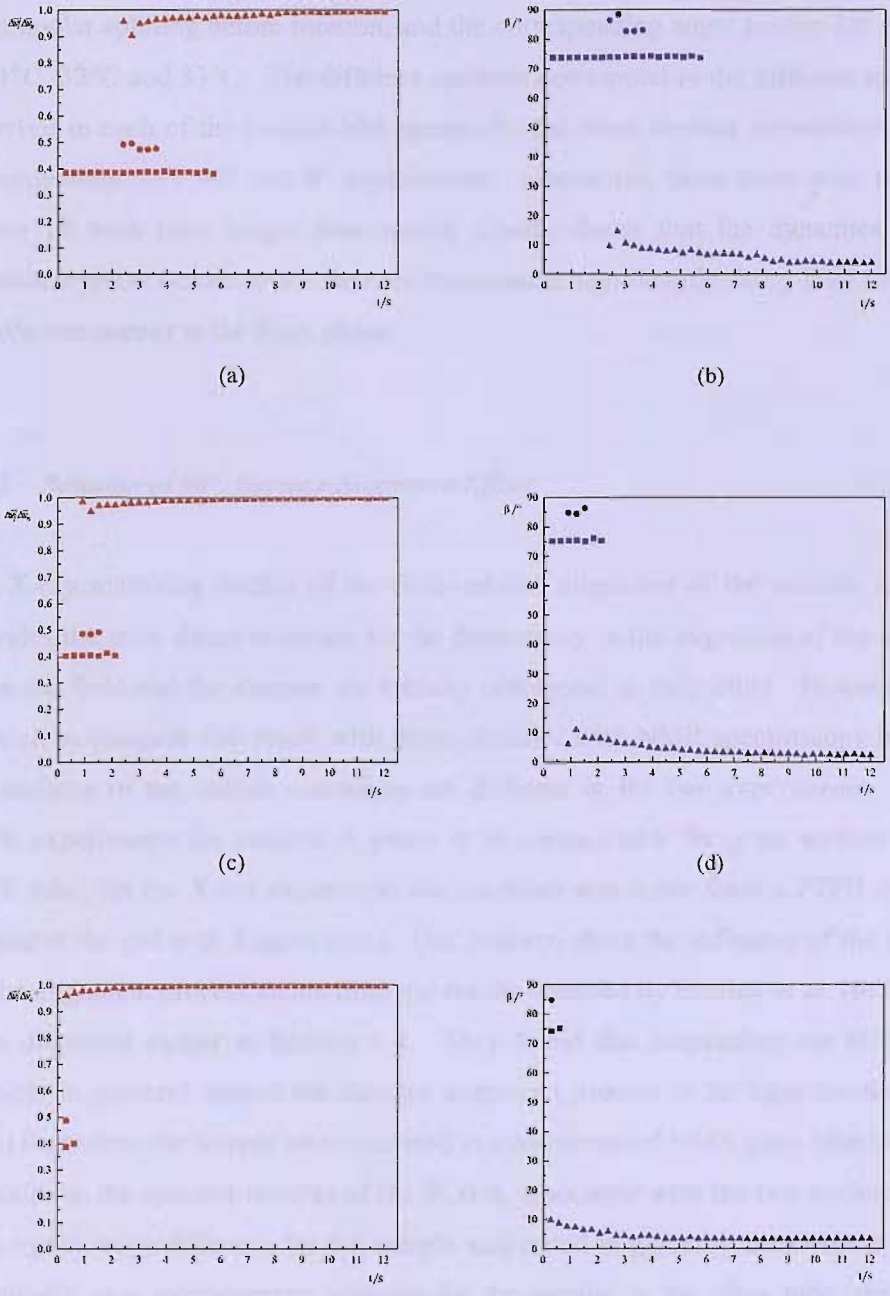


**Figure 23** The time dependence of $\Delta\tilde{\nu}/\Delta\tilde{\nu}_0$ for the SmA phase of 8CB-$d_2$ determined at (a) 31°C, (c) 32°C and (e) 33°C and the corresponding angle, β, made by the director with the magnetic field in (b), (d) and (f), respectively for the 75° sample rotation experiments. The different symbols represent different director orientations in the sample.

Figure 23 shows the time dependence of the ratio of the quadrupolar splitting and the quadrupolar splitting before rotation, and the corresponding angle for the 75° rotation at 31°C, 32°C and 33°C. The different symbols correspond to the different splittings observed in each of the powder-like spectra for the three director orientations that is approximately 75°, 90° and 0° experiments. Comparing these plots with those in Figure 18 with their longer time scales, clearly shows that the dynamics of the relaxation process close to the SmA-N transition is significantly faster than when the sample was deeper in the SmA phase.

### *6.6.3 Rotation of 90°: Surface Alignment Effect*

The X-ray scattering studies of the field-induced alignment of the smectic A phase provides the most direct evidence for the degeneracy in the alignment of the director when the field and the director are initially orthogonal to each other. However, it is difficult to compare this result with those obtained with NMR spectroscopy because the surfaces of the sample containers are different in the two experiments. In the NMR experiments the smectic A phase is in contact with the glass surface of the NMR tube; for the X-ray experiment the container was made from a PTFE cylinder capped at the end with Kapton discs. Our concern about the influence of the surface on the alignment process stems from the results obtained by Emsley *et al.* [6] that we have discussed earlier in Section 6.4. They found that suspending the 8CB-$d_2$ as droplets in glycerol caused the director alignment process to be significantly faster (60s) than when the sample was contained in a conventional NMR glass tube (60min). In addition, the spectral features of the 8CB-$d_2$ associated with the two surfaces were also significantly different, for the sample suspended in glycerol, the director moved essentially as a monodomain, whereas for the sample in the glass tube, the NMR spectra only showed features associated with the director oriented parallel and perpendicular to the magnetic field, with no indication of intermediate orientations (see Figure 5). In our 90° rotation experiments, we performed our experiments using two different surfaces, one in a conventional NMR glass tube, and one with the sample in a PTFE to be between Kapton discs in order to simulate the sample conditions in the X-ray experiments. This is to ensure that the conditions used for the NMR and X-ray experiment are strictly comparable. The alignment process for a 90°

rotation is of special interest because the alignment pathways, clockwise and counter-clockwise are degenerate. In the case of nematics, this results in a non-uniform director distribution with regions of the sample being separated by domain walls [11]. NMR spectroscopy certainly indicates a complex process for the smectic A phase, although it is X-ray diffraction which shows in the most direct manner the degeneracy in the field-induced alignment process [7]. However, the powder-like form of the initial NMR spectra shown in Figures 21, 23 and 25 for temperatures of 25°C, 28°C and 30°C, respectively, did suggest that the director adopted a wide range of orientations before being aligned parallel to the field. This is apparent from the appearance of two dominant peaks in the spectra associated with the director being parallel and perpendicular to the magnetic field. The spectral intensity from other director orientations is spread over a wide range of frequencies and so is too weak to be observed.

In studying the surface effects on the alignment process at 25°C in Figure 24, we show the results for the two surfaces. Despite the slight difference in the timescale, the behaviour of the directors during the alignment process is almost comparable. There was, however, a difference in the induction period, whereby for the PTFE/Kapton container, the time taken before the directors start to move was 48.96s, whereas that for the glass surface it was relatively faster at 27.9s.

At the higher temperature of 28°C, the induction period for the sample with the glass surface was 46.5s. On the other hand, for the sample in the PTFE/Kapton container, the induction period was only about 36.72s before the directors started aligning as can be seen from the spectra in Figure 26. Even at 30°C, the difference in the behaviour of the directors which is apparent from the two surface effects as seen from the spectra in Figure 28 are in the induction period. The induction period for PTFE/Kapton container was 24.48s, while for the glass surface, there was no induction period and directors started moving almost immediately upon rotation of the sample. However, a qualitative overview suggested that there was not a significant qualitative difference in the behaviour of the directors in both surfaces employed. Figures 22, 24 and 26 show the time dependence of the ratio of the quadrupolar splitting and the quadrupolar splitting before rotation, and the corresponding angle for the 90° rotation at 25°C, 28°C and 30°C, respectively, for the sample in the

conventional glass NMR tube and in between PTFE and Kapton discs. The plots show that the trend in the alignment process for both surfaces is the same.

*90° rotation at 25°C*

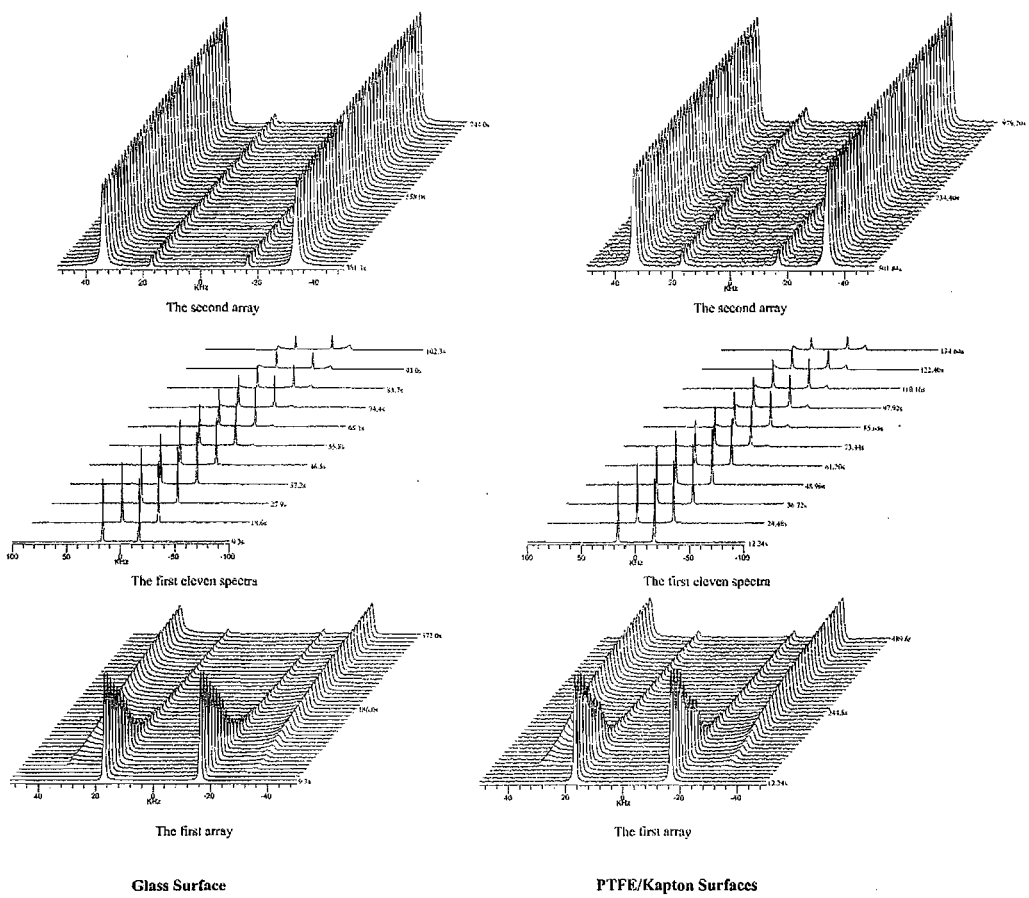


**Figure 24** Comparison of deuterium NMR spectra of the array acquisition for a sample rotation of 90° at 25°C for 8CB-$d_2$ contained in a glass surface and in a PTFE/Kapton cylinder. The times between the spectra are 9.3s and 12.24s for the glass surface and PTFE/Kapton container respectively.

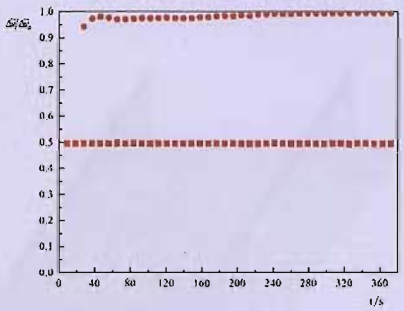


glass

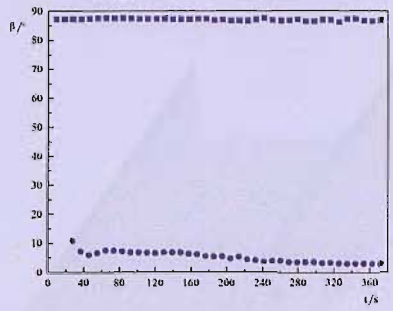


glass

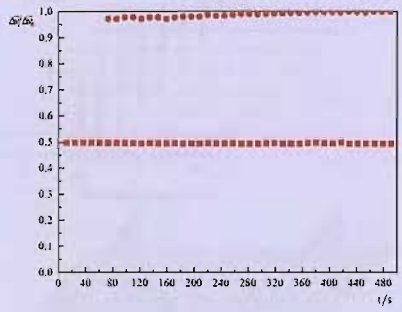


PTFE/Kapton

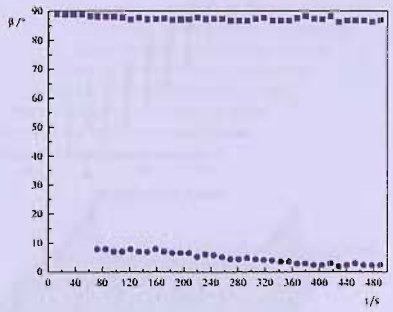


PTFE/Kapton

**Figure 25** The time dependence of $\Delta\tilde{\nu}/\Delta\tilde{\nu}_0$ for the SmA phase of 8CB-$d_2$ measured at 25°C sample in a glass and in the PTFE/Kapton container, and the corresponding angle, β, for the 90° sample rotation experiments. The different symbols represent different director orientations in the sample.

*90° rotation at 28°C*

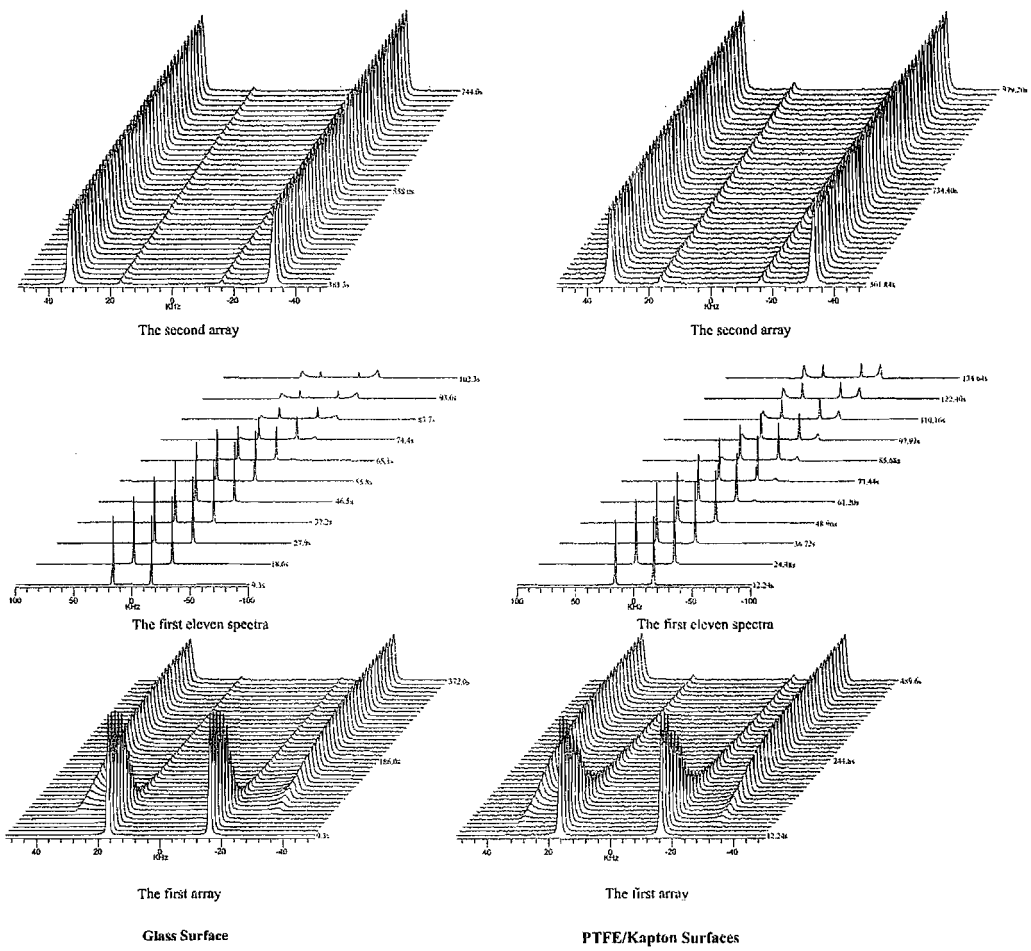


**Figure 26** Comparison of deuterium NMR spectra of the array acquisition for a sample rotation of 90° at 28°C for 8CB-$d_2$ contained in a glass tube and in a PTFE/Kapton cylinder. The time between scans are 9.3s and 12.24s for the glass surface and PTFE and Kapton surfaces, respectively.

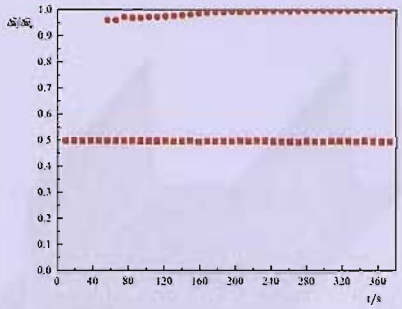


glass

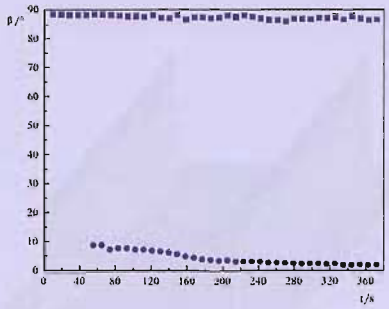


glass

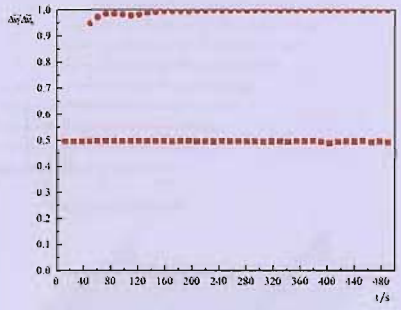


PTFE/Kapton

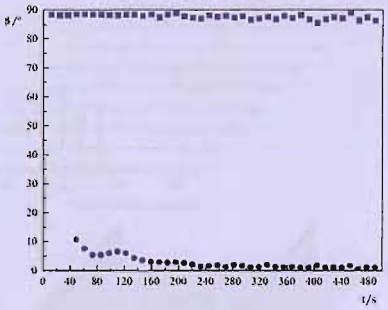


PTFE/Kapton

**Figure 27** The time dependence of $\Delta\tilde{\nu}/\Delta\tilde{\nu}_0$

*90° rotation at 30°C*

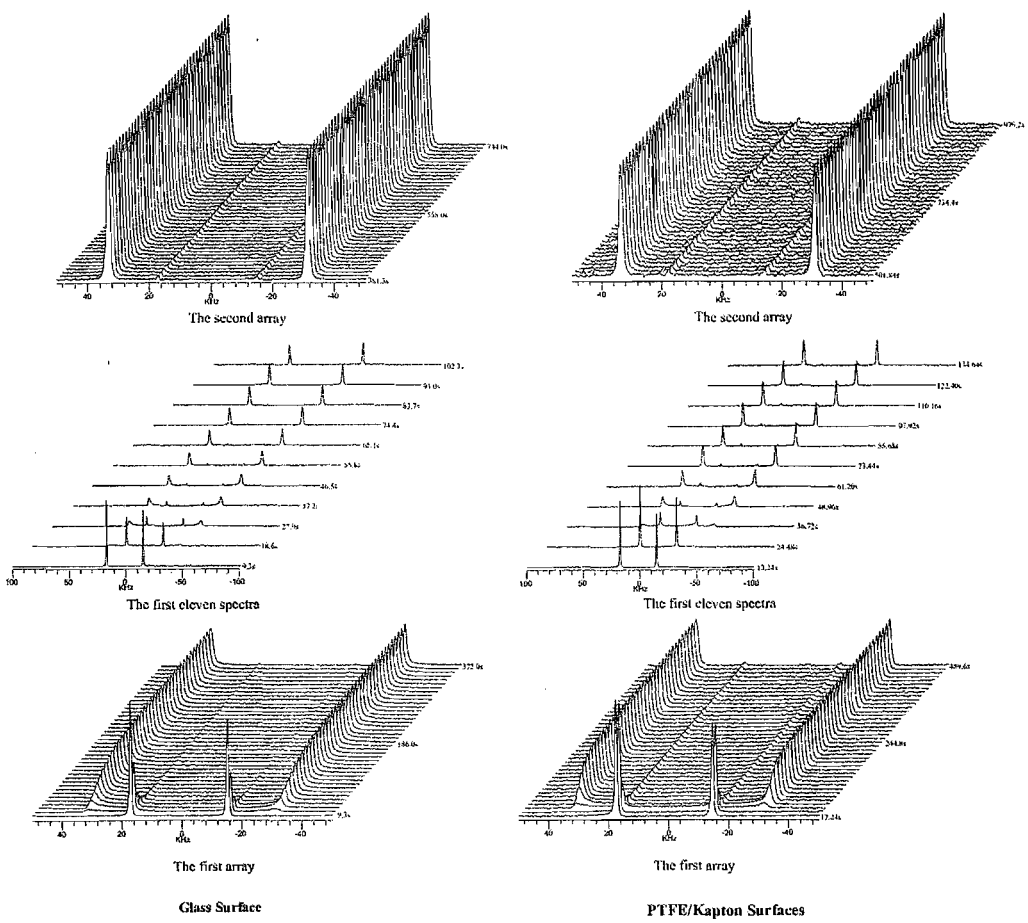


**Figure 28** Comparison of deuterium NMR spectra of the array acquisition for a sample rotation of 90° at 30°C for 8CB-$d_2$ contained in a glass tube and in a PTFE/Kapton cylinder. The time between scans are 9.3s and 12.24s for the glass surface and PTFE and Kapton surfaces, respectively.

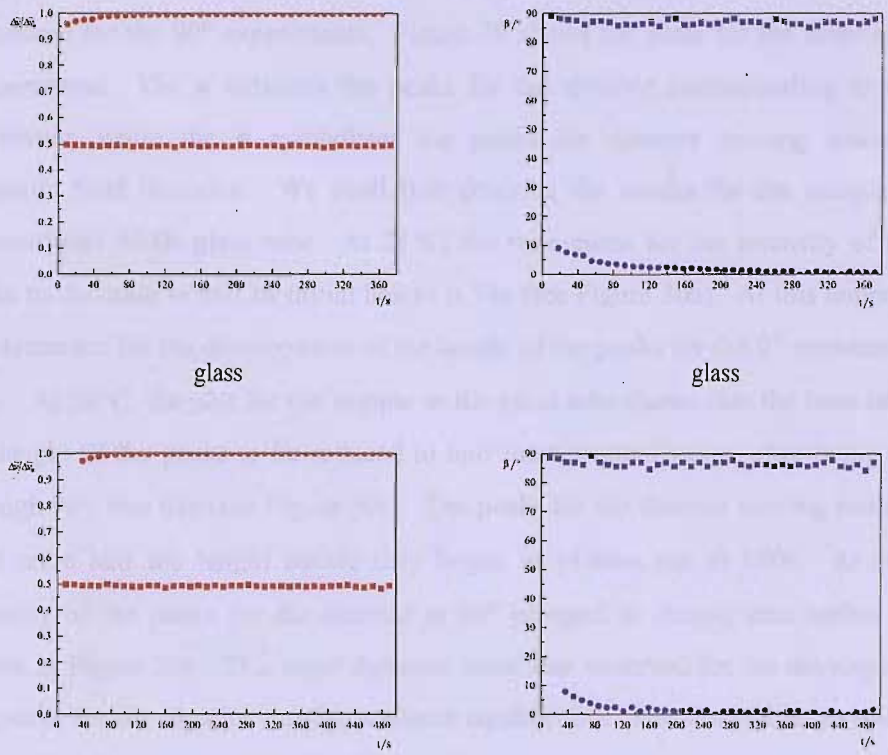


**Figure 29** The time dependence of $\Delta\tilde{\nu}/\Delta\tilde{\nu}_0$ for the SmA phase of 8CB-$d_2$ measured at 30°C sample in a glass and in the PTFE/Kapton container, and the corresponding angle, β, for the 90° sample rotation experiments. The different symbols represent different director orientations in the sample.

As for the 45° and 75° experiments, the heights of the peaks with time were also monitored for the 90° experiments. Figure 30 shows the plots for the three different temperatures. The ■ indicates the peaks for the director corresponding to the 90° orientation while the • symbolises the peaks for director moving towards the magnetic field direction. We shall first describe the results for the sample in the conventional NMR glass tube. At 25°C, the time taken for the intensity of the 90° peaks to decrease to half its initial height is 74s (see Figure 30a). At this temperature, the dynamics for the development of the height of the peaks for the 0° orientation was slow. At 28°C, the plot for the sample in the glass tube shows that the time taken for the height of the peaks to be reduced to half their original value, after being rotated through 90°, was 65s (see Figure 30c). The peaks for the director moving towards the field were half the height before they began to plateau out at 160s. At 30°, the intensity of the peaks for the director at 90° plunged to almost zero within 40s as shown in Figure 30e. This rapid dynamic were also observed for the development of the peaks for the director moving towards equilibrium. The time taken to reach half the height of the plateau was 47s for the glass surface.

As for the sample in the PTFE/Kapton container, at 25°C, the time taken for the height of the 90° peaks to decrease to half their original value is 98s (see Figure 30b). At 28°C, the plot shows that the time taken for the height of the peaks to be reduced to half their original value, after being rotated through 90°, was 86s (see Figure 30d). The peaks for the director progressing towards the field were half the height before they began to plateau out at 120s. As observed for the sample in the glass tube at 30°C, the height of the peaks for the director at 90° dropped to almost zero within 40s (see Figure 30f). The development of the height of peaks for the director parallel to the magnetic field was also rapid. The time taken to reach half the height of the plateau was approximately 31s for the PTFE/Kapton container. These results clearly suggest that the trend in the development of the intensity of the peaks is comparable for the sample in the glass tube and for the sample in the PTFE/Kapton container.

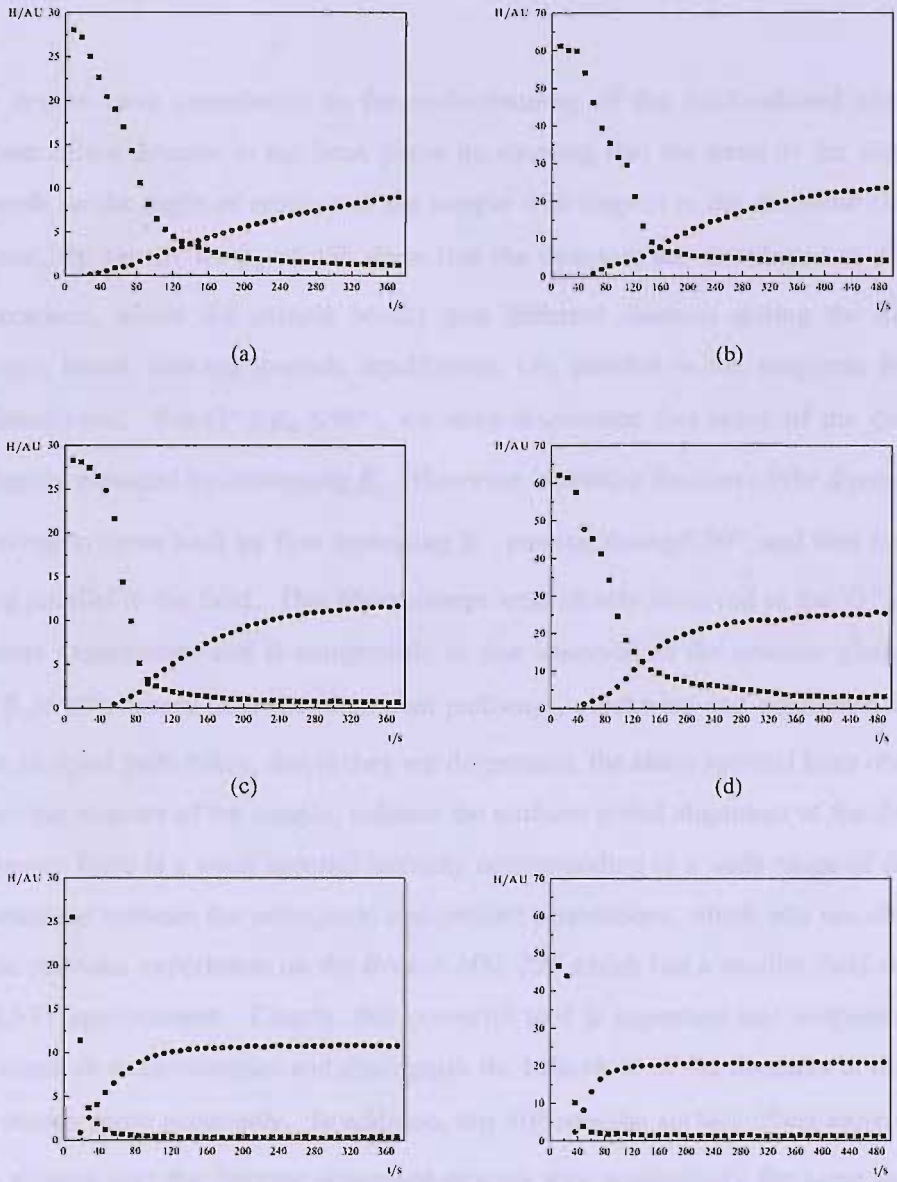


**Figure 30** The time-dependence of the intensity for the peaks in the NMR spectrum of SmA phase of 8CB-$d_2$ measured at 25°C for (a) and (b), 28°C for (c) and (d) and 30°C for (e) and (f) for the 90° rotation experiments for the sample in a glass (a, c, e) and in the PTFE/Kapton container (b, d, e). Here, H denotes heights of the peaks, and AU is arbitrary units. The different symbols represent different director orientations in the sample.

## 6.7 Conclusions

Our results have contributed to the understanding of the field-induced alignment process of the director in the SmA phase by showing that the trend of the alignment depends on the angle of rotation of the sample with respect to the magnetic field. In general, the results for $\beta_0$ of 45° show that the directors are distributed at different orientations, where the sample breaks into different domains during the aligning process, hence, moving towards equilibrium, *i.e.*, parallel to the magnetic field, at different rates. For $45° \leq \beta_0 \leq 90°$, we have discovered that some of the directors realign as expected by decreasing $\beta_t$. However, a smaller fraction of the directors are observed to move back by first increasing $\beta_t$, passing through 90°, and then return to being parallel to the field. This phenomenon were clearly observed in the 75° sample rotation experiments and is comparable to that observed in the nematic phase [18]. For $\beta_0$ at 90°, where both the alignment pathways, clockwise and counterclockwise, have an equal probability, that is they are degenerate, the sharp spectral lines observed following rotation of the sample, indicate the uniform initial alignment of the director. However, there is a weak spectral intensity corresponding to a wide range of director orientations between the orthogonal and parallel orientations, which was not observed in the previous experiment on the *Bruker MSL 200* which has a smaller field strength of 4.67T spectrometer. Clearly, this powerful tool is important and instrumental in our research to characterise and distinguish the behaviour of the directors at different $\beta_0$ rotation more accurately. In addition, our 90° rotation surface effect experiments also showed that the director alignment process was qualitatively the same for both the sample in the conventional NMR glass tube and in a PTFE/ Kapton cylinder. For all the experiments conducted, the dynamics of the director alignment became faster with increasing temperature. This was especially interesting for temperatures close to the transition to the nematic phase where there was a dramatic reduction in the relaxation time as seen in the 75° sample rotation experiments. This pretransitional behaviour is probably associated with an increase in the concentration of defects in the smectic A phase as the sample is heated close to the nematic phase.

## 6.8 References


[1] M. L. Magnuson, B. M. Fung, *J. Chem. Phys.* **100**, 1470 (1993).

[2] A. Sugimura, G. R. Luckhurst, *Nanotechnology and Nano-Interface Controlled Electronic Devices*, (Eds. M. Iwamoto, K. Kaneto, S. Masaki), Elsevier Science, (2003), Chap. 16.

[3] G. R. Luckhurst, T. Miyamoto, A. Sugimura, B. A. Timimi, *J. Chem. Phys.*, **116**, 5099 (2002).

[4] G. R. Luckhurst, T. Miyamoto, A. Sugimura, B. A. Timimi, *J. Chem. Phys.*, **117**, 5899 (2002).

[5] J. W. Emsley, J. E. Long, G. R. Luckhurst, P. Pedrielli, *Phys. Rev. E*, **60**, 1831 (1999).

[6] J. W. Emsley, G. R. Luckhurst, P. Pedrielli, *Chem. Phys. Lett.*, **320**, 255 (2000).

[7] W. Bras, J. W. Emsley, Y. K. Levine, G. R. Luckhurst, J. M. Seddon, B. A. Timimi, *J. Chem. Phys.*, **121**, 4397 (2004).

[8] G. R. Luckhurst, T. Miyamoto, A. Sugimura, T. Takashiro, B. A. Timimi, *J. Chem. Phys.*, **114**, 10493 (2001).

[9] G. Labrunie, J. Robert, *J. Appl. Phys.*, **44**, 4869 (1973).

[10] R. A. Wise, A. Olah, J. W. Doane, *J. Phys. (Paris)*, **36-C1**, 117 (1975).

[11] P. Esnault, J. P. Casquilho, F. Volino, A. F. Martins, A. Blumstein, *Liq. Cryst.*, **7**, 607 (1990).

[12] G. R. Luckhurst, A. Sugimura, B. A. Timimi, *Liq. Cryst.*, **32**, 1449 (2005).

[13] E. L. Hahn, *Phys. Rev.*, **80**, 580 (1950).

[14] E. L. Hahn, D. E. Maxwell, *Phys. Rev.*, **88**, 1070 (1952).

[15] I. Soloman, *Phys. Rev.*, **110**, 61 (1958).

[16] J. H. Davis, K. R. Jeffrey, M. Bloom, M. I. Valic, T. P. Higgs, *Chem. Phys. Lett.*, **42**, 390 (1976).

[17] C. P. Poole, Jr., H. A. Farach, *Relaxation in Magnetic Resonance*, Academic Press, New York, 1971.

[18] G. R. Luckhurst, A. Sugimura, T. Tetsuo, B. A. Timimi, *unpublished results* (2001).

# Chapter 7

# Phase Biaxiality and its Characterisation *via* NMR: Studies of a Crystal E Phase

## 7.1 Introduction

The thermotropic biaxial nematic phase is probably the most scrutinised and debated liquid crystal phase at present, especially in the unambiguous demonstration of its existence. The hunt for this elusive phase continues to be a challenging task, not only because of the difficulty of designing molecules of sufficient biaxiality [1] but also because of the problem of characterising the phase biaxiality beyond doubt [2]. While the existence of the biaxial nematic phase in lyotropic systems [3] is indisputable and the biaxiality is large, as large as the maximum of unity as reported by Nicoletta *et al.* [4], the opposite is true for thermotropic systems. In a recent publication on a thermotropic system by Madsen *et al.* [5], for example, the biaxiality in the quadrupolar tensor for a spin probe is reported to be merely 0.11. Are thermotropic systems so different from lyotropic systems that the phase biaxiality is easily masked? To this date, there is no successful report in finding a thermotropic biaxial nematic phase even though the molecular shape for the mesogens studied seems to suggest it is so. Despite the dilemma, we are convinced that NMR spectroscopy is indeed one of, if not, the most powerful tool with which to determine the symmetry of the phase. In this Chapter, we take a twist in solving the identification problem. We shall depart from the pursuit of the biaxial nematic, and focus instead, on the reliability of the NMR technique in order to establish a standard and robust methodology for characterising the phase symmetry.

To place these studies in the correct context, we begin our discussion on the significance of the biaxial nematic and its potential applications in Section 7.2. Section 7.3 will describe briefly the theoretical background which leads to the proposal of the biaxial nematic phase. This is followed by the characterisation

techniques used to investigate the biaxial nematic phase in Section 7.4. Our study of the crystal E phase to enhance our understanding on the phase biaxiality will be rationalised in 7.5. In Section 7.6, we will explain the NMR background of how the averaged quadrupolar tensor provides a measure of the phase biaxiality, while Section 7.7 will describe the order parameters and their relation to the phase biaxiality. 7.8 will discuss previous studies of the crystal E phase. Our experimental set-up is described in Section 7.9, which leads to our results and discussion in Section 7.10. Our concluding remarks are given in 7.11.

## 7.2 The Importance of the Biaxial Nematic Phase

The biaxial nematic phase has, potentially, significant technological applications in displays, telecommunications and optical devices, either in effectively improving the existing technologies or in being incorporated in technologies which require biaxiality for the operation of the application [6]. One possible application of the biaxial nematic phase is in devices that utilise defects, such as the zenithally bistable devices (*i.e.*, zero-power devices), which may improve switching properties [7]. Another potential application for the biaxial nematic is in optical compensation films, used to improve the viewing characteristic of twisted nematic (TN) displays [8]. Currently, manufacturers are already producing biaxial compensation films using non-uniform uniaxial nematics; nonetheless, the same effect could be produced using a uniformly aligned biaxial nematic, possibly with a simpler manufacturing process [6].

Apparently, the existence of a stable biaxial nematic phase could produce an entirely new class of liquid crystal devices. One proposed biaxial nematic device uses in-plane fields to rotate the minor director while keeping the major director fixed, in contrast with uniaxial devices which rotate the major director. This new device could have a fast response time, since rotation of the minor director may have a lower rotational viscosity than for rotation of the major director. However, before such devices can be made, there are many issues concerning engineering challenges, not least the question of surface alignment of the directors [6]. Whether or not both the major and minor directors of biaxial nematics can be aligned by simply rubbing the substrates is not known. A combination of applied fields and surface treatment may

be needed to produce the required alignment and any such system would make device operation and construction more complicated [6].

## 7.3 Background

It all began in 1970, when Freiser of IBM [9] predicted that the reduction in molecular symmetry from $D_{\infty h}$ to $D_{2h}$ should result in the formation, not only of the uniaxial nematic, but also of a new nematic phase, *i.e.*, the biaxial nematic phase. The uniaxial nematic phase, $N_U$, has $D_{\infty h}$ symmetry, while the biaxial nematic phase, $N_B$, has $D_{2h}$ symmetry. The term *uniaxial*, is borrowed from the field of optics, and indicates that plane-polarised light can travel along just one axis without a change in its state of polarisation. This axis is the optic axis, and in the common nematic phase, it corresponds to the director [10]. On the other hand, the biaxial nematic has two axes along which plane-polarised light can travel without a change in the state of polarisation. It is of great interest to note that neither of these axes corresponds to the directors. The idealised molecular organisation within the biaxial nematic phase composed of block-shaped molecules is depicted in Figure 1.

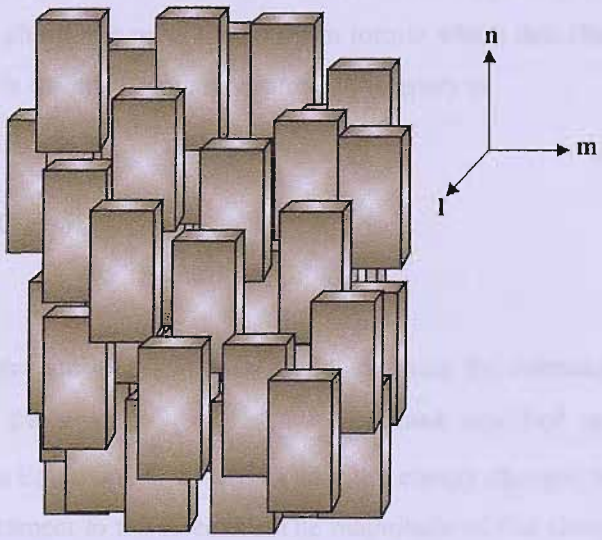


**Figure 1** The organisation of the molecular blocks in an idealised biaxial nematic phase. Here, the translational order is only short range.

At a macroscopic level in the uniaxial phase, tensorial properties of the nematic phase, such as the dielectric constant and refractive index, have cylindrical symmetry [11]. There are then two unique principal components of the property which, for the general case of a second rank tensor are denoted by $\tilde{Q}_{\parallel}$ and $\tilde{Q}_{\perp}$. Here we use the tilde, ~, to distinguish the quantities within a liquid crystal from those for a crystal.

In the case of a biaxial phase, at the macroscopic level, the three principal components of a second rank tensor would all be different, denoted by $\tilde{Q}_{ZZ}$, $\tilde{Q}_{YY}$, $\tilde{Q}_{XX}$. The three directors, **l**, **m** and **n**, correspond to the symmetry axes of the phase and are the principal axes for the tensorial properties such as the dielectric susceptibility. Conventionally, these directors are labelled such that the director **n** corresponds to the Z-axis along which the molecular long axes tend to be parallel. The director **l** is the director along the X-axis which, on average, the molecular short axes are parallel, while the director **m** is orthogonal to **l** and **n**, *i.e.*, the Y-axis.

It is to be expected that the molecular biaxiality, $\lambda$, *i.e.*, the biaxiality of the constituent molecules, determines the stability of the phase biaxiality [9,11, 12,13,14,]. This molecular biaxiality can be described within the context of the molecular field theory first used to predict the phase behaviour of the system [9,11,13,14]. For the uniaxial nematic phase, the potential of mean torque which describes the energy of a biaxial molecule in its anisotropic environment, is given as

$$U(\omega) = -\sum_{m=-2}^{2} X_{2m}^{*} C_{2m}(\omega), \qquad (1)$$

in which, $\omega$ denotes the spherical polar angles defining the orientation of the director in the molecular frame, and $C_{2m}(\omega)$ is a second-rank modified spherical harmonic. The expression in Equation (1) describes how the energy changes with the molecular orientation with respect to the director. The magnitude of this change is governed by the strength tensor, $X_{2m}$, which is related to the molecular anisotropy and the long-range orientational order parameters. The subscript 2 signifies the second-rank nature of the tensor, while $X_{20}$ is the major component of the strength tensor and $X_{22}$ is the

biaxiality in the tensor. The molecular biaxiality, $\lambda$, is defined by the ratio of these principal components, $X_{22}/X_{20}$, which under certain conditions is determined exclusively by anisotropy in the molecular shape. Thus for a molecule having a cuboidal shape with length, L, width, W, and breadth, B, the molecular biaxiality is, according to the surface tensor theory, given by Ferrarini *et al.* [15] as

$$\lambda = \frac{(3/2)^{1/2} L(B-W)}{\{L(B+W)-2BW\}}. \tag{2}$$

The expression in Equation (2) shows that in the limit of B = W, the molecular cross-section is square; hence the molecular biaxiality vanishes and $\lambda$ is zero. The opposite extreme to this rod-like molecule is the disc-like molecule which occurs when L = B; then $\lambda$ is $\sqrt{3/2}$. The most biaxial molecular shape, however, occurs in between these rod-like and disc-like extreme, which are uniaxial. This occurs when L, B, and W are related by the harmonic mean

$$\frac{\left(W^{-1}+L^{-1}\right)}{2} = B^{-1}, \tag{3}$$

for which $\lambda$ is $1/\sqrt{6}$, as we shall see. Although $\lambda$ has been estimated here using a model based solely on repulsive forces, it should be remembered that attractive forces also contribute to the biaxiality parameter [16].

The phase behaviour predicted by the molecular field theory as the molecular biaxiality is changed is shown in Figure 2. As expected, when $\lambda$ is zero, the system forms only a uniaxial nematic phase, $N_U$. As $\lambda$ deviates from zero, so a biaxial nematic phase is introduced in the phase diagram. With increasing $\lambda$, the uniaxial nematic-isotropic transition, $T_{N_UI}$, increases but not as rapidly as that between the biaxial and uniaxial nematic phases, $T_{N_BN_U}$. As a result, the two lines converge at a unique point, the *Landau point*, where the isotropic phase undergoes a transition directly to the biaxial nematic phase; this occurs when $\lambda$ is $1/\sqrt{6}$. As $\lambda$ increases

beyond this point, the molecule becomes more uniaxial and disc-like. Consequently, $T_{N_BN_U}$ falls until $\lambda$ is $\sqrt{3/2}$, where only a uniaxial nematic phase exists formed by the cylindrically symmetric molecular disc. In addition, the theory also predicts the order of the transitions which is important to help identify the $T_{N_BN_U}$ transition [9, 11, 12, 13, 14]. Thus, the $T_{N_UI}$ transition is first-order but as $\lambda$ increases, so the entropy change decreases until it vanishes at the Landau point, when the $T_{N_BI}$ transition is predicted to be second-order. This Landau point occurs when the value of $\lambda$ corresponds to the molecular maximum biaxiality which appears, as we can see in Figure 2 when $\lambda$ is 0.4082, *i.e.*, $1/\sqrt{6}$. In contrast to the $T_{N_UI}$ transition, the $T_{N_BN_U}$ transition is predicted to be second-order regardless of the magnitude of the molecular biaxiality. Therefore, on the basis of the molecular field calculations by Freiser [9], and others [13,14], it is apparent that any compound composed of biaxial molecules should, in principle, exhibit a biaxial nematic phase, and that the greater the molecular biaxiality, the greater the chance of observing the phase. However, the formation of the $N_B$ may be blocked by the formation of a smectic or a crystal phase; this possibility is indicated by the dashed line in Figure 2 which indicates that the $N_B$ phase may only be formed over a small range of molecular biaxiality.

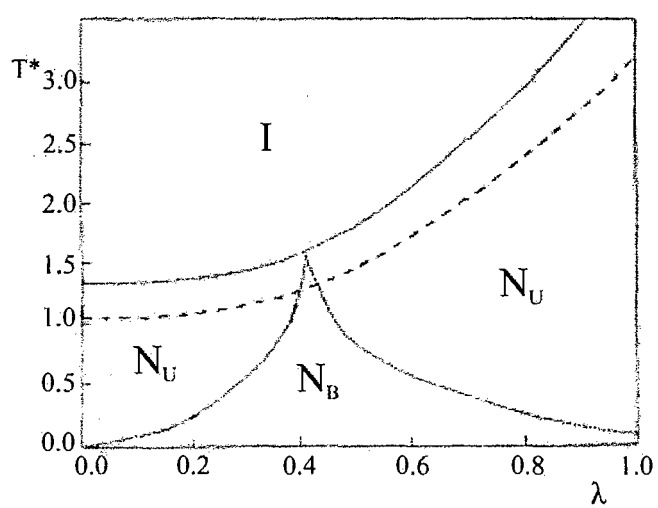


**Figure 2** The phase diagram predicted by the molecular field theory for a system of biaxial molecules as a function of the biaxiality parameter, $\lambda$; T* is the scaled temperature, $k_BT/u_0$, $u_0$ being the interaction energy, $k_B$ the Boltzmann constant, and T the absolute temperature. The dashed line shows the anticipated freezing point of the mesogen at a reduced temperature of 0.8 [11,12].

The phase in Figure 2 differs from that predicted by the theory derived by Sonnet *et al.* [17]; this new phase diagram is shown in Figure 3. In the phase diagram in Figure 3, the point on the line separating the $N_U$ and $N_B$ phases where the first- (solid line) and the second-order transition (dotted line) meet is a *tricritical point*, which is a distinctive feature of the model proposed by Sonnet *et al.* [17]. The same sequence of phases occurs until $\lambda \approx 0.22$, at the *triple point* when the three phases $N_U$, $N_B$, and I coexist. Above this value, a direct first-order transition from the isotropic phase into the biaxial nematic phase, $I - N_B$, is observed without an intermediate $N_U$.

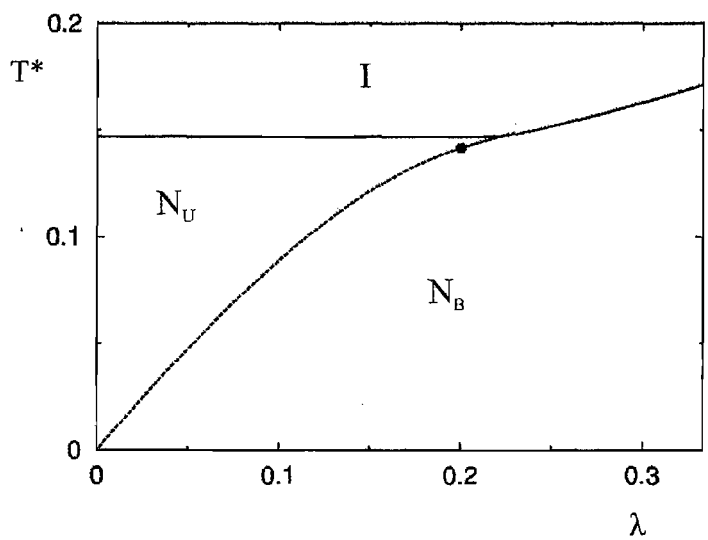


**Figure 3** The phase diagram showing the dependence of the scaled temperature, T*, on the biaxiality parameter, λ; T* is $k_BT/u_0$. The solid line represents the first-order transitions, while the dotted line represents the second-order $N_B - N_U$ transition [17].

As well as the ideal block shape, there are many forms that the molecule could take, in order to deviate from a cylindrical shape [18]. For example, a series of molecular shapes could be formed by linking rod-like, disc-like and semi-circular moieties together [19]. Such molecules would be long enough to exhibit a nematic phase and to deviate significantly from cylindrical symmetry to give a biaxial nematic. In fact, the first claimed discovery of a biaxial nematic [20] was for a compound formed of spoon-like molecules. Similar claims soon followed for cross-shaped [21] and bone-shaped molecules [22]. Perhaps the most recent shape of the mesogenic molecule explored is of a V-shaped [5, 11 ,23], in which two rod-like mesogenic groups are linked together through a central unit, as depicted in Figure 4.

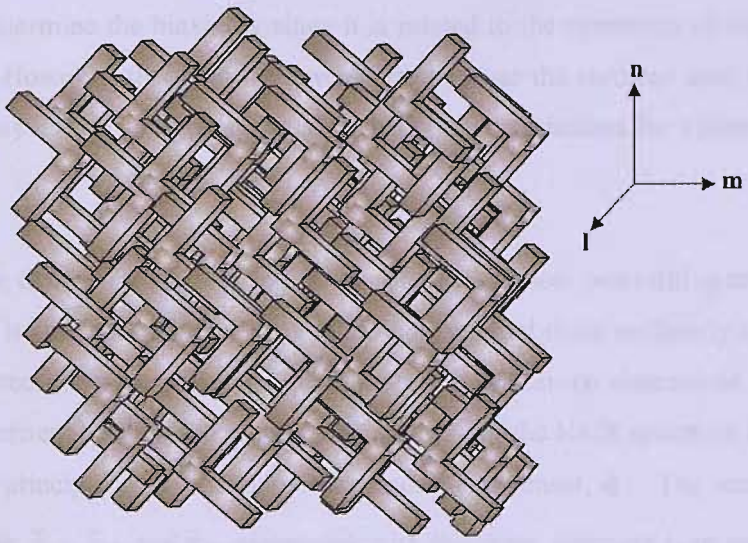


**Figure 4** The molecular organisation in an apolar biaxial nematic phase formed from V-shaped molecules.

## 7.4 Characterisation of the Biaxial Nematic Phase

A variety of techniques have been employed to identify the biaxial nematic phase [2], and one such method is based on the observation of the optical texture under the polarising microscope. Indeed polarising microscopy is usually a powerful technique with which to identify liquid crystal phases. For a biaxial nematic it had been argued that only a two-brush defect is formed [24, 25], as opposed to the four-brush defects found for a uniaxial nematic phase. More significantly, the observation of the biaxiality in tensorial properties, such as the refractive index (although formally, this is not a tensor) or dielectric permittivity should provide the most convincing demonstration of the phase symmetry. However, the determination of this biaxiality is not trivial as it is usually necessary to apply two constraints to the system to align two of the directors uniformly throughout the sample, while the third will follow the other two, thus creating a monodomain sample. One way to align the directors is to use a field, either magnetic or electric to align the director **n**, and subsequently surface forces to align one of the remaining directors. This would require, for example, the use of a thin sample confined between two surfaces which had been suitably treated to give the uniform planar alignment with the field applied across the film [26]. In the

case of the refractive index, conoscopy provides an extremely sensitive method with which to determine the biaxiality since it is related to the symmetry of the refractive index [2]. However, this is also its weakness because the surfaces used to align the thin film may induce an optical biaxiality that could be mistaken for a phase biaxiality [2].

In principle, deuterium NMR spectroscopy provides a more powerful approach as the bulk phase is studied, and the directors are not required to be uniformly aligned [27, 4]. The three components of the quadrupolar tensor can be determined in a single NMR experiment because the quadrupolar splitting of the NMR spectrum is related to one of the principal components of the quadrupolar tensor, $\tilde{\mathbf{q}}$. The measurements then provide $\tilde{q}_{XX}$, $\tilde{q}_{YY}$ and $\tilde{q}_{ZZ}$ associated with the three directors **l**, **m** and **n**. This NMR method has been applied to at least three compounds that were claimed to form a thermotropic biaxial nematic phase, and it was found that the nematic phase is, in fact, uniaxial [11, 28, 29,]. It would seem that although the molecules are certainly biaxial, the uniaxial nematic phase crystallises or is interrupted by a smectic phase before the anticipated biaxial nematic phase can be formed (see Figure 2).

Since the thermotropic biaxial nematic problem lies in large part with the technique of characterising the phase biaxiality, it is, therefore, crucial to test the viability of the technique in the first place. As stated earlier in Section 7.1, another burning issue is that if the biaxiality is large for lyotropic systems, why is it not so for thermotropic systems? In order to unravel these problems, we have therefore chosen a system in which the biaxiality is indisputable – the crystal E phase.

## 7.5 Crystal E phase of 4BT

The crystal E phase shows a clear biaxiality due to the herringbone arrangement of the molecular short axes in the layer orthogonal to the long axes [30] as depicted in Figure 5. The essential structural features of a crystal E phase are that the molecular long axes are orthogonal to a layer plane defined by the molecular centres and so exhibit long-range order. The molecular centres within the plane have a hexagonal arrangement. Overall the molecular centres have an orthorhombic distribution. The

molecular short axes have a herringbone arrangement which is also long range. However, the biaxiality depends on the angle made by the short axes with the glide plane. Thus the phase biaxiality will be a maximum when the angle is in between 0° and 45° but will vanish if the short axes are ≥ 45° to the glide plane. The phase would then have $D_{4h}$ rather than $D_{2h}$ symmetry.

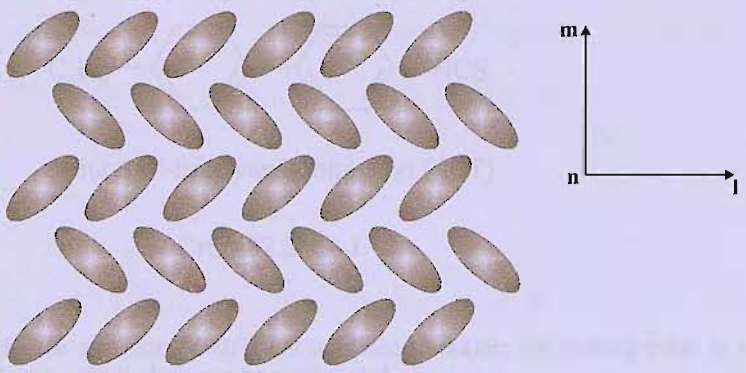


crystal E

**Figure 5** The herringbone organisation of the molecular short axes within a layer of a crystal E phase. The molecular long axes are orthogonal to the layer along the director **n**.

In the crystal E phase, the thermal motion of molecules is reduced to the extent that they arrange themselves in a herringbone pattern within a smectic layer [31]. In this herringbone organisation, the molecules remain disordered with respect to rotations of $\pi$ about both long and short molecular axes [32, 33]. Neutron scattering studies of the crystal E phase show that the molecules are rotating quite rapidly [33]. This situation results from the jump motions of the molecules about their long axes, such that they are generally restricted to $\pi$ rotations. The cooperative jumps are rapid with a frequency of about $10^{9\text{-}10}s^{-1}$, but the molecular planes can still be regarded as spending a greater proportion of their time in the biaxial herringbone arrangement featured in Figure 5.

In deuterium NMR spectroscopy, it is convenient to introduce deuterium into the sample by adding deuteriated probe molecules rather than face the difficult task of deuteriating the mesogenic molecule itself [11]. Moreover, most deuteriated liquid crystals are not commercially available, and so using deuteriated probe molecules

seems to be more convenient. The probe clearly needs to be selected so that the spectrum is especially sensitive to the phase biaxiality. To explore the relationship between the observed biaxiality and the molecular structure of the probe, we have chosen the crystal E phase, formed by 4-butyl-4′-isothiocyanatobiphenyl (4BT, see Figure 6) [34], whose biaxiality is not in doubt. In addition, 4BT has the advantage of staying in the E phase over a wide temperature range since this supercools easily.

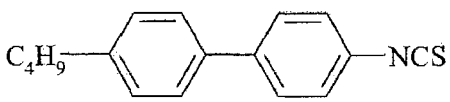


4-butyl-4′-thiocyanatobiphenyl (4BT)

CrE 82.2°C I

**Figure 6** The molecular structure of 4BT and its phase transition; the melting point is not known because the E phase can be supercooled.

The following section will describe the theoretical background of the determination of the phase biaxiality *via* deuterium NMR.

## 7.6 Theoretical Background

The analysis of the deuterium NMR powder pattern yields the components of the partially averaged quadrupolar tensor, $\tilde{\mathbf{q}}$, when the directors are randomly distributed with respect to the magnetic field of the spectrometer. The relative biaxiality in $\tilde{\mathbf{q}}$, defined by

$$\tilde{\eta} = \frac{\tilde{q}_{XX} - \tilde{q}_{YY}}{\tilde{q}_{ZZ}}, \tag{4}$$

provides a measure of the relative phase biaxiality, in which $\tilde{\eta}$ ranges from 0 (for a uniaxial phase) to the maximum of unity. These limiting values are obtained because $\tilde{\mathbf{q}}$ is traceless, *i.e.*, the sum of the diagonal elements vanishes, *i.e.*,

$$\tilde{q}_{XX} + \tilde{q}_{YY} + \tilde{q}_{ZZ} = 0, \tag{5}$$

with the axes labelled by convention such that,

$$|\tilde{q}_{ZZ}| > |\tilde{q}_{XX}| > |\tilde{q}_{YY}|, \quad \text{and} \quad \tilde{q}_{XX} - \tilde{q}_{YY} > 0. \tag{6}$$

Here, XYZ are the principal axes of $\tilde{\mathbf{q}}$ and correspond to the three directors for a biaxial phase, **n**, **l**, and **m**, as mentioned earlier in section 7.3. For the uniaxial phase, $\tilde{q}_{XX} = \tilde{q}_{YY}$ and so $\tilde{\eta}$ vanishes. At the other extreme, $\tilde{q}_{YY}$ vanishes and so $\tilde{q}_{XX}$ is $-\tilde{q}_{ZZ}$ (see Equation (5)). Hence from Equation (4), $\tilde{\eta}$ is equal to unity.

*Simulation of the NMR Spectra*

In a sample which consists of a distribution of the directors, the deuterium NMR spectrum is a superposition of quadrupolar doublets weighted by the singlet orientational distribution function $P(\beta,\alpha)$, which gives the probability of finding the magnetic field at the spherical polar angles β, α to the principal axes of $\tilde{\mathbf{q}}$. In our simulation, we assume a Lorentzian lineshape for each of the doublet components with a characteristic linewidth of $T_2^{-1}$. The overall spectrum, $I(\nu)$, can be obtained by integrating over all the possible angles,

$$I(\nu) = \int L\left[\nu, \Delta\nu(\beta,\alpha), T_2^{-1}\right] P(\beta,\alpha) \sin\beta \, d\beta \, d\alpha, \tag{7}$$

where L is the normalised Lorentzian function,

$$L(\nu) = 2T_2\left(\frac{1}{1+T_2^2(\nu-\nu_0)^2}\right), \tag{8}$$

where $T_2$ is the spin-spin relaxation time, and $\nu_0$ is the Larmor frequency. For a biaxial quadrupolar tensor, the positions of the peaks are given by

$$\begin{aligned}\tilde{\nu} &= \nu_0 \pm \frac{3}{4} q_{ZZ}\left( P_2(\cos\beta) + \frac{1}{2}\tilde{\eta}\sin^2\beta\cos 2\alpha \right) \\ &= \nu_0 \pm \frac{1}{2}\Delta\tilde{\nu}_0\left( P_2(\cos\beta) + \frac{1}{2}\tilde{\eta}\sin^2\beta\cos 2\alpha \right),\end{aligned} \tag{9}$$

where $P_2(\cos\beta)$ is the second Legendre function, $(3\cos^2\beta - 1)/2$. Taking $\nu_0 = 0$, and $\Delta\tilde{\nu}_0 = 1$, Equation (9) is simplified to

$$\tilde{\nu}(\beta,\alpha) = \pm\left( \frac{1}{2} P_2(\cos\beta) + \frac{1}{4}\tilde{\eta}\sin^2\beta\cos 2\alpha \right). \tag{10}$$

Hence the observed spectrum when the field is randomly oriented with respect to the principal axes of $\tilde{\mathbf{q}}$ is

$$I(\nu) = \int_0^{\pi}\int_0^{2\pi} \frac{T_2}{1 + T_2^2\left[ \nu \pm \left( \frac{1}{2} P_2(\cos\beta) + \frac{1}{4}\tilde{\eta}\sin^2\beta\cos 2\alpha \right) \right]^2} d\beta d\alpha. \tag{11}$$

In Equation (11) the linewidth, $T_2^{-1}$, is taken to be orientation independent. However in a biaxial phase, the three principal components $\tilde{q}_{XX}$, $\tilde{q}_{YY}$, and $\tilde{q}_{ZZ}$ determine the quadrupolar splittings when the magnetic field is along the principal axes, and we expect that in general, there will be different linewidths for these special orientations. These are denoted by $T_{XX}$, $T_{YY}$, and $T_{ZZ}$; strictly these are abbreviations for the more cumbersome expressions, $(T_2^{-1})_{XX}$, $(T_2^{-1})_{YY}$, and $(T_2^{-1})_{ZZ}$. It is now necessary to decide how the linewidth varies when B makes the spherical polar angles $\beta$, $\alpha$ with principal axes. The form of this angular dependence might be assumed to have a similar form as for quadrupolar splitting given in Equation (10). If so, then $T(\beta,\alpha)$ would be given by

$$T(\beta,\alpha) = \left\{ T_{ZZ} - \left( \frac{T_{YY} + T_{XX}}{2} \right) \right\}\cos^2\beta + \frac{T_{YY} + T_{XX}}{2} + \frac{1}{2}(T_{YY} - T_{XX})\sin^2\beta\cos 2\alpha. \tag{12}$$

This expression can be checked for the limiting orientations $\beta = 0$, $\beta = \pi/2$ $\alpha = 0$, and $\beta = \pi/2$ $\alpha = \pi/2$, corresponding to the field along the Z, X, and Y axes respectively. For these orientations along the principal axes of $\tilde{\mathbf{q}}$, the linewidths should be $T_{ZZ}$, $T_{XX}$, and $T_{YY}$ respectively, as they are.

There are two other simplifying situations, *i.e.*, (i) when the system is uniaxial $\left(T_{XX} = T_{YY} = T_{\perp}; T_{ZZ} = T_{\parallel}\right)$ and then the angular dependence of the linewidth is given by

$$T(\beta) = \left(T_{\parallel} - T_{\perp}\right)\cos^2\beta + T_{\perp} \tag{13}$$

and (ii) when the system is isotropic $T_{XX} = T_{YY} = T_{ZZ} = T_2^{-1}$; then the linewidth is independent of orientation and given by $T_2^{-1}$.

Figure 7 shows the simulation with various values of $\tilde{\eta}$, with the minimum value of zero to the maximum value of unity. The simulated deuterium NMR spectra for a system containing a single deuteron for which the directors are randomly distributed in three dimensions ($P(\beta,\alpha) = 1/4\pi$) are shown for a uniaxial and a biaxial phase. For the uniaxial phase, the spectrum consists of a pair of shoulders separated by $3\tilde{q}_{ZZ}/2$, and a pair of horns separated by $3\tilde{q}_{XX}/2 \equiv 3\tilde{q}_{YY}/2$.

When the phase is biaxial, another pair of shoulders appears, which allows all three components of $\tilde{\mathbf{q}}$, to be determined. For the maximum biaxiality, the splitting between the horns vanishes and the two sets of shoulders coalesce $\left(i.e., \tilde{q}_{XX} = -\tilde{q}_{ZZ} \text{ and } \tilde{q}_{YY} = 0\right)$ as observed in Figure 7 (although the signs of the splittings cannot be determined directly in such NMR experiments). The signature features of the spectrum show a clear indication of the biaxiality in $\tilde{\mathbf{q}}$, and hence the phase as $\tilde{\eta}$ increases from a value of zero. Indeed, NMR can be a definitive technique to confirm if the phase is biaxial or not. However, some spin probes can be blind to this biaxiality as discussed later in our results.

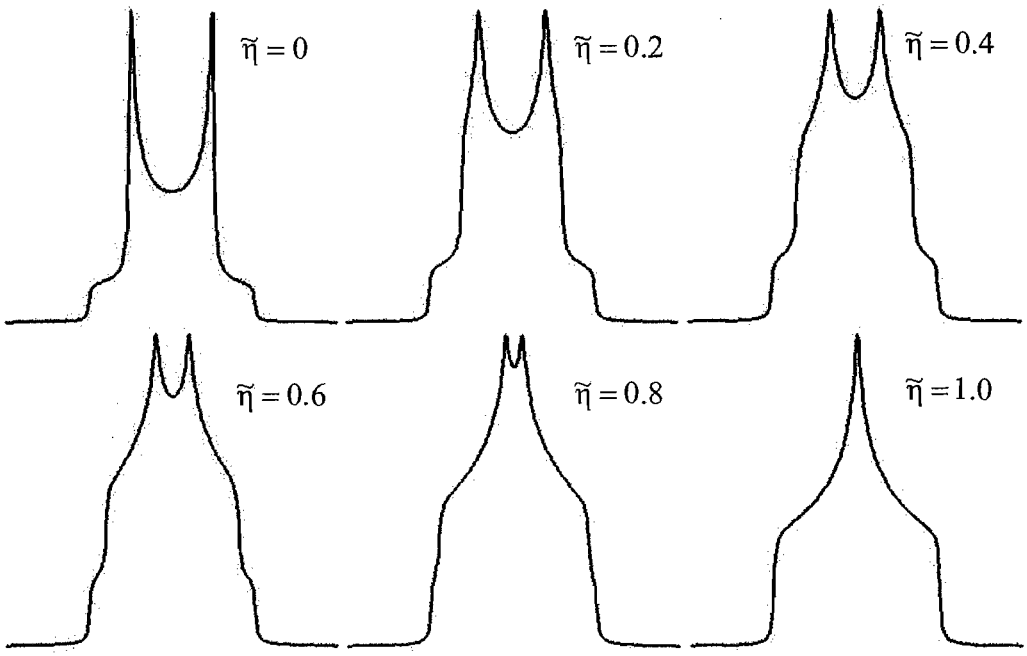


**Figure 7** Simulated 3D spectra for various values of $\tilde{\eta}$, the minimum value being zero and the maximum unity.

Although the spectral appearance clearly indicates the phase biaxiality, the quantification of this requires the determination of the principal components of $\tilde{\mathbf{q}}$. However, from the powder pattern it is difficult to determine these splittings directly, especially for a 3D spectrum with shoulders. In fact to determine the splittings from the experimental spectrum, it is necessary to simulate this in order to obtain the best fit by varying $\tilde{q}_{ZZ}$ (related to $\Delta\tilde{\nu}_0$), $\tilde{\eta}$ and $T_2^{-1}$. In the simulation, the maximum splitting is scaled to be 1. To determine the measurement point for the spectral shoulders, we run the simulation using the plot x-axis ranging from -0.5 to 0.5, *i.e.*, the maximum splitting of 1. We tested our results using three different values of the biaxiality, $\tilde{\eta}$ (*i.e.*, 0, 0.5, and 1), with the linewidth, $T_2^{-1}$, kept fixed. Figure 8 shows the results of the simulations. From the simulations, it can be seen that the separation for the shoulder should be measured at half-height of the shoulder, as indicated by the arrows. This is especially apparent for $\tilde{\eta} = 0.5$ because the sum of the inner splitting and the inner shoulder must equal to the outer shoulder. To satisfy this, the separation

for the shoulders must be measured at their half-height. For the inner doublet, the separation is measured from peak to peak. Of course, to obtain more precise values, those measured directly from the spectra can be used as the starting values for an iterative simulation of the experimental spectrum.

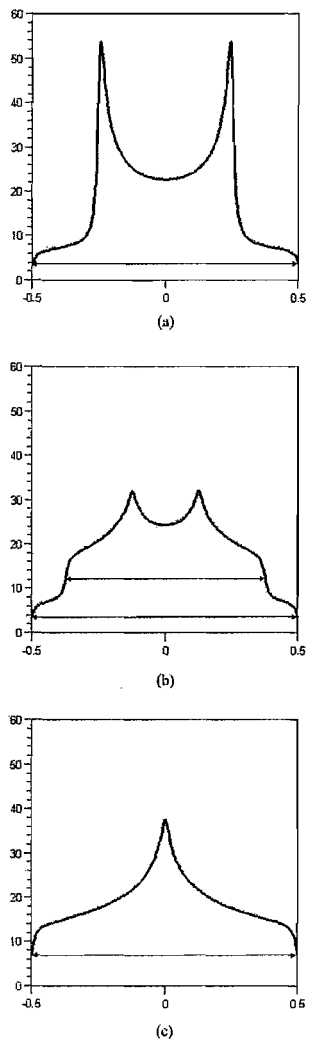


**Figure 8** Simulated spectra for three different values of $\tilde{\eta}$, *i.e.*, 0 for (a), 0.5 for (b) and 1 for (c). The maximum splitting is scaled to be 1. The simulations indicate that the splitting of the shoulder is measured at half-height, as shown by the arrows.

## 7.7 Order Parameters and their Relation to Phase Biaxiality

In this section, we shall discuss the relationship of the principal components of the partially averaged quadrupolar tensor, $\tilde{\mathbf{q}}$, obtained from the NMR experiment, to the

orientational order parameters. We first introduce the orientational order parameters used to define the order of the molecules in a biaxial phase.

### *7.7.1 Uniaxial Molecule in a Biaxial Phase*

Some of the probe molecules used in this project are uniaxial, and so, the simplest case to consider is that of a uniaxial molecule in a biaxial phase. Figure 9 shows a schematic diagram of a cylindrically symmetric molecule in a biaxial phase. XYZ are the phase symmetry axes and z is the molecule symmetry axis. The major order parameter, $S_{zz}^{ZZ}$, depends on the distribution function for the angle the molecule makes with the Z axis, and is given by

$$S_{zz}^{ZZ} = \left\langle \frac{3\ell_{zZ}^2 - 1}{2} \right\rangle, \tag{14}$$

where $\ell_{zZ}$ is the direction cosine for the two axes z and Z. This is analogous to the Saupe order parameter for a uniaxial molecule in a uniaxial phase.

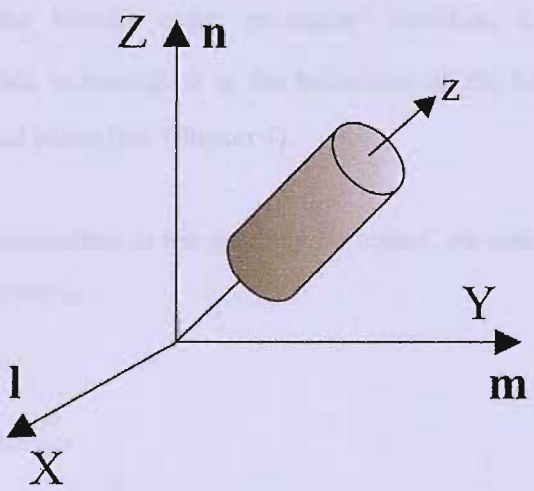


**Figure 9** Schematic diagram showing the orientation of a cylindrically symmetric (uniaxial) molecule in a biaxial phase.

The minor order parameters are then

$$S_{zz}^{XX} = \left\langle \frac{3\ell_{zX}^2 - 1}{2} \right\rangle \tag{15}$$

and

$$S_{zz}^{YY} = \left\langle \frac{3\ell_{zY}^2 - 1}{2} \right\rangle. \tag{16}$$

The sum of the squares of the direction cosines is unity, *i.e.*,

$$\ell_{zZ}^2 + \ell_{zX}^2 + \ell_{zY}^2 = 1 \tag{17}$$

and so

the ordering matrix is traceless,

$$S_{zz}^{ZZ} + S_{zz}^{XX} + S_{zz}^{YY} = 0. \tag{18}$$

The biaxial order parameter for the phase is then given as $\left(S_{zz}^{XX} - S_{zz}^{YY}\right)$. For a perfectly ordered system, the biaxial order parameter vanishes, *i.e.*, as $S_{zz}^{ZZ} \to 1$, so $\left(S_{zz}^{XX} - S_{zz}^{YY}\right) \to 0$ which is analogous to the behaviour of the behaviour of a biaxial molecule in a uniaxial phase (see Chapter 4).

To relate the order parameters to the quadrupolar tensor, we note that the quadrupolar splitting, $\Delta\tilde{\nu}_{ZZ}$, is given as

$$\Delta\tilde{\nu}_{ZZ} = \frac{3}{2}\tilde{q}_{ZZ} = \frac{3}{2}q_{CD}S_{zz}^{ZZ}, \tag{19}$$

where $q_{CD}$ is the component of the quadrupolar tensor for the deuteron in the $C-D$ bond which we take to be along the z-axis, *i.e.*, a principal axis system of the molecule. If the $C-D$ is at angle, $\theta$, to the molecular z-axis, $\Delta\tilde{\nu}_{ZZ}$ will then be

$$\Delta\tilde{\nu}_{ZZ} = \frac{3}{2} q_{CD} \left( \frac{3\cos^2\theta - 1}{2} \right) S_{zz}^{ZZ}, \tag{20}$$

assuming $q_{CD}$ is cylindrical [35]. When the magnetic field is along either of the other two principal axes of the phase then the quadrupolar splittings are given by

$$\Delta\tilde{\nu}_{XX} = \frac{3}{2}\tilde{q}_{XX} = \frac{3}{2} q_{CD} S_{zz}^{XX} \tag{21}$$

and

$$\Delta\tilde{\nu}_{YY} = \frac{3}{2}\tilde{q}_{YY} = \frac{3}{2} q_{CD} S_{zz}^{YY}, \tag{22}$$

where $\tilde{q}_{XX}$, $\tilde{q}_{YY}$, and $\tilde{q}_{ZZ}$ are the components of the partially averaged quadrupolar tensor, $\tilde{\mathbf{q}}$. To obtain these expressions, the C – D bond, about which the quadrupolar tensor is assumed to be cylindrically symmetric, is taken to be along the molecular z axis. In general, when the C – D bond makes an angle $\theta$ with the z axis, the quadrupolar splittings, $\Delta\tilde{\nu}_{XX}$ and $\Delta\tilde{\nu}_{YY}$, are given by expressions analogous to that for $\Delta\tilde{\nu}_{ZZ}$ in Equation (20). From Equation (4), the biaxiality in $\tilde{\mathbf{q}}$ for this general case can be rewritten as

$$\begin{aligned} \tilde{\eta} &= \frac{\left(q_{CD}\left(\left(3\cos^2\theta - 1\right)/2\right) S_{zz}^{XX}\right) - \left(q_{CD}\left(\left(3\cos^2\theta - 1\right)/2\right) S_{zz}^{YY}\right)}{q_{CD}\left(\left(3\cos^2\theta - 1\right)/2\right) S_{zz}^{ZZ}} \\ &= \frac{\left(S_{zz}^{XX} - S_{zz}^{YY}\right)}{S_{zz}^{ZZ}}. \end{aligned} \tag{23}$$

Equation (23) shows that the biaxiality parameter, $\tilde{\eta}$, is independent of the orientation of the C – D bond with respect to the molecular z axis. On the other hand, the individual order parameters are not independent of the molecular geometry.

In addition, the relationship of $\left(S_{zz}^{XX} - S_{zz}^{YY}\right)$ *vs* $S_{zz}^{ZZ}$ produces a curve for a fixed value of the biaxiality parameter passing through the limiting values

$S_{zz}^{ZZ} = 0$, $\left(S_{zz}^{XX} - S_{zz}^{YY}\right) = 0$ and $S_{zz}^{ZZ} = 1$, $\left(S_{zz}^{XX} - S_{zz}^{YY}\right) = 0$ and having a maximum value when $S_{zz}^{ZZ} \sim 0.5$. The relationship measures the deviation from cylindrical symmetry.

### *7.7.2 Biaxial Molecule in a Biaxial Phase*

Figure 10 shows the orientation of a biaxial molecule in a biaxial phase. XYZ are the phase symmetry axes, and xyz are the molecular symmetry axes. The orientational ordering of a biaxial molecule in a biaxial phase can be described by the supermatrix

$$S_{\alpha\beta}^{AB} = \left\langle \frac{3\ell_{A\alpha}\ell_{B\beta} - \delta_{AB}\delta_{\alpha\beta}}{2} \right\rangle, \tag{24}$$

where A and B denote the phase symmetry axes, and α and β are for the molecular symmetry axes [36].

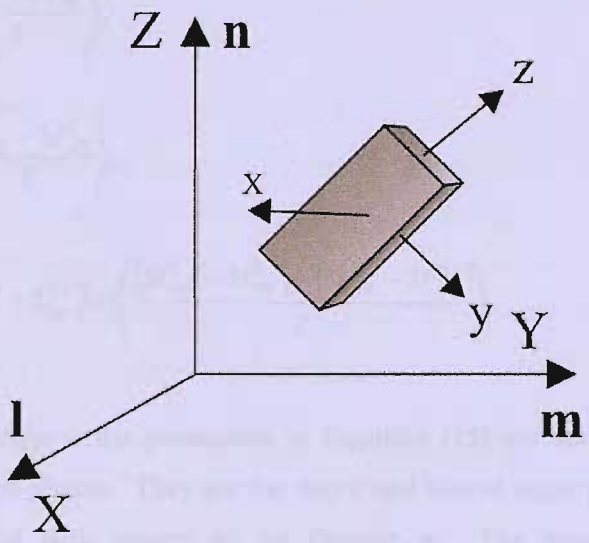


**Figure 10** Schematic diagram showing the orientation of a biaxial molecule in a biaxial phase.

In general, the supermatrix contains eighty-one non-zero elements, but the number of independent elements is just 25. This is due to the invariance under exchange of the indices, for example, x → y and X → Y, which leaves the supermatrix elements

unchanged; in addition, the properties of the direction cosines require that the trace of each submatrix vanishes. If the principal axes for both the phase and the molecular matrices are known, the number of independent components can be reduced. This leaves the nine diagonal elements, $S_{\alpha\alpha}^{AA}$, as non-zero, and because $\sum_{\alpha} S_{\alpha\alpha}^{AA}$ and $\sum_{A} S_{\alpha\alpha}^{AA}$ both vanish, we are left with just four independent elements of the supermatrix [37]. Physically, the $S_{\alpha\alpha}^{AA}$ are the ordering matrices for the principal molecular axes with respect to the three principal axes **l**, **m**, and **n** of the biaxial phase. The four independent components of $S_{\alpha\alpha}^{AA}$ used to describe the second rank orientational ordering of a biaxial molecule within a biaxial phase are defined to be (see Chapter 2, Section 2.5):

$$
\begin{aligned}
S_{zz}^{ZZ} &= \left\langle \frac{3\ell_{zZ}^2 - 1}{2} \right\rangle, \\
S_{xx}^{ZZ} - S_{yy}^{ZZ} &= \left\langle \frac{3\ell_{xZ}^2 - 3\ell_{yZ}^2}{2} \right\rangle, \\
S_{zz}^{XX} - S_{zz}^{YY} &= \left\langle \frac{3\ell_{zX}^2 - 3\ell_{zY}^2}{2} \right\rangle, \\
\left(S_{xx}^{XX} - S_{xx}^{YY}\right) - \left(S_{yy}^{XX} - S_{yy}^{YY}\right) &= \left\langle \frac{\left(3\ell_{xX}^2 - 3\ell_{xY}^2\right) - \left(3\ell_{yX}^2 - 3\ell_{yY}^2\right)}{2} \right\rangle.
\end{aligned}
\tag{25}
$$

The first two of these order parameters in Equation (25) are non-zero in both the uniaxial and biaxial phases. They are the major and biaxial order parameters for the molecule measured with respect to the director **n**. The remaining two order parameters vanish in the uniaxial phase, but are non-zero in the biaxial phase. $\left(S_{xx}^{ZZ} - S_{yy}^{ZZ}\right)$ is the minor biaxial order parameter for the molecule, while $\left(S_{zz}^{XX} - S_{zz}^{YY}\right)$ measures the biaxiality in the ordering of the molecular z axis with respect to the phase X and Y axes, *i.e.*, the minor biaxial order parameter for the phase. The final quantity is the difference in the phase biaxial order parameter for the molecular x and

y axes, or in other words, the major biaxial order parameter for the molecule and the phase. The dependence of these four order parameters on the direction cosines, $\ell_{\alpha A}$, allows the limiting forms to be easily identified since, in the limit of perfect order, these limits $\alpha A \rightarrow \delta_{\alpha A}$, *i.e.*, $\ell_{zZ} = 1$ while $\ell_{zX} = 0$. Then $S_{xx}^{XX} = S_{yy}^{YY} \rightarrow 1$ and $S_{xx}^{YY} = S_{yy}^{XX} = -\frac{1}{2}$, and so the high order limiting values with the molecular axes x, y, and z parallel to the phase axes X, Y, and Z, respectively, are

$$
\begin{aligned}
&S_{zz}^{ZZ} \rightarrow 1, \\
&S_{xx}^{ZZ} - S_{yy}^{ZZ} \rightarrow 0, \\
&S_{zz}^{XX} - S_{zz}^{YY} \rightarrow 0, \\
&\left(S_{xx}^{XX} - S_{xx}^{YY}\right) - \left(S_{yy}^{XX} - S_{yy}^{YY}\right) \rightarrow 3.
\end{aligned}
\tag{26}
$$

### *7.7.3 Molecular Geometry: The General Case*

Here we consider the relationships between the quadrupolar splittings and the four principal order parameters for the general case of a biaxial molecule in a biaxial phase. We shall not derive these results from first principles but shall use the result derived by Dunmur and Toriyama [38] for the magnetic susceptibility tensor of a biaxial phase. This tensor, like the quadrupolar tensor, is also second-rank but unlike the quadrupolar tensor, it is traceless. Allowing for this gives the three principal components of $\tilde{\mathbf{q}}$ as

$$
\tilde{q}_{ZZ} = \frac{2}{3}\left[ S_{zz}^{ZZ}\left( q_{zz} - \frac{1}{2}\left(q_{xx} + q_{yy}\right)\right) + \frac{\left(S_{xx}^{ZZ} - S_{yy}^{ZZ}\right)}{2}\left(q_{xx} - q_{yy}\right)\right] . \tag{27}
$$

$$
\tilde{q}_{YY} = -\frac{1}{3}\left[\begin{array}{l} \left(S_{zz}^{ZZ} + \left(S_{zz}^{XX} - S_{zz}^{YY}\right)\right)\left( q_{zz} - \frac{1}{2}\left(q_{xx} + q_{yy}\right)\right) + \\ \left\{\left(S_{xx}^{ZZ} - S_{yy}^{ZZ}\right) + \left(S_{xx}^{XX} - S_{yy}^{XX}\right) - \left(S_{xx}^{YY} - S_{yy}^{YY}\right)\right\}\frac{1}{2}\left(q_{xx} - q_{yy}\right) \end{array}\right] \tag{28}
$$

$$\tilde{q}_{XX} = -\frac{1}{3}\left[\begin{array}{l}\left(S_{zz}^{ZZ} - \left(S_{zz}^{XX} - S_{zz}^{YY}\right)\right)\left(q_{zz} - \frac{1}{2}\left(q_{xx} + q_{yy}\right)\right) + \\ \left\{\left(S_{xx}^{ZZ} - S_{yy}^{ZZ}\right) + \left(S_{xx}^{XX} - S_{yy}^{XX}\right) - \left(S_{xx}^{YY} - S_{yy}^{YY}\right)\right\}\frac{1}{2}\left(q_{xx} - q_{yy}\right)\end{array}\right]. \tag{29}$$

These expressions can be simplified somewhat by using the fact that the molecular quadrupolar tensor is also traceless; this means that $\left(q_{zz} - 1/2\left(q_{xx} + q_{yy}\right)\right)$ can be replaced by $3q_{zz}/2$. This gives

$$\tilde{q}_{ZZ} = S_{zz}^{ZZ} q_{zz} + \left(S_{xx}^{ZZ} - S_{yy}^{ZZ}\right)\frac{1}{3}\left(q_{xx} - q_{yy}\right) \tag{30}$$

$$\tilde{q}_{YY} = -\frac{1}{2}\left[\begin{array}{l}\left(S_{zz}^{ZZ} + \left(S_{zz}^{XX} - S_{zz}^{YY}\right)\right)q_{zz} + \left\{\left(S_{xx}^{ZZ} - S_{yy}^{ZZ}\right) + \left(S_{xx}^{XX} - S_{yy}^{XX}\right) - \left(S_{xx}^{YY} - S_{yy}^{YY}\right)\right\} \\ \frac{1}{3}\left(q_{xx} - q_{yy}\right)\end{array}\right] \tag{31}$$

$$\tilde{q}_{XX} = -\frac{1}{2}\left[\begin{array}{l}\left(S_{zz}^{ZZ} - \left(S_{zz}^{XX} - S_{zz}^{YY}\right)\right)q_{zz} + \left\{\left(S_{xx}^{ZZ} - S_{yy}^{ZZ}\right) + \left(S_{xx}^{XX} - S_{yy}^{XX}\right) - \left(S_{xx}^{YY} - S_{yy}^{YY}\right)\right\} \\ \frac{1}{3}\left(q_{xx} - q_{yy}\right)\end{array}\right]. \tag{32}$$

It is of interest that $\tilde{q}_{ZZ}$ depends only on the two order parameters that do not vanish in both the uniaxial and biaxial nematic phases. As is to be expected, the biaxiality in $\tilde{\mathbf{q}}$ is determined solely by the order parameters in which do vanish in the uniaxial but not in the biaxial nematic phase; thus

$$\tilde{q}_{XX} - \tilde{q}_{YY} = \left(S_{zz}^{XX} - S_{zz}^{YY}\right)q_{zz} + \left\{\left(S_{xx}^{XX} - S_{yy}^{YY}\right) - \left(S_{xx}^{YY} - S_{yy}^{YY}\right)\right\}\frac{1}{3}\left(q_{xx} - q_{yy}\right). \tag{33}$$

The sensitivity of the result for this biaxiality in $\tilde{\mathbf{q}}$ and the relative biaxiality to the location of the $C-D$ bond is of particular concern. Here we consider three special cases in which the $C-D$ bond is directed along each of the three principal axes of the molecular ordering tensor. In evaluating the resulting phase biaxiality it is convenient and realistic to neglect the small biaxiality in the molecular quadrupolar tensor, $\tilde{\mathbf{q}}$.

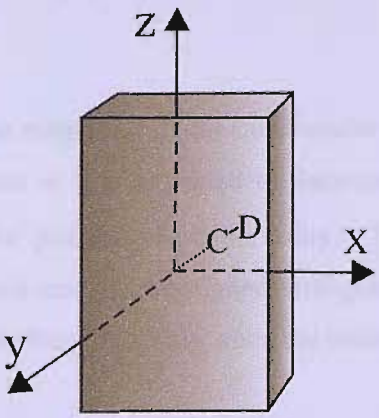


**Figure 11** A schematic representation of a biaxial molecule showing its principal axis system.

I. $C-D \parallel$ z-axis:

When the $C-D$ bond is parallel to the z-axis the diagonal components of $\tilde{\mathbf{q}}$ are

$$q_{zz} = q_{CD}$$

$$q_{xx} = -\frac{1}{2} q_{CD} \tag{34}$$

$$q_{yy} = -\frac{1}{2} q_{CD},$$

and so $(q_{xx} - q_{yy})$ vanishes. This gives the major element of $\tilde{\mathbf{q}}$ and its biaxiality as

$$\tilde{q}_{ZZ} = S_{zz}^{ZZ} q_{CD}$$

$$\tilde{q}_{XX} - \tilde{q}_{YY} = (S_{zz}^{XX} - S_{zz}^{YY}) q_{CD}. \tag{35}$$

The relative biaxiality is then

$$\tilde{\eta} = \frac{\left(S_{zz}^{XX} - S_{zz}^{YY}\right)}{S_{zz}^{ZZ}} \tag{36}$$

which is independent of the magnitude of the quadrupolar coupling constant. As the orientational order increases so $\tilde{\eta}$ is expected to decrease which suggests that this location is not the best for probing phase biaxiality. This is especially the case because the molecular z-axis tends to be aligned orthogonal to the XY plane and so will not be able to probe the phase biaxiality when the ordering is high.

II. $C-D \parallel$ y-axis:

When the $C-D$ bond is parallel to the y-axis, the diagonal elements of $\tilde{\mathbf{q}}$ are

$$\begin{aligned} q_{zz} &= -\frac{1}{2} q_{CD} \\ q_{yy} &= q_{CD} \\ q_{xx} &= -\frac{1}{2} q_{CD}, \end{aligned} \tag{37}$$

which gives the biaxiality in $\tilde{\mathbf{q}}$ as

$$q_{xx} - q_{yy} = -\frac{3}{2} q_{CD}. \tag{38}$$

Substitution of these into the expressions for $\tilde{\mathbf{q}}$ gives the following results

$$\tilde{q}_{ZZ} = -\frac{1}{2} q_{CD}\left[S_{zz}^{ZZ} + \left(S_{xx}^{ZZ} - S_{yy}^{ZZ}\right)\right] \tag{39}$$

for the major component and for the biaxiality

$$\tilde{q}_{XX} - \tilde{q}_{YY} = -\frac{1}{2} q_{CD} \left[ \left( S_{zz}^{XX} - S_{zz}^{YY} \right) + \left( S_{xx}^{XX} - S_{yy}^{XX} \right) - \left( S_{xx}^{YY} - S_{yy}^{YY} \right) \right] \tag{40}$$

These expressions for $\tilde{\mathbf{q}}$ are given in terms of the four order parameters characterising the ordering of a biaxial molecule in a biaxial phase (see Equations 25). We see that the biaxiality in $\tilde{\mathbf{q}}$ is determined by the dominant biaxial order parameter and so it is anticipated that the location of the C – D bond along the y-axis is favourable for the determination of the phase biaxiality especially when the order is high.

Although it is helpful to have $\tilde{\mathbf{q}}$ expressed in terms of the four order parameters, it is possible to simplify the equations for the components of $\tilde{\mathbf{q}}$. This is achieved by using the fact that $S_{\alpha\alpha}^{AA}$ is traceless when summed over $\alpha$ and A. Using the summation over $\alpha$ allows us to write

$$\begin{aligned} S_{zz}^{ZZ} + S_{xx}^{ZZ} &= -S_{yy}^{ZZ}, \\ S_{zz}^{YY} + S_{xx}^{YY} &= -S_{yy}^{YY}, \\ S_{zz}^{XX} + S_{xx}^{XX} &= -S_{yy}^{XX}. \end{aligned} \tag{41}$$

Substitution of these relations into Equations (39) and (40) leads to the simpler results

$$\tilde{q}_{ZZ} = q_{CD} S_{yy}^{ZZ} \tag{42}$$

and

$$\left( \tilde{q}_{XX} - \tilde{q}_{YY} \right) = q_{CD} \left( S_{yy}^{XX} - S_{yy}^{YY} \right) \tag{43}$$

with the relative biaxiality

$$\tilde{\eta} = \frac{\left( S_{yy}^{XX} - S_{yy}^{YY} \right)}{S_{yy}^{ZZ}}. \tag{44}$$

These biaxialities are expected to be large provided the molecular y axis tends to be aligned in the XY plane.

III. $C-D \parallel$ x-axis:

In this final example, the $C-D$ bond is aligned parallel to the molecular x-axis. The diagonal components of $\tilde{\mathbf{q}}$ are then

$$q_{zz} = -\frac{1}{2} q_{CD}$$

$$q_{yy} = -\frac{1}{2} q_{CD} \tag{45}$$

$$q_{xx} = q_{CD};$$

this gives the biaxiality as

$$q_{xx} - q_{yy} = \frac{3}{2} q_{CD}. \tag{46}$$

Substitution of these results into Equations (30) and (33) for the components for the partially averaged quadrupolar tensor, $\tilde{\mathbf{q}}$, as

$$\tilde{q}_{ZZ} = -\frac{1}{2} q_{CD} \left[ S_{zz}^{ZZ} - \left( S_{xx}^{ZZ} - S_{yy}^{ZZ} \right) \right] \tag{47}$$

for the major component and

$$\left( \tilde{q}_{XX} - \tilde{q}_{YY} \right) = -\frac{1}{2} q_{CD} \left[ \left( S_{zz}^{XX} - S_{zz}^{YY} \right) - \left\{ \left( S_{xx}^{XX} - S_{yy}^{XX} \right) - \left( S_{xx}^{YY} - S_{yy}^{YY} \right) \right\} \right] \tag{48}$$

for the biaxiality. As is to be anticipated, these results are analogous to the case when the C – D bond is parallel to the y-axis. Consequently, the biaxiality in $\tilde{\mathbf{q}}$ is expected to be large. In the same way we found when the C – D bond is parallel to the y-axis, these equations can be simplified to

$$\tilde{q}_{ZZ} = q_{CD} S_{xx}^{ZZ} \tag{49}$$

and

$$\tilde{q}_{XX} - \tilde{q}_{YY} = q_{CD}\left(S_{xx}^{XX} - S_{xx}^{YY}\right) \tag{50}$$

which gives the relative biaxiality as

$$\tilde{\eta} = \frac{\left(S_{xx}^{XX} - S_{xx}^{YY}\right)}{S_{xx}^{ZZ}}. \tag{51}$$

This is also expected to be significant provided that the molecular x-axis tends to be aligned in the XY plane of the biaxial nematic phase.

## 7.8 Previous Studies on Crystal E Phase

Before we proceed to our results on the crystal E phase of 4BT using the spin probes, we shall first discuss the results for the crystal E phase found in other systems. Of parallel interest is a study by Vaz *et al.*, [30] who had described the first detailed deuterium NMR study of the molecular orientational ordering in a crystal E phase exhibited by a binary mixture of liquid crystals. The following subsection gives a brief account of their investigation.

*Binary mixture of 4O.8-$d_4$ and 8OCB*

The binary system studied by Vaz *et al.*, [30] was composed of 50wt.% 4-butoxybenzylidene-4'-octylaniline-2,3,5,6-$d_4$ (4O.8-$d_4$), in which the aniline has been

deuteriated in the ring) and 50wt.% 4-octyloxycyanobiphenyl (8OCB). The crystal E phase only appears in the binary mixture and not in the pure form of the two liquid crystalline materials. This is a feature that appears to have some generality in that equimolar mixtures of 8OCB and several other *n*O.*m* Schiff base materials also exhibit a crystal E phase [30]. For the system studied, the phase sequence was:

Cr 15°C E 52.9°C SmB 83°C SmA 104°C SmA + I 107.5°C I.

The NMR experiment was carried out by heating the sample into the isotropic phase, and data were then recorded in a slow cooling cycle. The NMR spectra were recorded at several selected temperatures as a function of the angle, θ, made by the original field direction with the sample. Figure 12 shows some very unusual spectral patterns found by Vaz *et al.* [30] for the crystal E phase at 20°C.

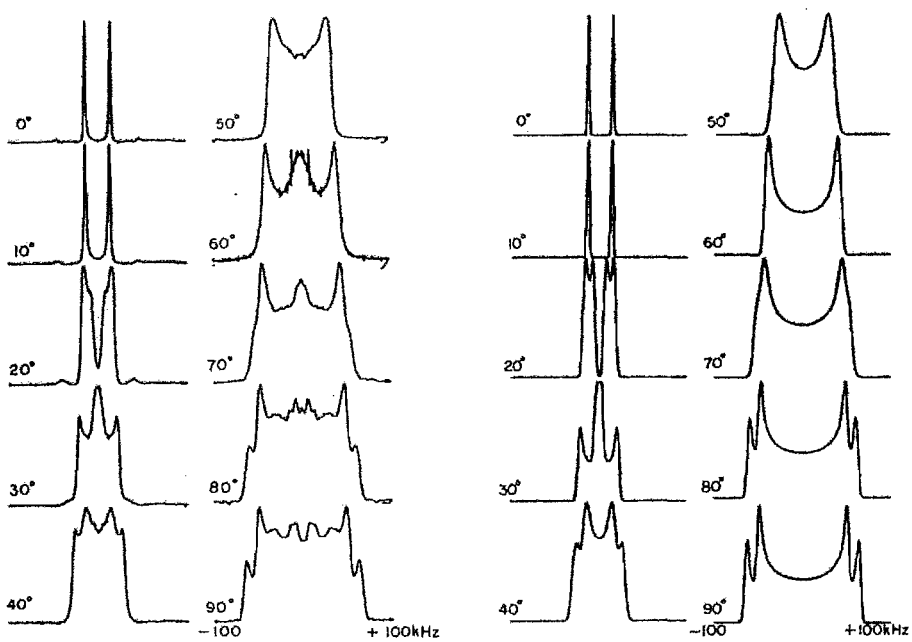


**Figure 12** The orientation dependence of the deuterium NMR spectra at 20°C in the crystal E phase of the binary mixture of 4O.8-$d_4$ and 8OCB and the simulated spectra with the value of $\tilde{\eta} = 0.57$ [30].

In the preceding aligned SmA and SmB phases, their uniaxial character is demonstrated by the observation of a single quadrupolar splitting whose angular dependence is given by

$$\Delta\tilde{\nu}_\theta = \Delta\tilde{\nu}_0 P_2(\cos\theta), \quad (52)$$

where $\Delta\tilde{\nu}_\theta$ is the quadrupolar splitting of the NMR spectrum when the director makes an angle, $\theta$, with the magnetic field and $\Delta\tilde{\nu}_0$ is the quadrupolar splitting when the director is parallel to the magnetic field. Equation (52) shows that with increasing $\theta$, the quadrupolar splitting decreases, passes through zero at the magic angle (*i.e.*, 54.74°), and then increases to one half the original splitting, $\Delta\tilde{\nu}_0$, when the director is perpendicular to the magnetic field. Evidently, the spectra recorded for the crystal E phase deviates from this angular dependence in Equation (52) and shows peculiar spectral patterns which are more complex than a single quadrupolar doublet found in the uniaxial phases (see Figure 12). The spectral width for the orientation perpendicular to the applied magnetic field is much larger than at 0°, which contrasts with the results obtained for the SmA and SmB phases. In the SmA phase the director is aligned parallel to the magnetic field and this alignment is preserved on cooling into the SmB and then the crystal E phase but the minor directors are not aligned by the field.

To explain this curious phenomenon, Vaz *et al.* [30] proposed some possible molecular motional models for the aromatic ring within the crystal E phase from the simple geometry of a herringbone lattice, which are able to account precisely for the measured values of the time-averaged quadrupolar coupling constant and biaxiality parameter which was found to be 0.57. In addition, from the models and their experimental data, it was observed that the orientational order of the para axis for the aromatic ring relative to the axis of the magneto alignment (layer normal) in the crystal E phase is approximately unity.

The molecular motion within the crystal E phase should consists primarily of (i) a rapid ($\tau \sim 10^{-5}$s) localised diffusive motion perpendicular to the smectic layers, and (ii) on-site librational (oscillational) motions of the short axis of the aromatic ring with an order parameter of 0.8. In addition, it is suggested that only the aromatic ring may be flipping and that other segments of the molecule may be rotating more freely. This observation comes from the angular-dependent spectral patterns of 50wt.% 4O.8-$d_{21}$

(perdeuteriated alkyl chain) mixed with 50wt.% 8OCB, which narrow at the orientation of 90° [39], rather than broader, as found in the study by Vaz *et al.* [30].

## 7.9 Experimental

The sample of 4BT was kindly given to us by Professor Roman Dabrowski from the Institute of Chemistry at the Military Technical Academy, Warsaw, Poland, and was not purified further. 4BT exhibits exclusively the crystal E phase with the transition to the isotropic phase at 82.2°C [34]. However, we did not check this transition. In addition, 4BT also undergoes supercooling. The details of the synthesis of 4BT are reported in [34]. We have used various probe molecules for this study which were, hexamethylbenzene-$d_{18}$ (also used in the investigation of the supposed biaxial nematic phase of other mesogens [5, 29]), acetonitrile-$d_3$, chloroform-$d_1$, methylene dichloride-$d_2$, and p-xylene-$d_6$; the molecular structures of these probes are shown in Figure 13. The choice of the probe molecules are such that they possess either uniaxial or biaxial molecular biaxiality, in order to obtain a substantial amount of information concerning the effect of the probe structure on the biaxiality of the quadrupolar tensor in the crystal E phase.

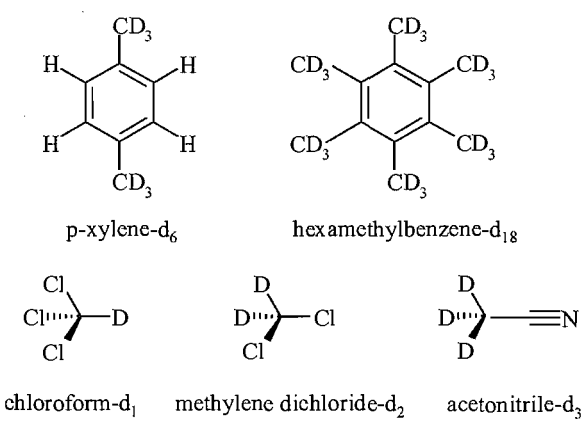


**Figure 13** The deuteriated spin probes used in the investigation.

Each sample was individually prepared in a 5mm o.d. 4mm i.d. NMR tube, about 3.5cm long. The NMR tube was heat-sealed completely after quenching the sample in liquid nitrogen to prevent the solute from evaporating. Finally, the sample was heated into the isotropic phase in order to homogenise the mixture (so that the probe

is evenly distributed) and cooled to room temperature before placing it in the magnetic field of the spectrometer. The short NMR tubes are necessary because the tube is placed horizontally in the NMR probe which is only 7cm in diameter. In addition, a Vortex plug was used in order to prevent the sample from flowing out of the NMR tube.

The deuterium NMR measurements were performed on a *Varian Infinity Plus 300* spectrometer with *Spinsight* software for data acquisition and processing, using the Solaris Operating Environment on a SUN *Microsystem* workstation. The spectra were recorded using a quadrupolar echo sequence $(\pi/2-\tau_1-\pi/2-\tau_2)$, where both $\tau_1$ and $\tau_2$ were 33μs (in most of the experiments conducted), while the length of the $\pi/2$ pulse was 5μs. The free-induction decay was averaged over several thousand transients. The spectral width was within the range of 100-200kHz. The temperature was controlled *via* a thermocouple located in the probe head connected to a *Varian* temperature control unit, with a stability of 0.1K. The air flow rate was set at $50ft^3/h$.

## 7.10 Results and Discussion

The NMR spectra show a range of behaviour for the various probes. There is usually a central peak from an isotropic component due to the low solubility of the probes in the highly ordered crystal E phase. In essence, the magnetic field of the spectrometer is unable to align the crystal E phase, which results in a random distribution of the directors, and hence, a three-dimensional powder pattern spectrum is obtained. Our simulations were performed using MAPLE 10.0. In the simulation, three parameters were optimized, the linewidth, the major quadrupolar coupling, $\tilde{q}_{zz}$, and the biaxiality parameter, $\tilde{\eta}$, in order to get the best fit to the experimental spectra. The inclusion of the isotropic peak in our simulation is also important to fit our experimental results, and here too, the linewidth of the single peak was optimized to fit the experimental spectra.

*7.10.1 Hexamethylbenzene-$d_{18}$*

Figure 14 shows the experimental and simulated spectra of hexamethylbenzene-$d_{18}$ in 4BT. The form of the experimental spectrum suggests that the biaxiality in $\tilde{\mathbf{q}}$ is small, and the simulation of the spectrum gives a value for $\tilde{\eta}$ of just 0.05. This result

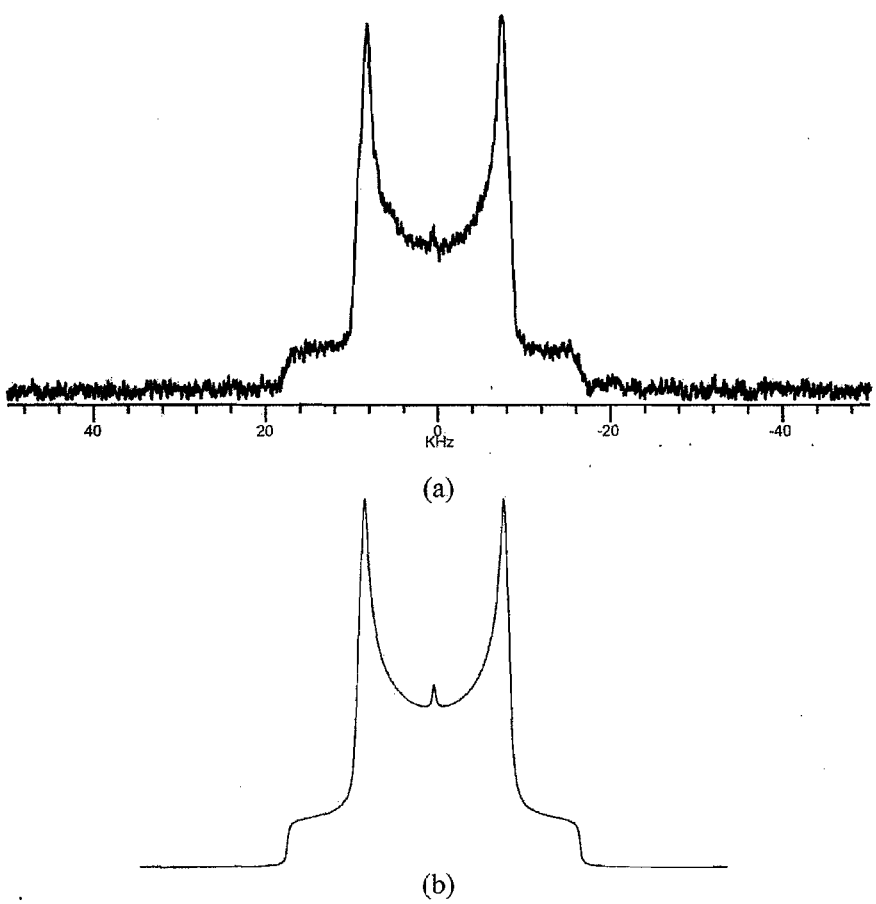


**Figure 14** (a) The deuterium NMR spectrum of hexamethylbenzene-$d_{18}$ in 4BT at 25°C and (b) the spectrum simulated with $\tilde{\eta} = 0.05$.

seems to be comparable with that obtained by Madsen *et al.* [5] who used hexamethylbenzene-$d_{18}$ as a probe for the nematic phase formed by V-shaped molecule ODBP-Ph-$C_7$ (short for 2,5-bis(4-hydroxyphenyl)-1,3,4-oxadiazole); they found $\tilde{\eta}$ to be about 0.11. However, our results differ in that the orientational order in the two phases are quite different; thus $\Delta\tilde{\nu}_0$ is 34.2kHz whereas in the nematic phase

formed by ODBP-Ph-$C_7$ [5], $\Delta\tilde{\nu}_0$ is only 5.98kHz. This large difference suggests that the ordering in E phase of 4BT is extremely high which is to be expected; however it prompted us to study the crystallised phase of pure hexamethylbenzene-$d_{18}$.

*Pure Hexmethylbenzene-$d_{18}$*

Figure 15 shows the deuterium NMR spectra of pure hexamethylbenzene-$d_{18}$ in various conditions. Figure 15a shows the spectrum of the hexamethylbenzene-$d_{18}$ in its crystalline state. When the sample was melted into the isotropic phase in the spectrometer and subsequently cooled to 25°C, the spectrum obtained was that shown in Figure 15b. The spectrum is not very much different from that of hexylmethylbenzene-$d_{18}$ in 4BT shown in Figure 14, except, of course, for the extraneous peaks. We rotated the sample by 90° from the direction of the magnetic field and the spectrum obtained is shown in Figure 15c. The spectrum looks different from that shown in Figure 15b, and so we attribute this difference to the different orientations of the crystal axes created when the sample was cooled from the isotropic phase. When the sample was rotated through a subsequent 90° rotation (see Figure 15d), the spectrum obtained was the same as that obtained in Figure 15b when the sample was cooled from the isotropic phase. Despite the different spectral forms, the splittings of the spectrum of the pure hexamethylbenzene-$d_{18}$ and hexamethylbenzene-$d_{18}$ in 4BT are almost the same; the outer splitting for the pure hexamethylbenzene-$d_{18}$ shown in Figure 15b is 33.1kHz which compares well with the value of 34.2kHz found in 4BT. Another similarity is the shape of the horns which suggest that as in 4BT, there is a small biaxiality in the quadrupolar tensor. This is unexpected because the internal rotation of the $-CD_3$ groups about its hexad axis should average any biaxiality to zero.

The observed small biaxiality has been attributed by Hoatson *et al.* to the distortions of the molecular geometry of the ring [40]. However, the similarity of the quadrupolar tensor in pure hexamethylbenzene-$d_{18}$ and that in 4BT strongly suggests that this probe does not dissolve at all in 4BT and so the observed biaxiality in $\tilde{\mathbf{q}}$ is unrelated to that of the crystal E phase. This is not the case for the studies of the symmetry of the nematic phases formed by several mesogens where

hexamethylbenzene has been used as a probe [5, 11, 29]. Here the largest component of the quadrupolar tensor is only about 5kHz which is significantly smaller than that found for the crystal phase of the probe. It clearly indicates considerable rotational disorder and hence that the probe has dissolved in the host.

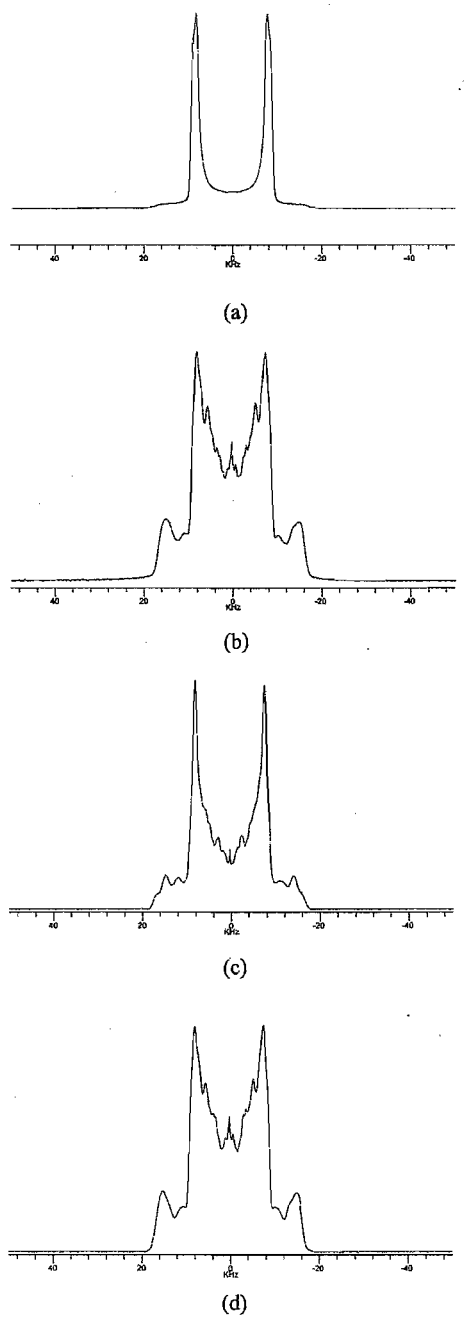


**Figure 15** The deuterium NMR spectrum of pure hexamethylbenzene-$d_{18}$ at 25°C (a) in crystalline form, (b) after cooling from the isotropic phase, (c) after rotation of 90° and (d) after a second 90° rotation .

*7.10.2 Acetonitrile-$d_3$*

Just as in the case of hexamethylbenzene-$d_{18}$, the $\tilde{\eta}$ for the deuterons of acetonitrile-$d_3$ in 4BT also shows a low value, as evidenced from the spectrum in Figure 16. The form of the horns clearly deviates slightly from that expected for a uniaxial system. Simulation of the spectrum gives a value for the biaxiality, $\tilde{\eta}$, of about 0.04. The largest quadrupolar splitting is 35.9kHz. The agreement between the simulated and experimental spectra is close but not perfect and this probably results from the assumption that the linewidth independent of the orientation.

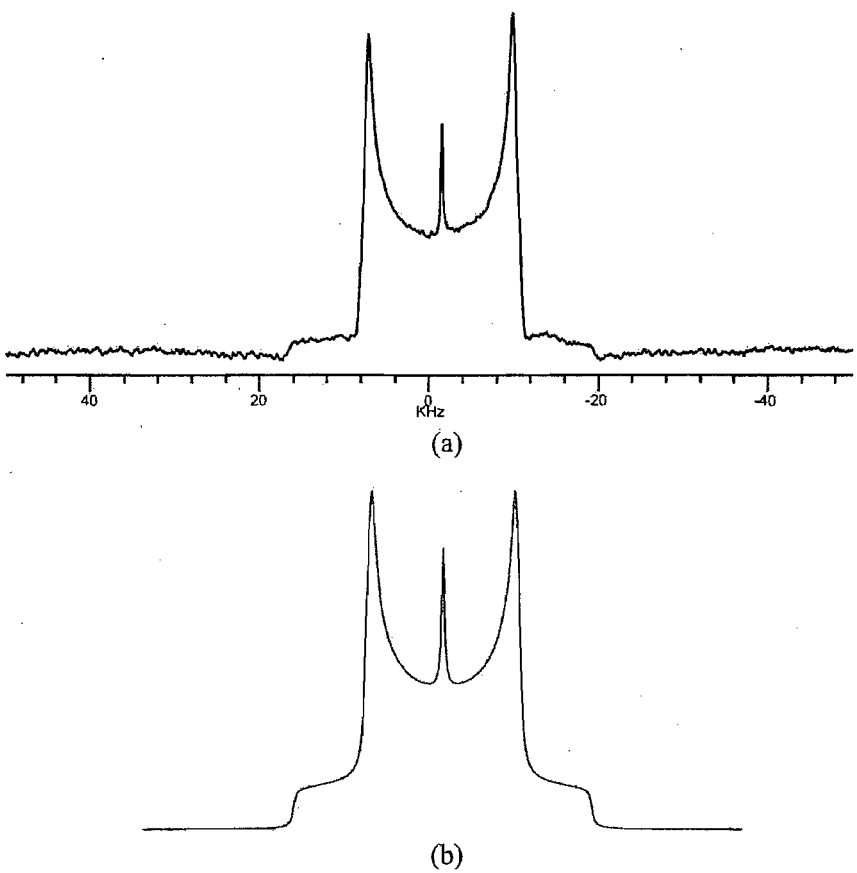


**Figure 16** (a) The deuterium NMR spectrum of acetonitrile-$d_3$ in 4BT at 27.5°C, and (b) the spectrum simulated with $\tilde{\eta} = 0.04$.

We now consider the order parameters for the symmetry axis which can be determined from the quadrupolar splittings. Since the C – D bond makes an angle, θ, with respect to the molecular z-axis, then according to Equation (20),

$$\Delta\tilde{\nu}_{XX} = \frac{3}{2} q_{CD} \left( \frac{3\cos^2\theta - 1}{2} \right) S_{zz}^{XX}, \tag{53}$$

and

$$\Delta\tilde{\nu}_{YY} = \frac{3}{2} q_{CD} \left( \frac{3\cos^2\theta - 1}{2} \right) S_{zz}^{YY}, \tag{54}$$

assuming a tetrahedral angle, 109.5° and $q_{CD}$ is taken to be 168kHz. The quadrupolar splittings $\Delta\tilde{\nu}_{ZZ}$, $\Delta\tilde{\nu}_{XX}$, and $\Delta\tilde{\nu}_{YY}$ are 35.9kHz, 18.7kHz, and 17.2kHz respectively for acetonitrile-$d_3$ in 4BT. However, we are unable to measure the signs of the splittings although we know that their sum must vanish. If we take the largest splitting to be positive, then the other two will be negative and the three order parameters will be

$$S_{zz}^{ZZ} = 0.427$$

$$S_{zz}^{YY} = -0.222$$

$$S_{zz}^{XX} = -0.205.$$

Thus with this choice of signs the molecule behaves as a rod as might be expected from its shape. This choice of signs which combined with the major order parameter gives a relative biaxiality, $\tilde{\eta}$, of 0.04 (see Equation (23)). The biaxial order parameter $\left(S_{zz}^{XX} - S_{zz}^{YY}\right) = 0.017$. The observation of such a small biaxiality in $\tilde{\mathbf{q}}$ for acetonitrile is hard to understand. The major order parameter is essentially in the middle of its range at which point we might have expected the biaxiality in $S_{zz}$ to be a maximum. It would seem that the probe is located in a region of the E phase where the biaxiality is small. For example, the polarity of acetonitrile might mean that it will tend to

associate with the thiocyanato group. This is somewhat remote from the biphenyl group and it is this which creates the biaxiality in the E phase.

### *7.10.3 Chloroform-$d_1$*

Again, there is good but not quite perfect agreement between the simulated and experimental spectrum. In contrast with the spin probe acetonitrile-$d_3$, chloroform-$d_1$ shows a relatively large $\tilde{\eta}$. The experimental spectrum in Figure 17 clearly exhibits the two pair of shoulders and a pair of inner horns corresponding to the three different principal components of $\tilde{\mathbf{q}}$ (see Figure 17b).

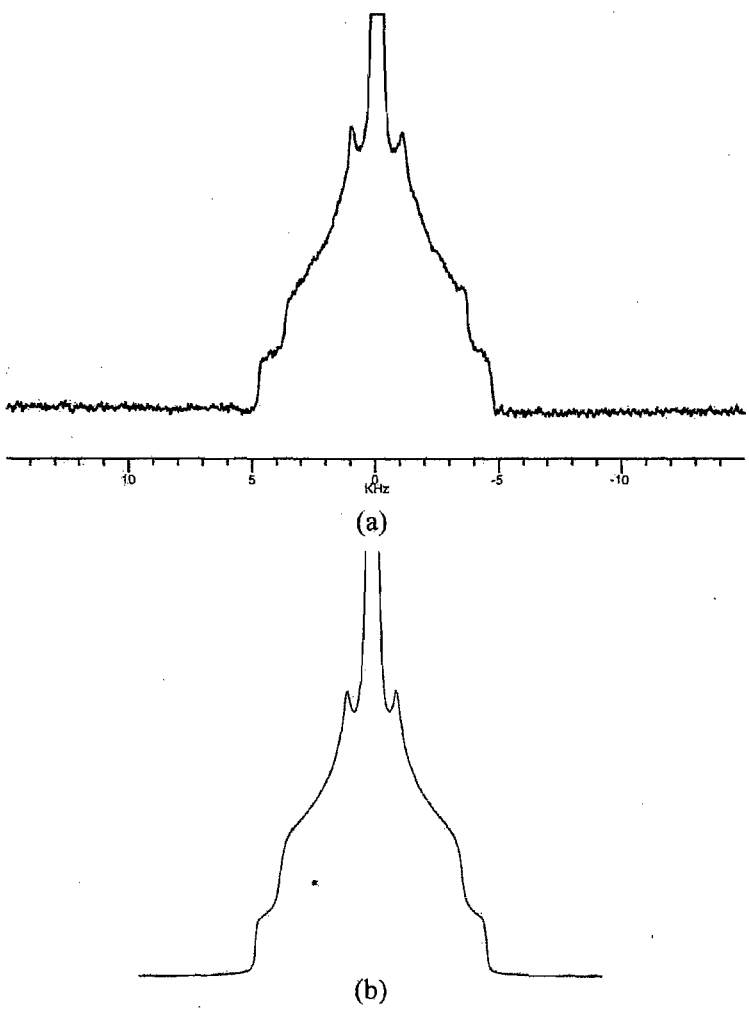


**Figure 17** (a) The deuterium NMR spectrum of chloroform-$d_1$ in 4BT at 25°C and (b) the spectrum simulated with $\tilde{\eta} = 0.57$.

Simulation of the spectrum suggests that $\tilde{\eta}$ is 0.57; in addition there is a strong isotropic peak coming from chloroform that has not dissolved in 4BT.

For the chloroform-$d_1$, the values found for the three splittings are 9.5kHz, 7.5kHz, and 2.0kHz respectively. In order to use Equations (20)-(22) to determine the order parameters from the quadrupolar splittings, we require their signs but as we know, they are not available from NMR spectra. Since a chlorine atom is larger than a deuteron it seems reasonable to treat chloroform as though it will align as a disc with the symmetry axis orthogonal to the Z axis of the phase, that is tending to be orthogonal to the molecular long axis of 4BT. This reasonable assumption gives the three principal order parameters as

$$S_{zz}^{ZZ} = -0.038$$

$$S_{zz}^{XX} = 0.030$$

$$S_{zz}^{YY} = 0.008.$$

The biaxial order parameter, $\left(S_{zz}^{XX} - S_{zz}^{YY}\right)$, is then 0.022 when the major order parameter is $-0.038$. Both order parameters are small although the relative biaxiality, $\tilde{\eta}$, is large at 0.57. The smallness of the order parameters makes it difficult to interpret the value of $\tilde{\eta}$ in terms of specific interactions; however if the $C-D$ does tend to be orthogonal to the Z-axis, then it will sense the difference in the ordering with respect to the X and Y axes more reliably.

*7.10.4 Methylene Dichloride-$d_2$*

The results are more exciting for methylene dichloride-$d_2$ for this gives the largest value of the relative biaxiality in $\tilde{\eta}$ for all of our experiments, *i.e.*, 0.8! The experimental spectrum given in Figure 18 shows that the two sets of outer shoulders seem to have coalesced, *i.e.*, $\tilde{q}_{XX} = -q_{ZZ}$, as found when $\tilde{\eta}$ is unity. However, this cannot be exact because simulation of the spectrum gives the optimum value for $\tilde{\eta}$ as

0.80. At the centre of the spectrum there are two horns on either side of the isotropic peak showing that $\tilde{\eta}$ is not quite unity. The three quadrupolar splittings given by the simulation are 7.3kHz, 6.6kHz and 0.7kHz.

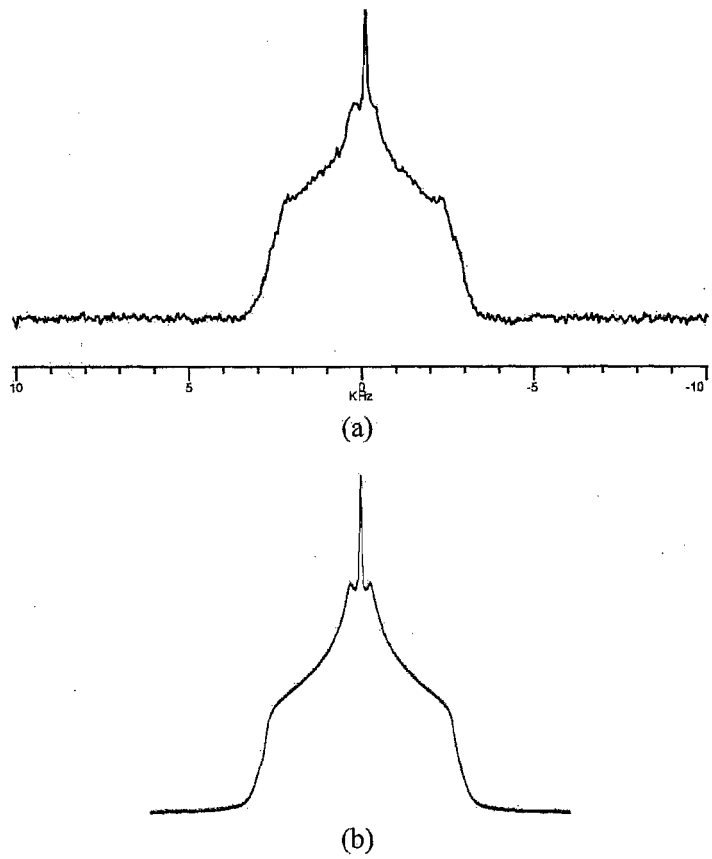


**Figure 18** (a) The deuterium NMR spectrum of methylene dichloride-$d_2$ in 4BT at 20°C and (b) the spectrum simulated with $\tilde{\eta} = 0.80$.

To relate the measured quadrupolar splittings for methylene dichloride to the four order parameters needed to describe the ordering of a biaxial molecule in a biaxial phase (see Equations 25) it is necessary to define the principal axes for the molecule. These are shown in Figure 19 and follow from the two mirror planes of symmetry, giving a point group symmetry of $C_{2v}$. Given the larger size of chlorine with respect to deuterium, the z-axis is taken as parallel to the chlorine-chlorine vector. The y-axis bisects the DCD bond angle and x is orthogonal to both x and z.

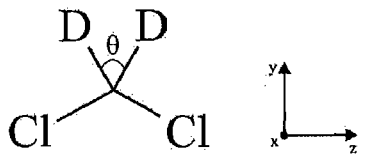


**Figure 19** The principal axes system for methylene dichloride-$d_2$.

If we assume that methylene dichloride has a regular tetrahedral structure, that is $\theta = \cos^{-1}(-1/3)$, then the diagonal components of the molecular quadrupolar tensor are

$$q_{zz} = -\frac{1}{2}q_{CD}$$

$$q_{yy} = \frac{1}{2}q_{CD} \tag{55}$$

$$q_{xx} = 0.$$

This gives the biaxiality in **q** as

$$q_{xx} - q_{yy} = -\frac{1}{2}q_{CD}. \tag{56}$$

Substituting these results for **q** into Equations (30)-(32) for the partially averaged quadrupolar tensor, $\tilde{\mathbf{q}}$ as

$$\tilde{q}_{ZZ} = -\frac{1}{2}q_{CD}\left(S_{zz}^{ZZ} + \frac{1}{3}\left(S_{xx}^{ZZ} - S_{yy}^{ZZ}\right)\right) \tag{57}$$

$$\tilde{q}_{YY} = \frac{1}{4}q_{CD}\left[S_{zz}^{ZZ} + \left(S_{zz}^{XX} - S_{zz}^{YY}\right) + \frac{1}{3}\left\{\left(S_{xx}^{ZZ} - S_{yy}^{ZZ}\right) + \left(S_{xx}^{XX} - S_{yy}^{XX}\right) - \left(S_{xx}^{YY} - S_{yy}^{YY}\right)\right\}\right] \tag{58}$$

and

$$\tilde{q}_{XX} = \frac{1}{4} q_{CD} \left[ S_{zz}^{ZZ} - \left( S_{zz}^{XX} - S_{zz}^{YY} \right) + \frac{1}{3} \left\{ \left( S_{xx}^{ZZ} - S_{yy}^{ZZ} \right) + \left( S_{xx}^{XX} - S_{yy}^{XX} \right) - \left( S_{xx}^{YY} - S_{yy}^{YY} \right) \right\} \right]. \tag{59}$$

The biaxiality in $\tilde{\mathbf{q}}$ is then

$$\left( \tilde{q}_{XX} - \tilde{q}_{YY} \right) = -\frac{1}{2} q_{CD} \left[ \left( S_{zz}^{XX} - S_{zz}^{YY} \right) + \frac{1}{3} \left\{ \left( S_{xx}^{XX} - S_{yy}^{XX} \right) - \left( S_{xx}^{YY} - S_{yy}^{YY} \right) \right\} \right] \tag{60}$$

and the relative biaxiality is

$$\tilde{\eta} = \frac{\left[ \left( S_{zz}^{XX} - S_{zz}^{YY} \right) + \frac{1}{3} \left\{ \left( S_{xx}^{XX} - S_{yy}^{XX} \right) - \left( S_{xx}^{YY} - S_{yy}^{YY} \right) \right\} \right]}{\left[ S_{zz}^{ZZ} + \frac{1}{3} \left( S_{xx}^{ZZ} - S_{yy}^{ZZ} \right) \right]}. \tag{61}$$

It is not possible to simplify these expressions for the principal components of $\tilde{\mathbf{q}}$ any further and so the values of $\tilde{q}_{ZZ}$ and $\left( \tilde{q}_{XX} - \tilde{q}_{YY} \right)$ are insufficient to unravel the four order parameters. To determine all of these requires two additional pieces of information and it is not possible to determine these for deuteriated methylene dichloride. In principle, they might be available for protonated methylene dichloride if the three components of the partially averaged dipolar coupling could be determined. Since the dipolar interaction is cylindrically symmetric about the inter-proton vector, that is the x-axis, then the principal components of the partially averaged dipolar vector would yield $S_{xx}^{ZZ}$ and $\left( S_{xx}^{XX} - S_{xx}^{YY} \right)$. We have not been able to undertake these proton NMR experiments but would note that they have been performed by Thayer *et al.* [41], although using a crystal E performed by a mixture of 4.O8 and 8OCB with the same composition to that studied by Vaz *et al.* [30] but with a 5-10wt% of $CH_2Cl_2$. The biaxiality in the dipolar tensor is repeated as 0.208 which is significantly different to that which we have found for the quadrupolar tensor $\tilde{\mathbf{q}}$. This difference is large which might be expected because they are for different axes in

the methylene dichloride. However, it must also be remembered that the concentration of methylene dichloride is different and more importantly the mesogens forming the crystal E phase are significantly different.

*7.10.5 p-xylene-$d_6$*

Figure 20 shows the experimental and the simulated spectra of p-xylene-$d_6$ in 4BT. Our simulation suggests that $\tilde{\eta}$ is 0.47, which is still relatively large. The largest quadrupolar splitting is 5.6kHz. It might have been anticipated that the biaxiality of the p-xylene molecule would have made the extraction of the order parameters from the quadrupolar splittings difficult (see Section 7.7.3). However, because of the averaging of the molecular quadrupolar tensor of the methyl deuterons by rotation about the C – C bond, this is not the case. The two methyl groups elongate the molecule and so the para-axis tends to align parallel to the director in a uniaxial nematic; we therefore label the para-axis as the z-axis. The y-axis is orthogonal to the phenyl ring and the x-axis is in the plane of the ring and orthogonal to x and y. With this assignment of the principal axes for the ordering matrix the diagonal elements of **q** averaged over the methyl group rotation and assuming tetrahedral geometry are

$$q_{zz} = -\frac{1}{3}q_{CD}$$

$$q_{yy} = \frac{1}{6}q_{CD} \qquad (62)$$

$$q_{xx} = \frac{1}{6}q_{CD}.$$

This gives the biaxiality in **q** as zero which means that this is comparable to the case when the C – D is parallel to the z-axis (see Section 7.7.3). Thus the major component is

$$\tilde{q}_{ZZ} = -\frac{1}{3}q_{CD}S_{zz}^{ZZ} \qquad (63)$$

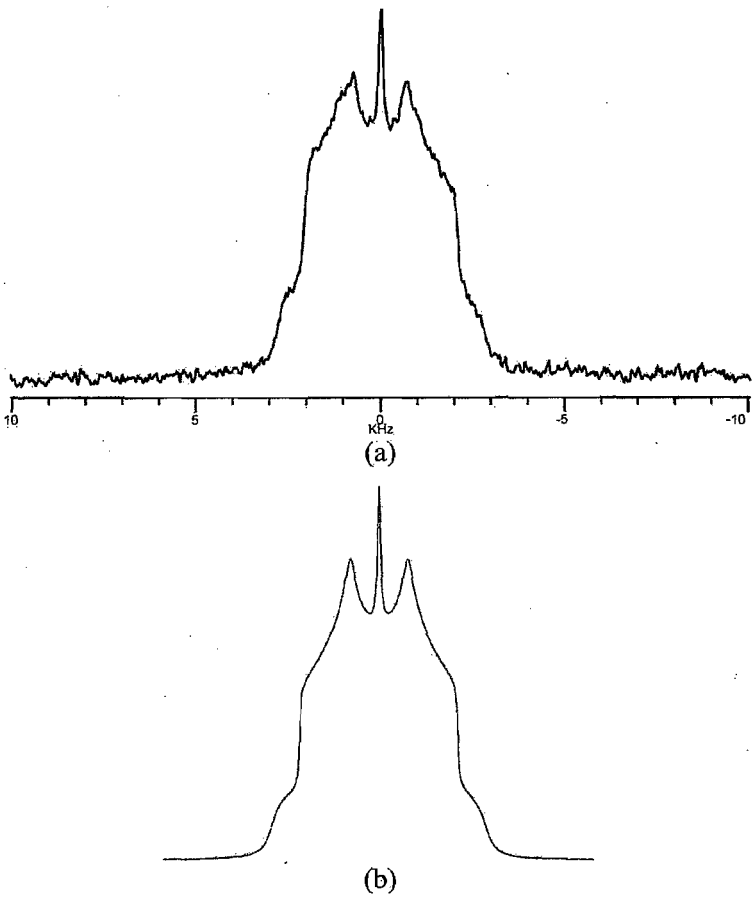


**Figure 20** (a) The deuterium NMR spectrum of p-xylene-$d_6$ in 4BT at 25°C and (b) the spectrum simulated with $\tilde{\eta} = 0.47$.

and the biaxiality is

$$\left(\tilde{q}_{XX} - \tilde{q}_{YY}\right) = -\frac{1}{3} q_{CD} \left(S_{zz}^{XX} - S_{zz}^{YY}\right), \tag{64}$$

which gives the relative biaxiality as

$$\tilde{\eta} = \frac{\left(S_{zz}^{XX} - S_{zz}^{YY}\right)}{S_{zz}^{ZZ}}. \tag{65}$$

The observed quadrupolar splittings then give the order parameters as $S_{zz}^{ZZ} = -0.066$ and $\left(S_{zz}^{XX} - S_{zz}^{YY}\right) = 0.032$. In this calculation, $\tilde{q}_{ZZ}$ is taken to be negative in keeping with the result found for nematic hosts and consequently the other two components of $\tilde{\mathbf{q}}$ are taken to be positive.

### *7.10.6 Pure 4BT-$d_2$*

In order to compare the results of the deuteriated pure sample and the doped samples which we had investigated, Professor Dabrowski prepared some deuteriated 4BT. The deuteriation is restricted to the two aromatic rings but is not in one specific position as shown in Figure 21. Fortunately it is expected that various C – D bonds make, essentially, the same angles with the principal axes of the supermatrix so that the spectra associated with the different deuteriated sites should essentially be the same. The experimental spectrum measured at 75°C is shown in Figure 22. It appears that there are just three major features, two sets of shoulders and one pair of horns as expected for a biaxial phase. However, closer inspection reveals an extremely weak isotropic peak possibly resulting from the high temperature which is close to the E-I transition. In addition, there is a pair of weak, relatively sharp peaks on the inside of the dominant horns and these may result from different deuteriation sites in the biphenyl moiety. We shall, however, ignore this second pair of horns when simulating the spectrum to determine the major quadrupolar coupling $\tilde{q}_{ZZ}$ and the relative biaxiality, $\tilde{\eta}$. As in the previous simulation, the linewidths were also varied to optimise the fit with the experimental spectrum. The optimised simulated spectrum is shown in Figure 22 and gave a relatively large value for $\tilde{\eta}$ of 0.51.

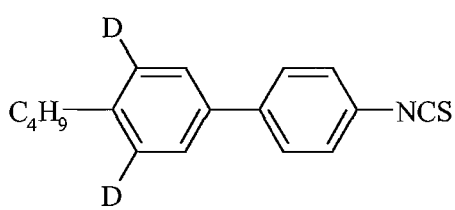


**Figure 21** The molecular structure of the specifically deuteriated 4BT used in our study.

Given the biaxiality of 4BT and of the phase, these two parameters are insufficient to determine the four order parameters which are needed to characterise the orientational order (see Section 7.10.4 for methylene dichloride-$d_2$). Instead we consider the model proposed by Vaz *et al.* [30] in which the biaxiality in the quadrupolar tensor, $\tilde{\mathbf{q}}$, is taken to result from the internal motion of the phenyl rings through the $\pi$-flips. This motion must occur because without it, the powder pattern observed would be that for the isolated C – D, that is with a form corresponding to a uniaxial quadrupolar tensor with the largest component, $\tilde{q}_{ZZ}$, being equal to ~ 186kHz. This is clearly not observed and the internal motion is involved to induce a biaxiality. In the E phase, the para-axis of the biphenyl group is likely to be aligned parallel to the Z-axis. The jump motion of the phenyl ring will not change the quadrupolar tensor components along this axis or indeed along the X and Y axes. These axes are shown with respect to the phenyl rings of 4BT in Figure 23.

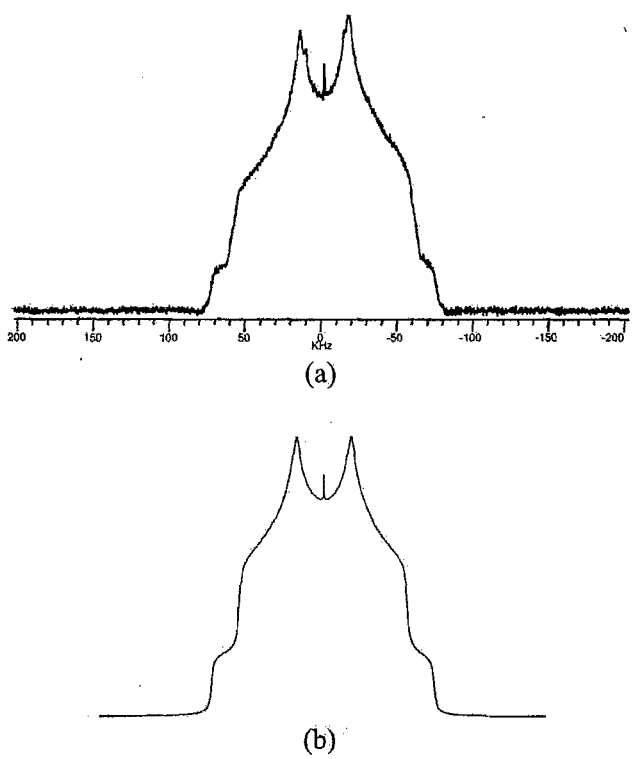


**Figure 22** The deuterium NMR spectrum of 4BT-$d_2$ at 75°C, and the simulated spectrum with $\tilde{\eta} = 0.51$.

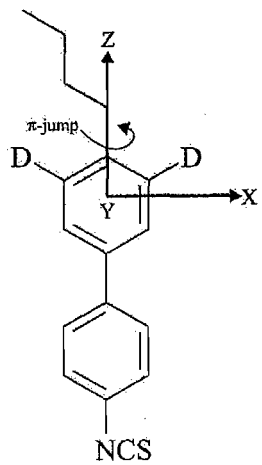


**Figure 23** The schematic representation of the laboratory axes of 4BT-$d_2$.

Assuming a regular hexagonal structure for the phenyl ring and a cylindrical symmetry for the quadrupolar tensor, the X, Y and Z components of $\tilde{\mathbf{q}}$ are given by

$$\tilde{q}_{ZZ} = -\frac{1}{8}q_{CD}$$

$$\tilde{q}_{YY} = -\frac{1}{2}q_{CD} \qquad (66)$$

$$\tilde{q}_{XX} = \frac{5}{8}q_{CD}.$$

Interestingly the largest components of $\tilde{\mathbf{q}}$ is $\tilde{q}_{XX}$ and so according to the convention introduced in Section 7.6, the components should be relabelled as

$$\tilde{q}'_{ZZ} = \frac{5}{8}q_{CD}$$

$$\tilde{q}'_{YY} = -\frac{1}{2}q_{CD} \qquad (67)$$

$$\tilde{q}'_{XX} = -\frac{1}{8}q_{CD}.$$

This gives the biaxiality as

$$(\tilde{q}'_{XX}-\tilde{q}'_{YY})=\frac{3}{8}\tilde{q}_{CD} \qquad (68)$$

and the relative biaxiality as $\tilde{\eta}=3/5$. This value of 0.60 is close to the experimental value of 0.51 and the agreement could be improved if allowance was made for deviations of the geometry of the phenyl ring from a regular structure. For example, if the angle made by the C – D bond with the Z-axis is taken to be 61° rather than 60° than $\tilde{\eta}$ is predicted to be 0.54 which is closer to the observed value. Exact agreement is found when the angle made by the C – D bond with the Z-axis is given the value 61.7° which is not unreasonable. The model can also be tested by predicting the absolute value of the largest quadrupolar splitting, $\tilde{q}'_{ZZ}$. With an angle of 61.7°, this is predicted to be 185kHz. The experimental value of 148.0kHz is somewhat smaller and suggest that there is some librational motion of the phenyl ring in the crystal E plane. Similarly, the predicted value for $\tilde{q}'_{XX}$ is 45.4kHz, which is larger than the experimental value of 32.3kHz. However, these values are also sensitive to the assumed geometry. For example, if we return to the regular hexagonal geometry then $\tilde{q}'_{ZZ}$ is calculated to be 174kHz and the smallest principal component, $\tilde{q}'_{YY}$, is calculated to be 34.9kHz; these are much closer to the experimental values.

If the origin of the biaxiality in the quadrupolar tensor, $\tilde{\mathbf{q}}$, is indeed the jump rotation of the phenyl rings or indeed of the entire molecule, then it is to be expected that the spectrum should be temperature dependent, *i.e.*, as the temperature is lowered so that the rate at which the C – D changes its orientation will be reduced. Since the jump rotation modulates the components of the quadrupolar tensor in the laboratory frame, then the linewidths should change and eventually the line positions. To test this expectation, we have measured the NMR spectrum of 4BT-$d_2$ as a function of temperature from 75°C down to 0°C; the spectra obtained are shown in Figure 24. As we have already seen, the spectrum at 75°C is a standard powder pattern for a biaxial quadrupolar tensor, which suggests that at this temperature, the jump rotation is fast on the NMR timescale. As the temperature is lowered so the appearance of the spectrum changes; the difference to the high temperature spectrum becomes

especially noticeable at 45°C. Thus the outer shoulders become more peak-like while the inner shoulders are rather flat. The shape of the horns does not change to any significant extent. At the lowest temperature of 0°C, these trends have clearly continued. Thus the outer shoulders now appear as two peaks; the inner shoulders have a much stronger peak-like appearance although the widths are considerably larger than the outer pair. The horns have the same form as at higher temperature but with a much lower intensity. We should note that although the appearance of the spectral features does change as the temperature is lowered from 75°C to 0°C, their location does not. In contrast, the spectra found for the probes acetonitrile-$d_3$, chloroform-$d_1$, methylene dichloride-$d_2$ and p-xylene-$d_6$ do not change with temperature.

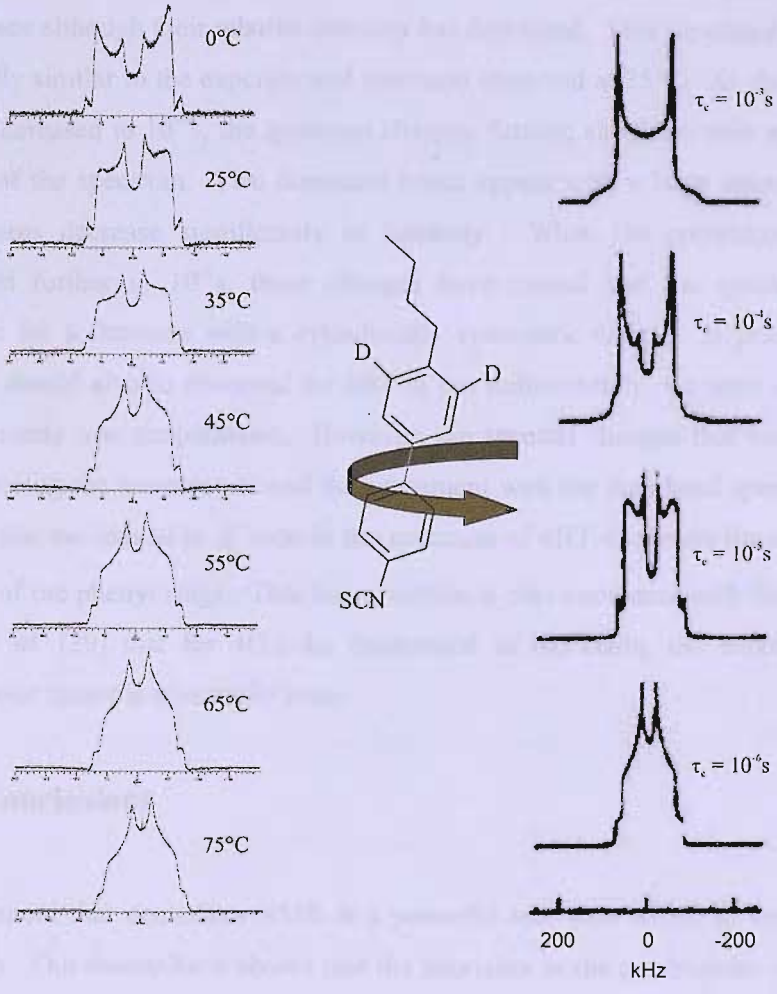


**Figure 24** The temperature dependence of the deuterium NMR spectra of pure 4BT, and the simulated spectra for a π-flip model as a function of the correlation time, $\tau_C$ [42].

We are able to use the temperature dependence of the NMR spectra to confirm the jump rotation of the phenyl rings as the source of the biaxiality because the changes have been simulated. The simulation is for a randomly oriented sample of molecules in which the deuteriated phenyl ring undergoes jumps through 180° [42]. The spectra were simulated for a range of correlation times, $\tau_c$, characterising the jump dynamics. The results are shown in Figure 24 for a range of correlation times, for $10^{-6}$s to $10^{-3}$s. For the smallest time, the simulated spectrum has the appearance expected for a powder pattern of a deuteron with a biaxial quadrupolar tensor. This simulated spectrum is essentially identical to that measured for 4BT-$d_2$ at the highest temperature. When the correlation time is $10^{-5}$s, both the inner and outer spectral shoulders have developed a peak-like form while the horns have not changed in appearance although their relative intensity has decreased. This simulated spectrum is essentially similar to the experimental spectrum observed at 25°C. As the correlation time is increased to $10^{-4}$s, the spectrum changes further; shoulders now appear at the outside of the spectrum. Two dominant horns appear with a large intensity and the inner horns decrease significantly in intensity. When the correlation time has decreased further to $10^{-3}$s, these changes have ceased and the spectrum is that expected for a deuteron with a cylindrically symmetric tensor. In principle, these changes should also be observed for 4BT-$d_2$ but unfortunately, we were unable to go to sufficiently low temperatures. However, the spectral changes that were observed on decreasing the temperature and the agreement with the simulated spectra strongly suggest that the biaxial in $\tilde{\mathbf{q}}$ seen in the spectrum of 4BT-$d_2$ results from the $\pi$-jump rotation of the phenyl rings. This interpretation is also consistent with the finding by Dong *et al.* [39] that for 4O.8-$d_{21}$ deuteriated in the chain, the biaxiality in the quadrupolar tensor is essentially zero.

## 7.11 Conclusions

It is apparent that deuterium NMR is a powerful tool with which to explore phase biaxiality. Our results have shown that the biaxiality in the quadrupolar tensor, $\tilde{\mathbf{q}}$, is related to the probe structure. In addition, the magnitude of $\tilde{\eta}$ can be influenced by the extent of the orientational order of the probe as well as by its symmetry. For the uniaxial probe, acetonitrile-$d_3$ $\tilde{\eta}$ is essentially zero. In contrast, the uniaxial probe

chloroform-$d_1$ has a high biaxiality in $\tilde{\mathbf{q}}$. The two biaxial probes, methylenedichloride-$d_2$ and p-xylene-$d_6$, both have large values of $\tilde{\eta}$. In addition, the ring-deuteriated pure mesogen can also yield a measure of biaxiality, as observed in the results for deuteriated 4BT, which gives a large value of $\tilde{\eta}$, comparable with the lyotropic biaxial nematics. However, care is required to interpret biaxiality from NMR in the presence of internal motion. Indeed for this system, the observed biaxiality in $\tilde{\mathbf{q}}$ is thought to result from the $\pi$-jumps of the phenyl rings containing the deuterons.

This rich variety of behaviour provides a valuable route to understanding, at a theoretical level, the biaxial interactions between the probe molecule and its biaxial environment. At a pragmatic level, it shows that considerable care needs to be exercised in the selection of probe molecules to explore the symmetry of liquid crystal phases. Indeed it seems essential to use a selection of spin probes in such studies.

## 7.12 References


[1] D. W. Bruce, *Chem. Rec.*, **4**, 10 (2004).

[2] Y. Galerne, *Mol.Cryst.Liq.Cryst.*, **323**, 211 (1998).

[3] L. J. Yu, A. Saupe, *Phys. Rev. Lett.*, **45**, 1000 (1980).

[4] F. P. Nicoletta, G. Chidichimo, A. Golemme, N. Picci, *Liq. Cryst.*, **10**, 665 (1991).

[5] L. A. Madsen, T. J. Dingemans, M. Nakata, E. T. Samulski, *Phys. Rev. Lett.*, **92**, 145505 (2004).

[6] P. D. Brimicombe, 2nd Southampton International Symposium on Biaxial Nematics (http://www.slci.soton.ac.uk/Biaxiality_meeting_Jan06.htm), 27th January, 2006.

[7] P. Brimicombe, *Soft Matter Mathematical Modelling Workshop*, Cortona, 11th - 16th September, 2005.

[8] J-J Lyu, C-H Lee, H-S Chang, *U.S. Patent Publication*, **US 2003/0043325 A1** (2003).

[9] M. J. Freiser, *Phys. Rev. Lett.*, **24**, 1041 (1970).

[10] G. R. Luckhurst, *Angew. Chem. Int. Ed.*, **44**, 2834 (2005).

[11] G. R. Luckhurst, *Thin Solid Films*, **393**,40 (2001).

[12] A. Ferrarini, P. L. Nordio, E. Spolaore, G. R. Luckhurst, *J. Chem. Soc. Faraday Trans.*, **91**, 3177 (1995).

[13] J. P. Straley, *Phys. Rev. A*, **10**, 1881 (1974).

[14] N. Boccara, R. Mejdani, L. de Seze, *J. Phys.*, **38**, 149 (1977).

[15] A. Ferrarini, G. R. Luckhurst, P. L. Nordio, S. J. Roskilly, *J. Chem. Phys.*, **100**, 1460 (1994).

[16] G. R. Luckhurst, C. Zannoni, P. L. Nordio, U. Segre, *Mol. Phys.*, **30**, 1345 (1975).

[17] A. M. Sonnet, E. G. Virga, G. E. Durand, *Phys. Rev. E*, **67**, 061701 (2003).

[18] G. R. Luckhurst, *Nature*, **430**, 413 (2004).

[19] K. Praefcke, B. Kohne, B. Gundogan, D. Singer, D. Demus, S. Diele, G. Pelzl, U. Bakowsky, *Mol. Cryst. Liq. Cryst.*, **198**, 393 (1991).

[20] J. Malthête, H. T. Nguyen, A. M. Levelut, *J. Chem. Soc. Chem. Commun.*, 1548 (1986).

[21] S. Chandrasekhar, B. R. Ratna, B. K. Sadashiva, N. V. Raja, *Mol. Cryst. Liq. Cryst.*, **165**, 123 (1988).

[22] K. Praefcke, B. Kohne, D. Singer, D. Demus, G. Pelzl, S. Diele, *Liq. Cryst.*, **7**, 589 (1990).

[23] B. R. Acharya, A. Primak, S. Kumar, *Phys. Rev. Lett.*, **92**, 145506 (2004).

[24] S. Chandrasekhar, G.G. Nair, D. S. Shankar Rao, S. K. Prasad, K. Praefcke, D. Blunk, *Curr. Science*, **75**, 1042 (1998).

[25] C. Chiccoli, I. Feruli, O. D. Lavrentovich, P. Pasini, S. V. Siyanovskii, C. Zannoni, *Phys. Rev. E*, **66**, 030701 (2002).

[26] S. Chandrasekhar, G. G. Nair, D. S. Shankar Rao, K. Praefke, D. Blunk, *Liq. Cryst.*, **24**, 67 (1998).

[27] P. J. Collings, D. J. Photinos, P. J. Bos, P. Ukleja, J. W. Doane, *Phys. Rev. Lett.*, **42**, 996 (1979).

[28] S. M. Fan, I. D. Fletcher, B. Gundogan, N. J. Heaton, G. Kothe, G. R. Luckhurst, K. Praefcke, *Chem. Phys. Lett.*, **204**, 517 (1993).

[29] J. R. Hughes, G. Kothe, G. R. Luckhurst, J. Malthete, M. E. Neubert, I. Shenouda, B. A. Timimi, M. Tittlebach, *J. Chem. Phys.*, **107**, 9252 (1997).

[30] N. A. Vaz, M. J. Vaz, J. W. Doane, *Phys. Rev.*, **30**, 1008 (1984).

[31] M. R. Fisch, S. Kumar, in *Liquid Crystals: Experimental Study of Physical Properties and Phase Transitions*, (Ed. S. Kumar), Cambridge University Press, United Kingdom (2001).

[32] R. M. Richardson, A. J. Leadbetter, J. C. Frost, *Mol. Phys.*, **45**, 1163 (1982).

[33] A. J. Leadbetter, J. C. Frost, J. P. Gaughan, M. A. Mazid, *J. Phys. (Paris)*, **C3**, 185 (1979).

[34] S. Urban, K. Czupryński, R. Dabrowski, B. Gestblom, J. Janik, H. Kresse, H. Schmalfuss, *Liq. Cryst.*, **28**, 691 (2001).

[35] C. A. Veracini, *Nuclear Magnetic Resonance of Liquid Crystals, NATO ASI Series*, (Ed. J. W. Emsley) D. Reidel Publishing Co., Dordrecht (1985), Chap. 5.

[36] G. R. Luckhurst, in *Physical Properties of Liquid Crystals: Nematics*, (Eds. D. A. Dunmur, A. Fukuda, G. R. Luckhurst), INSPEC, London (2001), Chap. 2.1.

[37] M. A. Bates, G. R. Luckhurst, *Phys. Rev. E*, **72**, 051702 (2005).

[38] D. Dunmur, K. Toriyama, *Handbook of Liquid Crystals, Vol. 1*, (Eds. D. Demus, J. Goodby, G. W. Gray, H. W. Spiess, V. Vill) , WILEY-VCH, Weinheim, (1998), Chap. VIII.

[39] R. Y. Dong, H. Schmiedel, N. A. P. Vaz, Z. Yaniv, M. E. Neubert, J. W. Doane, *Mol. Cryst. Liq. Cryst.*, **98**, 411 (1983).

[40] G. L. Hoatson, R. L. Vold, T. Y. Tse, *J. Chem. Phys.*, **100**, 4756 (1994).

[41] A. M. Thayer, M. Luzar, A. Pines, *Liq. Cryst.*, **2**, 241 (1982).

[42] R. J. Schadt, E. J. Cain, A. D. English, *J. Phys. Chem.*, **97**, 8387 (1993).